TÉCNICO LISBOA

UNIVERSIDADE DE LISBOA
INSTITUTO SUPERIOR TÉCNICO

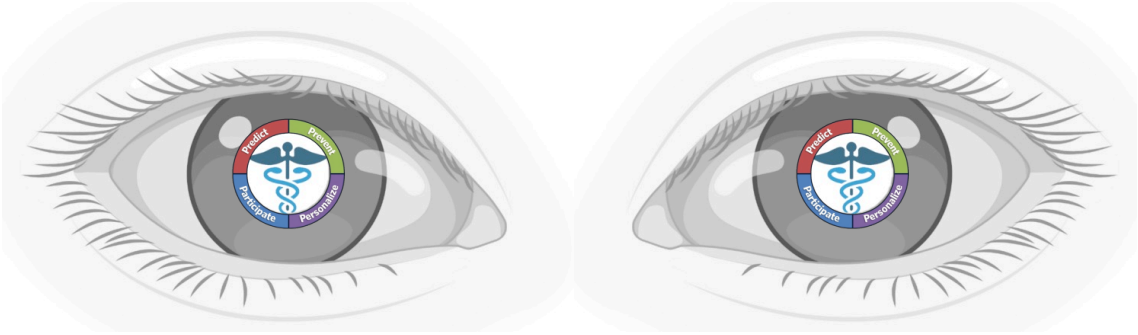

Nanoparticle-based (Bio)sensors:

Blowing Tailwinds of Information to Wellness and Healthcare

Rui Pedro Oliveira Silva

Supervisor: Doctor Duarte Miguel de França Teixeira dos Prazeres

Co-supervisors: Doctor Nuno João de Oliveira e Silva
Doctor Pedro Miguel Neves Ribeiro Paulo

Thesis approved in public session to obtain the PhD Degree in Biotechnology and Biosciences
Jury final classification: Pass with Distinction

2022

TÉCNICO LISBOA

UNIVERSIDADE DE LISBOA
INSTITUTO SUPERIOR TÉCNICO

Nanoparticle-based (Bio)sensors:

Blowing Tailwinds of Information to Wellness and Healthcare

Rui Pedro Oliveira Silva

Supervisor: Doctor Duarte Miguel de França Teixeira dos Prazeres

Co-supervisors: Doctor Nuno João de Oliveira e Silva
Doctor Pedro Miguel Neves Ribeiro Paulo

Jury

Chairperson: Doctor João Pedro estrela Rodrigues Conde, Instituto Superior Técnico da Universidade de Lisboa

Members of the Committee:

Doctor Daniel Aili, Linköping University, Sweden
Doctor João Pedro estrela Rodrigues Conde, Instituto Superior Técnico da Universidade de Lisboa
Doctor Duarte Miguel de França Teixeira dos Prazeres, Instituto Superior Técnico da Universidade de Lisboa
Doctor João Diogo Osório de Castro Conde, NOVA Medical School|Faculdade de Ciências Médicas, Universidade Nova de Lisboa

Thesis approved in public session to obtain the PhD Degree in Biotechnology and Biosciences
Jury final classification: Pass with Distinction

FUNDING INSTITUTION

FCT – Fundação para a Ciência e a Tecnologia

2022

To all those who’ve fueled my eagerness
for personal and intellectual growth

Abstract

The process of gather, analyze, and convert information into knowledge is a crucial step to assess the state of a system. Modern medicine is not an exception to this premise, and therefore the usage and development of (bio)sensors as a tool to harvest information about a patient's health condition is critical to enable adequate response. Hence, the scope of this thesis is to push the limits of (bio)sensors by exploring the features of nanomaterials. To do so, I explored three independent concepts:

- A magnetic thermometer resorting to nanoparticles with a sharp magnetic transition around 42˚C was prepared and tested as a non-volatile logic-gate. The Iron Selenide (Fe_3Se_4) nanoplatelets determined the occurrence of temperature overshoots during hyperthermia treatments *in vitro* using a prostate cancer (PC-3) cell line as a model.
- A plasmophore composed of gold-coated silver triangular nanoprisms (Ag@Au NTs) operates as support and optical antenna for ATTO-655. The ability and efficiency to detect nucleic acid sequences using the fluorescent nanocomposite was assessed. Confocal fluorescence lifetime microscopy characterized the optical properties of the hybrid constructions, unveiling that emission from a single nano-object is a 1000-fold brighter than that from a single dye label.
- For last, dark-field microscopy was employed to determine proteolytic activity in real-time at a single particle level. The particle's optical response is monitored as the cleavage of the peptide layer on the AuNRs' surface by the protease induces changes in the local refractive index. With hundreds of milliseconds of time resolution, this design rendered powerful insights about the kinetics of the reaction. Also, the ratio between two competitive mechanisms – peptide cleavage and non-specific adsorption – enabled to overcome the non-trivial response of the substrate-limited sensor. Quantification of active enzyme over three orders of magnitude as working range with detection limits of a few nanomolar was achieved.

Overall, I aspire that the principles underlying the (bio)sensors developed within the framework of this thesis can significantly contribute to fields and concepts such as P4 medicine by enabling access, either discretely in time or through continuous monitorization, to information previously considered unattainable.

Keywords: Nanomaterials, Biosensors, Nanothermometry, Plasmonic-based Fluorescence Enhancement, Proteolytic activity in Real-time

Resumo

O processo de recolha informação e sua conversão em conhecimento é um passo crucial para avaliar o estado de determinado sistema. A medicina moderna não é exceção a esta premissa. Por este motivo, a utilização e desenvolvimento de (Bio)ssensores está intimamente ligada com a capacidade de recolher informação relevante sobre o estado de saúde de um paciente, permitindo uma resposta adequada e "educada". Neste âmbito, esta tese focou-se no desenvolvimento de (bio)ssensores com potencialidade para serem integrados em diagnóstico médico e controlo de processo e/ou tratamentos. Aqui é apresentado o design e desenvolvimento experimental e três conceitos de (Bio)ssensores independentes:

- Um nanotermómetro composto de Seleneto de Ferro (Fe_3Se_4) com propriedades de magnetos duros foi preparado e testado como porta-lógica não-volátil. Simultaneamente estes nanodiscos apresentam uma transição magnética abrupta em torno dos 42˚C. Procedente das suas propriedades magnéticas peculiares, as nanoplacas foram capazes de determinar a ocorrência de sobreaquecimento durante tratamentos de hipertermia *in vitro* utilizando como modelo uma linha celular de cancro da próstata (PC-3).
- Um plasmóforo constituído por nanoprismas triangulares de prata revestida a ouro (Ag@Au NTs) que operam como nanoantena ótica para a emissão do fluoróforo ATTO-655 na deteção de ácidos nucleicos foi desenvolvido. As propriedades óticas do nanomaterial híbrido resultante foram caracterizadas utilizando microscopia por tempos de vida de fluorescência em modo confocal. Assim, foi possível verificar que o nanohíbrido possuía uma emissão 1000 vezes superior à emissão de um fluoróforo individual.
- Por fim, nanobastonetes de ouro (AuNRs) foram aplicados na determinação de atividade proteolítica em tempo-real sob microscopia de campo escuro. O corte da camada peptidíca existente à superfície dos AuNRs induz uma alteração no índice de refração local que é sondado pela alteração das propriedades óticas dos AuNRs. O biossensor resultante possibilita observação de partícula individual com possibilidade de mapeamento espacial. Também, permite a monitorização da atividade proteolítica com uma resolução temporal na ordem das centenas de milissegundos e ao longo de três ordens de magnitude de concentração desde 1 até 300 nanomolar.

Idealmente é desejado que os princípios subjacentes aos (bio)ssensores desenvolvidos no contexto desta tese possam contribuir significativamente na área de sensores e em conceitos como o de medicina P4 por facilitação do acesso a informação previamente inatingível sobre a ocorrência de eventos discretos no tempo ou por monitorização continua do processo.

Palavras-chave Nanomateriais, (Bio)ssensores, Nanotermometria, Fluorescência Intensificada por Partículas Plasmónicas, Atividade Proteolítica em Tempo-real.

Acknowledgments

First and foremost, if you are reading this and expecting to see your name but do not find it, please do not be discouraged. It is impossible to express gratitude to every individual who contributed in some way to the completion of this thesis. I apologize in advance to those whose names may be omitted in this section. However, please understand that this does not diminish my heartfelt appreciation and recognition of your contributions and impact.

Have you ever wondered what your superpower is? Growing up, this daydream crossed my mind many times. Among all my strengths and weaknesses, I believe my superpower is "Mirroring." It may not have the most exciting name, but the reality is that every time I have the opportunity to interact and spend time with someone, I try to understand what I admire most about that person and then try to incorporate that quality into my own life. This might seem vague, but, I believe that recognizing this has allowed me to surround myself with interesting people and try to get the most out of these interactions. This leads me to express my gratitude to the "giants" on whose shoulders I stood, attempting to see further - my supervisors: Professor Miguel Prazeres, Nuno João Silva, Pedro M. Paulo and the "unseen protagonist" Peter Zijlstra.

If true heroism is defined as "fighting against an equal or stronger opponent to protect someone weaker in whom you believe," then I would like to thank Professor Miguel for always being a constant support and for always "covering my back" throughout my journey. I hope to have acquired his boundless patience that enabled us to navigate our countless pre-weekend and wide-ranging discussions, projects, and challenges we encountered throughout this journey.

Nuno was the only supervisor I knew before I began this endeavor, and our professional relationship dates back to the days when we barely had a bench to work. I could attribute many qualities to him, like my other supervisors, but his true love for his craft and courage to step out of his comfort zone and take risks stand out to me. Interestingly, in a world that preaches to "think outside the box," he effortlessly taught me that innovation can also arise from thinking about "what's inside the box." Thank you for all the freedom, trust, and for always feeling close, despite often being physically far away.

I always felt welcome at IST, but it wasn't until I started working closely with Pedro that I started cementing my path. Frankly, I see Pedro as my scientific "older brother." He was always extremely accessible and available and even when my ideas seemed far-fetched, he never discouraged me without proper reasoning. Remarkably, with a simple longpass filter, he managed to get me out of the "peer-reviewed induced Dunning-Kruger" which saved me a lot of time and enabled me to redirect my research towards a better path. My admiration for Pedro lies in his ability to "motivate through care." For example, after training me to use the microscope, it was enough to hand me the keys for some voluntary weekend "self-enslavement" to happen...

I am incredibly grateful for my time at TU/e and in the Netherlands. The experience exceeded all of my expectations (the weather though…) and I am especially grateful for the opportunity to be a part of such an open and ambitious group with such stimulating working culture. I am thankful for Peter's guidance and support, and for the opportunity to be involved in a

collaborative and energizing environment where I could focus on doing research-related tasks instead of losing energy with pointless bureaucratic and slow-paced affairs. Peter's skillset is incredibly diverse and well-rounded (his player card would certainly be very close to the perfect “pentagon”), covering a range of subjects from physics to biology and engineering, making it exciting to work on multidisciplinary innovative projects. One of the most valuable lessons I have learned from Peter is the importance of effectiveness, both professionally and personally. I am grateful for the clear and concise messages and ideas that he has shared with me that I constantly recall. I promise that I will continuously strive to acquire this skill set that I clearly lack (😅 🤣).

As “wildcard”, I would like to share a personal story that had a profound impact on me. Right after the 1st quarantine, I was visiting Maastricht and practicing some longboard dancing tricks in the main square. A little girl in a wheelchair, who I later learned was 5 years old, shouted out "that's awesome!" and we struck up a conversation. She challenged me to a race and I was faced with the question of whether or not to let her win. I ultimately decided to win while trying my best to make it look competitive and enjoyable, and I encouraged her to keep training so next time she could win. What struck me most about this encounter was the little girl's joyful spirit and excitement as she was just smiling and spinning around in her wheelchair. Effortlessly, she reminded me of the importance of staying focused on the big picture and the path that I wish to navigate towards to... It is interesting that in this “paperocratic world” based on (fake) “productivity” metrics, it was this little girl that found a simple, yet right attitude to give me a boost of motivation through a very important lesson. From Barbara I intend to “steal” the Smile 😊

It goes without saying that I am very grateful to all the people I have had the privilege of meeting for one reason or another. This has undoubtedly been an interesting, crazy journey that would not make as much sense without all of you. Whether my opinion about you is good or bad, I am grateful either way. After all, good experiments often need both "positive" and "negative" controls, and most sensing technologies rely on the usage of "calibration curves". Therefore, I believe that everyone was able to contribute to creating a "better version of me". Nonetheless, and to be honest, I only plan to keep around those who keep raising the bar and making me strive for higher goals, because, after all, one day I want to be able to look you in the eyes and say right to your face, "I told you so!" 👊🏻 *wink

I am very grateful to all my long-time friends for sticking by my side for all these years, even though sometimes I am not the easiest person to deal with. A special heartfelt acknowledgment goes to my everlasting friend Dani for the many adventures, thoughts, and lessons that we’ve shared throughout our history together. Even though, our carbon-carbon experiences are no longer an option, I am sure I will continue to use my “augmented reality” features to keep you right by my side. Hence, if my “Peter Pan Syndrome” (which we often joked about) is real, you are now something like my “Tinker Bell”. #sorrynotsorry 🌟 💫 💖

“Behind a great man there’s always a great woman”. From this sentence I may doubt if I classify as a “great man”, but I don’t doubt for a second that Joana is a great woman and a wonderful human being. From the bottom of my heart and the center of my brain, thank you

"$very\ much^{100000}$" for keeping the ground steady, the heart pumping, and the blood flowing. ❤️🔥

It is a clear understatement to say that I would need an entire dissertation to explain why I am thankful for all these years, how you have made me a better human being and why I owe you so much. By now you should all know that, so I'll keep it simple and say: thank you for accepting me as a "maverick" and for making me proud of be "shameless".

Lastly, but not least, thank you little Simão "Zephy" for putting an end to this madness… 🍼👶

Table of Contents

Figure Index

Figures Contextualization

Figures P(lasmon)E(nhanced)F(luorescence)

Figures PEF (SI)

Table PEF (SI)

Figures M(agnetic) L(ogic)-G(ate)

Tables M LG (SI)

Figures M LG(SI)

Figures L(ocalized)S(urface)P(lasmon)R(esonance) P(roteolytic)A(ctivity)

Figures LSPR PA (SI)

Tables LSPR PA (SI)

Figures M(onitoring) P(roteolytic)A(ctivity) R(eal)T(ime)

Figures Patent

Summary and Objectives

Objectives on conveying information

The term technology refers to the integration and application of scientific knowledge into our daily lives. As society keeps progressing towards a more technological future, multidisciplinarity and interdependency between many scientific areas of knowledge are increasingly becoming the status-quo. The research topic underlying this dissertation is no exception to this premise as it involves concepts regarding biology, physics, chemistry, among others – either directly or indirectly.

The pace of scientific output in the overviewed topics is immense and, as a result, extensive covering would be an ineffective task. Furthermore, human's "attention span" seems to be rapidly decreasing[i] due to technology and accessibility to information, which can critically impair the learning process. Except for the technical chapters,[ii] most of the thesis will be exposed according to Da Vinci's motto: "simplicity is the ultimate sophistication"[iii], while aiming to maintain scientific accuracy.

As the primary goal of publishing a Ph.D. thesis is to disseminate its findings, and with the aim of democratizing[iv] the access to the knowledge produced, the following elements are used in this document:

- Visual elements such as conceptual images, mindmaps and others to condensate information and facilitate interpretation.
- Headers that guide the reader in the technical chapters.
- Comprehensible footnotes explaining concepts and ideas, providing notes or external links to non-peer reviewed websites or streaming videos.[v] References sections are almost exclusively dedicated to peer-reviewed publications.
- For a curious audience aiming for more complex explanations or ideas, a section named "glossary and notes" is included.
- Experimental chapters are independently presented and do not follow a specific sequence. This gives the audience the opportunity to freely decide its path.[vi]
- Lastly, the "PDF version" includes multimedia interactions to facilitate navigation throughout the document. Ultimately, an "audio version" in the form of episodes should be released in freely access platforms.[vii]

Hopefully, these changes will provide a concise idea of the work developed throughout my Ph.D. to a broader audience in an engaging way and reverberate within the community.

---

[i] People born from 1997-2012 (aka "Gen Zers) appear to have an average Attention Span of 8 seconds (source: Forbes "5 differences between Marketing to Millenials vs. Gen Z")

[ii] For the non-specialized audience brief and easier summaries are provided instead.

[iii] Resembling the popularly denominated as "101" or "for dummies" books.

[iv] Accessible and comprehensible to a larger group of individuals – independent of gender, race, geolocation…

[v] References sections are exclusively dedicated to peer-reviewed publications.

[vi] A tentative sequence is suggested elsewhere.

[vii] ~5 billion have access to the internet (source: https://www.statista.com/statistics/617136/digital-population-worldwide/ - date April 2022)

Objectives concerning scientific research and achievements

Curiosity boosts the learning process, which can be explained as it increases our attentiveness, will to explore, and happiness – a state made famous by Archimedes interjection "Eureka!".[viii] This intimate connection between curiosity, eagerness to access and understand information, along with novel materials and technologies, spark opportunities to dig deep into previously unreachable realms. Operating at the same scale as molecular and cellular processes whilst maintaining quantum-derived properties, nanotechnology shines a light onto many unexplored concepts. Throughout this thesis the development and/or usage of nanoparticles will be the central link to the sensing mechanisms developed herein.

Nowadays, nanoparticles and sensors are probably two of the most appealing research areas due to their immense potential in many areas – from the environment, to tracking of supply chains conditions, fundamental studies, and many others. Due to the versatility provided by the combination of both research fields, instead of concentrating on a specific topic, I opted to focus on developing (Bio)sensors towards a wellness-based personalized medicine – namely P4 medicine.

This dissertation is then sub-divided in seven main sections:

- The Preface briefly wanders about the concept of information and how it seems to be developing into gathering and storing it in a reliable way, culminating in the process of comprehending it to enable informed decisions.
- The Contextualization section is the broadest section when it comes to diversity of concepts. In a generic way, intentions are to sew a continuous line through the fabric of history, motivations, technologies, and concepts impacting the work (directly or indirectly). Hopefully, this will feed the reader noteworthy information while cementing the fundamental concepts underlying the journey of developing a nanoparticle-based (bio)sensor.
- As demonstrated during the recent Covid-19 pandemic, accessibility to trustable diagnostic tools based on nucleic acids and immediacy to obtain results is still missing. Extremely-sensitive and portable diagnostic methods that avoid the need for PCR-based process are demanded. A potential alternative to this end, can be the usage of metallic nanoparticles as antennas that significantly boost the brightness of fluorophore molecules. Research on this topic is described in the first section of the Results.
- Aging of the population is an undeniable reality in modern societies. Being an age-related disease, cancer tends to become more frequent, leaving a heavy trail of death and/or disability. To tackle this burden and aiming to increase treatment efficiency and survivability, hyperthermia treatments are reaching the hospitals as co-adjuvant treatment of chemo- and radiotherapy. However, so far, poor understanding or control over the temperature can have nefarious side-effects and ultimately result in death. Intuitively, a nanothermometer enabling to evaluate and assess the process can be a pivotal tool to understand hyperthermia at a fundamental level or to dynamically adjust the treatment. Research on this topic is described in the second section of the Results.

[viii] (Author comment): as an experimentalist who strongly appreciates to try some occasionally serendipity my self-expression to these moments is "What about that?!!.." *Include fingerslap

- Many metabolic processes involve a family of enzymes named proteases, which are essential to ensure homeostasis. These proteases have some peculiarities such as the need for post-translational activation and further strict regulation. As maintaining this delicate equilibrium can differentiate between health or disease, the monitoring of proteolytic activity is a reliable postulate to assess metabolic processes such as tissue recovery, metastatic behavior, and many others. Research on this topic is described in the third section of the Results.
- A Conclusion and Future Perspectives section.
- An Epilogue, with a personal and expanded view of the author onto the potential unwinding's of the topic.

The (bio)sensors developed and presented herein are still far from being used in real-life situations. Nevertheless, in my mind I cogitated the following scenario (Figure below):[ix] a person arrives at the hospital in needs of a diagnostic. Unfortunately, news are not good and a metallic nanoparticle-fluorophore sensor indicates that cancer seems to be the result. Then, to comprehend and validate the efficiency of a prescribed hyperthermia treatment process, a nanothermometer is used as a sensor. Lastly, after treatment, a follow-up metabolic sensor is used to assess treatment effectiveness, spreading or recurrency. Hopefully, by the end of the day, in this hypothetic scenario, "patient-doe" swiftly gets back home cancer-free, without substantial side effects while maintaining its quality of life, to live happily ever after…

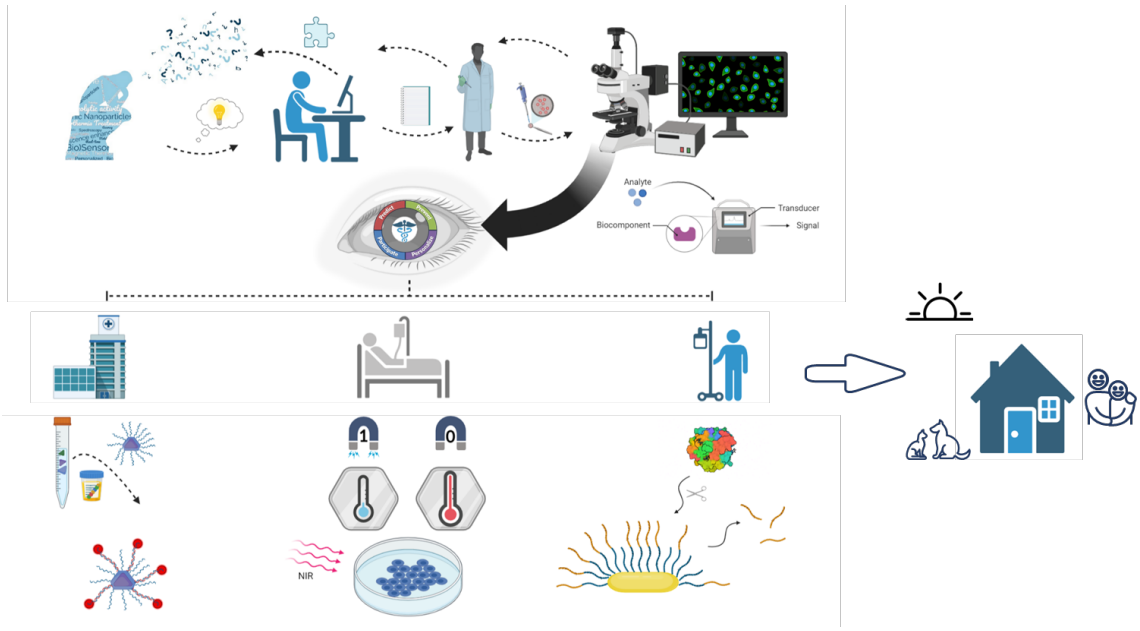

[ix] Created using Biorender

Conceptualization – The trails of information: How do we know what we know?

Scrolling through history, we realize that the human perception of the world correlates with the contemporary knowledge. Often, this knowledge is an extension of the lessons learnt from past events, social context, and the experience of a revolution—either intellectual or technological. These revolutions sporadically trigger an acute impact in our lifestyle, leading to shifts in our paradigms. Since the 1st industrial revolution, these changes have been so abrupt that within the timeframe of one generation we lose track of the old ways and our ancestors' stories become almost unimaginable. If this trend was already an obvious reality, unforeseen global events such as the current pandemic from Covid-19 and a modern version of the "cold war" pushed us even further. Consequently, and concomitantly with dawn of 4.0 industries the development of technologies related to communication and sensors are skyrocketing.

Logically, information underlies many aspects of our quotidian and plays a central role in modern society and its progression. Yet, if we take a step back and ask ourselves "What is information?" or "What does it mean?", most of us will struggle to find a trivial and appropriate answer to these questions. However, when asked "Is information important?", the intuitive answer seems to be "Yes!". Then, why is information so difficult to define while seemingly being so important?

From the universe around us down to our genetic library (genome) and history books, information exists in many forms, and can be obtained in many ways. In fact, all living beings and viruses possess some kind of sensors that helps them to assure prevalence. In our case, five senses, body position and balance sensors are crucial for us to analyze the surrounding environment and adapt to it. For millennia, we relied solely on these ancestral tools to thrive while basing our actions on instinctive reactions. The amazingness of these inbuilt capabilities is undeniable. However, a swift change in Human evolution started when we expanded beyond our biological intricacies, taming fire, using tools, domesticating dogs, or "inventing" agriculture. As a species, these adaptations twisted the course of our history, marking the transition from nomadism to settle as societies.

Even though it may feel far-fetched, our ability to gather and analyze information, endowed us with the skill to adapt and overcome many sorts of challenges. Nevertheless, understanding and adaptation were just the first steps—after all, many animals also possess these capabilities… Thus, to assure our progress the next step was to learn how to communicate and/or store that information, ensuring it can reach our peers and further generations. Once suggested as *homo stupidus,*[x] *neandertals living in the Iberian Peninsula (Spain) ~115000 years ago were the first to solve this charade by craving petroglyphs* and/or pictographs using marine shells.[1] Either intended to be depicted as "art" or a way to communicate, it is indeed fascinating that our ancestors almost all around the globe swiftly felt the need to develop tools to engrave their traditions/behaviors while making their history prevail.

For millennia, humanity basis of communication was based on primitive languages and unsophisticated drawings. Intuitively, languages evolved as "social Darwinistic" (Herbert

[x] So Long, 'Homo Stupidus.' Hello, Intelligent, Compassionate Neanderthals from Forbes

Spencer's influence)[xi] tools to provide better and more reliable ways to communicate and express complex ideas. However, and despite the amazingness of our brains, human memory is critically flawed.[xii] In our brains storage and retrieval of information is often a simultaneous process and therefore one can critically influence the other. Thus, relying merely on "mouth to mouth" communication was untrustworthy. Invented independently at least four times throughout human history,[xiii] full writing-systems are the ultimate tool to fairly dissociate the processes of storage from retrieval of information. Henceforward, information could be stored in a perpetual and immutable fashion.

One of the oldest manuscripts (~2500 years old) containing valuable insights that are still relevant in modern society is the "Art of War"[xiv] from Sun-Tzu. Interestingly, it is worth to note that the author emphasizes the importance of collecting good and reliable information, and therefore stressing the central role of "spies". Far from those military teachings, a similar thought process can be applied in other contexts of our daily lives such as biology and medicine.

Thereby, as a product of human evolution and through exploitation of modern tools like Information Technology (IT), in this thesis I will focus on the war against other types of enemies such as diseases by means of developing "white hat" spies, for temperature, genetic and metabolic processes, denominated as (Bio)sensors.

[xi] evolution of species and how behavior of the individual organism adapts through interaction with the environment; Herbert Spencer From Britannica
[xii] 'Brain Bugs': Cognitive Flaws That 'Shape Our Lives' from NPR
[xiii] Where did writing begin? From British Library
[xiv] Sun Tzu | The Art of War From Einzelgänger

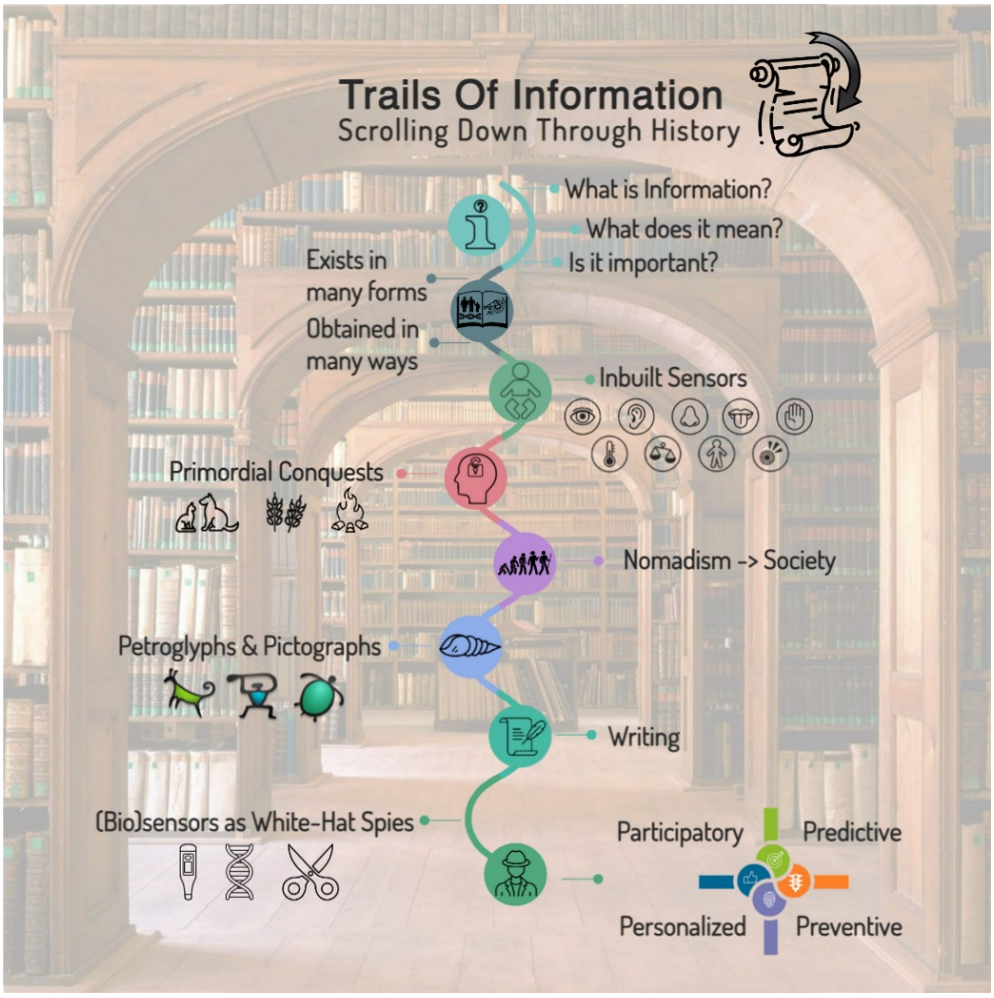

(1) L, H. D.; E, A. D.; Valentín, V.; Josefina, Z.; João, Z. Symbolic Use of Marine Shells and Mineral Pigments by Iberian Neandertals 115,000 Years Ago. *Sci Adv* **2022**, *4* (2), eaar5255. https://doi.org/10.1126/sciadv.aar5255.

Contextualization – Understanding the hermeneutic cycle of healthcare

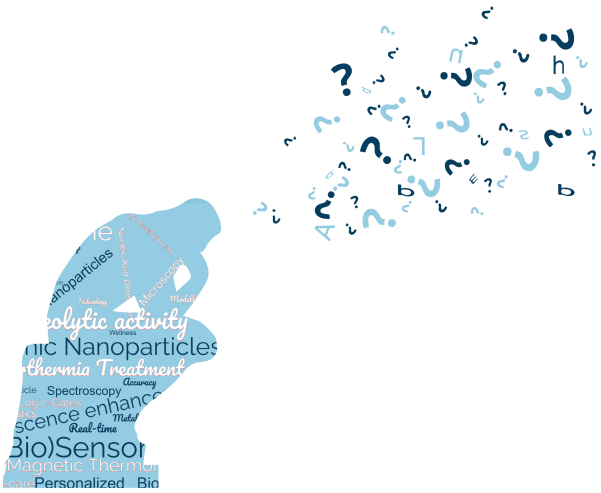

The subliminal reveries of history.

Biologic evolution – particularly in large animals – is a slow and dynamic process. Thus, precisely pinpointing a time and place for the origin of modern humans (*Homo sapiens*) [xv] is almost a guessing game. Nonetheless, predominantly characterized by its large and rounded braincase to accommodate our brains, narrow pelvis[xvi] and other characteristics, it seems consensual that we originated in Africa hundreds of thousands of years ago by compilation of genes of species living nearby. Beyond hunting and excavating fossils, digging into our genes can be more informative in understanding charts of migrations, movements and what guided and shaped the evolution of our ancestors'. [1,2xvii]

Originally described by Richard Dawkins, the concept of "Meme" is an analogue to "genes" in the context of memory.[xviii] Exactly, like genes, and demonstrated by the concept itself, memes tend to effortlessly spread across brains and can be perceived as the building block of cultural evolution.[3] To give an example, in hindsight, to me there are two "Memes" that accurately evoke a significant part of a dissertation:

- Rodin's statue "The Thinker", as it depicts the iterative process of back-and-forth cycle of introspections, daydreaming, questioning, reasoning...
- Newton's famous quote "If I have seen further it is by standing on the shoulders of giants.". Inherent to this message is the recognition that our knowledge is boosted by the intellectual progress previously achieved.

Intuitively and intertwined with the idea presented on the "Chapter 0 - trails of information", this implies that "dissertations" are inserted within a societal and historical framework, which crucially skews the outcome. To avoid further *ad nauseum* argumentation or mazy explanations, alternative strategies or concepts that were not explored are cited here but

[xv] From the Latin "wise man".
[xvi] Consequence of millions of years of walking standing.
[xvii] An Evolutionary Timeline of *Homo sapiens* From Smithsonian Magazine (2021)
[xviii] Author's note: Attributed to W. Churchill "history is written by the victors" but "memes" as sayings, language itself and even prejudice can be a persistent/resilient stamp of historical facts.

often simplified, cited, or skipped altogether. Hence, in this section, broad contextualization of our society and takes on the underlying motivations, technological developments and concepts inherent to the work developed within the framework of this thesis are discussed, outlining the relevance of nanoparticle-based (bio)sensors as promising tools for P4 Medicine.

Describing the World's history since the emergence of farming until today, John J. Finnigan jotted "…for the first twelve thousand years nothing happened and then, in the last 200 years everything happened".[4] Even though his sentence feels simplistic, he strikes the argument that "A peasant in China in 1000 BC was just as well off as a peasant in Europe in 1000 AD". This advocates that despite the remarkable human achievements, such as the Roman Aqueducts, the Egyptian pyramids, intercontinental sailing and globalized trading routes, amusing pieces of art and cities, still, for centuries the life conditions of the vast majority of the population were roughly stagnant. This was mostly a consequence of lacking a proper societal and philosophic structure to provide a foundation to a striving technological-based civilization. A simple way to grasp this fact is by exploring the influence of key technological developments in the growth of human population over the centuries. Thus, in Contextualization - Figure 1, the estimate of the human population over time from the "Worldometers database" [xix] is combined with the marking of several keystone (selected by the author) inventions or the arising of concepts and technologies.[xx] Here, I section this in three phases, with the 1st being the previously mentioned "stagnant phase" that lasted for Millenia until the beginning of the XVIIth century. Then, the development and implementation of the Scientific Method marks the beginning of the 2nd phase. This phase loosely resembles the "lag phase" of bacterial growth, and despite bluntly observed this timeframe provided a new framework of thinking, reasoning, experimenting, and documenting conclusions, leading to ground break discoveries and inventions. For this reason, this timeframe is denominated as "Proto-technologic" or "Proto-industrial" as it provides the foundation to the "industrial revolution". This phase marks the dawn of a new era of humanity's fate, by means of industrial activity, food production, urbanization, and countless others, leading to a swift blooming of machinery and consequent digitalization of society. Observing Contextualization - Figure 1 the landmarking technological improvements are extremely condensed in this timeframe.[xxi] This unprecedented era and exponential growth have been constantly fueling paradigm changes that critically deflect Humankind's path.

[xix] https://www.worldometers.info/ (2022)

[xx] "Technology" refers to the application of scientific knowledge to the practical aims of human life. From Britannica (2022)

[xxi] Examples of landmarks selected by the author

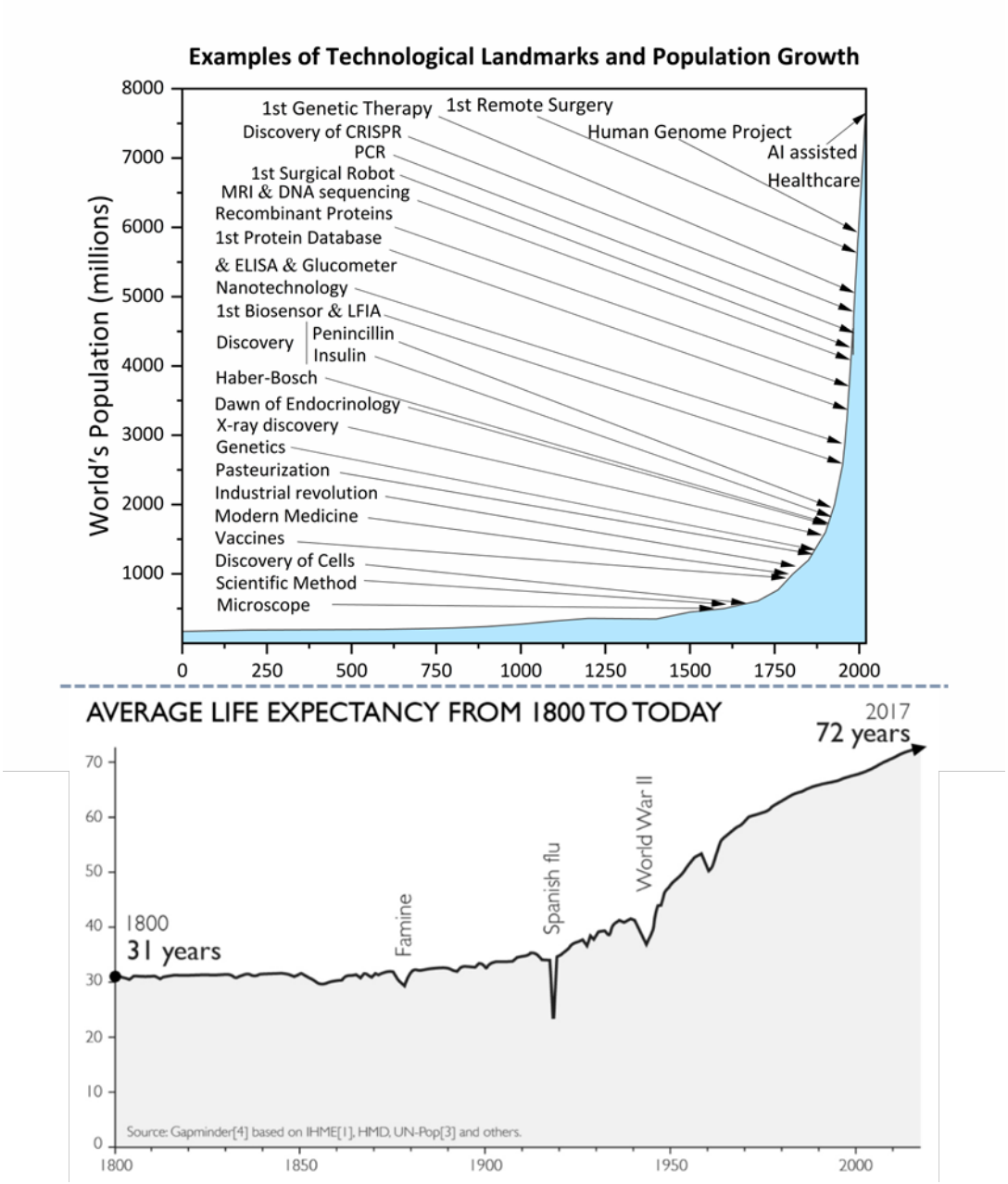

*Contextualization - Figure 1 - **The unfolding of human progression.** A) growth of the world's population over the centuries, pin-pointing some selected examples of historical major events. B) average human's life expectancy from 1800 to 2017*[xxii]

Nevertheless, it is important to note that a single correlation between technological achievements and population growth can be misleading and result in incomplete interpretations. Thus, the evolution of life expectancy over the last centuries (Contextualization - Figure 1) is also assessed, as a complementary metric. Analyzing the data from both graphs in Contextualization - Figure 1, for the period from 1800 to ~1950, it is notable that both profiles are out of phase. During this period, the population went from 1 billion to over 2.5billion, while the life expectancy remained essentially unchanged. However, after 1950, a fast (exponential) increase in the life expectancy and a correlation with the population growth is observed. This

[xxii] Life Expectancy from Gapminder

can be explained by the sudden change in human collective awareness and the motivations underlying our technological progression from the 1st to the 2nd half of the XXth century. Until approximately ~1950 (give it or take) human history was marked by continuous occurrence of conflicts and by the "struggle for dominance", which is emphasized by two consecutive World Wars and diverse colonial disputes, as countries were fighting to impose their own sovereignty. These pushed governments and the public to a war-oriented mindset that l focused on developing military-related arsenals - guns, tanks, airplanes, battleships and even bombs like the ones that destroyed Hiroshima and Nagasaki.

Those devastating events evidenced the grievous side that technological advances can have and pinpointed the moment at which humanity gained the ability to jeopardize itself.[xxiii] The silver lining lesson was that direct conflicts between super powerful countries were no longer a viable option, thus, opening an avenue for new mindsets to arise. Therefore, the 2nd half of the century was marked by the swift appearance of peaceful collaborative projects as the "European Union" or skirmishless disputes like the "space race".[5xxiv] The latter campaign ignited major technological leaps, ultimately propelling us far beyond the edge of our planet and the limits of our imagination.

Where to look next?

The influence of the cosmos in life is undeniable. An intriguing example is given by David Eagleman in his book "Livewired" where he speculates about "why do we dream?". Briefly, Eagleman reasons that, because of our brain plasticity, dreaming is an evolutionary tool to cope with the night periods and prevent space from our visual cortex from being conquered by the other senses while not being used (as in blind people). Furthermore, for several reasons, many animals evolved to be nocturnal. Besides being a source of fewer photons, and similarly to us, many of them found in the twinkling night sky a reliable navigation tool.[xxv] Humans were "gifted" with the largest prefrontal cortex in the animal kingdom, a structure that enables us to orchestrate complex thoughts and actions. However, we are intrinsically constrained by our sensors and limited to our "scale". This bounder our perception to a thin part of reality and confines our imagination. Yet again, providing us with a variety of events from marvellous aurora borealis, days suddenly becoming night due to eclipses or even catastrophic falls of asteroids, the universe, along with life itself, have been the biggest source of our inquiries. For aeons these were the catalyst of human wonders pushing the limits of our imagination and making us eager to progress and expand our knowledge. From praising to the celestial entities/gods to landing on the moon, we came a long way. In fact, "the pale blue dot"[xxvi] monologue illustrated by videos from the mission "Voyager 1" from Carl Sagan is one magnificent reminder of how we are a sort of "teensy weensy quarks" embedded in an everlasting universe.

[xxiii] Fermi Paradox - Where are all the Aliens? from Kurzgesagt (2015)
[xxiv] The Space Race from simple history
[xxv] Nocturnal Animals Use Stars for Orientation from Sci-News; From dung beetles to seals, these animals navigate by the stars from National Geographic
[xxvi] Carl Sagan's Pale Blue Dot (3min) from carlsagandotcom

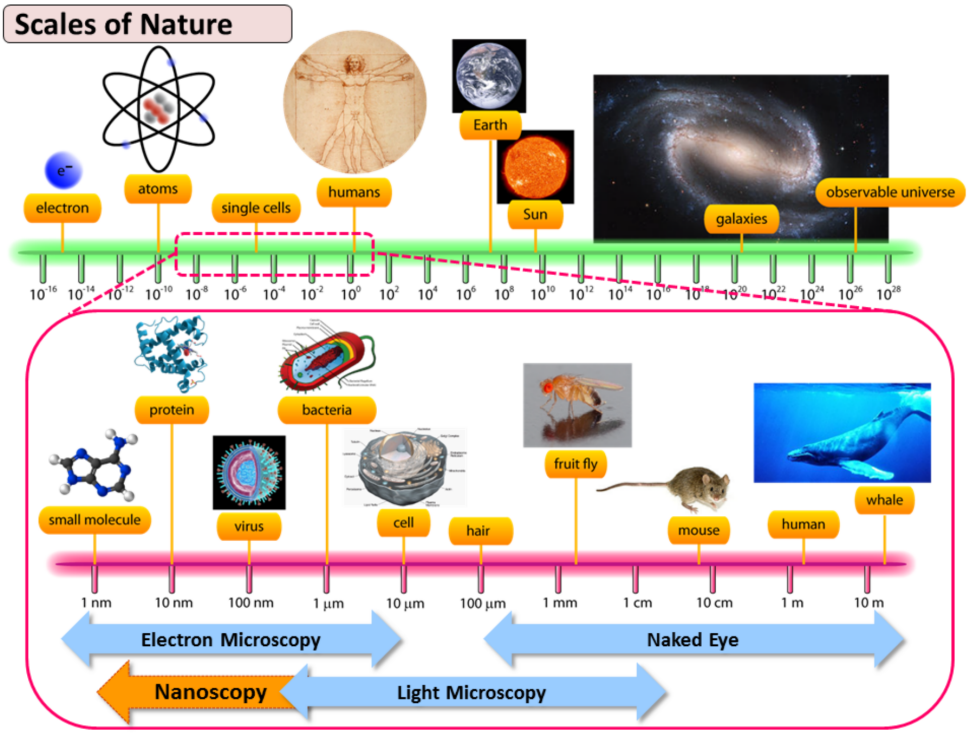

*Contextualization - Figure 2 - **The Scales of Nature**[xxvii] - from quarks to Laniakae [xxviii] and beyond…*

Down we go…

Intriguingly, the "giant leap for mankind" and many other events that bookmarked our modern history would not have been achieved without "small steps" in the direction of the "nano realm". Despite being on opposite sides of the scale (Contextualization - Figure 2), it is evident that both Astronomy and Nanotechnology share many technologies (e.g., lenses, detectors, etc). Less recalled but reminiscent in modern lifestyles and culture, the development of Integrated Circuits (ICs) and information technology (IT) induced a sharp shift in many paradigms of our society. Remarkably, the Apollo program (AP) was a major propeller of the ICs era, as it thrusted the technology to be small and powerful enough to help the Apollo Guidance Computer (AGC) that guided Mankind to the moon. In fact, it is estimated that by 1963, the Apollo program was responsible for the consumption of ~60% of the domestic production of this fresh and still unproven technology.[6] A subsequent boost and exponential growth of the ICs/chips industry, baptized as "Moore' law", was achieved by means of miniaturization and development of "top-down" nanofabrication strategies (detailed below). [xxix]

This bookmarked the dawn of a digital era, where information can immediately cross the globe through the internet, humongous amounts of data[xxx] can be tracked and analyzed, among other capabilities…. For this reason, the contribution of "top-down"-based nanotechnology is undeniable by its mere existence, extent, and reachability. However, this

[xxvii] Scales of Nature from Gould Research lab (Bates)
[xxviii] Laniakea: Our home supercluster from Nature video
[xxix] Transistors - The Invention That Changed The World From Real engineering (2016)
Inside The Worlds' Largest Semiconductor Factory from BBC click (2019)
The most powerful computers you've never heard of from Veritasium (2022)
[xxx] Your Mobile Phone vs. Apollo 11's Guidance Computer from RealClearScience (2019)

dissertation mostly explores concepts underlying "bottom-up" strategies, which will thus gather our major focus. Nevertheless, both strategies share similar principles and are entangled in many examples, thus, "top-down" strategies are not overlooked but rather exposed in softer fashion, when it becomes convenient/ relevant.

The enticing nanoworld

Materials based on micro-, and nanotechnology have been around for centuries,[xxxi] but without proper knowledge and understanding about their properties. In 1959, Richard Feynman, sparked the first light on the field during his talk "There's plenty of room at the bottom"[7] when he incited the investigation on the construction of atomic and molecular assemblies. Later denominated as "Nanotechnology",[xxxii] this new paradigm of designing and operating at nanoscopic scales would enable "strange phenomena" to occur in complex situations. As a teaser, Feynman stated physicists should build better microscopes and biologists should use math. As provocative as this may sound, by accepting this premise, questions that seemed farfetched - "what is the sequence of bases in the DNA?"; "how are proteins synthesized?"; and "how is the base order in the DNA connected to the order of the amino acids in the protein?" - are now trivial.

New features, analogous dimensions, deeper insights…

Before digging deep into the nano-realm a disclaimer is essential. Due to the complex and extensive nature of the topic, several nuances and over exposition will be avoided. Instead, attention will be given to concepts, technologies, and examples impactful to the modern medicine and the so-called P4 medicine ecosystem.

The following section aims to provide fundamental understanding on what guides the properties of nanomaterials; and aspects influencing synthesis.

Properties of nanomaterials:

The properties of materials in bulk are purely determined by the average of all forces affecting the atoms in their constitution. As things get smaller, there is a turning point where the specific behavior of individual atoms or molecules start to become significant. Because the behavior of individual atoms can be very different from the collective aggregates found in bulk materials, properties can also drastically change with size. For example, insulators like silicon become conductors, inert materials become catalysts (platinum) and many others…

Why does size matter?

Nanotechnology studies objects that comprise at least one dimension with 1-100 nm. As materials enter this scale, they break a size barrier below which the quantization of energy for the electrons existing in the solid becomes relevant.

[xxxi] Nanotechnology is ancient history from NanOpion (2012)
Iranians enjoyed nanotechnology 3000 years ago...? from Nanowerk (2007)
Nanotechnology in cosmetics - 2000 years ago...? from Nanowerk (2006)
[xxxii] Prefix "nano-" corresponds to (10^{-9}) meaning that a a nanometer is 1 billion times smaller than a meter

At glance, the first advantage of operating at extremely small scales is miniaturization. For instance, IBM recently announced their "2 nm chip" technology, which makes it possible to fit up to 50 billion transistors[xxxiii] on a chip with the size of a fingernail. This has direct consequences not only in the processing capacity but also in battery life, faster object detection, etc…[xxxiv]

As nanomaterials find themselves in a "No Man's Land" between atoms, small molecules, and their bulk counterparts, both size and quantum effects can predominantly influence their properties. Also, matching the scale of cellular and metabolic processes, opens a venue to many fundamental studies and applications that is yet to be explored.

Morphology[xxxv]

As materials shrink, surface atoms (%) become more representative. This increase in atom density at the surface gets even more pronounced for particles below 10 nm (Contextualization - Figure 3– left side).[8] As particles decrease in size, they become more susceptible to changes in their surroundings whilst atoms are prone to exposure to the environment. Therefore, size, structure, and shape have major implications in electronic conductivity, optical properties, chemical reactivity magnetic and mechanical properties.

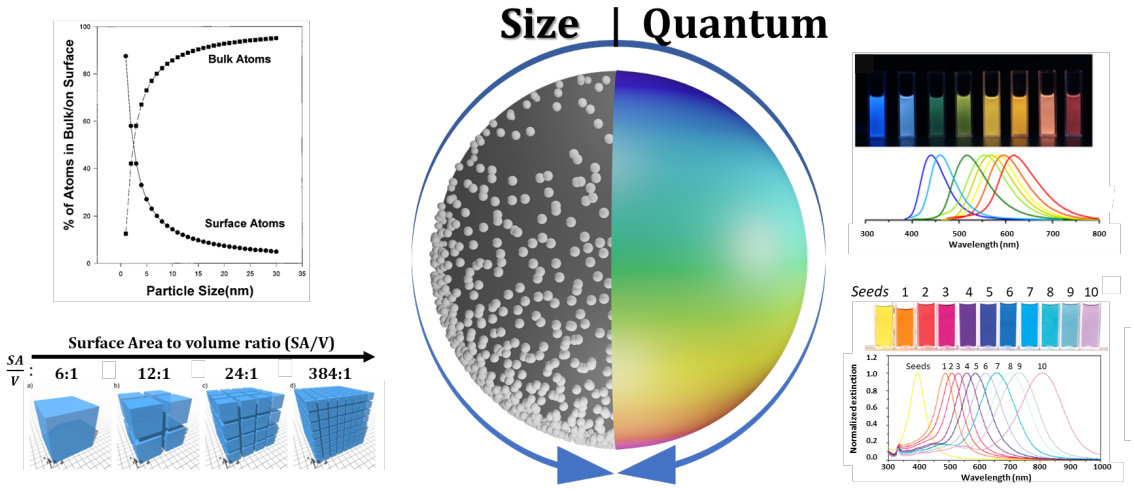

*Contextualization - Figure 3 – **Size Matters: the intertwining of morphology and quantum effects guiding nanomaterials properties**. (central) Illustration of "morphology" (left) and "quantum" (right) effects determining nanomaterials properties. (Top left): estimated surface to bulk ratios in solid metal particles vs size;*[8] *(Bottom left): Increments of surface area vs volume by decreasing the size of units (the total volume is normalized to 1 cubic unit);*[9] *(Top Right) Multicolor fluorescence emission from Carbon Dots (Cdots).*[10] *(Bottom right) Samples of silver triangular nanoplates with different sizes and respective Uv-vis spectra.*[11]

- **Size**: Accessibility, surface energy and surface-to-volume ratio are inversely proportional to size. Especially relevant for particles below 10 nm, these features dramatically increase at the nanoscale, which often correlates with higher efficiency and better performance. Catalytic materials such as "Nanozymes" are an intuitive and noteworthy example of a forefront technology in many bioapplications.[12]

[xxxiii] Transistors - The Invention That Changed The World from Real Engineering
[xxxiv] IBM Unveils World's First 2 Nanometer Chip Technology, Opening a New Frontier for Semiconductors from IBM newsroom (2021).
[xxxv] Disambiguation: morphology relates to size, shape, and structure of the materials.

- **Structure**: Reducing dimensions also impacts the atomic arrangement within the crystalline structure. This assertive correlation even allows to estimate nanocrystals' (grain) size based on its crystallinity.[13][xxxvi] For example, these structural configurations are known and exploited to render new or to alter magnetic properties of widely used nanomaterials (detailed later).[14–16]
- **Shape**: Due to their high surface energy and poor crystallinity, extremely small particles (< 10 nm) tend to acquire isotropic forms such as spheres. Yet, as size increases, more complex and anisotropic shapes – such as the ones explored throughout this thesis[xxxvii] – are possible. Since anisotropy implies the break of symmetry at least along one axis, properties of materials can be altered and enhanced.

Quantum Size effects

Expressions like "Quantum mechanics" or "Quantum physics" are of often perceived as a sort of "black box" that no one fully understands. This arises from the counterintuitive nature of many phenomena occurring from the nano- to the subatomic scale.[xxxviii,xxxix] Since these phenomena don't have a macroscopic and observable equivalent, it is difficult for our minds to fully understand them. However, in a simple way, the word quantum derives from the observation that some physical quantities only vary in discrete amounts and not in continuous fashion.[17]

The right side of Contextualization - Figure 3 represents the quantum aspects guiding the properties of nanomaterials. As the particle size decreases, the movement of free electrons is confined [xl] and the energy levels of the material become discrete originating a bandgap. Especially pronounced below 10 nm, the quantum effects start to dominate the behavior of matter, influencing its optical, electrical, and magnetic properties.[18–20] This "Quantum confinement" effect is evident in semiconductor Quantum Dots (QDs), as color emission is precisely controlled by their size. [xli] Carbon Quantum Dots (top) and Silver nanoprisms (bottom), which have optical properties precisely tuned either by doping or by controlling the size, respectively, constitute examples of these effects (Contextualization - Figure 3(right)).[10,11]

The holy grail of nanotechnology is to fully comprehend, predict and utterly manipulate the properties of nanomaterials. A list of miscellaneous videos is suggested in Appendix – Table 1 as examples of how nanotechnology is already influencing our daily lives and how it can pave the way for many future applications.

[xxxvi] As size ↓ the peaks measured get broader (←→), enabling to correlate them.
[xxxvii] Hexagonal nanoplatelets; Triangular nanoprisms; Nanorods;
[xxxviii] What Is Quantum Mechanics? Explained from "insane curiosity" (2022)
If You Don't Understand Quantum Physics, Try This! from "domain of science" (2019; intermediate)
[xxxix] Recommendation: From quantum mechanics to nanoparticles and their applications from Quantum Spinoff – includes instructions on "how to build and homemade spectrophotometer" (You're welcome and have fun!)
[xl] Quantum Confinement from Payne's video (2014)
[xli] Color by Size: Quantum Dots from SciToons (2018)

A "fourth" dimension: 0-, 1-, 2-, 3D

Properties of nanomaterials are intimately connected with size and morphology aspects such as shape. As the symmetry along at least one axis is "broken", isotropy is loss and dimensions of nanomaterials can scale above 100nm. For this reason, based on their three-dimensional size and morphology, nanomaterials are sorted into four categories, as shown in Contextualization - Figure 4.

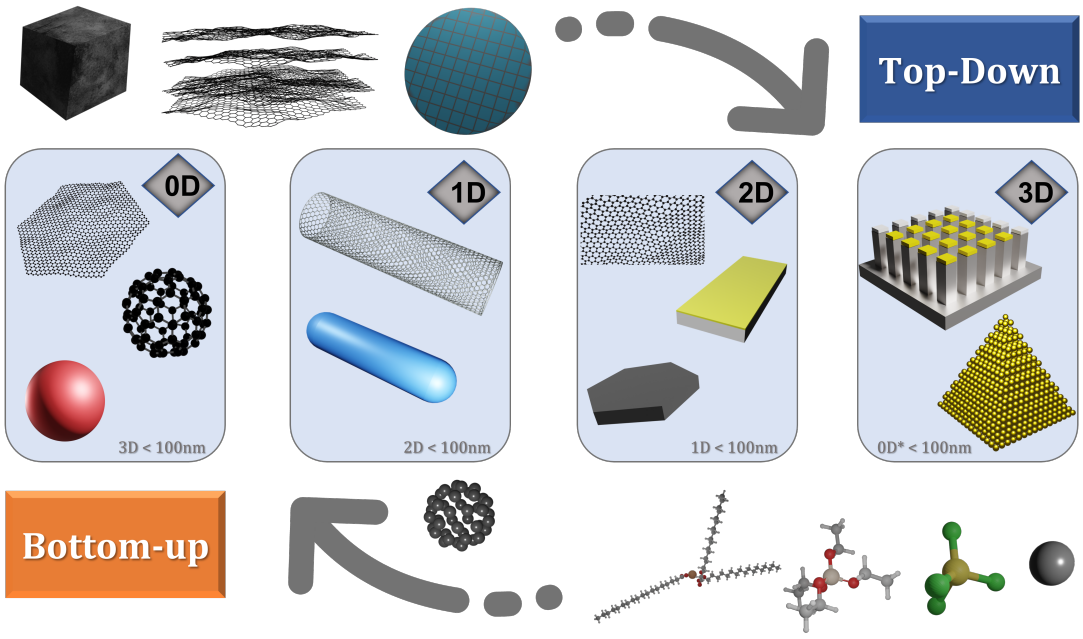

*Contextualization - Figure 4 – **Nanomaterials grouped according to their dimensions and examples of starting materials in top-down and bottom-up approaches**. List of examples: (**top-down**) Bulk object (i.e CuO), graphite sheet and silicon wafer. (**Bottom-up**): Atom, molecules ($HAuCl_4$, TEOS, iron (III) stearate) and a cluster of atoms. (**0D**) graphene quantum dot, fullerene, and gold nanosphere. (**1D**) Carbon nanotube and gold nanorod. (**2D**) iron selenide hexagonal nanoplatelet, graphene and gold thin film; (**3D**) Array of nanopillars partially covered with a gold layer; pyramid-shaped assembly of gold nanospheres. *Structure comprises elements/objects at the nanoscale. **Objects are not to scale**. All the illustrations were prepared and rendered using Blender v3.2.*

Carbonaceous and plasmonic nanomaterials are two of the common examples used to illustrate the influence of dimensions onto the properties of materials. For example, carbon materials with similar crystalline (graphite-like) structure have vastly distinct properties, as (0D) Graphene quantum dots are luminescent, while (1D) carbon nanotubes are extremely rigid[xlii] and lastly, (2D) graphene is used to make malleable and conductive surfaces. Intuitively, there is no "one size fits all" strategy to their nanofabrication, thus selecting the appropriate method is crucial.

Nanofabrication: coming down or going up?

Nowadays a wide variety of nanofabrication methodologies are available. Endowed with a vast range of tools and instruments, nanofabrication strategies can be adjusted precisely to fit the requirements of the desired product and application. Fundamentally, synthesis of nanomaterials can either be considered "Top-down"[xliii] or "Bottom-up"[xliv] based on the size of

[xlii] One of the stiffest materials known to man
[xliii] The size of the starting materials is above the nanoscale (> 100nm)
[xliv] "Top-down" are often referred as physical methods while "bottom-up" as chemical methods

the starting materials.[xlv] Briefly, as illustrated Contextualization - Figure 4, top-down approaches use techniques that rely on starting materials with sizes above the nanoscale (i.e., bulk and surfaces). while bottom-up approaches use atoms, molecules or small clusters as starting materials.

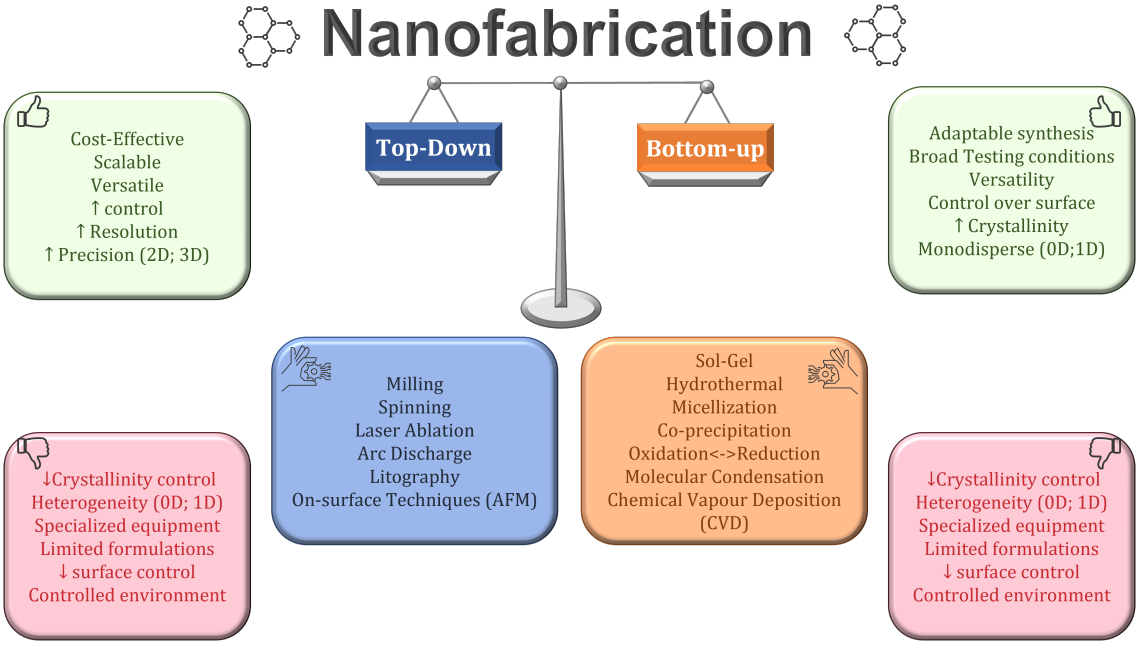

*Contextualization - Figure 5 – **Overview of the nanofabrication processes available**: Top-down vs Bottom-up approaches.*

Extensive coverage of nanofabrication processes would fall outside the scope of this dissertation, and information can be found elsewhere.[21–25] Instead, common techniques and underlying principles are portrayed, and general advantages and disadvantages are summarized in Contextualization - Figure 5.

A straightforward way to aggregate the general principles underpinning Top-down techniques is according to their underlying principles:

- Breaking-down the starting material - milling, ablation, arc discharge.
- Printing - i.e., spinning and sputtering.
- Photo- and electron beam lithography.

Briefly, “breaking” techniques rely on the usage of mechanical or electrical force to break the structure of materials into their nanosized counterparts. These techniques are the most cost-effective and scalable, however they have poor control over size and crystallinity, and formulations are limited to the starting material. Printing techniques, on the other hand, are automatable and allow precise production of thin films (i.e. solar cells). Nevertheless, these techniques are often restricted to the fabrication of 2D materials and formulations are limited. Lastly, lithography is the most versatile and precise top-down approach (with sub-atomic resolution). Nevertheless, and even though lithography is yet the most scalable and cost-

[xlv] Uses atoms, small molecules or cluster as starting materials.

effective methodology for precise production of complex technological nanoconstructions, it often relies on the usage of expensive machinery, trained personnel, and controlled environment. For these reasons, as rule of thumb, Top-down approaches are generally used to produce low-cost nanomaterials or 2- and 3D nanostructures that require high precision. Due to their easy[xlvi] implementation, automation and scalability, Top-down techniques are employed to fabricate most nanomaterials commercially available.

Bottom-up approaches are convenient way for testing different formulations and for the development of novel materials. This arises from fundamental self-assembly process occurring during nanoparticle (NPs) formation, which offers versatility to alter the internal structure of the particle and allow smaller sizes and a wide variety of aspect ratios/shapes. However, scalability issues remain the biggest challenge to overcome, hindering the widespread commercial applications. Nonetheless, this reality began to change as products, such as QLED displays and standard "antigen tests" for COVID-19, are already paving their way into our daily lives, alongside with many others.[xlvii]

Brick by Brick

Colloidal,[xlviii] chemical, and physical properties of nanoparticles are key aspects in the development of the sensors developed in the context of this dissertation. Herein, plasmonic (silver and gold) and chalcogenide[xlix] (iron selenide; Fe_3Se_4) nanoparticles were tested due to their exquisite and tunable optical and magnetic properties. All the nanoparticles were inorganic and prepared via solvothermal synthesis,[l] namely chemical reduction of metals and thermal decomposition. Thereby, the fundaments underlying such strategies is the primary focus in the following sections.

Thermal decomposition and chemical reduction are two of the most reliable bottom-up strategies to obtain monodisperse nanocrystals (NCs) with high reproducibility, reasonable tunability and versatility. Yet, achieving proper control over the nanoparticle-formation process is essential, especially considering that NCs preparation is controlled by an intimate relationship between thermodynamics and/or kinetics.[li] This implies that in thermodynamically controlled synthesis specific sizes or aspect ratios are not favored compared with others, while in kinetic controlled synthesis parameters involving particle growth are difficult to adjust.[26] Hence, comprehension of concepts inherent to the bottom-up strategies is essential to guarantee that high quality nanomaterials with the desired properties are attained by educated design strategies rather than burdensome trial-and-error. Interested readers can find extensive and detailed reviews describing the kinetics and thermodynamics of bottom-up NP formation are available in the literature.[27–31]

[xlvi] Note: Albeit some top-down strategies requiring highly trained personnel and expensive machinery, and require cleanrooms, in most of the cases the desired nanomaterials are still unattainable via bottom-up.
[xlvii] QDs market prospects (2021-2026) from marketsandmarkets
Global Gold Nanoparticles Market to Reach $7.9 Billion by 2026 from "Cision"
[xlviii] A colloid is a mixture in which a substance consisting of microscopically dispersed insoluble particles is suspended in another substance. In nanotechnology usually refers to nanoparticles stably dispersed in solution. Colloids from Tyler Dewitt
[xlix] Chalcogenide from wikipedia
[l] Building blocks are mixed in solution and exposed to growth conditions for a given time.
[li] Thermodynamics vs Kinetics from Khan Academy

Lamer and beyond – the foundations of nucleation and growth…

Preparation of nanomaterials is often a straightforward task, yet systematic control over dimensions and properties is still challenging in many cases as it demands precise management over the nanoparticle-formation process. Solvothermal synthesis is a convenient, versatile, and productive strategy with unparalleled ability to control size and shape. When aiming to obtain monodisperse nanoparticles, a common motto within solvothermal synthesis is that "all the particles should have a similar story". Despite not 100% accurate per se, the idea underlying this motto is that, in an ideal scenario, all the phases comprised in nanoparticles preparation are well-defined and occur in distinct moments. However, control over these phases can be challenging, especially in cases in which the pool of adjustable variables, such as precursors, is limited. An ingenious way often used to evade this limitation is using cation or anion exchange procedures. The underlying principles of these are reviewed elsewhere. [32–34]

Precursors are the raw materials which are converted into monomers to provide the elemental building blocks to the NCs formation (Contextualization - Figure 6A). These monomers then further aggregate to form small clusters, which ideally turn into stable nuclei that can further grow into larger NCs. Primarily, described by Lamer,[35] the growth of NCs in solution via solvothermal synthesis is segmented in three or four distinct phases, depending on the occurrence of particle-mediated growth or not.

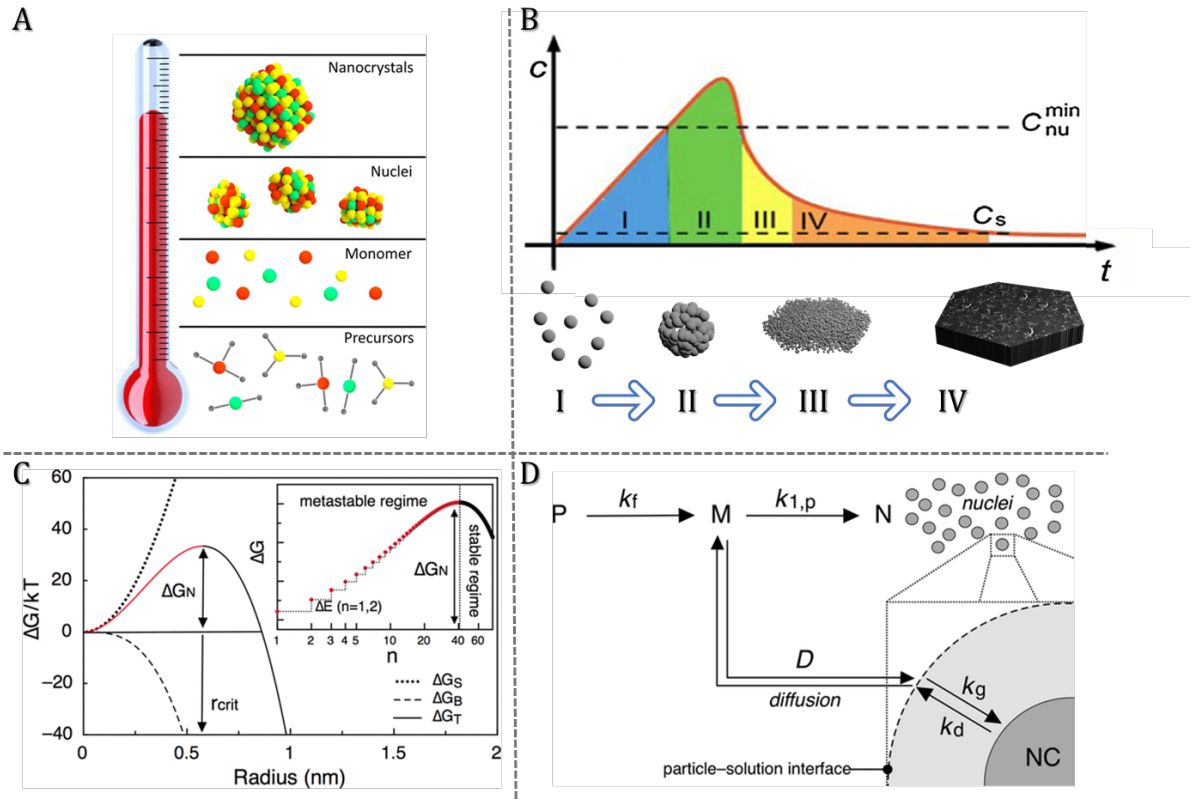

*Contextualization - Figure 6 – **Basic concepts inherent to bottom-up approaches.** A) Evolution from precursors to nanocrystals formation by thermal decomposition[lii].[27]; B) Lamer curve including a phase IV comprising particle mediated growth – adapted from [28]; (particles illustrated from I to IV were rendered using Blender 3.2); C) Free Gibbs*

[lii] Thermal decomposition is common strategy in bottom-up NP synthesis that the conversion from precursors to monomers is induced by an increase of temperature.

(ΔG) energy vs. critical radius (r_{crit}) of the nuclei. Inset: illustration of energy variation (ΔE) as atoms aggregate to form clusters. Transition from the metastable to stable regime [27]; D) Kinetics of particle formation process and diffusion processes at particle-solution interface; k_f - constant of monomer formation.[27]

As depicted in Contextualization - Figure 6B – I to IV, these phases are segmented and characterized by:

I Phase (I): precursors are gradually converted into free monomers that will later constitute the NCs. During this phase, small clusters of monomers form, which are nonetheless unstable and may redissolve.

II Nucleation (II): when the concentration of free monomer surpasses the "critical nucleation concentration" (C_{nu}^{min}), free monomers can aggregate and form stable nuclei. Nucleation happens while the concentration of free monomer is above C_{nu}^{min}.

III Growth (III): after nucleation, when the concentration of free monomer breaks down C_{nu}^{min}, the free monomer diffuses into the particles surface and aggregate leading to particle growth. In most cases the reaction terminates at this stage, lasting until the solubility concentration (C_S) is reached.

IV Particle-mediated growth (IV): in some cases, a new phase also arises to promote growth. This phase differs from phase III because growth is promoted by particle aggregation rather than free monomers.

Preparation of NCs is highly dependent on the thermodynamic and kinetic aspects guiding the process. During the nuclei formation, due to its miniscule sizes, the surface-to-volume ratio is high and consequently the surface energy is also high, and thereby, for very small nuclei, the Surface free energy (ΔG_S) is dominant. This indicates that the stability of clusters and small nuclei is compromised and reversible dissolution into free monomers is favored, hence the designation "metastable regime" (Contextualization - Figure 6C; red line). In opposition, as the nuclei gets larger by monomer aggregation (Contextualization - Figure 6C inset) the Bulk free energy (ΔG_B) becomes the predominant factor. After crossing the thermodynamic barrier (ΔG_N), particles reach a "critical radius" (r_{crit}), thus entering the "stable regime". Since a system always spontaneously evolves to lower its free energy, one can perceive r_{crit} as the boundary governing the fate of the nuclei. If $r_{nuclei} < r_{crit}$, dissolution of the particle is preferred (metastable regime), when $r > r_{crit}$ the growth of the NC is favored (stable regime).

As mentioned before, the formation of NCs is not exclusively dependent on thermodynamic aspects but it also depends on kinetics. Thereby, Contextualization - Figure 6D illustrates the kinetics involved during the formation of NCs. As observed, k_f corresponds to the "formation rate" at which the precursor P is converted into monomer M. Then, depending on the pathway (phase II or III), monomers can either be consumed to form new nuclei (N) at a "nuclei formation rate $k_{1,p}$", or supplemented by dissolution at the particle-solution interface at a "dissolution rate k_d". Despite metastable nuclei being prone to dissolution, it can also occur in larger particles through various mechanisms (explained later). For this reason, the NCs' growth is guided by the ratio between the "growth rate constant" (k_g) and the "dissolution rate constant" (k_d). This relationship is one of the key aspects to comprehend the possible growth mechanisms and how parameters such as washing, and particle stabilization affect, for example, their shelf life. Understanding the thermodynamics and kinetics involved during nuclei formation is a powerful tool to evaluate the behavior of the reaction and its outcomes which ultimately helps speeding-up the adaptation of reaction conditions/parameters to obtain the desired nanomaterial. An

interested reader can find meticulous information and deeper insights regarding these aspects elsewhere. [27,36,37]

Precursor paving the road towards monodispersity

Controlling the nucleation step (phase II) is crucial for monodispersity of the sample. In an ideal scenario, nucleation occurs rapidly in a single and homogenous step,[liii] hence the motto aforementioned and the designation of "burst nucleation". Indeed, this challenging aspect frequently undermines the quality of the NCs. To circumvent this limitation, alternative strategies were developed by introducing small alterations in the procedures. Injection-based techniques[liv] are an easy way to surpass this limitation, as they allow to pre-condition the reaction pot and swiftly initiate precursor to monomer conversion and optimize the nucleation step. However, its practicality and scalability are limited due to poor heat management and heterogeneous nucleation[lv,lvi], thus making it unsuitable for large scale production and, for this reason, these strategies are becoming outdated with exception of the preparation of metallic seeds.[27,38] Seed-mediated growth is yet another strategy, which relies on the separation of nucleation from the growth phase. Comparing with solvothermal synthesis, precise control over the growth and the shape of the materials is relative straightforward by adjusting the parameters of the reaction. However, isolation of the nucleation phase still involves a large amount of trial and error, and reproducibility can be affected due to underlying aspects – i.e., concentration and size of seeds.[26] Acknowledging the perks of the strategies mentioned, nonetheless, they were used to prepare the nanomaterials tested in this dissertation when convenient, due to their convenience and versatility. Furthermore, recognizing that some fundamental aspects are similar to all the strategies, solvothermal synthesis will be used as key example in the following section.

In general, the reaction pots contain limited number of components and comprise only precursors, ligands, and solvents. Aiming to perceive how reactants and products evolve throughout an optimized synthesis procedure, the progression of these aspects across the different phases is presented in Contextualization - Figure 7A – for a standard Lamer synthesis.[lvii] For detailed information about particle-mediated growth and the importance of "oriented attachment" read elsewhere.[28,39]

- Monomer formation (I): concentration of precursor (P) reaches its maximum and gradually decreases over time, as it is converted into free monomer. This increase in monomer concentration leads to supersaturation (S).[lviii] In homogeneous nucleation,

[liii] Nuclei are formed uniformly through a "parent phase". These processes are thermodynamically described by the total free energy ΔG_T -> sum of ΔG_S and ΔG_B

[liv] Simple Synthesis of Lead Halide Perovskite Quantum Dots from Sci-FunHub

[lv] Nucleation occurs at structural inhomogeneities (i.e., impurities, air bubbles…). In liquid, heterogeneous nucleation is favoured since stable nuclei are already present. This can easily be visualized by putting a frozen grape (for example) in a glass of cold water. Immediately, ice will be formed around the grape. Note: for this reason, materials previously used for synthesis need to be properly cleaned, as for example with aqua regia in the case of metallic NPs.

[lvi] Nucleation occurs at structural inhomogeneities (i.e., impurities, air bubbles…). In liquid, heterogeneous nucleation is favored since stable nuclei are already present. This can easily be visualized by putting a frozen grape (for example) in a glass of cold water. Immediately, ice will be formed around the grape. Note: for this reason, materials previously used for synthesis need to be properly cleaned, as for example with aqua regia in the case of metallic NPs.

[lvii] Assuming particle-mediated growth doesn't occur or is irrelevant

[lviii] Concentration of free monomer is above its solubility.

reaching the supersaturation is not sufficient to form stable nuclei. This occurs because of the high energetic barrier for the formation of a new solid when the surface area to volume ratio is very high.[40] Consequently, the nucleation rate (dN/dt) and NCs mean size are zero.

- Nucleation: When the S level crosses above the "critical nucleation concentration" (C_{nu}^{min}), free monomers aggregate forming nuclei, thus dN/dt quickly evolves from infinitesimal to a maximum value and the concentration of [NCs] in solution increases swiftly. During this phase, concentration of free monomer in solution depends on both monomer formation (↑conc) and aggregation onto nuclei surface (↓conc). During this stage, a small growth in particle size (<r>) is observed, yet the standard deviation (SD) raises steeply to a maximum. Ensuring controlled homogeneous nucleation, rather than heterogenous is pivotal to render monodisperse NCs. This is the most challenging and critical step dictating the fate of the NCs.
- Growth: the nucleation phase is considered finished after dN/dt reaches its peak and S falls below (C_{nu}^{min}). After this point, new nuclei are no longer formed, and the free monomer starts to aggregate and to promote particle growth. As dN/dt abruptly slows a small decrease of [NCs] is also observed due to dissolution of the metastable nuclei (early time ripening – ETR) consequently decreasing the SD. Throughout the rest of the growth phase, all the [P] still remaining in solution is converted to monomer which diffuses to the NCs. This step finishes when equilibrium is reached, and S goes to approximately zero.
- Equilibrium: At this stage, reaction is considered complete and NCs should be isolated and purified to avoid classical Oswald Ripening, a process during which smaller NCs dissolve and redeposit onto larger NCs which commonly induces polydispersity.

Other parameters, such as temperature and/or strength of the reductant molecule also influence the size, the SD and the final [NCs]. Under "acceptable" conditions, fast precursor to monomer conversion - either by high heating rate or using a strong reductant – will induce nucleation faster and for a narrower period, thus resulting in a higher [NCs], yet of small size and with lower SD. For example, this is the reason why tiny gold and silver nanoparticles denominated as "seeds" are usually synthesized using $NaBH_4$, instead of slower reductant agents as citric or ascorbic acid.

The combination of precursor and ligand chemistry is a key consideration in solvothermal synthesis, as it defines the monomer and its stability, and ultimately it determines the NCs characteristics. In general cases, precursor to monomer conversion is guided by the activation energies (E_A), which are critically influenced by the precursor and ligands. A comparison between different precursors with three increasing reactivities and the influence in the resulting NCs is shown in Contextualization - Figure 7B.

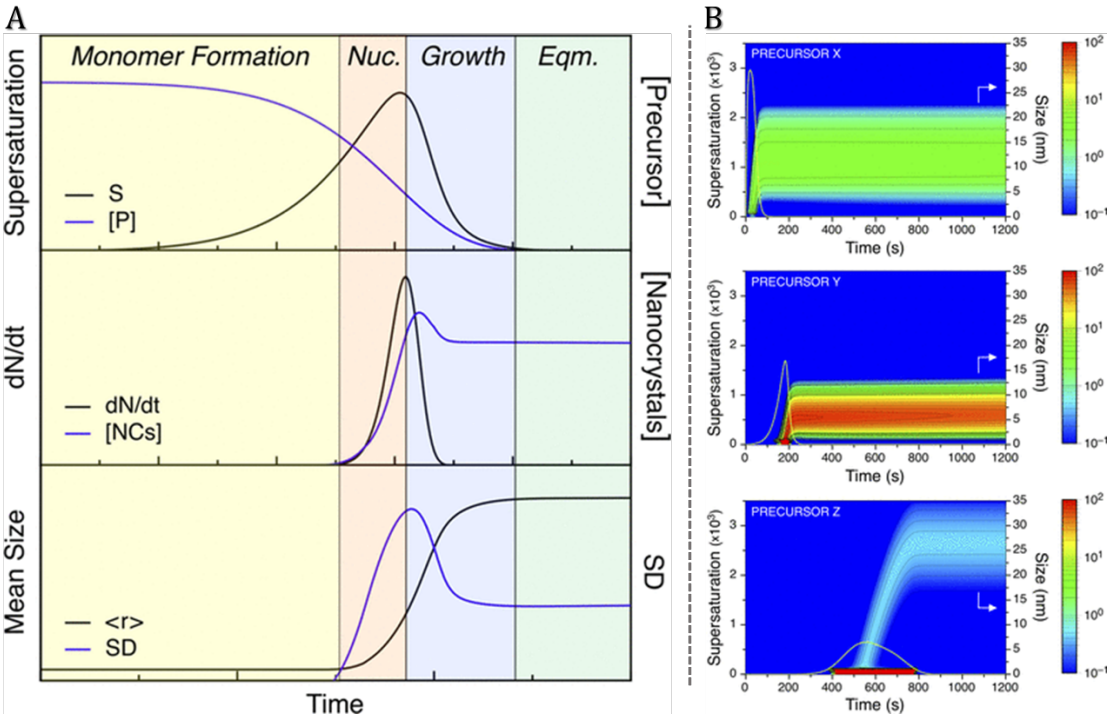

*Contextualization - Figure 7 – **Evolution of NCs synthesis**. A) Simulated evolution of the prominent reaction parameters during NCs synthesis.[27] B) Simulated evolution profiles of NCs employing different precursors - X, Y, Z correspond to High, Medium, and Low reactivity, respectively.[27]*

- Precursor X (↑ reactivity; E_A = 60 KJ mol^{-1}) – a rapid formation of monomer is observed by the rapid increase in the supersaturation at earlier times. This induces a quick nucleation and fast growth of the NCs, which results in a broad size distribution (12.4 ± 4.6 nm; SD ~ 37%) and reasonable yield (7 µM);
- Precursor Y (moderate reactivity; EA = 80 KJ mol^{-1}) – the formation of free monomer occurs gradually overtime, and nucleation occurs after approximately 180 seconds and over a short duration. Furthermore, this less reactive precursor also inhibits NCs growth during the nucleation phase, resulting in a good yield (~50 µM) and narrower size distribution (6.7 ± 1.9 nm; SD ~ 28%);
- Precursor Z (↓ reactivity; E_A = 110 KJ mol^{-1}) – formation of monomer is slow, and nucleation is only reached after ~400 seconds, continuing for a long period of time (~400s). This very slow rate of precursor dissociation, and consequent monomer formation, prevents the nascent nuclei from growing. This implies that only small clusters (1-2nm) exist, which are constantly dissolving and reforming due to nucleation. Eventually, supersaturation reaches a point that larger clusters have consumed a significant amount of free monomer and C_{nu}^{min} cannot be reached anymore, thus, nucleation stops. Then, these large clusters consume the free monomer still available. The resulting NCs have a medium size distribution (26.5 ± 5.5 nm; ~21%) but a very poor yield (< 1µM).

Assuming the element provided by the "precursor" is identical, the composition of the NC is independent from reactivity. However, it is important to note that in some specific cases, such as iron oxide (Fe_3O_4) the oxidation states are also important aspects to be considered. For instance, this can be solved by adjusting the ligands or the solvent itself.[41–43] Within a precursor, if applicable, the ligand is the coordination molecule which is responsible for stabilizing the

element composing the NCs structure.[43] The strength of the coordination and stability of the complex (element-ligand) is correlated with the E_A, meaning that if the coordination is weak, then the E_A is low, and vice-versa.[31] In case of interactions between metals and ligands, usually the strength of the interaction follows the "Hard Soft Acid Basis" (HSAB) principle.[44][lix]

In Focus – fundamental growth mechanisms

Stabilization is yet another crucial aspect guiding the fate of NCs. The primary role of a stabilizer is to control growth and confer colloidal stability to the NCs by regulating the aggregation behaviour of atoms, clusters, or particles. During nucleation, the stabilizing molecules adsorb onto the surface of the freshly formed nuclei, providing them stability via repulsive forces (electrostatic stabilization, i.e., citric acid) or steric stabilization (i.e., polymers such as polyethylene glycol). [31] Depending on the strength of this coordination, the surface energy of the NCs changes, which influences the critical radius (r_{crit}). If the coordination complex is strong, then the surface energy decreases and r_{crit} also decreases, and vice-versa.[31] However, decreasing the surface energy also diminishes reactivity, which potentially undermines the growth and leads to polydisperse NCs or very low yields (known as Finke-Watzky and exemplified as Precursor Z), which implies a crucial role of surface energy in determining the fate of NCs. Furthermore, it is important to note that strongly adsorbed stabilizers can be persistently attached to the nanoparticles, rendering the surface unavailable or non-reactive, and undermining further applications, such as catalysis, or other functionalization by making the surface unavailable or by rendering it a non-reactive. After nucleation, and as particles grow, their crystalline structure[lx] starts to be defined, impacting both properties and stability, as consequence of different crystalline facets of the material having distinct surface energies hence directional growth can be promoted (illustrated later). Those mechanisms implicitly have major influence in the mono- or polydispersity by promoting the convergence of particles to the same size (focusing) or the divergence of particle size (defocusing).[45] These mechanisms can be segmented as following - Contextualization - Figure 8

- Ostwald ripening – during the nucleation, the nuclei formed can have different sizes. As stability is intimately related with size, especially relevant for long times, smaller particles tend to redissolve known, consequently refueling the growth of larger particles. In opposition, digestive ripening occurs when larger seeds dissolve and feed the growth of smaller particles. Depending on the conditions and/or situation both phenomena can contribute either to the focusing[lxi] or defocusing of the sample, contributing to mono- or polydispersity.
- "Growth by diffusion" – smaller nanoparticles have higher surface energy, smaller radius and ligand coverage, which results in higher growth rate when compared to larger particles.[46]
- Finke-Watzky – like example from "precursor Z", there's no temporal distinction between the nucleation and growth phases. The slow continuation phase can be represented as conversion monomers (M) into nuclei (N), while the autocatalytic surface

[lix] Hard Soft Acid Base Theory from Professor Adams

[lx] Note that not all the particles are crystalline, thus materials can also be amorphous (non-crystalline)

[lxi] In general, focusing means that a sample is heterogeneous and overtime monodispersity is promoted, in opposition to defocusing. For instance, Oswald ripening leads to the dissolution of smaller particles. If the monomers favor controlled growth of the bigger particles the sample the size dispersity decreases, hence the sample was focused. If growth is uncontrolled and size dispersity increases, then it promoted defocusing of the sample.

growth is the aggregation of free monomer into the nuclei but without diffusion control.[30]

This phenomenon contributes for size defocusing.[47]

- Intraparticle ripening – changes in the particle over time are induced by the discrepancy on the surface energy between different facets.[30]
- Coalescence – growth is promoted by attachment of particles within each other's vicinity. This phenomenon is non-organized, meaning that crystallographic planes are not aligned during the process and often leads to polydispersity or aggregation. When growth is promoted by coherent attachment, the process is named "Oriented attachment" which, intuitively, often promotes anisotropy.[28]

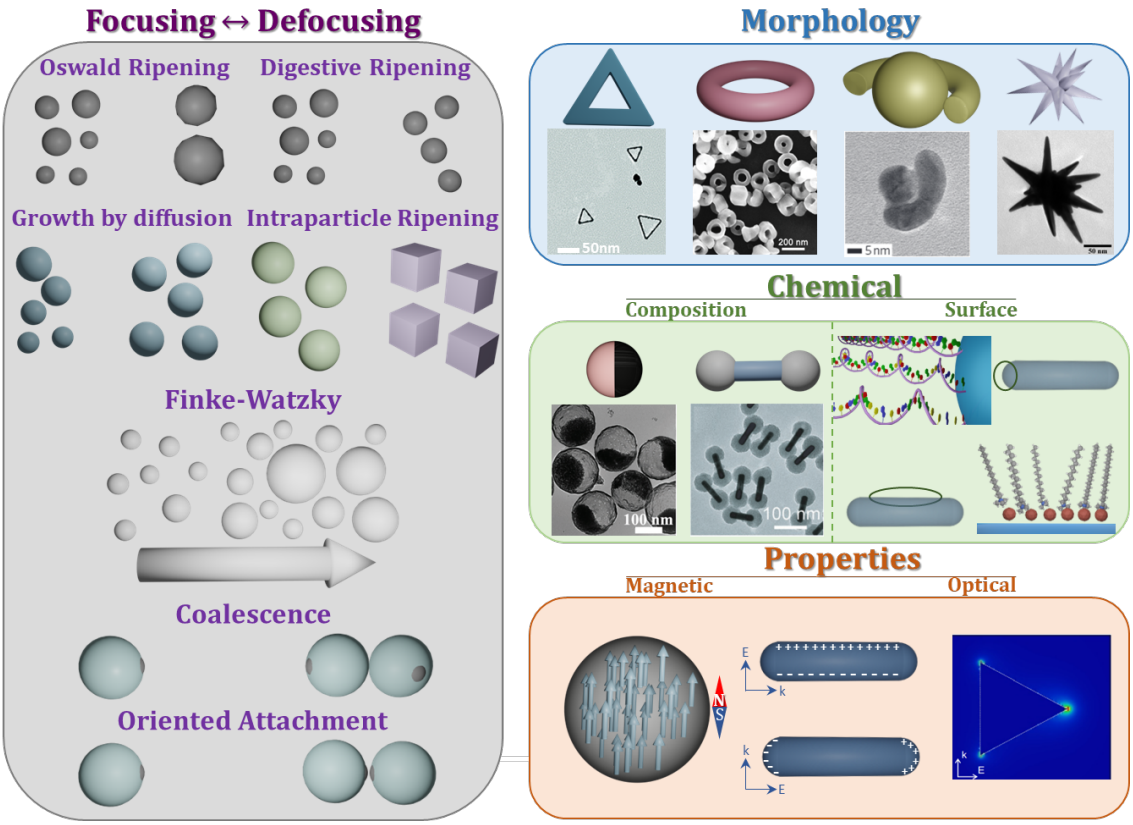

Contextualization - Figure 8 – (Left panel) ***Growth mechanisms influencing Focusing or Defocusing of size dispersion****. (Right Panels)* ***Categories of anisotropy****. Morphology: Gold Hollow nanotriangles[48]; Iron Oxide Nanorings[49]; Gold "nanobridged nanogap particles"[50]; Gold Nanostars[51]; Chemical: Composition Ying-yang "oleic acid–NaYF4:Yb,Er@hollow porous SiO_2 nanoparticles"[52]; Gold(nanorod)-SiO_2(spheres) hybrid nanoparticle[53]; Chemical: Surface – Gold nanorod with tip-specific functionalization comprising ssDNA molecules at the tips and CTAB molecules at the sides[54]; Properties: Transversal and longitudinal Localized Surface Plasmon Resonance (LSPR) of a metallic nanorod; Map of the Field enhancement of a triangular nanoprism; Orientation of the magnetic field within a spherical nanoparticle.*

Unfortunately, models precisely describing and predicting the formation growth and coalescence of NPs, such as colloidal metal and chalcogenide NCs, and the influence of modifying the synthesis conditions are not yet available. Therefore, refinement of the preparation of nanomaterials still comprises trial-and-error. Nonetheless, understanding the thermodynamic and chemical intricacies that underlie the preparation of colloidal NCs is essential to recognize how variables are influencing the process to achieve control and develop a reliable nanofabrication procedure. To this end, *in situ* characterization and real-time probing can contribute with vital knowledge about the thermodynamics and kinetics of the process while, in

some cases, it provides a mean to assess the quality control of the process itself.[55–57] Nevertheless, the transition from "alchemy" to "predictive chemistry"[58–61][lxii] is being steadily paved whilst the field of bottom-up synthesis is maturing. Consequently, we are endowed with a vast pool of novel and advanced colloidal nanomaterials that are popping and materializing in an overwhelming range of possibilities.[62–72]

At the edge – colloidal stability and beyond

Solvothermal synthesis is a versatile strategy suitable with both organic and aqueous media, the latter often referred to as Hydrothermal. While organic media typically renders higher concentration of nanoparticles with better control over size, aqueous synthesis is more friendly, and the pool of reactants is often larger. The role of stabilizers in managing aspects related to nuclei stabilization and growth processes was already recognized. However, the role of such molecules in guaranteeing colloidal stability and providing chemical functionality is yet to be uncovered. Recognizing that the surface is where "everything happens", with its pivotal role in driving stability, programmability, and interactions with the surrounding environment, the following section discusses aspects related to particle-particle and surface chemistry mediated interactions.

DLVO Theory

Particle aggregation in solution is mediated by both attractive and repulsive forces, as described by the DLVO theory,[lxiii] which was originally described to explain the colloidal stability of charged particles (illustrated in). The balance between attraction-repulsion that is at the core of the DLVO theory is commonly expandable to particles stabilized with non-charged molecules like polymers. Nevertheless, it is important to acknowledge that non-DLVO interactions, such as hydrophobic and bridging interactions, steric, depletion and hydration forces, are also possible.[73] These non-classical interactions or forces can lead to phenomena as for instance Pickering emulsions,[74] oil-water separation[75] or surfactant-free stabilization[76] , which cannot be described by classical DLVO theory.

In the classical example, if the surface potential is different from zero, particles in solution that are either positively or negatively charged will be pushed apart and redispersed by electrostatic forces.[lxiv] Contrarily, approaching particles made from the same material will become susceptible to the so called "Hamaker attraction", because of van der Walls interactions. As described in the DLVO "plot", (Contextualization - Figure 9) the difference between repulsive and attractive forces, as the distance between particles decrease, contributes to an energy potential. In the general example depicted here, as particles approach each other, interactions began to arise – red and orange lines. At the shallowest and secondary minimum of energy possible, particles are considered flocculated, meaning that aggregation is still reversible by agitating or sonication, for example. As particles keep approaching, repulsive forces become predominant, either due to electrostatic repulsion, steric hinderance or to the creation of a

[lxii] Predictive Chemistry: The Holy Grail for Chemicals & Materials from alchemy cloud
[lxiii] Named Boris Derjaguin and Lev Landau, Evert Verwey and Theodoor Overbeek.
DLVO theory from Hagen@Cal Poly - highly recommended channel for physical chemistry concepts
[lxiv] This is the reason why citrate is often used to stabilize gold nanoparticles – as firstly described by Turkevich for gold nanoparticles

hypertonic (saturated) environment, which promotes water to flow in between and redisperses them. Nevertheless, this energy barrier can be diminished by increasing salt concentration, which shields electrostatic repulsion, or it competes with the stabilizing agent (e.g., citrate), removing it from the surface. When high concentrations of solutes are present (above Critical coagulation concentration)[lxv], the concentration of solute between approaching particles decreases, creating an osmotic pressure that promotes the diffusion of water into solution, favoring aggregation. If the particles manage to cross the energy barrier and enter each other's vicinity, coagulation occurs. Lastly, and although not accounted in the originally formulas, as atoms get exceptionally close, electron-electron and nucleus-nucleus interactions (Born forces) will contribute to a strong repulsion. Surface engineering – from Colloidal stability and surface chemistry to programmability and beyond.

In charged particles, repulsive electrostatic forces stabilize the colloid, hence making it less prone to aggregate by increasing the energy barrier. A common technique to assess colloidal stability is by measuring the zeta potential.[lxvi] Note, however, that due to the presence of ions in solution, that strongly interact with the surface to minimize its energy (Contextualization - Figure 10), the measurement doesn't retrieve the charge of the particle's surface itself, but rather the charge at the double layer (slipping plane). Intuitively, the zeta potential of the particle correlates with its colloidal stability as highly[lxvii] charged particles tend to be more stable.[lxviii] Concomitantly, zeta potential measurements are semi-quantitative and non-destructive enabling not only to evaluate the native chemistry of the surface (as prepared), but also surface modifications or its interactions with the environment.[77,78] As the surface guides interactions between the nanoparticle and the surrounding media, introduction or modification[lxix] of functional groups (Contextualization - Figure 10) is a reliable and versatile strategy to tailor these interactions.[79–82] A range of functional groups provides the possibility to perform specific and guided surface modifications, instead of uncontrolled and often non-specific physical adsorption.[83,84]

Surface modifications can be used in many ways accordingly to its intended purpose or desired application. For instance, surface modifications can be engineered to promote phase exchange between media (Contextualization - Figure 10) which helps overcoming challenges and optimize preparation of materials or enabling reusability.[87–89] Furthermore, using examples from biomedicine and biosensors, biorecognition ligands, such as antibodies and nucleic acids can be anchored to the NPs to promote specific interactions,[90–93] while positively-charged "cell penetrating peptides" encourage cellular internalization of particles[94] and polymers can be used as antifouling to avoid unspecific interactions. [lxx95,96]

[lxv] critical coagulation concentration derivation from Hagen@cal Poly

[lxvi] https://en.wikipedia.org/wiki/Zeta_potential; Zeta Potential Tutorial from nanoComposix

[lxvii] Either positive or negative

[lxviii] Note that the zeta potential depends on both the surface and the surrounding liquid. For instance, micelles composed by fat molecules have high zeta potential which prevents them to coalesce. If acid is added, the zeta potential will decrease and the fat droplets will coalesce/aggregate and consequently forming cheese.
Note: the pH is a critical aspect influencing the zeta potential measurements.

[lxix] Through a process named "functionalization"

[lxx] Nanoparticle-based drug delivery in the fight against cancer from Institute for Molecular Bioscience

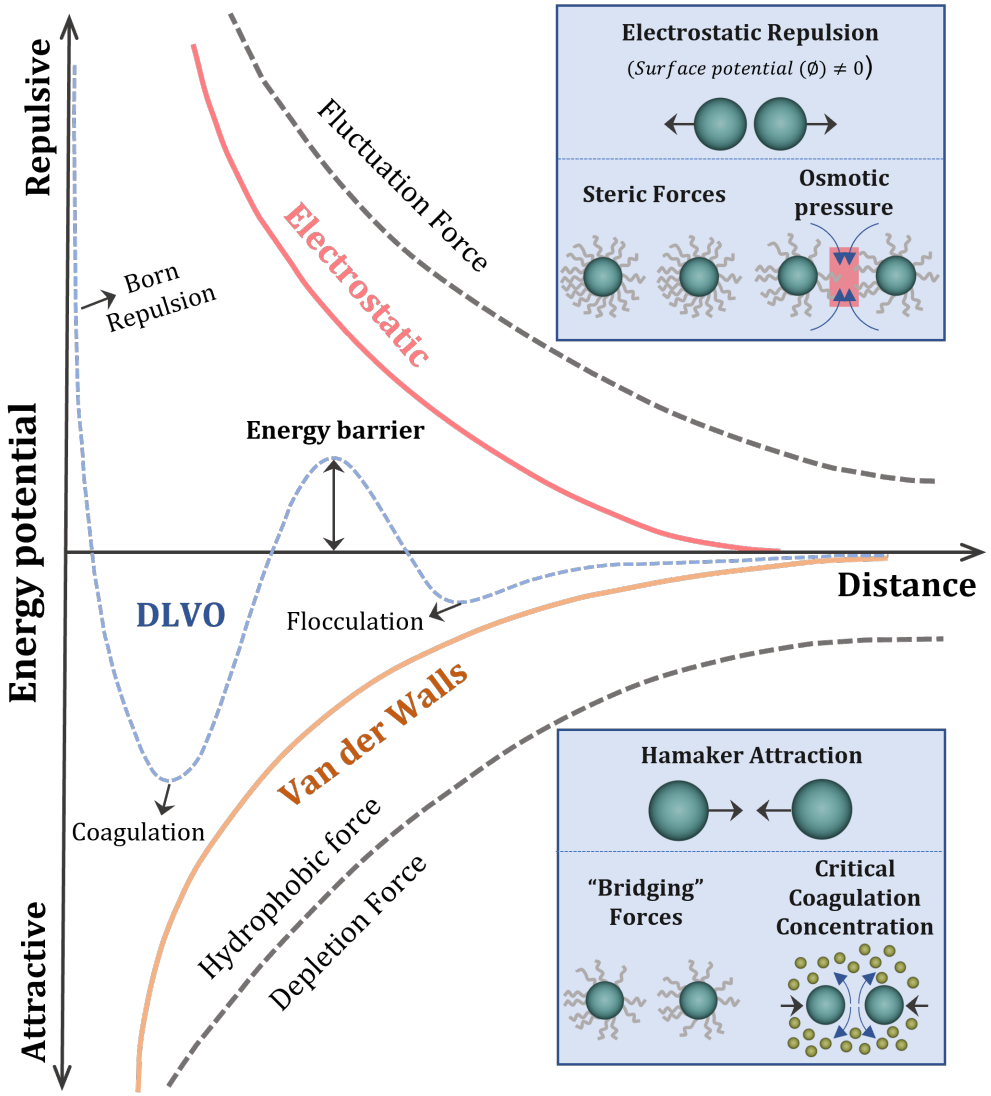

*Contextualization - Figure 9 – **Classical DLVO plot representing aspects underlying colloidal stability of nanoparticles**. Dashed lines in grey represent non-DLVO interactions – adapted from*[73]

As nanomaterials become exposed to increasingly complex environments, its surface is prone to form a corona[lxxi] by interaction with the surrounding media (Contextualization - Figure 10). The formation of corona is usually a rapid and dynamic phenomenon driven by the occurrence of hydrogen bonding and hydrophobic, Van der walls and electrostatic interactions. The most common and widely known type of corona is the protein corona and it is a key aspect to consider in nanomedicine and (bio)sensors. For instance, while in specific examples is favorable by making the particles evade the immune system, and consequently avoid rapid clearance from the body, it can also critically undermine efficiency, for example, by shielding interactions between the biorecognition element and its target. As consequence of the complex and dynamic nature of the corona formation, research on protein corona formation is extremely challenging and often requires advanced techniques, such as super-resolution microscopy.[97,98] Yet, and despite some fundamentals about corona formation being already known, such as its

[lxxi] Unspecific adsorption by molecules present in the medium.

dependence on the material composition, size, morphology and surface chemistry, the overall formation processes are largely unpredictable. [85,86,99]

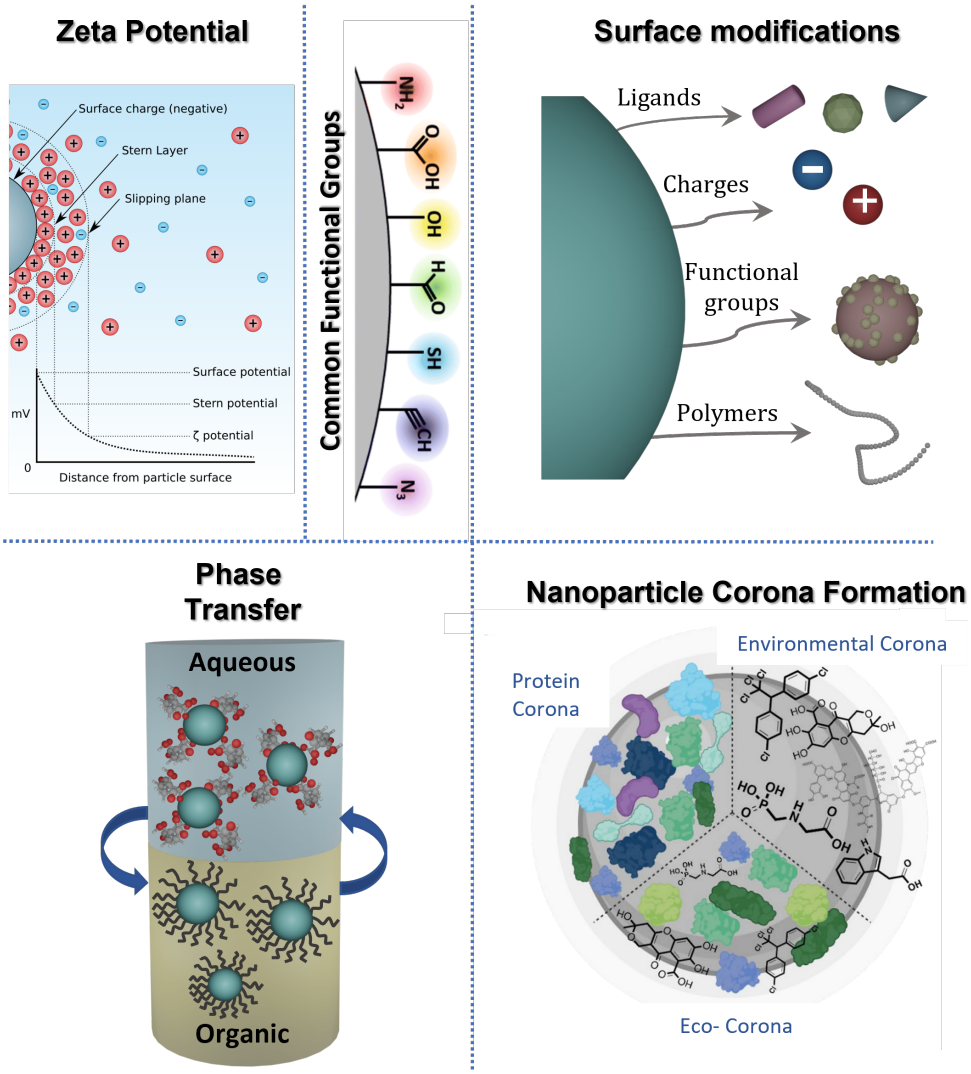

Contextualization - Figure 10 – ***Fundamental aspects guiding stability, functionality, programmability, and the fate of nanomaterials****. Illustration of the zeta potential of a particle in solution (from Wikipedia); Common types of chemistry groups used to functionalize nanomaterials (from*[79]). Types of surface modifications (adapted from[85]). Illustration of phase transfer of nanomaterials. Corona formation on nanomaterials (from [86])

Engineering of nanomaterials relies intimately on the relationship between the properties of the core nanomaterial, its surface, and anisotropy. The correlation between each of such aspects towards functionality and programmability is uncovered in the next section.

A Bakerian light at the nanoscale

From the 1st observations on metallic colloids made by Faraday [100,101] to the Turkevich method for the synthesis of metallic nanoshperes,[102,103] the preparation of nanoobjects evolved remarkably.

So far, only the influential role of ligands[lxxii] in precursor reactivity was mentioned. Stabilizers are also key elements, although non-exclusively, in biasing the underlying phenomena during growth mechanisms, and consequently skewing the fate of the NCs.[104] In this regard, contrary to precursor molecules that have limited options available, the pool of ligands, stabilizers and/or even templates are rich, adaptable, and expandable.[82,105,106] [lxxiii] Furthermore, even though shape and size of the core majorly determine the properties of a nanomaterial, stabilizing agents' are at the interface and subsequently mediate the interactions of nanomaterial-environment. Therefore, ligands and/or stabilizers are crucial tools to guide and discern the resulting NCs by influencing composition, structure, shape, and surface chemistry.

The versatility provided by such components opens an enormous venue of prospects and combinations to anisotropic nanomaterials. Considering the materials and strategies underlying this dissertation, the following section will predominantly focus in metallic and magnetic materials as examples of common principles and concepts that rely on anisotropy to shape enhanced properties. Lastly, phase transfer and self-assembly procedures are mildly addressed as means to reinforce, optimize, and expand the possibilities of nanomaterials.

Functionality through shaping

Anisotropy is a fundamental property of our universe. By breaking symmetry, objects potentially acquire programmability that allows the creation of structures with high degrees of functional complexity.[26,107] From our ability to perceive colours, to the strength of our bones, to endowing virus with the ability to infect target cells, nature provides us with countless examples of functionality acquired through anisotropy.[lxxiv] Despite morphological anisotropy being the most intuitive, other forms of anisotropy related to chemical/composition and material properties are also possible and desirable (Contextualization - Figure 8). Acknowledging the resourcefulness and capabilities conferred by anisotropy, scientists have tried to emulate nature's ability to exploit such structures. As a result, the number of strategies and conditions to prepare anisotropic materials are countless. A few examples were selected as described next.[108–112]

[lxxii] Regularly the same molecule acts as ligand and as stabilizer (not mandatory).
Disambiguation: Ligand is the name given to the molecule coordinating the precursor, thus ligands influence the Activation energy (E_A); Stabilizer is the name given to the molecule coordinating the monomer and/or the NCs and dictate its surface energy. If convenient, multiple stabilizers can be used.
[lxxiii] They can be exchanged overtime, i.e., by appearance of new facet during growth.
[lxxiv] Why Is Blue So Rare In Nature? From Be smart

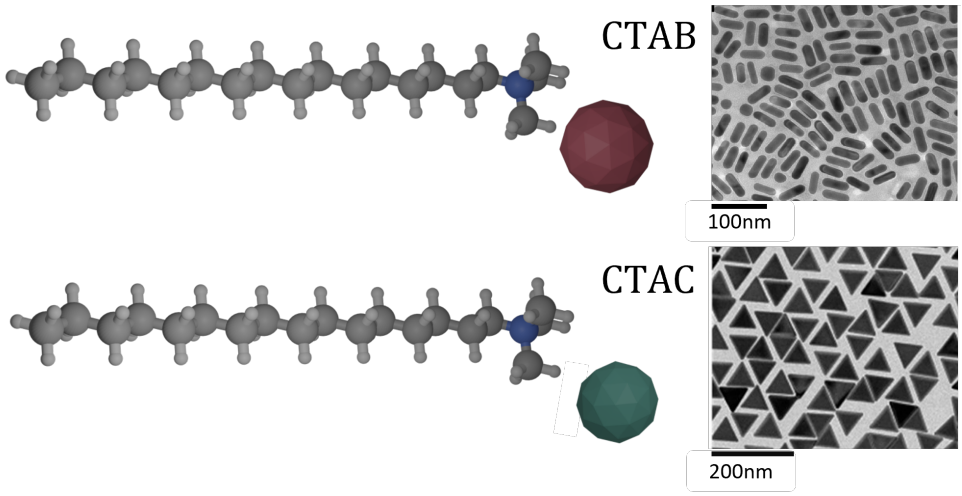

Contextualization - Figure 11 – ***illustration of CTAB (Cetyltrimethyl ammonium bromide) & CTAC (Cetyltrimethyl ammonium chloride) molecules****. (top) Gold nanorods synthesized using CTAB as ligand/stabilizer;*[117] *Gold triangular nanoprisms synthesized using CTAB as ligand/stabilizer.*[118]

Templated synthesis relies on the usage of external components to guide the morphology of nanomaterials. These strategies rely on "solid-state" templates, hence the denomination "hard-templating", whereas "soft-templating" uses "fluid-like" component such as surfactants.[113] Selective molecular adsorption can be seen as a soft templating method as it influences the growth of NCs such as AuNRs.[53,114,115] Despite its convenience, it is important to note that soft-templating strategies are driven by a thin balance between thermodynamics and kinetic factors that involves not only the diffusion of precursors, but also the equilibrium between adsorbed and free-molecules in solution, interfacial strain, facet-dependent deposition rates, and molecular affinity.[116] To grasp how these strategies are dynamic and sensitive even to small variations, Contextualization - Figure 11[117,118] illustrates two different morphologies of gold nanoparticles: nanorods and triangular nanoprisms. In both cases, preparation is performed by seed-mediated growth. However, the swapping of small amounts of $AgNO_3$ [lxxv]for NaI[lxxvi] and of CTAB[lxxvii] for CTAC (bromine to chlorine) dictates if nanorods or triangular nanoprisms are obtained, respectively. Despite silver-free methods to prepare AuNRs exist, full comprehension of its role and influence in nanorod synthesis is still yet to be unveiled.[119–121] Nonetheless, what strikes the most is that even though CTAB and CTAC molecules are close to identical, during synthesis they are not interchangeable.[118,122]

Beyond shape per se, the relative size across directions is another aspect influencing morphological anisotropy and the properties of the nanomaterial. For instance, gold nanorods (AuNRs) are a classical example of anisotropy guiding its optical properties as differences in aspect ratio (AR)[lxxviii] induces a red-shift in the wavelength of the longitudinal plasmonic mode (detailed later) almost linearly. As mentioned, differences in the AuNRs aspect ratio is promoted by inhibiting axial growth, and consequently controlling thickness and length by changing parameters such as pH, introducing new stabilizers, etc.[121]

[lxxv] Silver nitrate
[lxxvi] Sodium iodide
[lxxvii] Cetyltrimethyl ammonium bromide or chloride – CTAB or CTAC
[lxxviii] Relationship between length and width

Functionality through chemistry

Imparting directionality in the chemical properties of a nanomaterial is yet another type of anisotropy. This is called chemical anisotropy (Contextualization - Figure 8), and its most intuitive form is when the nanomaterial is composed of different materials that are partitioned within its structure. Janus nanoparticles are a popular example of how such heterostructures can enhance (multi-) functionality.[123–127] Another distinct type of chemical anisotropy regards the surface chemistry of the nanomaterials. This has been explored, for instances, by promoting the specific immobilization of single stranded DNA molecules at the tip of AuNRs. Here, advantage is taken of the well-established fact that CTAB bilayers used in AuNRs' stabilization have a packing density that critically decreases around curved surfaces (i.e., the tips of AuNRs). More specifically, CTAB is used above its CMC[lxxix] (~ 1mM at RT) to stabilize the AuNRs in solution by forming a double layer, which confers the particles a strongly positive zeta potential. During immobilization at concentrations slightly above the CMC (10 mM), the CTAB layer pushes the ssDNA molecules towards the tips, thus the resulting in AuNRs with different surface densities of DNA at the tips and edges (Contextualization - Figure 8).[54] As consequence of both molecules having opposite charges, a major challenge to overcome while immobilizing ssDNA onto CTAB-coated AuNRs in solution is to avoid particle aggregation.

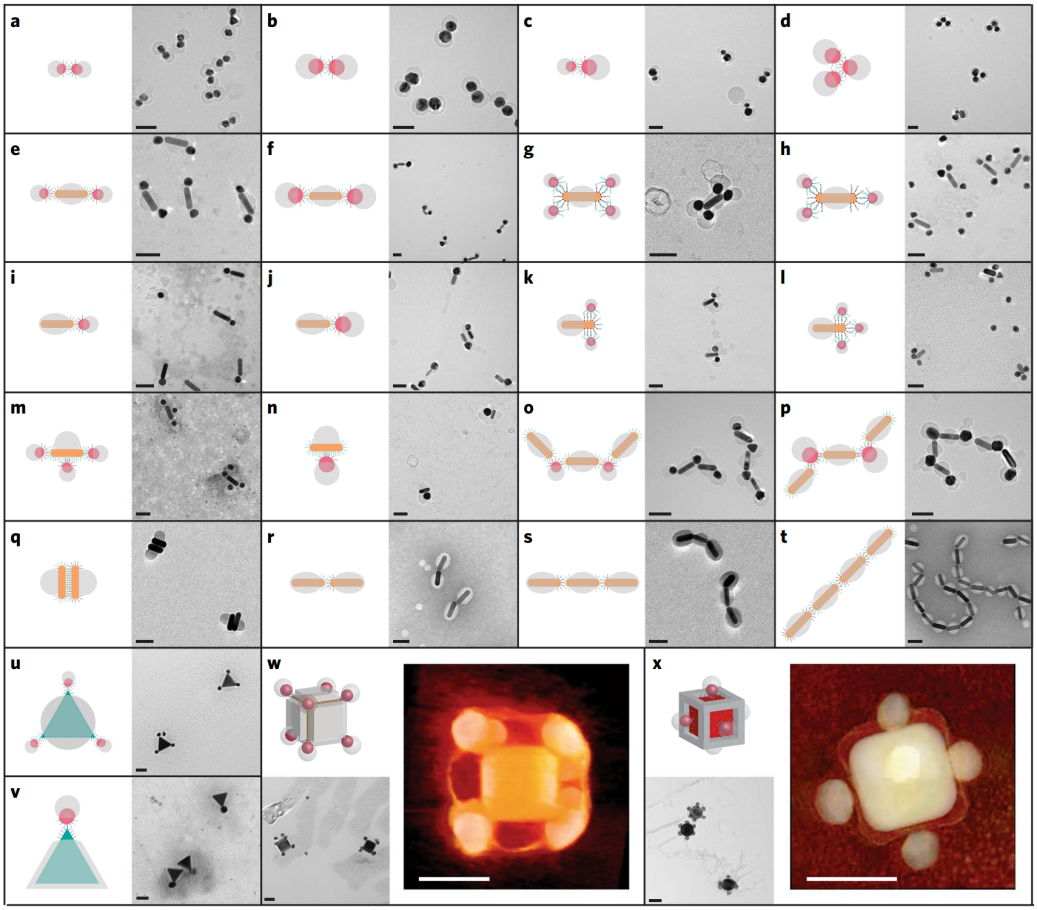

Contextualization - Figure 12 – ***TEM images from programmable self-assemblies using chemically anisotropic gold nanoparticles*** *– originally published elsewhere;*[128] scale bars 50nm.

[lxxix] Critical micellar concentration: Below CMC micelles are absent and above CMC micelles are formed.

Despite their inherent differences, both composition and surface chemical anisotropies can be used concomitantly to further boost multifunctionality, stability and programmability. In this regard, regioselective coating and functionalization of the surface to encode nanoparticles for programmable self-assembly in solution is an exciting example.[128] Briefly, using a mixture of polymers and solvents in different conditions, researchers were able to favor the coating formation along faces, tips, and edges in materials with distinct dimensions (0D to 3D). This versatile strategy relies on the thermodynamic equilibrium of the polymers and the particle surface to promote selective molecular adsorption and promote extreme control over the coating. Besides promoting colloidal stability, the coating selectively obstructs surface access, thus guiding the immobilization of biomolecules, such as ssDNA, towards the exposed surfaces.

As illustrated in Contextualization - Figure 12, by combining this selective coating strategy with the direct programmability of DNA sequences, it was enabled the design of a variety of self-assembly structures. By the end, the authors further speculate that their strategy is likely to be expandable to other shapes and yet other materials such as QDs and magnetic nanoparticles. Moreover, programmable self-assembly can encompass technologies such as patching and DNA origami,[lxxx] further boosting nanoconstructions and bringing chirality and logical computation to bottom-up nanostructures.[129–133]

These examples display how chemical anisotropy is a reliable tool to propel multi-physical or multi-chemical functionalities or both, thus pushing the limits of advanced functional and/or smart materials.

Functionality through properties

Lastly, and frequently intertwined with the morphological and the surface, the properties can also present anisotropy (Contextualization - Figure 8). A common and intuitive example of “properties anisotropy” is the magnetic orientation within a spherical iron oxide nanoparticle. Even though they are morphologically and chemically isotropic, their magnetic properties can be oriented as “north” and “south” - Contextualization - Figure 8. Properties of metallic nanoparticles can also present anisotropy due to Localized Surface Plasmon Resonance (LSPR). In nanospheres, which are isotropic, the LSPR is a single and broad peak whose position depends on the radius of the particle.[lxxxi] In gold nanorods, however, symmetry is broken and the LSPR is split into 2 distinct peaks (transversal and longitudinal). Also, control over the aspect ratio (width over height) makes it possible to adjust the position of longitudinal LSPR within the red to infrared window.[134] Interestingly, “ultranarrow optical properties” of AuNRs could be obtained using a post-synthesis strategy that resorted to femtosecond laser pulses.[135] This strategy was proven extremely efficient as the LSPR profile of the overall sample converged and approximated to a spectrum of a single particle. Lastly, optical properties of plasmonic nanoparticles are also distorted when in the vicinity of other plasmonic material, giving rise to hybridized plasmonic modes in structures such as those shown in Contextualization - Figure 8.

Until this point, the intertwined relationship of nanoscale objects and respective dimensions with properties was congregated with the fundamentals of bottom-up synthesis and

[lxxx] Complex 3-D DNA structures from Massachusetts Institute of Technology (MIT)
Nanobase DNA origami database
[lxxxi] (In water) from ~520 nm for small NPs (12nm) to <600nm for larger NPs (100nm)

the types of anisotropy. Based on the framework of this thesis, the following section is devoted to (separately) reveal magnetic and plasmonic properties at the nanoscale as they provide the fundamental properties of the developed sensors.

Magnetism 101

Saying that magnetism has been around us since ever feels like an understatement. [lxxxii] Even though it was discovered in ancient Greece in the city of "Magnesia", hence the denomination "magnetism", it wasn't until recently that magnetism paved its way to integrate our technologies.[lxxxiii] Firstly discovered as a magnetite-based mineral named "lodestone", magnetic materials started cementing their importance in society as navigation tools in the form of compasses. Few centuries have passed since then, and from kid's games to hard drives in our computers, to MRI contrast agents, technologies relying on magnetism are everywhere. Interestingly, ferromagnetism, the most widely recognizable type of magnetism, is yet another phenomenon correlated with anisotropy.

Intimately related with anisotropy, the properties of ferromagnetic materials[lxxxiv] are critically dependent not only on their intrinsic properties, such as atomic and molecular (crystal) structures, but also on morphological aspects related with their shape and the surfaces.[26,111,136–139] Magnetocrystalline and shape anisotropy are interesting aspects to be considered to understand why magnetization is directionally preferred along a certain crystallographic direction that we call easy axes rather than others that we call hard axes (Contextualization - Figure 13).[lxxxv] Nevertheless, a thorough explanation of the thermodynamic aspects involved would be cumbersome, but the interested reader can find it elsewhere.[136] Instead, to provide the fundamentals to understand the magnetic sensor explored, the next section will uncover the importance of size in domain formation and its influence in the magnetic properties.

Magnetic ordering commonly arises in materials comprising elements such as iron, nickel, cobalt and gadolinium, arising from the electronic interactions of electrons[lxxxvi], which consequently directionally pins their magnetic moment within the structure. As size decreases towards the nanoscale, electrons get confined and hence ferromagnetism becomes size-dependent. As consequence, the magnetic properties – coercivity, remanence, hysteresis,[lxxxvii] and saturation magnetism – can be tuned by composition, size, shape, and surface.

As illustrated in Contextualization - Figure 13, as size decreases, the magnetic properties of a material change. As the particle "shrinks" the boundaries between the domains cease to exist, and below D_{sd}, the magnetic nanoparticle becomes composed by a single domain. Comparing

[lxxxii] Disclaimer: For sake of simplicity diamagnetism and quantum locking will be avoided altogether. Nevertheless, the following are recommended: Diamagnetism: How to Levitate a Frog from SciShow and Everything Is Magnetic! Moving Water With Magnets And Levitating Frogs from Action Lab; Mind-Bending Effect of Ferrofluid on a Superconductor from Action Lab

[lxxxiii] Magnets - History of Magnetism from Lammas Science

[lxxxiv] MAGNETS: How Do They Work? From minutephysics

[lxxxv] Note: in solution, particles are "free" to rotate. hence magnetic ordering can interfere with colloidal stability – depending on the interactions between dipoles.
Note 2: Ferrofluids are a noteworthy example of strongly stabilized nanoparticles in which the colloid can be manipulated using magnetism - Ferrofluid display cell bluetooth speaker from DAKD Jung

[lxxxvi] Spin-spin or Spin-orbit interactions

[lxxxvii] Materials with intrinsic low hysteresis are called "soft magnets" while materials with high hysteresis are "Hard Magnets"

single- with multi-domain ferromagnets it is possible to see that coercivity is significantly larger than in multi-domain. This occurs because after removing the external magnetic field, some of the domains partially lose their magnetic moment (orient in different directions), hence diminishing the coercivity value. If size further decreases, the superparamagnetic region is entered. The superparamagnetic phenomena can only occur at the nanoscale and its properties lie between paramagnetism (magnetism of single atoms) and ferromagnetism. This makes superparamagnetic a special class of magnets with high susceptibility (quickly magnetized by applying a "weak" magnetic field and high magnetization) with no remanence neither coercivity.

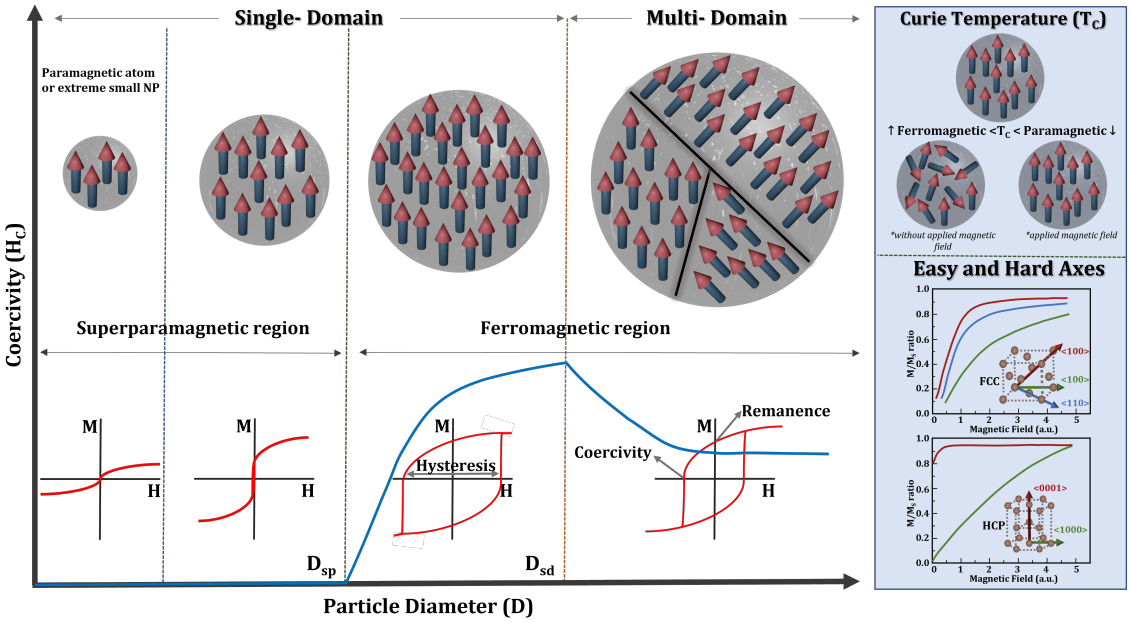

Contextualization - Figure 13 – ***Schematic illustration of the coercivity (H_C) behavior vs particle diameter (D)*** *– represent by the blue line. D_{sp} – Maximum Diameter for superparamagnetism to occur; D_{sd} – maximum diameter for single domains to exist; Adapted from* [140]; Sketch of Curie Temperature; Demonstration of magnetization of Easy and Hard axes using "fcc-Co" and "hcp-Co" crystals as examples – adapted from[136]

Even though these properties can be disadvantageous in context such as data storage, [lxxxviii] due to its versatility, remote maneuverability, programmability, and other features,[141–144][lxxxix]superparamagnetism has been proven worthful in many contexts like biomedical applications and micro-/nanorobots.

The Curie Temperature (T_C) is another intrinsic property of magnetic materials. Ferromagnetism, and consequently coercivity, is a result of the "magnetic" ordering from the spins of electrons within the material (as mentioned above). As temperature increases, the thermal energy (k_BT)[xc] also increases leading to a higher thermal agitation, which favors the disordering of the spins. Thus, the T_C bounds the temperature at which, in the absence of an external field, the system properties transits from an ordered to a disordered state (Contextualization - Figure 13).[xci] This magnetic transition critically depends on the composition of the nanomaterial and its crystal

[lxxxviii] Superparamagnetic limit from Alexandr Kolesnikov
Scientists Found New Way To Clean Your Blood! From seeker
[xc] K_B – Boltzmann constant (1.380649×10^{-23} m^2 kg $s^{-2}K^{-1}$)
[xci] Curie temperature demonstration from Mopatin

structure as it will be later demonstrated in the section dedicated to the magnetic (bio)sensor developed herein.

(Localized) Surface Plasmon Resonance - (L)SPR – A goose that lays golden eggs?

Surface Plasmons (SP) are characterized by the collective and coherent oscillation of the free electrons ("electron gas") confined at the interface between a material and a dielectric. Initially described by R. H. Richie for metals,[145] SPs originated by coupling of photons with the free electrons[xcii] and, depending on the material' dimensions, it can be categorized as: propagating (SPR; thin films) and localized (LSPR; 0- 1D; Contextualization - Figure 14) – being the later the main focus herein.[xciii] Conventionally, noble metals like Silver and Gold are used to study SPs due to their abundant number of free electrons which results in a resonance frequency located in the visible and NIR[xciv] regions.

Nevertheless, semiconductors or 2D structures can also present or be engineered to present SP properties. In Contextualization - Figure 14 it is depicted how different types of material, depending on their number of free electrons interact with different regions of the electromagnetic spectrum.[146]

The LSPR of metallic nanoparticles, which is responsible for the particle's strong absorption and light scattering, displays a spectral lineshape given by a "Lorentzian peak" around the resonance frequencies (Contextualization - Figure 14). Fundamentally, the LSPR profile and peak position in the electromagnetic spectrum is critically dependent on the intrinsic optical properties of the material composing the nanoparticle, its size and shape and it is also influenced by the properties of the dielectric material surrounding the particle.[xcv]

As result of sharp interaction with light, plasmonic nanoparticles have strong and well-defined colors. Interestingly, gold and silver nanoparticles have been around for centuries and were used to color objects such as the Lycurgus cup (Contextualization - Figure 14), or glasses in cathedrals. In the midst XIXth century, the first photographic technique – the daguerreotype – based on plasmonic effects was invented (Contextualization - Figure 14).[147,149] However, these admirable inventions were created far before we were able to understand SPs or nanotechnology; hence, control over the preparation of the nanomaterials was limited. Nowadays, plasmonic nanomaterials can be accurately tuned due to the precise control over nanofabrication processes. As an illustrative example of this accurate control, the original painting and a microsized replica of Monet's "Impression Sunrise" printed using plasmonic (Al) materials, are presented in Contextualization - Figure 14.[147,148] Still in this framework, recently, plasmonic nanostructures have been proposed as dynamic color generators for functional materials.[150xcvi]

[xcii] Especially at the nanoscale, this implies that excitement of the SP is promoted by a "specific" wavelength

[xciii] Comparing LSPR and SPR for Diagnostics from Lambdagen

[xciv] Near Infrared

[xcv] Note: Cu and Al have reliable optical properties but are unstable under environmental conditions while Pd and Pt have high absorption in the visible and NIR, hence these materials are poor candidates in many plasmonic applications.

[xcvi] Note that the polarization of the applied electric field (E) accounts for the plasmonic profile around the particle as it excites the transversal or longitudinal modes, i.e. nanorods.

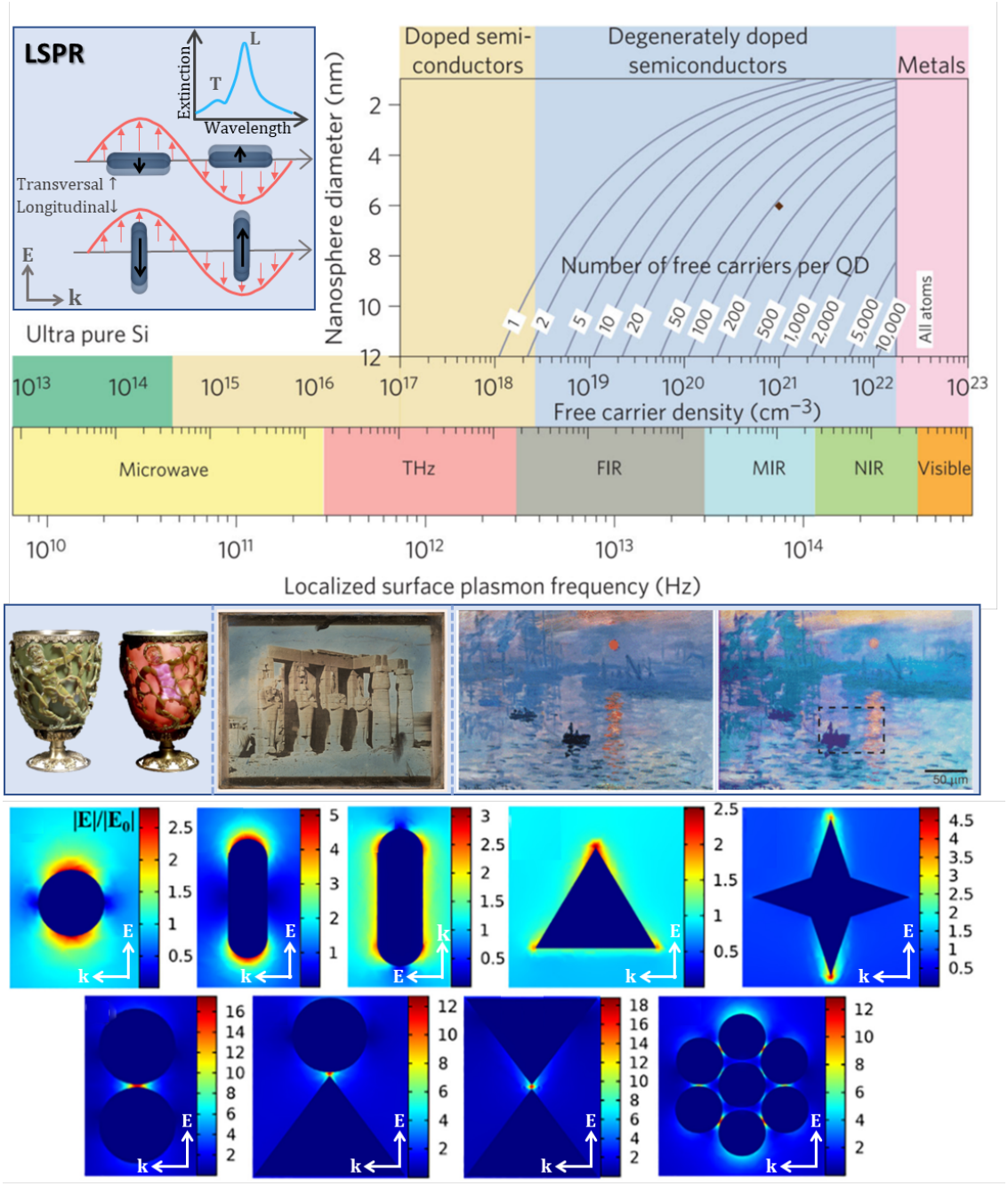

*Contextualization - Figure 14 - **Surface Plasmons**; (L)SPR illustration: Representative illustration of LSPR spectrum from a single gold nanorod, representing the transversal mode (T) and Longitudinal mode (L) frequencies; Excitation of the "transversal" and "longitudinal" plasmonic modes. Plasmon frequencies vs number of free electrons: Correlation of the resonance frequency in semiconductors and metals with number of free electrons. Plasmonic colour generation: Lycurgus Cup (300 A.D; British Museum);*[xcvii] *Daguerreotype of Pharaohs Ramses II's temple in Thebes (1844; Metropolitan Museum of Art);*[147] Microsized realistic reproduction of Monet's "Impression Sunrise" coloured using plasmonic nanomaterials.[148] COMSOL Multiphysics simulations: simulation of the distribution of the electric field across different gold nanostructures.

Another key feature of plasmonic materials is their inherent ability to dramatically enhance light-mater interactions at subwavelength scales.[151] Simulations of the spatial profile of the SPs across gold nanoparticles with different morphologies and nanostructures of gold assemblies are shown in Contextualization - Figure 14.[152] Immediately, it is possible to observe that the electric

[xcvii] Nanoplasmonics from Nanowerk; Ancient Cup Made With "Nano-Technology? From Mystery History

field concentrates (i.e. is stronger) around curvatures and even more dramatically around tips, which thus receive the denomination "hot-spots". This efficient confinement of optical energy at the nanoscale allows a local increase of the electric field by orders of magnitudes.[151,152] These features combined with the ability activate remotely, and tuneability of aspects like morphology, optical properties, surface chemistry and others, make plasmonic materials promising tools in many areas including biomedicine and sensing.[153–156]

SP-based sensors have been growing at a strong pace for the last couple decades. Due to strong light-matter interaction and intrinsic optical properties, plasmonic materials empower many detection schemes and strategies like Surface Enhancement Raman Spectroscopy (SERS), Surface Enhancement Infra-red absorption (SEIRA), plasmonic enhancement of fluorescence (PEF) and refractive index-based sensing. In general, these sensors enable monitorization in real-time, they require small sample size, and render accurate results at low-cost. Acknowledging the potential and flexibility provided by plasmonic nanoparticles, and in line with the scope of this thesis, the next section will be dedicated to uncovering the mechanisms underlying SPs sensors with focus on label-free (L)SPR sensing and plasmon enhanced fluorescence (PEF).

Surface Plasmons on duty…

Metal nanoparticles don't suffer from photo-fatigue and are sensitive to refraction index changes in a nanometric volume surrounding their surface, which makes them promising materials for optical transduction, particularly in real-time label-free sensing applications.

LSPR "Spying on the neighbourhood" 101

Depending on the propagating distance of SPs (δ_{SPP}), sensors can be categorized as Surface Plasmon Resonance (SPR), when the surface waves propagate, or localized surface plasmon resonance (LSPR), when particle diameter is much smaller than δ_{SPP} (~ 2-20µm). The other two characteristics distances determining the (L)SPR profile of the sensor are δ_{metal} and δ_{diel} (Contextualization - Figure 15), which correspond to the distances that the propagating wave can penetrate either in the metal or the dielectric, respectively. Since δ_{metal} is small in both cases ($\leq 5nm$), the major difference between SPR and LSPR arises from δ_{diel}, which becomes the most relevant aspect in determining sensing volume. In the case of SPR, δ_{diel} typically ranges from 250-1000 nm, whereas δ_{diel} of LSPR sensors is typically in the range of 20-40 nm and quickly decays with the distance. Predominantly in SPR sensors, this results in the so called "Bulk-effect" and makes it susceptible to non-specific targets in solution and imposes a challenge when dealing with complex matrixes as it may significantly increase the noise and ultimately lead to false-positives.

Plasmonic optical properties and sensor's performance

Sensitivity is a defining aspect of sensor performance and corresponds to shift of the (L)SPR wavelength in response to changes in the refractive index typically expressed in nm.RIU^{-1}. In both (L)SPR, sensitivity is differentiated by:

- Bulk Sensitivity (S) – corresponds to sensor's response to changes in the bulk environment, for example by changing solvents with different refractive indexes – from η = 1.33 to η = 1.55 (Contextualization - Figure 15).

- Surface sensitivity (S_S) – corresponds to sensor's response to changes near the surface as a result of binding or unbinding events. In this case, surface interactions may be mediated by specific receptors for target capture.

Besides peak position, extinction cross-section (ca. 10^{-3} μm^2) and linewidth (meV) are the other aspects defining the optical properties of the (L)SPR profile. Loosely, the extinction cross-section determines the total interaction of the plasmon with light, comprising both scattering and absorption phenomena ($\sigma_{ext} = \sigma_{abs} + \sigma_{scat}$). Hence, the extinction coefficient is related with the "ability to harvest light", which increases the signal, and consequently boosting the optical performance of the sensor by increasing the signal-to-noise ratio (SNR).[xcviii] The absorption cross-section is proportional to the particle's volume, while the scattering cross-section scales with the squared particle's volume, and both are sensitive to the refractive index (Contextualization - Figure 15). This becomes relevant regarding the optical signal used for detection, for instance, photothermal or photoluminescence detection depend on light absorption by the particle, and thus its signal intensity scales with the particle's volume. On the other hand, dark field microscopy based on total internal reflection detects scattered light by the particle and, therefore, its signal scales with the squared volume of the particle.

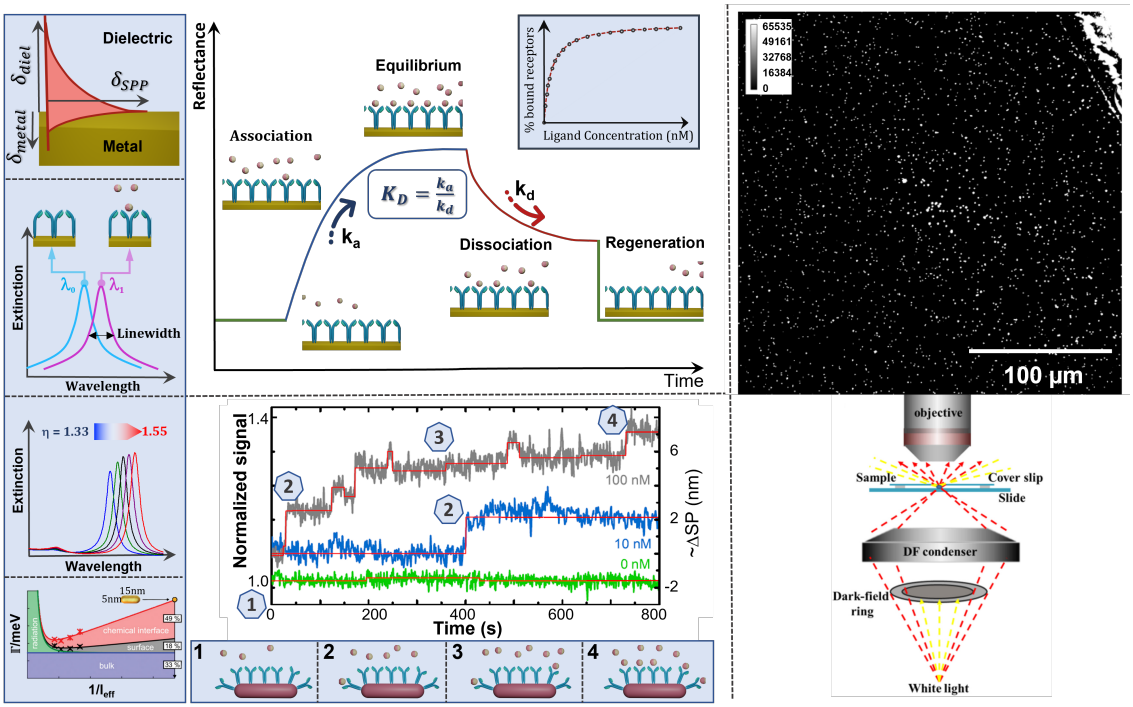

Contextualization - Figure 15 – ***Representation of the penetration and propagation distances. Bounding of analyte inducing a red-shift in the optical properties of the sensor. Symbolic response of an LSPR sensor when increasing the refractive index of the solvent. Damping mechanisms vs size*** *- Linewidth (Γ) contribution for each damping mechanism as a function of effective path length (l_{eff}) from.*[157] ***Comparison of illustrative results obtained using SPR vs LSPR****. The sensogram presented simulates the results obtained using an SPR device based on antibody detection of an analyte. "k_a" and "k_d" represent the association and dissociation rates, respectively while "K_D" represents the dissociation constant. The inset depicts the response of the sensor to several experiments with different concentrations of analyte (in equilibrium). In the LSPR example, the results correspond to single molecule experiment to streptavidin using Gold Nanorods.*[158] **Representative image from a sample of gold nanotriangles using Dark-field microscopy**

[xcviii] This is one of the reasons why gold nanoparticles are used to give the colour in the Covid-19 antigen testing (explained later).

resorting to a dark-field condenser (non-published data). Schematic representation of a dark-field microscope illuminated through a dark-field condenser.

Lastly, and probably the most critical aspect determining the performance of the sensor is the linewidth (or full width at half maximum, FWHM). Intuitively, if the (L)SPR peak is broad, the center is difficult to determine with precision and small changes on the refractive index will be less pronounced, in opposition to sharp well-defined peaks. The homogeneous linewidth originates from damping mechanisms that dephase the plasmon oscillation. As illustrated in Contextualization - Figure 15, damping mechanisms can be divided into 4 categories:

- Bulk damping – is an intrinsic property of the plasmonic material and corresponds to electronic transitions (inter/intraband) within the metal. As it is material-dependent, its influence on the linewidth is constant.[xcix]
- Radiation damping – negligible for smaller particles (<25 nm) it originates from radiative phenomena such as photoluminescence.
- Surface damping – is a damping pathway corresponding to phenomena occurring at the interface between the plasmonic material and surrounding material. It is critically dependent on the size, morphology, and composition of the material.
- Chemical interface damping – corresponds to the influence of the chemical environment on the linewidth.

Collectively, these four damping mechanisms determine the homogeneous linewidth of the plasmonic material and hence influence its performance. Extensive covering on damping mechanisms can be found elsewhere.[157]

Plasmonic as sensors: from mere quantification to kinetics.

SPR sensors already reached a large degree of maturity with many options being commercially available. For example, the SPR sensor depicted in Contextualization - Figure 15, detects binding of a target molecule (analyte) to an antibody (receptor) immobilized at the metal's surface and allows to follow this process over time. The frequency of binding events is correlated with the concentration of the analyte, while the portion of receptors occupied in equilibrium is correlated with the affinity between the analyte and the receptor. Thus, (L)SPR sensors are not only good for mere quantification but also render kinetic information about the system. For this reason, these cost-effective sensors are a reliable tool in many contexts such as drug development, food safety, environmental analysis, and others.

Succinctly, in an SPR experiment, the initial response is the background signal due to the absence of analyte. As the analyte starts flowing into the sensing volume, a change in signal is observed due to the association of the analyte with receptors, which enables the determination of the binding rate constant (k_a). After a while, the rate of binding and unbinding of analyte will equalize, thus, reaching a situation of chemical equilibrium. At this point, the signal is proportional to the fraction (%) of analytes bound to receptors and is concentration dependent (if all surface receptors are not yet saturated). Then, after reaching equilibrium, the analytes are washed from the solution, dissociating from the receptors at a dissociation rate (k_d), which is

[xcix] This is the reason why Ag is the best plasmonic contender regarding optical properties to sense in the visible and NIR range. However, it is also prone to oxidation and surface roughness, which can negatively impact its applications, while gold optical properties, although worst in comparison, have increased environmental and chemical stability.

also dependent on the analyte-receptor affinities. Consequently, the dissociation equilibrium constant (K_D; M^{-1})[c] of an analyte-receptor pair can be determined using the measured values of k_a and k_d. Lastly, the sensor can be regenerated, by promoting complete unbinding of the analyte, and reusing it. Furthermore, measuring the signal at equilibrium for different concentrations allows one to obtain a dose response curve for a given analyte (inset - Contextualization - Figure 15).

Construction of SPR sensors impose some engineering challenges.[ci] For starters, resonant conditions (only) in SPR to promote the occurrence of the evanescent field are not achievable in air, hence the use of a prism is mandatory. Furthermore, as the target analyte binds to the surface, the (L)SPR peak position red-shifts from λ_0 to λ_1 (Contextualization - Figure 15), inducing an alteration on the resonance angle that enforces the usage of adaptable optics. Lastly, as SPR optics need to be extremely controlled, temperature control is mandatory while LSPR is almost temperature independent.

Other major advantage of LSPR comparing with SPR is that resonant conditions are achieved solely by using a light source with adequate wavelength. These benefits critically simplify the engineering of the device ultimately able to reach single molecule detection. Consequently, LSPR sensing is a versatile and robust tool adjustable to a wide variety of assays that can be integrated in a device in noteworthy requirements, like scalability, miniaturization and suitable to integrate portable devices as it requires less energy. Beyond the intrinsic optical properties, as explained above, LSPR confines and enhances the electric field at the nanoscale, which enables building of plasmon sensors with ultra-small probe volumes down to attoliters. This increases the sensor's specificity because only a restricted volume at the particle's surface, where receptors are attached, is probed. The rationale about the influence of the aspect ratio in bio-sensing can be read elsewhere.[159]

The advantages of LSPR sensing have been enabled to reach the ultimate sensitivity of single-molecule detection. This feature is illustrated in (Contextualization - Figure 15) which shows results from a single particle experiment using photothermal microscopy to determine binding of streptavidin (0-100 nM) in real-time. Like with SPR sensors, when the analyte molecule binds to the receptor at the particle surface, a red-shift in plasmon resonance wavelength is observed. However, contrary to SPR experiments in which the shift occurs gradually, the LSPR shift occurs in discrete steps indicating binding of single molecules one at a time. Furthermore, due to the stochastic nature of the binding events it is possible that the waiting time needed to observe the binding of the first molecule is much larger for the 10 nM experiment, when compared with the 100 nM sample.[160] Besides the advantages aforementioned, this unveils yet another key advantage of LSPR vs SPR sensors as they render deeper insights about molecular dynamics with the ultimate ability to uncover process heterogeneities.[161]

A major challenge in ultrasensitive sensors is the lack of statistics, for example in diluted samples such as 10 nM, it is possible to observe that the waiting time for a single event to occur is of the order of hundreds of seconds. To overcome this limitation, wide-dark-field microscopy enables

[c] Concentration at which 50% of the receptors are bound to the analyte and is a key aspect determining the efficiency of a system in many contexts.
[ci] Comparing LSPR and SPR for Diagnostics - LambdaGen

monitorization of hundreds of particles simultaneously with single particle and ultimately single molecule resolution.[160] For mere illustrative purposes, a darkfield microscopy image of gold nanotriangles is shown and underlying the setup configuration using a dark field condenser (Contextualization - Figure 15).[cii] Each spot corresponds to the point spread function (PSF) of a single particle of particles (except for sporadic clusters).[ciii]

LSPR is unquestionably a powerful tool for label-free sensing. However, it is still limited for targeting molecules with low molecular weight like small proteins or micro-RNA, and is aggravated at minute concentrations, which cannot induce a perceptible alteration in the local refractive index to be sensed. This is aggravated by unspecific interactions or protein corona formation that can interfere with measurements. To tackle these limitations, plasmon enhanced strategies with specific labels can provide a reliable alternative for detection of specific small molecular targets.

Plasmon Enhanced Fluorescence (PEF) – A bright synergy

Control and focus of light are a standard procedure in our daily lives. With mirrors, filters, optical fibers, waveguides, and photonic crystals, we manipulate light in microscopes, displays and countless other devices. Nonetheless, these are diffraction limited[162] and the preparation of such designs is often burdensome and restricted. Due to their inherent optical properties, plasmonic nanomaterials can function as nanoantennae for other emitters concentrating the electric field, while enabling control over the radiation direction, polarization state and tuneability of the emission spectra.[163] This is tremendously relevant considering that most emitters from atoms to molecules or even nanoparticle emitters, like QDs, have dimensions comparable or below nanometer scale (< 10 nm), but their optical cross-sections are smaller than their physical size. On the other hand, plasmonic materials have optical cross-sections that are larger than their physical cross section, which highlights their ability as optical antennas.[163] Acknowledging these features, several different strategies for signal enhancement of emitters using plasmonic materials as optical antennas have been explored.[164–166] Likewise, optical properties of plasmonic materials are also intensively studied outside the scope of sensing such as in photocatalysis, heat generation, non-linear optics… [167–170] The next section will review general aspects regarding fluorescence enhancement in metal-fluorophore assemblies and challenges of PEF. Comprehensive reviews on metal enhanced fundamentals and applications can be found elsewhere. [151,163,171–174]

Available in many colors, shapes and materials, luminescence can be seen as one of nature's brightest "inventions".[civ] Inspired and originally endowed by nature, many luminescent materials were engineered to provide us with a series of products and applications like tv screens, bioimaging, sensors... According to the excitation mechanism, luminescence can be divided into different categories, being electroluminescence, chemiluminescence and photoluminescence the most common. In photoluminescence, the atom or molecule is excited

[cii] Upgrading a microscope to darkfield from microbehunter microscopy
[ciii] What is a point spread function (psf)? From Craig Daly
https://en.wikipedia.org/wiki/Point_spread_function
[civ] Fantastic fluorescence! from Brainiac75;
Basics and principle of Fluorescence & Phosphorescence measurement from practical ninjas.

from the ground-state to the excited state by absorption of a photon (hv_{exc} ; k_{exc}) with the appropriate wavelength (Contextualization - Figure 16). After photon absorption, these excited-states can either be "singlet" (S_n , $n \geq 1$; electron spins in opposite directions) or "triplet" (T_n , $n \geq 1$; electron spins aligned in the same direction), and emission from these states to a singlet ground state (S_0) is differentiated, respectively, as fluorescence (allowed transition, timescale of ns) or phosphorescence (forbidden transition, timescales from μs to s). If excitation is performed to excited states higher than S_1, then transition between these higher excited states to lower energy excited states occurs through internal conversion, vibrational crossing, or intersystem crossing. Then, from the lower singlet excited (S_1) state,[cv] the molecule is able to relax to the ground-state through a radiative (k_r) process that results in photon emission or through a non-radiative (k_{nr}) process. The lifetime (τ) and the quantum yield (QY or Φ_f) are two photophysical parameters used to characterize the emission of luminophores:

$$\tau = \frac{1}{k_r + k_{nr}} \; and \; \Phi_f = \frac{k_r}{k_r + k_{nr}}$$

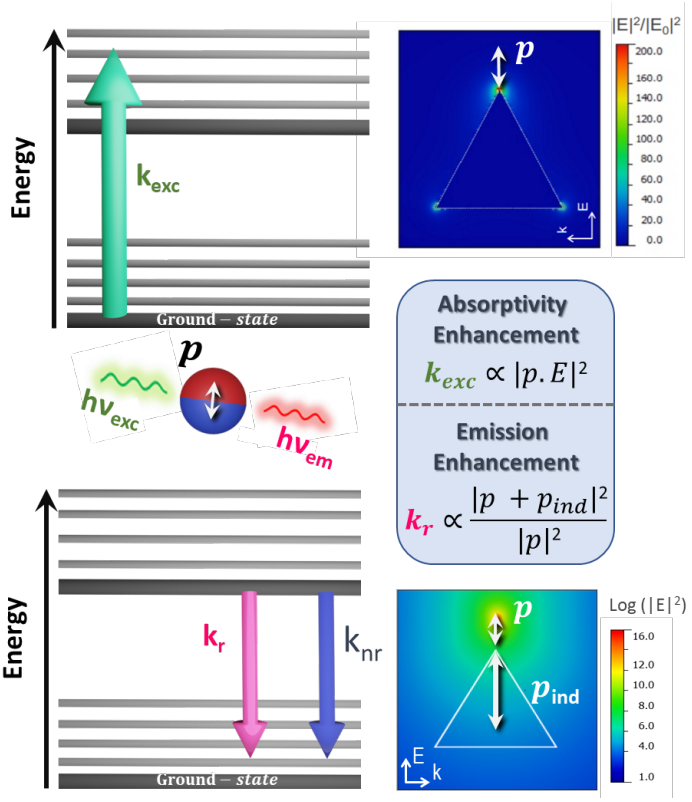

Contextualization - Figure 16 – ***Simplified Perrin-Jablonski diagram illustrating the excitation from the ground-state to an excited state and subsequent decay through radiative and non-radiative pathways****. Discrete Dipole approximation (DDA) maps illustrating the concentration of the electric field using a plasmonic triangular nanoprisms are shown as example.*

In fluorophores, the lifetime is usually in the order of nanoseconds, while in phosphorescence materials it ranges from microseconds up to seconds. Since τ is absolute, then by employing emitters that have a lifetime dependence on environmental properties, it is possible to probe

[cv] Few exceptions are known by Kasha's rule

such properties and even to perform spatial mapping, like in fluorescence lifetime imaging microscopy (FLIM).[cvi].

Plasmon resonance can contribute to enhance both excitation and emission of an emitter. Many experiments have been dedicated to understanding and optimizing the excitation-emission efficiency of plasmophores (plasmonic particle+fluorophore). From the excitation perspective, matching the LSPR peak with excitation wavelength of the fluorophore is expected to render the highest excitation efficiency, because k_{exc} benefits from the local enhanced plasmon field sometimes by orders of magnitude compared to free space. As shown in Contextualization - Figure 16 (map on the top), this effect is more pronounced at the plasmon hot-spots and closer to the metal surface. Unfortunately, from the perspective of fluorophore's emission, if the light emitter is too close to the plasmonic material, then energy transfer can occur to plasmonic modes acting as energy acceptors, thus, strongly quenching fluorescence emission. On the other hand, the dipole induced (p_{ind}) by the molecule's emitting dipole within the plasmonic material can promote the radiative decay rate (k_r) and consequently increase Φ_f. For these reasons, optimization of a plasmophore requires the adjustment of the distance and location of the emitter to obtain a compromise between optimal excitation and emission enhancements. Anisotropic nanoparticles, such as gold nanorods, present optical asymmetry due to both transversal and longitudinal modes of the LSPR, and allow for tuning the longitudinal peak wavelength, by changing the rod's aspect ratio, in order to simultaneous match the plasmon's optical spectrum to the excitation and emission wavelengths of the fluorophore.[175]

The current state-of-art of PEF systems still entails many operational and engineering challenges. Yet, the potential of PEF systems is irrefutable as it brings intrinsically weak emitters, like proteins or metal complexes obscured by low Φ_f's, back into the game, enhancing their emission up to millions of times.[176] Also, as oblique technologies arise and progress, they converge with plasmonic particles and enable materials with superior features. This can be further boosted by improvements in nanofabrication and assembling processes to render programmability through functionalization and immobilization. Irrespective of future developments, PEF detection systems are already mature enough to be considered a promising tool for early and fast diagnostics, including in portable devices.[177]

Spying on biology: Nanomaterials meet (bio)sensors

For the past few decades, the number of scientific publications on the field of nanotechnology steadily increased at a fast pace (Contextualization - Figure 17). This endowed us with versatile top-notch technologies that change our paradigms – hopefully, with many more yet to come. As we answer fundamental questions, new concepts and new technologies can be envisioned to boost our standards of living. Expectably, by operating at the same scale that most of our molecular, metabolic, and cellular phenomena, y nanotechnology has proven its worth in many biological applications and areas – from single particle/molecule fundamental studies, genetic engineering, quality control and tracking of products to countless others.

[cvi] Fluorescence Lifetime Imaging (FLIM) from Excelitas PCO

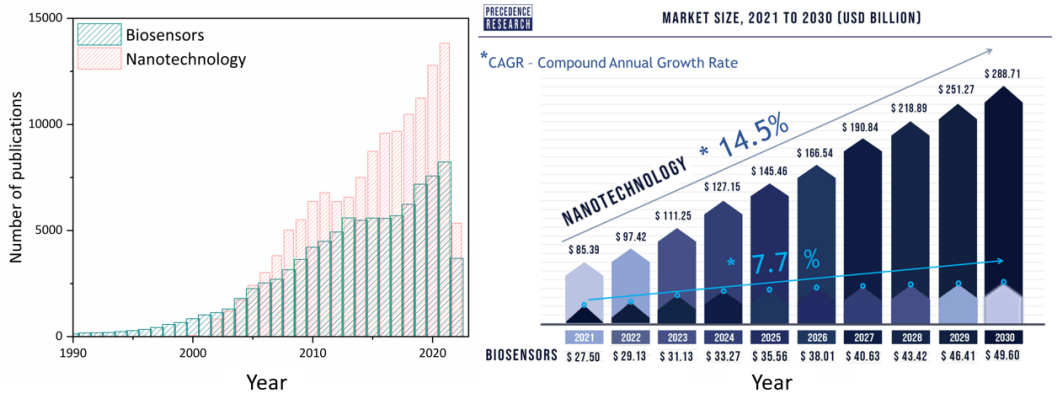

*Contextualization - Figure 17 – **Annual scientific output** of the fields of "nanotechnology" and "biosensors" – source Pubmed. Expected market size and growth from 2021-2030 of both "nanotechnology" and "biosensors" – source Precedence research*[cvii]

Conceptualized almost simultaneously, the intersection between the fields of nanotechnology and biosensors is enormous, as revealed by the almost entangled profiles of the scientific output and economic expect growth (CAGR) of both fields (Contextualization - Figure 17). Furthermore, as our understanding and control over nanofabrication and increased functionality of nanomaterials progressed, nanoparticles swiftly took over the (bio)sensors stage by merging or surpassing their organic counterparts or ultimately enabling novel applications that assess previously unreachable information.

(Bio)sensors in Healthcare: Hippocrates' little helper

Hippocrates is undisputedly the father of scientific-based Medicine. From the get-go he set guidelines to conduct the medical profession that, despite some slight updates, survived until modern days in the form of the "Hippocrates oath". [178][cviii] By denying diseases to be sort of a punishment from the gods, his non-reductionist perception recognized that the human body acts as a unique "coherent and integrated whole" organism embedded in its own physical and social environment. Remarkably, by acknowledging this he understood the transition from healthy to ill as a continuum process in opposition to an unavoidable and uncontrolled discrete event. Hippocrates fostered the importance of physician-patient relationship (Participatory and Personalized), while also stressing that "the best physician is the one who can prevent and predict". Dating from 400 BC, these revolutionary ideas led Darwin, in 1868, to write "*…I wish I had known of these views of Hippocrates before I had published, for they seem almost identical with mine - merely a change of terms" [179]. Today, these ideas still perfectly reverberate with our vision of medicine during this "-omics" era [179–182] – now popularized as P4, P5, or "P4+C^n" … [183–187]*

Throughout the course of history, medicine experienced many shifts, challenges, and advancements. Gradually, the field of medicine and treatments evolved from almost a "guessing game", full of myths and speculations, to an increasingly informed and coordinated approach.

[cvii] Biosensors market
Nanotechnology market
[cviii] Hippocratic Oath from Britannica

Living in a "post-genomic era"[cix], our knowledge and fundamental understanding about biology, chemistry and many other technological areas is infinitely extended from Hippocrates reality. Nowadays, the doctor's-patient relationship expanded beyond a mere "trustful interaction" to include a range of analytical parameters that feed critical information to enable educated decisions. This reality makes (bio)sensors a vital piece of the puzzle.

The history of (bio)sensors: unhealthy habits saving lives…

Starting with Leland Clark, the story of biosensors is rather a peculiar one. Described by Clark himself,[cx] the heart-lung machine is "a symphony of chemistry". However, in his original design, the oxygen levels in blood were monitored and evaluated merely based on its colour (redness) and, if needed, manually adjusted by trained personnel (often Clark himself). Obviously, this process was extremely inefficient and prone to human errors due to its ambiguous nature. Acknowledging this critical flaw, he actively researched different electrode designs to develop a sensor to monitor oxygen. As a solution, Clark envisioned a platinum electrode (the Clark electrode) that could sense the oxygen levels in the blood stream by converting oxygen to hydrogen peroxide and water. Naively, in his first experiments, Clark neglected the protein corona formation at the surface of the sensor, which blocked the oxygen to reach the electrode's surface. As proteins adsorbed to the surface, a quick decrease in the signal was observed even for fixed oxygen levels. Allegedly, after considering this hypothesis, his solution consisted in simply wrapping the electrode with an oxygen-permeable cellophane plastic from a pack of cigarettes.[188] This, effectively avoided proteins from reaching the surface of the sensor, while maintaining oxygen permeability and enabling continuous monitoring of the oxygen levels during cardiopulmonary bypass surgeries.[189] It comes without saying that this technology was just the "tip of the iceberg" and quickly disseminated both in space and applications.

Another of Clark's revolutionary inventions – and the first "official" biosensor – was almost an "organic" consequence of the latter. To calibrate the oxygen sensor, test solutions were deoxygenated by adding small amounts of glucose and glucose oxidase, which converted the existing oxygen into hydrogen peroxide. Intuitively, Clark realized that this principle could be used to measure glucose itself. In his first prototype, glucose oxidase was immobilized onto the oxygen electrode and the concentration of glucose (↑) was inversely proportional to the measured signal (oxygen ↓), enabling detection and quantification of glucose.[188cxi]

Since the inception of the field, as observable in the timeline (Contextualization - Figure 18), many inventions related with Bio(sensors) were created and became paramount in areas like molecular biology, quality control and healthcare. Third generation and wearable glucose sensors, which are critically important in the managing of diabetes,[cxii] are already available

[cix] Timeframe after completion of the "Human Genome Project" The Human Genome Project | Genetics | Biology from FuseSchool; Lessons from the Human Genome Project from National Human Genome Research Institute

[cx] Leland Clark from Chemical & Engineering News

[cxi] Note: Describing himself, Clark once said that his eagerness for inventing was like being a bird in flight with one wing being lifted by pure curiosity and the other one lifted by the joy of building new things and not by the applications itself.

[cxii] Today, glucose monitoring biosensors represent ~43% (~11.7B) of the total market share of biosensors (27.5B - Contextualization - Figure 17) and have an expected CAGR of ~8% - Blood Glucose Monitoring Devices Market Size from Grand view research

(Contextualization - Figure 18). Briefly, the 1st generation faced operational problems related with oxygen solubility and energy consumption,[190] in the 2nd generation this was solved by introducing redox mediators. [190] However, these mediators are highly toxic and hampered implantable and needle-type devices for continuous monitoring *in vivo*. This was fixed in the 3rd generation by using organic conducting materials that enabled direct transfer of electrons between the enzyme and the electrode.[191] These advancements in Glucose Biosensors lifted the quality standards to a reasonable portion of the 415 million (500+ millions by 2040) living with diabetes[cxiii] and continuous developments may give a glimmer of hope to others to whom they are yet unreachable.

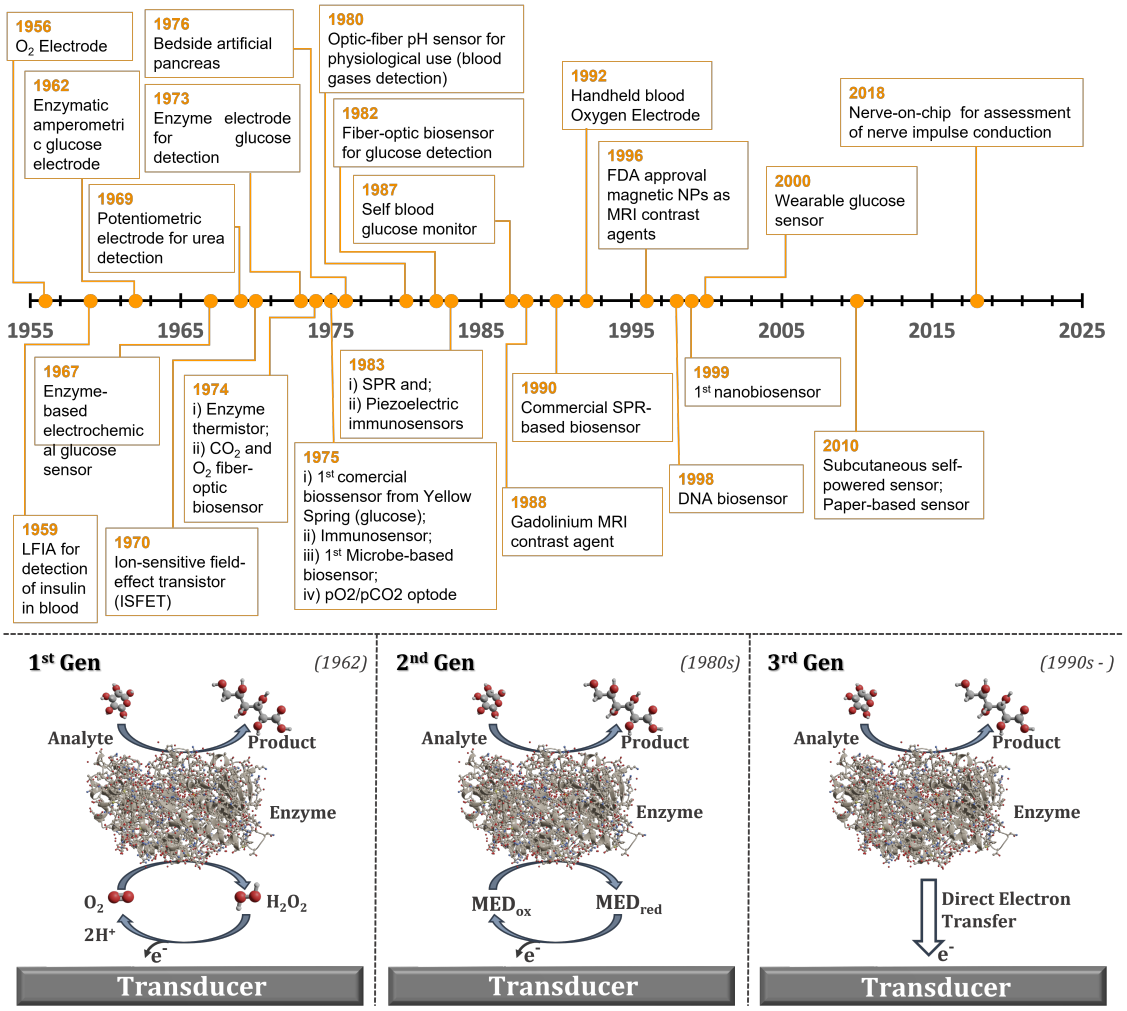

Contextualization - Figure 18 – ***Timeline of selected examples elucidating the evolution of (Bio)sensors and related achievements.***[190,192] **Different generations of glucose biosensors**. MED_{ox} and MED_{red}: Oxidized and reduced forms of mediator molecule (i.e., ferrocene or methylene blue), respectively.

A bit more than half century later and in the wake of a post-pandemic experience, stating that Clark's inventions were a game changer that shifted many of our paradigms is obvious. As witnessed in Contextualization - Figure 17 and Contextualization - Figure 18, the community was clearly motivated to thoroughly explore and develop (Bio)sensors to apply in different areas and for various purposes and contexts. However, due to an immensity of possibilities and aiming

[cxiii] World Diabetes Day from Centers for Disease Control and Prevention.

to keep within the framework of this dissertation, the next section will be dedicated to uncovering the fundamental aspects of characterizing a (bio)sensor.

(Bio)sensors 101: inspecting biology

In a broad definition, a sensor is a device or module that detects changes in physical quantities such as temperature, magnetism, light, current, and then, translates this signal to a detectable and analyzable form. In the specific case of (Bio)sensors,[cxiv] they are defined as analytical devices that produce a measurable signal that corresponds to the presence or concentration of a target analyte or physical parameter with biological relevance.

A general step-by-step representation of the workflow and molecules/materials comprising a (bio)sensor is illustrated in Contextualization - Figure 19.

1. Analyte or biomarker: is a characteristic molecule or parameter that is measured to assess the state of biological process, a pathophysiological event or to evaluate the response to a therapeutic intervention. Research focus: finding novel biomarkers, determine boundary limits, drug development... [cxv193–197]
2. Receptor:[cxvi] (not mandatory) is the component, commonly a biological-related element,[cxvii] responsible for recognizing/guiding the interaction between the analyte and the transducer. The process of "signal production" or "signal alteration" derived by the interaction analyte<->receptor is called biorecognition.
3. Transducer: a device/element that responds to the event (i.e. analyte binding receptor) or parameter (i.e. T or pH) being analysed and, consequently, produces a measurable signal. Research focus: new materials like nanoparticles and/or nanostructures and optimization of detection schemes, i.e. dark-field microscopy.
4. Read-out: is the unit used to discern the results in a readable and understandable way. Research focus: user interface, portability, energy consumption…

Starting from the range of analytes and contexts where (Bio)sensors can be a valuable tool, the combinations of designs and strategies are enormous. Considering that, ideally, a (bio)sensor should: be sensitive, deliver fast results, be "low-cost"/ "cost-effective", enable multiplexing[cxviii] and allow miniaturization/portability, four illustrative examples of were selected to be included in Contextualization - Figure 19: Bio-FET, Nanopore, Cantilever and Lateral Flow Assays.[cxix]

In a (Bio)-FET sensor, the receptors are immobilized at the sensing channel (grey wire), which connects the source (S) and drain (D) electrodes (yellow boxes). Also, a bias potential is applied and modulated to the gate electrode (big yellow box). Then, as the (charged) analytes bind to the receptors, they induce a change in the current flow between S and D, proportional to its

[cxiv] Note that within the framework of this dissertation the conventional definition of biosensor was expanded to include biological relevant parameters such as temperature, pH, ions… For disambiguation this aggregated is denoted as (Bio)sensors.

[cxv] As an output of this dissertation a "complementary chapter" "entitled "Monitoring Proteolytic Activity in Real Time" is included separately.[208]

Biomarkers: discovery, development and assay validation from Bioanalysis Zone

[cxvi] Note that some designs, may disregard the use of a receptor. An intuitive example is measuring temperature as it is measuring an environmental parameter, hence molecular recognition isn't needed.

[cxvii] Unnatural variations of biological elements can be used. For example, D-aminoacids or Locked Nucleic Acids.

[cxviii] Detecting 2 or more analytes simultaneously

[cxix] Note: magnetic and optical sensors based on fluorescence and LSPR-based sensors feel these requirements but were intentionally left out since they are presented later in the experimental sections.

concentration. [199,203] [cxx] Similarly, nanopores monitor the change in the measured current as molecules flow through them. Commonly, both sides of the pore have opposite potential to promote molecules to flow through. Besides single molecule capabilities, nanopores can also distinguish between nucleotides or protein residues, hence being valuable tools in sequencing.

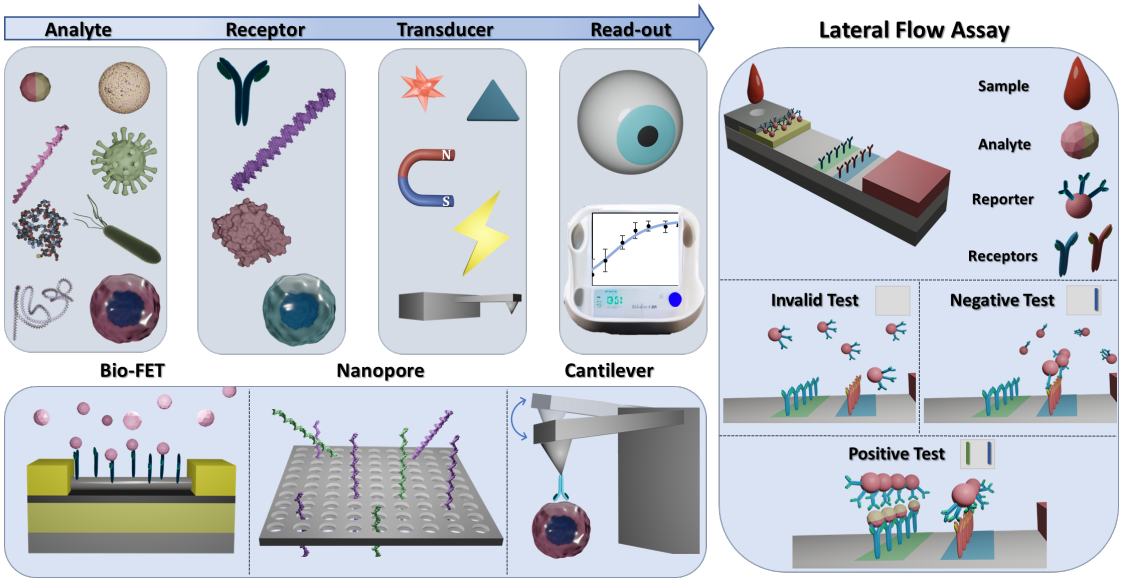

*Contextualization - Figure 19 – **General illustration of the operation principles underlying a biosensor.** A target molecule interacts with a receptor (actuator) that induces a response of the transducer method and output is evaluated – visually or digitally. Analytes (organized ↓): Ions or small molecules; RNA (Nucleic acids); Peptides and proteins; Genome; Exosomes; Virus; Bacteria; Diseased cell; Receptors: Antibody; DNA (Nucleic acids); Enzymes; Cells. Transducers: Organic Fluorophore; Plasmonic nanoparticle (optical detention); Magnetic detection; Electro-based detection; (gravimetric) Mass-based Detection;[cxxi] Read-out: "naked-eye" observation or digital reader[cxxii] . **Schematic representation of different biosensors' design**: Lateral flow Assay detection of an analyte from a blood sample using antibodies as bioreceptor and antibody-conjugated gold nanoparticles as reporters. Results are evaluated as stripes.[198][cxxiii] Bio-FET (Field-Effect Transistor-based Biosensor): Analyte is detected by changes in the electric current between source and drain electrodes.[199] Nanopore: Simultaneous detection of 2 nucleic acid chains. As Analytes flow through the hole a barcoded change in the electric current is measured.[200] Cantilever: Mapping the surface of a cell using an AFM tip functionalized with a receptor molecule.[201,202] [cxxiv] Response of the tip is proportional to the antibody interactions.*

The cantilever constitutes a good example of how humans overcome a given problem by resorting to a natural solution. While the resolution of human's vision is limited to about 40 microns in the best-case scenario, our tactile perception reaches the nanoscale (tens of nanometers).[204] With this in mind, and putting it into layman terms, Atomic Force Microscopy (AFM) can be compared to a blind person reading braille. In an AFM cantilever, the tip scans the surface and detects its defects, morphology or even chemistry. In the selected example, one may imagine a probe functionalized with a receptor molecule that it will "mildly glue" to the analyte, enabling its mapping at the surface of a single cell or a tissue.

Acknowledging that "simplicity is the ultimate sophistication", a standard lateral flow assay (LFA) was selected as key example. Accelerated by the Covid-19 pandemic, and already popularized

[cxx] nanoHUB-U Nanobiosensors from Professor Muhammad A. Alam (nanohubtechtalks) is a highly recommended "course".
[cxxi] MEMS - High Sensitivity, Cantilever Based Sensors from Panorama Synergy
[cxxii] The background image used as device was created using an "AI generative art" platform - Midjourney
[cxxiii] Lateral flow immunoassay works from Abingdon Health
[cxxiv] Atomic Force Microscopy - AFM Principle- Basic Training from Park systems

in the form of pregnancy tests, LFAs are a notable example of how bottom-up synthesis can impact our daily lives. As previously explained, the LSPR of gold nanoparticles provides them a high extinction cross section that makes them exceptionally "colorful". This makes the results more perceptible to the human eye in lower concentrations, discarding the need of any machinery. Undeniably, LFAs were a key tool enabling us taming the Covid-19 pandemic and as it gradually fades away, it can confidently be said that LFAs are here to stay…

Judging performance of (bio)sensors.

LFAs possess many of the desired perks for a (bio)sensor, yet in their simplest forms they are merely qualitative, providing only a "Yes" or "No" answer. Understandably, in many other contexts a precise and accurate quantification is paramount. A good example is the detection of cardiac troponin for diagnostic of Acute Myocardial Infarction (AMI), which is a leading cause of death and disability. Quantitation is especially relevant here given that AMI symptoms are common in emergency rooms but only 10% of those patients are diagnosed with AMI. Additionally, cardiac troponin is not a specific biomarker of AMI, and episodic events or less severe conditions can also trigger its presence in blood. For this reason, the guideline in developed countries is to measure troponin levels at least twice with an interval of 2-3 hours (a third measurement is possible after 6 hours). Only then can the patient be ruled-out – assuming the troponin level stays below the threshold or diminishes.[205,206] These prolonged waiting times come with high emotional, financial, and humanitarian costs for both patients and healthcare providers, while stressing emergency rooms.[207] This is yet another example of a fast growing billion dollar market that urges for a reliable solution.[cxxv] In this regard, solutions can comprise the development of high sensitive and specific point-of-care (POCs) devices that eventually could even integrate emergency vehicles.

Countless other examples could be cited to reason about the relevance of (Bio)sensors in healthcare, especially considering that as technologies progress novel opportunities can arise – one of such examples is the monitorization of proteolytic activity as alternative of mere quantification. The fundamentals and merits of this transition was published in the context of this dissertation and can be found in the "other relevant outputs" section.[208]

Intuitively, numerous designs of quantitative (bio)sensors can be envisioned for a given application. However, their performance and features need to be characterized based on several parameters, even to enable comparison. Personally, considering you are targeting a specific analyte individually and you know its molecular mass, rule number 1 is to evaluate in molar concentration units rather than mass. Molecular mass of biomarkers can vary by orders of magnitude and kinetic parameters are directly connected with the sensor' performance like the dissociation constant (K_D) in Molar units. This simple conversion from mass to molar makes interpretation and comparison between sensors and performance much more intuitive/friendly.

To evaluate the performance of the sensor's response to different concentrations of the target analyte (M), a dose response curve is measured from which several parameters and features can be extracted/identified – represented in Contextualization - Figure 20:

[cxxv] Troponin market size 2022-2030 (1.43b in 2021; CAGR 8.7%) from Biospace and Cardiac Biomarkers 2020-2030 (13.98 in 2021; CAGR 14.7%) from Grandview Research.

- R_B – is the "blank response", which correspondes to the sensors response to a sample without analyte (specific or non-specific). This is also denoted as "background".
- LOD – is the smallest value of concentration that can be measured with reasonable certainty and confidence. It corresponds to R_B plus 3 times the standard deviation of R_B;
- Dynamic range – corresponds to the "scale" of biomarker concentrations to which the biosensor produces a measurable response that can be addressed to a given concentration of analyte.
- Operating Range – measurable amplitude of the transducer in response to a given concentration of analyte.
- Sensitivity- corresponds to the ability of the sensor to discriminate concentrations that are proximate to each. This can be enhanced by increasing the SNR and/or the Slope.
- Specificity (selectivity) - is the ability of the sensor to responde uniquely to the target analyte or how much the sensor responds to spurious non-target molecules (represented by the orange line). This can be improved, for example, by mitigating corona formation or by a more adequate selection of biomarker<->receptor.

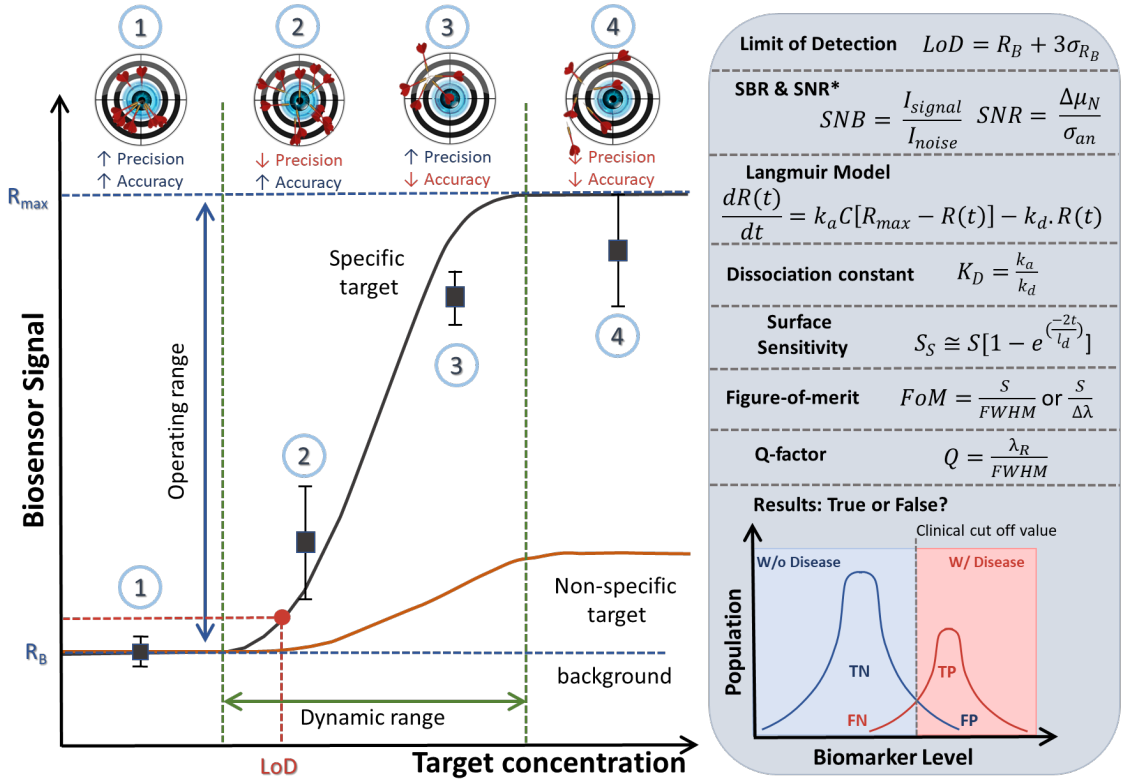

*Contextualization - Figure 20 – **Dose Response Curve**. **Illustrative curves are presented for the background (experiment from a blank sample; dashed blue), the sensors' response to a non-specific target (orange), and response to the target analyte (black)**. The Lower Detection Limit (LOD) is represented by the red dot while the dynamic range is represented in green. Accurate? Precise? Or both?... The targets depict the differences between accuracy and precision and addressed to representative values for the detection of the target analyte. Blue box: Parameters to characterize the performance of a biosensors – focused on surface-immobilized refractive index sensor. Legends: R_B – Blank result; R_{max} – maximum surface concentration of the complex, hence nº of receptors. σ_{R_B} – Standard Deviation from the blank result; SNB – signal-to-background ratio; SNR – Signal-to-noise ratio; R(t) – surface concentration of analyte-receptor complex at a given time; R_{max} – maximum surface concentration of complex (analyte – receptor); k_A and k_D -affinity and dissociation constants, respectively; k_{on} and k_{off} – rate of complex formation and complex dissociation, respectively; l_d – evanescent field decay length; FWHM – Full width at half maximum from the spectrum peak; λ_R – Resonance wavelength; TN & TP – true negative and true positive, respectively; FN & FP - false negative and false positive, respectively*

Other crucials aspects of (Bio)sensors, and also illustrated in Contextualization - Figure 20, are its precision and accuracy. As it can be seen by the dart boards and respective demonstrative results, precise sensors return values with low standard deviation, however, these values don't necessarily match the real concentration. On the other hand, results from accurate sensors compass around the real concentration but standard deviation can be elevated. Therefore, aiming for a precise and accurate (bio)sensor is the way to hit "Bullseye".

The box in Contextualization - Figure 20 elucidates how to determine other relevant features to assess the performance of (Bio)sensors – note, however, that despite these parameters being common to (bio)sensors, formulas may slightly vary across different designs. Hence, the parameters presented assume an optical sensor comprising receptors immobilized in a surface with a stoichiometry 1:1 between the receptor and analytes:

- Signal-to-background (SBR) or signal-to-noise-ratio(s)(SNR): SBR is the relationship between the signal intensity and the background intensity while the SNR corresponds to the ration between the change in the mean intensity and the "noise from the analyte" $SNR = \frac{\Delta\mu_N}{\sigma_{an}}$
- Langmuir Model: allows to estimate the number of molecules bounded to the surface receptors at a given time.
- Dissociation Constant: concentration at which 50% the receptors are bounded to the analyte and 50% are free. Selectivity can be estimated by comparing the binding affinity (K_A) of potentially competing analytes – assuming absence of unspecific binding. $K_A \approx \frac{1}{K_D}$
- Bulk (S) and Surface sensitivity (S_S): is the sensitivity of the sensor/transducer to detect changes comprising entire sensing volume (S) or the sensitivity to binding events at the surface (S_S);
- Figure-of-merit: a dimensionless number used to grade the design and optimization of the transducer characterizing the ability of the sensor to detect small changes
- Q-factor: evaluates the quality of the resonator

Regrettably these values are not always disclosed in the literature or easy to analyse. Nevertheless, determining these parameters is pivotal to comprehend, anticipate, and characterize a (Bio)sensor performance while enabling comparison with alternative strategies. Ideally an operational biosensor aims to be sensitive; selective; stable; have good and appropriate LoD; "miniaturizable" and convenient; reproducible; and have good response time (especially relevant for monitorization). Extensive coverage on Biosensors and underlying aspects can be found elsewhere.[153,209–216]

Multiplexing[cxxvi] and multiparametric capabilities is yet another aspect that can boost and benefit the performance of the (Bio)sensor. Parallelization of assays assisted by micro- and nanofluidics is often a reliable strategy for multiplexing,[217–220] however, it may require a higher amount of sample. Furthermore, in some circumstances, to evaluate synergistic aspects and/or

[cxxvi] Ability to measure multiple analytes simultaneously. Disambiguation: multiplexing can either occur in the same chamber or in parallel chambers relying for example on microfluidics.

dynamic processes related with the biomarker is more accurate if performed within the same assay which opens the possibility to unveil correlations.[221]

Furthermore, the transition between health and disease is not "black and white", thus at boundary conditions results may be misleading due to occurrence of false results – both positive and negative – as illustrated in Contextualization - Figure 20. For this reason, depending on the circumstance (analyte) and the expected performance of the (bio)sensor available, a "clinical cut off value" is established. Intuitively, this cut off value determines the boundaries of the "grey" area at which false results, therefore, if a cut off is set to avoid "false negatives", then the likelihood of rendering "false positives" increases and vice-versa. This is a critical aspect to be determined in the context of healthcare with special relevance in clinical diagnosis.

Biosensors in wellness and Healthcare: the good, the bad and the ugly…

In a world running away from a disease-centered healthcare towards wellness and precision medicine, tools to render trustworthy information are pivotal to understand and mitigate many health-related inconveniences and side-effects. As Hippocrates taught us, disease management involves care, both at the upstream level, via prevention and participation, but also downstream, through correct diagnosis, treatment, and proper adaptation. For instance, pregnancy, Covid-19, and diabetes are standard examples to portray participation of individuals in managing wellness and disease upstream. The use of (bio)sensors empowers individuals with better understanding of their own condition, and prepares them to make their own decisions, consequently, making medicine more efficient. Furthermore, (bio)sensors can also provide quality control of the environment, food, water, pharmaceuticals, hence avoiding problems related with contamination or lack of quality. Acknowledging the crucial impact that these devices can have in our daily lives and the rapid advancements in digital technologies and mobile health (m-health), ideally, (bio)sensor technologies should follow the REASSURED[222] (real-time connectivity, easy specimen collection, affordable, sensitive, specific, user-friendly, rapid, and robust, equipment-free and deliverable to end users) guidelines, often underlying the development of point-of-care (POC) or Point-of-use (POU) devices.

On the other edge, the role of (bio)sensors downstream is more intuitive, as it goes from diagnostics to adequation/personalization of treatments, and to follow-up of the disease and treatment progression.

The good: all together now

Putting into perspective, modern medicine comprises an amalgam of technologies congregating towards a better and more effective healthcare. Remote and robotics-assisted surgeries,[cxxvii] 3D bioprinting,[cxxviii] advanced and high-throughput machinery[cxxix] and many others

[cxxvii] Robot-assisted surgery brings precision, problems from CBC news
Robotic Surgery's Third Wave | T. Sloane Guy, MD from Tedx talks
Heart Surgery: Standing on the shoulders of giants | David D'Alessandro from Tedx talks
[cxxviii] 3D printing in medicine and healthcare from medical futurist
[cxxix] Next Generation Sequencing (NGS) from applied Biological Materials
Nanopore DNA sequencing from National Database
qPCRTag Analysis: High Throughput, Real-Time PCR Assay For Sc2.0 Genotyping from JOVE

are becoming increasingly available and synergistically expanding and complementing the potential of (bio)sensors in healthcare.[cxxx]

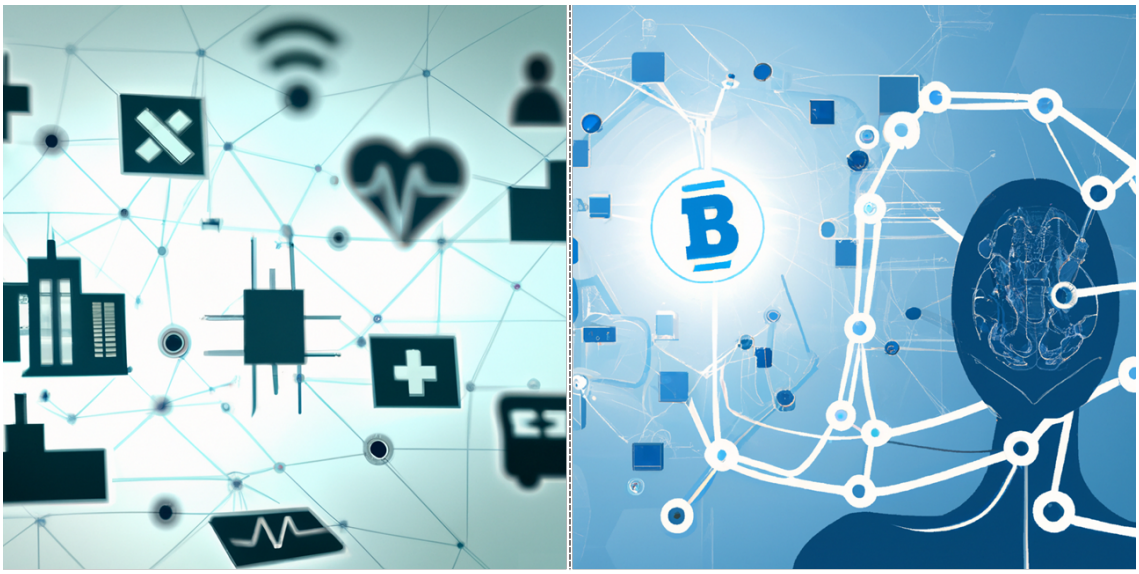

*Contextualization - Figure 21 – **AI-generated artwork of IO(M)T and Blockchain**. Images generated using Dall-E platform using the prompts "internet of medical things connected to a central entity sensing and communicating" and "healthcare sensors using blockchain to communicate."*

Additionally, maturation of IT technologies such as wireless communication,[223] machine learning and artificial intelligence (AI),[cxxxi] smart contracts and NFTs through blockchain[224–227cxxxii] for example are also positioning themselves as pivotal tools to complement and facilitate advancements in (bio)sensing via, i.e., wireless, and AI-assisted diagnostics,[228–230] Internet of Medical Things (Io(M)T),[231] data storage, privacy management and countless others (Contextualization - Figure 21).[cxxxiii]

(Bio)sensors are already intricately embedded in modern societies, and the tendency is to for them to become increasingly more reliant on tools to collect/evaluate biologically pertinent information. Hopefully, these technologies will converge and become interconnected (Contextualization - Figure 21), thus making healthcare more efficient and cost-effective boosting our standards of living.

The Bad: Managing the Hyp(e)idemics

The relevance of (bio)sensors in healthcare and wellness, directly or indirectly, is indisputable. Unfortunately, as seen many times throughout history this tends to push us to an overexcited state. Despite non-exclusive to financial and investment markets this feverish state

---

[cxxx] Here Is How Digital Health Devices Helped Me Recover From A Serious Infection From "The Medical Futurist"
[cxxxi] What's The Deal With Artificial Intelligence in Healthcare? From "The Medical Futurist"
[cxxxii] Blockchains: how can they be used? From "Simply Explained"
3 Ways How Blockchain Will Change Healthcare From "The Medical Futurist"
Note: alternative decentralized technologies such as Directed Acyclic Graph (DAG) are also emerging aiming to tackle blockchain scalability issues.
What is DAG? From "Intricity 101"
IOTA's Tangle From "Simply Explained"
[cxxxiii] The Future Of Hospitals, The Hospitals Of The Future! From "The Medical Futurist"

comes from our human natural tendency to suffer from "FOMO (fear of Missing Out)" which ultimately originates the so-called market "bubbles". Biotech and the field of (bio)sensors are not immune to these feelings. From the academic perspective, this leads to an increase of scientific publications with low-quality and low accuracy. Besides being a waste of resources, this triggers poor training and promotes "dishonesty".[232] This overwhelming list of literature makes it challenging to navigate and comprehend properly. This recalls me a lesson from Professor Teixeira Dias in which he implies that "excess of information is similar to absence of the information". Hereby, I would like to expand his idea by stating that excess of information can be even worse than absence of it, as it can create cognitive biases[233][cxxxiv] or misconceptions, or by giving the idea you can learn something useful, when eventually resulting in a mere waste of time and resources.[232,234–237] The beliefs underlying these pitfalls can expand from the Lab to the clinics and healthcare, for instance, by diagnosing non-symptomatic diseases (i.e., by genetic testing) or due to a false-positive triggered by "over testing", can increase patient stress and induce the "nocebo effect".[238][cxxxv]

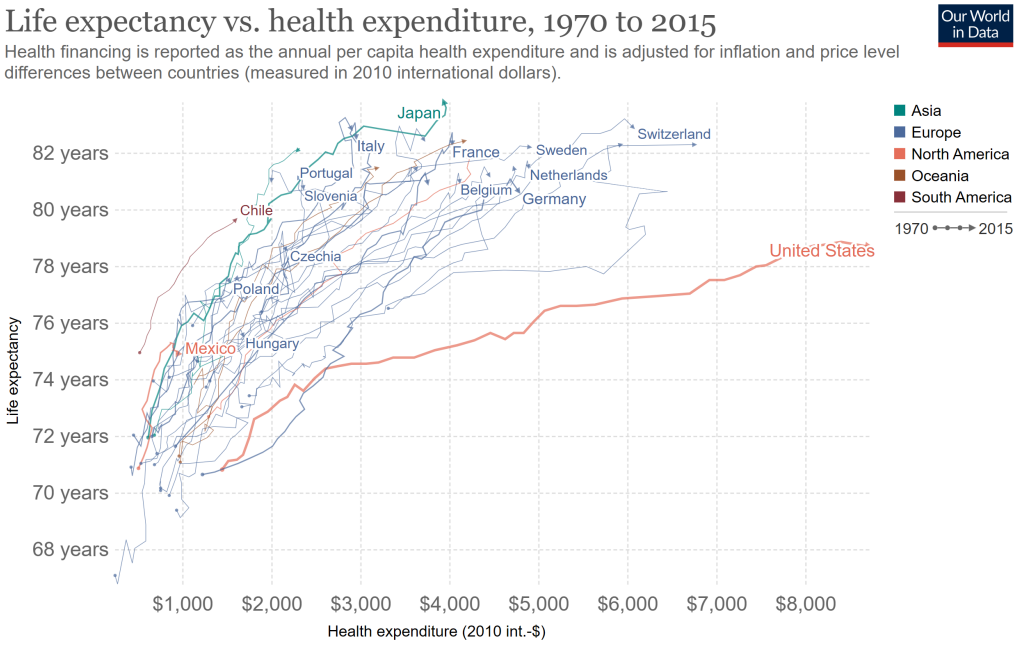

*Contextualization - Figure 22 – **Life expectancy vs. Health expenditure** - from*[cxxxvi]

Despite extremely tempting, one needs to be aware that the idea of a fully predictable and controllable medicine still lies beyond our knowledge and capabilities. And, without aiming to tame any conceptual and/or technological advancements, we should constantly perform a "reality check" to avoid waste of resources and money as it is the case of the current "biotech bubble".[239,240]

Besides the obvious downturns, this creates very poor dynamics to the space because it creates opportunities to immature projects and to skip important development steps when aiming to get extra funds. Later, the poor experience can "traumatize" the investors which leads them to

[cxxxiv] i.e., Einstellung effect From Wikipedia
Can Learning Make You Dumb? Yes From "Vsauce2"
[cxxxv] Placebos & Nocebos: How Your Brain Heals and Hurts You From "SciShow"
[cxxxvi] The link between life expectancy and health spending: Us focus from Ourworldindata.

stop investing in the ecosystem or to demand higher compensations, ultimately penalizing fresh comers arriving the market. Furthermore, to some extent, this can influence the end consumer as it may contribute to a relative increase to the cost of healthcare (Contextualization - Figure 22).[cxxxvii]

The Ugly: A grain of Salt…

Acknowledging the rapid advancement of technology experience for the past few decades, and as tempting as it may seem to be an early adopter or a 1st-mover, one should be pragmatic and remember that "slow and steady wins the race". Unfortunately, sometimes the eagerness to "leave our mark in society" combined with over excitement, results in a hyperbolic behavior searching for money and fame which is ultimately confronted with reality. This seems to be the case of Elizabeth Holmes that promised to revolutionize diagnostics and founded a company named Theranos". Recently, along with his executive manager, Elizabeth Holmes was found "guilty for defrauding investors and patients".[cxxxviii]

Contextualization - Figure 23 – ***Satirical image portraying the poor judgment and lack of "social responsibility" by many of the people and institutions involved*** *- generated by AI (Dall-E).*

The bottom line here, is not only the undeniable "hypothecation of people's lives" but also how bluntly celebrities, social journals (like Forbes and Fortune), and investors jumped – without any due diligence - to promote and endorse Elizabeth Holmes and "Theranos". This creates a sort of *Argumentum ad verecundiam*, known as Argument from authority (a type of fallacy), which feeds a self-fulfilling prophecy that pushes the least educated investors towards FOMO state and many patients that became whiling to explore novel technologies to jeopardize their own health (Contextualization - Figure 23).

Although, out of the scope of this thesis, as these technologies become foreseen, we should learn from this (and other) past event and bring to discussion, not only its impacts in our healthcare, but also win our social structures, ethics, and ultimately legislative aspects.[241–243]

[cxxxvii] Accounting for the cost of US health care From McKinsey (December 2008)
[cxxxviii] Former Theranos exec Ramesh Balwani convicted of fraud From "Politico"
Elizabeth Holmes: The 'Valley of Hype' behind the rise and fall of Theranos From "Yahoo Finance"

R4 Sensing: Reasonable, Reliable, Referable and Responsible.

Recognizing the perks and pitfalls of (Bio)sensors in modern society, and our inherent tendency to congregate ideas into acronyms, based on the information's previously exposed, hereby I rationalize about the concept of "R4 Sensing":

- Reasonable: aiming to mitigate over testing, the occurrence of false positives and stressing the patients, measurements to a given should only be performed if a satisfactory justification exists.
- Reliable: the methodology used should be reproducible and adequate to the situation.
- Referable: keeping a record of patient can be a pertinent tool in "Precision medicine". For example, a sample from a "newborn" may contain useful information, however, as mentioned previously, finding a condition can only create stress among the parents and can create conflicts about the physician-patient communication. For this reason, I propose that, assuming reasonable, sample is collected and properly stored until proven worth to measure.
- Responsible: Health will always be a top priority in a society, hence, all the players and stakeholders involved in wellness and healthcare should act responsibly and be held accountable when "promiscuous" behavior is observed.

Since history is usually the best source of lessons for the future, I believe that the mythological story of "Daedalus and Icarus" is an appropriate metaphor. As the field of nanotechnology, (bio)sensors, and synergistic technologies evolves and expands, our willingness to "escape the maze" by revolutionizing modern societies is virtually inevitable. Nevertheless, we should always keep in mind that just because we are endowed with the ability to fly, both flying low imposes the risk of drowning while flying close to the sun imposes the risk of bursting in flames. Therefore, healthcare professionals should make use the tools at their disposal responsibly, while modern-day technologists should make their best efforts to provide the appropriate sensors so that the "flying adventure" of Icarus is nothing but a smooth sail...

References – Contextualization

1. Schroeter, E. R., Cleland, T. P. & Schweitzer, M. H. Deep Time Paleoproteomics: Looking Forward. *Journal of Proteome Research* vol. 21 9–19 Preprint at https://doi.org/10.1021/acs.jproteome.1c00755 (2022).

2. Warinner, C., Korzow Richter, K. & Collins, M. J. Paleoproteomics. *Chem Rev* **122**, 13401–13446 (2022).

3. Dawkins, R. *The selfish gene*. (New edition. Oxford ; New York : Oxford University Press, 1989., 1989).

4. Finnigan, J. J. Society as a complex system: Can we find a safe and just operating space for humanity? *Journal and Proceedings of the Royal Society of New South Wales* **150**, 31–47 (2017).

5. Witze, A., Levy, A., Launius, R. D. & Seed, D. Nature Collection: 50 years since the Apollo Moon landing. https://www.nature.com/collections/bfhghadfcc (2019).

6. David Laws. Silicon Chips Take Man To The Moon. *Computer History Museum* (2019).

7. Feynman, R. P. There's Plenty of Room at the Bottom. *Eng Sci* **23**, 22–36 (1960).

8. Klabunde, K. J. *et al.* Nanocrystals as Stoichiometric Reagents with Unique Surface Chemistry. *J Phys Chem* **100**, 12142–12153 (1996).

9. Portilla, L. Functionalization of Metal Oxide Nanostructures via Self-Assembly. Implications and Applications. (2017).

10. Ding, H., Yu, S.-B., Wei, J.-S. & Xiong, H.-M. Full-Color Light-Emitting Carbon Dots with a Surface-State-Controlled Luminescence Mechanism. *ACS Nano* **10**, 484–491 (2016).

11. Kelly, J., Keegan, G. & Fournet, M. Triangular Silver Nanoparticles: Their Preparation, Functionalisation and Properties. *Acta Phys. Pol., A* **122**, 337–345 (2012).

12. Liang, M. & Yan, X. Nanozymes: From New Concepts, Mechanisms, and Standards to Applications. *Acc Chem Res* **52**, 2190–2200 (2019).

13. Monshi, A., Foroughi, M. R. & Monshi, M. Modified Scherrer Equation to Estimate More Accurately Nano-Crystallite Size Using XRD. *World Journal of Nano Science and Engineering* **2**, 154–160 (2012).

14. Hu, M. *et al.* Shaping the Assembly of Superparamagnetic Nanoparticles. *ACS Nano* **13**, 3015–3022 (2019).

15. Koplovitz, G. *et al.* Single Domain 10 nm Ferromagnetism Imprinted on Superparamagnetic Nanoparticles Using Chiral Molecules. *Small* **15**, 1804557 (2019).

16. Oliveira-Silva, R. *et al.* Temperature-responsive nanomagnetic logic gates for cellular hyperthermia. *Mater Horiz* (2019) doi:10.1039/C8MH01510D.

17. Wang, G. Nanotechnology: The New Features. (2018).

18. Dutta, D. & Bahadur, D. Influence of confinement regimes on magnetic property of pristine SnO2 quantum dots. *J Mater Chem* **22**, 24545–24551 (2012).

19. Das, R., Khan, G. G., Varma, S., Mukherjee, G. D. & Mandal, K. Effect of Quantum Confinement on Optical and Magnetic Properties of Pr–Cr-Codoped Bismuth Ferrite Nanowires. *The Journal of Physical Chemistry C* **117**, 20209–20216 (2013).

20. Zhu, S. *et al.* The photoluminescence mechanism in carbon dots (graphene quantum dots, carbon nanodots, and polymer dots): current state and future perspective. *Nano Res* **8**, 355–381 (2015).

21. Meyer, R. & Green, J. Shaping the future of nanomedicine: anisotropy in polymeric nanoparticle design: Shaping the future of nanomedicine. *Wiley Interdiscip Rev Nanomed Nanobiotechnol* **8**, (2015).

22. Baig, N., Kammakakam, I. & Falath, W. Nanomaterials: a review of synthesis methods, properties, recent progress, and challenges. *Mater Adv* **2**, 1821–1871 (2021).

23. Fu, X. *et al.* Top-down fabrication of shape-controlled, monodisperse nanoparticles for biomedical applications. *Adv Drug Deliv Rev* **132**, 169–187 (2018).

24. Tang, Z. & Wei, A. Fabrication of Anisotropic Metal Nanostructures Using Innovations in Template-Assisted Lithography. *ACS Nano* **6**, 998–1003 (2012).

25. Abid, N. *et al.* Synthesis of nanomaterials using various top-down and bottom-up approaches, influencing factors, advantages, and disadvantages: A review. *Adv Colloid Interface Sci* **300**, 102597 (2022).

26. Pearce, A. K., Wilks, T. R., Arno, M. C. & O'Reilly, R. K. Synthesis and applications of anisotropic nanoparticles with precisely defined dimensions. *Nat Rev Chem* **5**, 21–45 (2021).

27. van Embden, J., Chesman, A. S. R. & Jasieniak, J. J. The Heat-Up Synthesis of Colloidal Nanocrystals. *Chemistry of Materials* **27**, 2246–2285 (2015).

28. You, H. & Fang, J. Particle-mediated nucleation and growth of solution-synthesized metal nanocrystals: A new story beyond the LaMer curve. *Nano Today* **11**, 145–167 (2016).

29. Kwon, S. G. & Hyeon, T. Formation Mechanisms of Uniform Nanocrystals via Hot-Injection and Heat-Up Methods. *Small* **7**, 2685–2702 (2011).

30. Thanh, N. T. K., Maclean, N. & Mahiddine, S. Mechanisms of Nucleation and Growth of Nanoparticles in Solution. *Chem Rev* **114**, 7610–7630 (2014).

31. Polte, J. Fundamental growth principles of colloidal metal nanoparticles – a new perspective. *CrystEngComm* **17**, 6809–6830 (2015).

32. Li, X. *et al.* Cation/Anion Exchange Reactions toward the Syntheses of Upgraded Nanostructures: Principles and Applications. *Matter* **2**, 554–586 (2020).

33. Lim, Y., Lee, C.-H., Jun, C.-H., Kim, K. & Cheon, J. Morphology-Conserving Non-Kirkendall Anion Exchange of Metal Oxide Nanocrystals. *J Am Chem Soc* **142**, 9130–9134 (2020).

34. Rivest, J. B. & Jain, P. K. Cation exchange on the nanoscale: an emerging technique for new material synthesis, device fabrication, and chemical sensing. *Chem Soc Rev* **42**, 89–96 (2013).

35. LaMer, V. K. & Dinegar, R. H. Theory, Production and Mechanism of Formation of Monodispersed Hydrosols. *J Am Chem Soc* **72**, 4847–4854 (1950).

36. Talapin, D. v, Rogach, A. L., Haase, M. & Weller, H. Evolution of an Ensemble of Nanoparticles in a Colloidal Solution: Theoretical Study. *J Phys Chem B* **105**, 12278–12285 (2001).

37. Kwon, S. G. *et al.* Kinetics of Monodisperse Iron Oxide Nanocrystal Formation by "Heating-Up" Process. *J Am Chem Soc* **129**, 12571–12584 (2007).

38. Ghorpade, U. *et al.* Towards environmentally benign approaches for the synthesis of CZTSSe nanocrystals by a hot injection method: a status review. *Chemical Communications* **50**, 11258–11273 (2014).

39. Salzmann, B. B. v, van der Sluijs, M. M., Soligno, G. & Vanmaekelbergh, D. Oriented Attachment: From Natural Crystal Growth to a Materials Engineering Tool. *Acc Chem Res* **54**, 787–797 (2021).

40. Hiemenz, P. C. & Rajagopalan, R. *Principles of Colloid and Surface Chemistry, Revised and Expanded*. (CRC Press, 2016). doi:10.1201/9781315274287.

41. Kim, B. H. *et al.* Large-Scale Synthesis of Uniform and Extremely Small-Sized Iron Oxide Nanoparticles for High-Resolution T1 Magnetic Resonance Imaging Contrast Agents. *J Am Chem Soc* **133**, 12624–12631 (2011).

42. Park, J. *et al.* Ultra-large-scale syntheses of monodisperse nanocrystals. *Nat Mater* **3**, 891–895 (2004).

43. Bronstein, L. M. *et al.* Influence of Iron Oleate Complex Structure on Iron Oxide Nanoparticle Formation. *Chemistry of Materials* **19**, 3624–3632 (2007).

44. PEARSON, R. G. Hard and Soft Acids and Bases. in *Survey of Progress in Chemistry* (ed. SCOTT, A. F.) vol. 5 1–52 (Elsevier, 1969).

45. Mozaffari, S. *et al.* The role of nanoparticle size and ligand coverage in size focusing of colloidal metal nanoparticles. *Nanoscale Adv.* **1**, 4052–4066 (2019).

46. Reiss, H. The Growth of Uniform Colloidal Dispersions. *J Chem Phys* **19**, 482–487 (1951).

47. Watzky, M. A. & Finke, R. G. Transition Metal Nanocluster Formation Kinetic and Mechanistic Studies. A New Mechanism When Hydrogen Is the Reductant: Slow, Continuous Nucleation and Fast Autocatalytic Surface Growth. *J Am Chem Soc* **119**, 10382–10400 (1997).

48. Ivaskovic, P. *et al.* Spectral dependence of plasmon-enhanced fluorescence in a hollow nanotriangle assembled by DNA origami: towards plasmon assisted energy transfer. *Nanoscale* **10**, 16568–16573 (2018).

49. Jia, C.-J. *et al.* Large-Scale Synthesis of Single-Crystalline Iron Oxide Magnetic Nanorings. *J Am Chem Soc* **130**, 16968–16977 (2008).

50. Lim, D.-K. *et al.* Highly uniform and reproducible surface-enhanced Raman scattering from DNA-tailorable nanoparticles with 1-nm interior gap. *Nat Nanotechnol* **6**, 452–460 (2011).

51. Chatterjee, S. *et al.* Manipulating acoustic and plasmonic modes in gold nanostars. *Nanoscale Adv.* **1**, 2690–2698 (2019).

52. Chen, X. *et al.* Engineering of Yin Yang-like nanocarriers for varisized guest delivery and synergistic eradication of patient-derived hepatocellular carcinoma. *Nanoscale Horiz.* **4**, 1046–1055 (2019).

53. Wang, F., Cheng, S., Bao, Z. & Wang, J. Anisotropic Overgrowth of Metal Heterostructures Induced by a Site-Selective Silica Coating. *Angewandte Chemie International Edition* **52**, 10344–10348 (2013).

54. Botequim, D. *et al.* Fluorescent dye nano-assemblies by thiol attachment directed to the tips of gold nanorods for effective emission enhancement. *Nanoscale* **12**, 6334–6345 (2020).

55. Engelbrekt, C., Jensen, P. S., Sørensen, K. H., Ulstrup, J. & Zhang, J. Complexity of Gold Nanoparticle Formation Disclosed by Dynamics Study. *The Journal of Physical Chemistry C* **117**, 11818–11828 (2013).

56. Leffler, V., Ehlert, S., Förster, B., Dulle, M. & Förster, S. Nanoparticle Heat-Up Synthesis: In Situ X-ray Diffraction and Extension from Classical to Nonclassical Nucleation and Growth Theory. *ACS Nano* **15**, 840–856 (2021).

57. Abécassis, B. *et al.* Real-Time in Situ Probing of High-Temperature Quantum Dots Solution Synthesis. *Nano Lett* **15**, 2620–2626 (2015).

58. Kovnir, K. Predictive Synthesis. *Chemistry of Materials* **33**, 4835–4841 (2021).

59. Kim, E. *et al.* Materials Synthesis Insights from Scientific Literature via Text Extraction and Machine Learning. *Chemistry of Materials* **29**, 9436–9444 (2017).

60. Kim, E. *et al.* Machine-learned and codified synthesis parameters of oxide materials. *Sci Data* **4**, 170127 (2017).

61. McElfresh, C., Harrington, T. & Vecchio, K. S. Application of a novel new multispectral nanoparticle tracking technique. *Meas Sci Technol* **29**, 065002 (2018).

62. Wang, X. *et al.* Continuous Synthesis of Hollow High-Entropy Nanoparticles for Energy and Catalysis Applications. *Advanced Materials* **32**, 2002853 (2020).

63. Gupta, S. K. & Mao, Y. Recent Developments on Molten Salt Synthesis of Inorganic Nanomaterials: A Review. *The Journal of Physical Chemistry C* **125**, 6508–6533 (2021).

64. de Oliveira, P. F. M., Torresi, R. M., Emmerling, F. & Camargo, P. H. C. Challenges and opportunities in the bottom-up mechanochemical synthesis of noble metal nanoparticles. *J Mater Chem A Mater* **8**, 16114–16141 (2020).

65. Miao, Y. *et al.* Solvent-free bottom-up patterning of zeolitic imidazolate frameworks. *Nat Commun* **13**, 420 (2022).

66. Rivest, J. B. & Jain, P. K. Cation exchange on the nanoscale: an emerging technique for new material synthesis, device fabrication, and chemical sensing. *Chem Soc Rev* **42**, 89–96 (2013).

67. Li, X. *et al.* Cation/Anion Exchange Reactions toward the Syntheses of Upgraded Nanostructures: Principles and Applications. *Matter* **2**, 554–586 (2020).

68. Lim, Y., Lee, C.-H., Jun, C.-H., Kim, K. & Cheon, J. Morphology-Conserving Non-Kirkendall Anion Exchange of Metal Oxide Nanocrystals. *J Am Chem Soc* **142**, 9130–9134 (2020).

69. Yarbrough, R., Davis, K., Dawood, S. & Rathnayake, H. A sol–gel synthesis to prepare size and shape-controlled mesoporous nanostructures of binary (II–VI) metal oxides. *RSC Adv* **10**, 14134–14146 (2020).

70. Liu, H., He, Z., Jiang, L.-P. & Zhu, J.-J. Microwave-Assisted Synthesis of Wavelength-Tunable Photoluminescent Carbon Nanodots and Their Potential Applications. *ACS Appl Mater Interfaces* **7**, 4913–4920 (2015).

71. Tighe, C. J., Cabrera, R. Q., Gruar, R. I. & Darr, J. A. Scale Up Production of Nanoparticles: Continuous Supercritical Water Synthesis of Ce–Zn Oxides. *Ind Eng Chem Res* **52**, 5522–5528 (2013).

72. Marks, L. D. & Peng, L. Nanoparticle shape, thermodynamics and kinetics. *Journal of Physics Condensed Matter* vol. 28 Preprint at https://doi.org/10.1088/0953-8984/28/5/053001 (2016).

73. Zhang, J. & Zeng, H. Intermolecular and Surface Interactions in Engineering Processes. *Engineering* vol. 7 63–83 Preprint at https://doi.org/10.1016/j.eng.2020.08.017 (2021).

74. Kim, K. *et al.* Processable high internal phase Pickering emulsions using depletion attraction. *Nat Commun* **8**, (2017).

75. Meyer, E. E., Rosenberg, K. J. & Israelachvili, J. Recent progress in understanding hydrophobic interactions. *Proceedings of the National Academy of Sciences* (2006).

76. Merk, V. *et al.* In situ non-DLVO stabilization of surfactant-free, plasmonic gold nanoparticles: Effect of Hofmeister's anions. *Langmuir* **30**, 4213–4222 (2014).

77. Oliveira-Silva, R., Pinto da Costa, J., Vitorino, R. & Daniel-da-Silva, A. L. Magnetic chelating nanoprobes for enrichment and selective recovery of metalloproteases from human saliva. *J Mater Chem B* **3**, 238–249 (2015).

78. Carrola, J. *et al.* Metabolomics of silver nanoparticles toxicity in HaCaT cells: structure–activity relationships and role of ionic silver and oxidative stress. *Nanotoxicology* **10**, 1105–1117 (2016).

79. Geißler, D., Nirmalananthan-Budau, N., Scholtz, L., Tavernaro, I. & Resch-Genger, U. Analyzing the surface of functional nanomaterials-how to quantify the total and derivatizable number of functional groups and ligands. *Microchimica Acta* **188**, (2021).

80. Madamsetty, V. S., Paul, M. K., Mukherjee, A. & Mukherjee, S. Functionalization of Nanomaterials and Their Application in Melanoma Cancer Theranostics. *ACS Biomater Sci Eng* **6**, 167–181 (2020).

81. Sanità, G., Carrese, B. & Lamberti, A. Nanoparticle Surface Functionalization: How to Improve Biocompatibility and Cellular Internalization. *Frontiers in Molecular Biosciences* vol. 7 Preprint at https://doi.org/10.3389/fmolb.2020.587012 (2020).

82. Heuer-Jungemann, A. *et al.* The Role of Ligands in the Chemical Synthesis and Applications of Inorganic Nanoparticles. *Chem Rev* **119**, 4819–4880 (2019).

83. da Costa, J. P., Oliveira-Silva, R., Daniel-da-Silva, A. L. & Vitorino, R. Bionanoconjugation for Proteomics applications — An overview. *Biotechnol Adv* **32**, 952–970 (2014).

84. Bilal, M., Asgher, M., Cheng, H., Yan, Y. & Iqbal, H. M. N. Multi-point enzyme immobilization, surface chemistry, and novel platforms: a paradigm shift in biocatalyst design. *Critical Reviews in Biotechnology* vol. 39 202–219 Preprint at https://doi.org/10.1080/07388551.2018.1531822 (2019).

85. Park, S. J. Protein–nanoparticle interaction: Corona formation and conformational changes in proteins on nanoparticles. *International Journal of Nanomedicine* vol. 15 5783–5802 Preprint at https://doi.org/10.2147/IJN.S254808 (2020).

86. Wheeler, K. E. *et al.* Environmental dimensions of the protein corona. *Nat Nanotechnol* **16**, 617–629 (2021).

87. Yang, J., Lee, J. Y. & Ying, J. Y. Phase transfer and its applications in nanotechnology. *Chem Soc Rev* **40**, 1672–1696 (2011).

88. Cook, E., Labiento, G. & Chauhan, B. P. S. Fundamental methods for the phase transfer of nanoparticles. *Molecules* vol. 26 Preprint at https://doi.org/10.3390/molecules26206170 (2021).

89. Avugadda, S. K. *et al.* Highly Emitting Perovskite Nanocrystals with 2-Year Stability in Water through an Automated Polymer Encapsulation for Bioimaging. *ACS Nano* (2022) doi:10.1021/acsnano.2c01556.

90. Morales, M. A. & Halpern, J. M. Guide to Selecting a Biorecognition Element for Biosensors. *Bioconjug Chem* **29**, 3231–3239 (2018).

91. Yang, J., Li, L. & Kopeček, J. Biorecognition: A key to drug-free macromolecular therapeutics. *Biomaterials* vols 190–191 11–23 Preprint at https://doi.org/10.1016/j.biomaterials.2018.10.007 (2019).

92. Vandooren, J., Opdenakker, G., Loadman, P. M. & Edwards, D. R. Proteases in cancer drug delivery. *Advanced Drug Delivery Reviews* vol. 97 144–155 Preprint at https://doi.org/10.1016/j.addr.2015.12.020 (2016).

93. Rico, F., Russek, A., González, L., Grubmüller, H. & Scheuring, S. Heterogeneous and rate-dependent streptavidin–biotin unbinding revealed by high-speed force spectroscopy and atomistic simulations. *Proc Natl Acad Sci U S A* **116**, 6594–6601 (2019).

94. Xie, J. *et al.* Cell-Penetrating Peptides in Diagnosis and Treatment of Human Diseases: From Preclinical Research to Clinical Application. *Frontiers in Pharmacology* vol. 11 Preprint at https://doi.org/10.3389/fphar.2020.00697 (2020).

95. Ding, F. *et al.* Antifouling and pH-Responsive Poly(Carboxybetaine)-Based Nanoparticles for Tumor Cell Targeting. *Front Chem* **7**, (2019).

96. Chen, Q. *et al.* Impact of Antifouling PEG Layer on the Performance of Functional Peptides in Regulating Cell Behaviors. *J Am Chem Soc* **141**, 16772–16780 (2019).

97. Wang, Y. *et al.* Multicolor Super-Resolution Microscopy of Protein Corona on Single Nanoparticles. *ACS Appl Mater Interfaces* **14**, 37345–37355 (2022).

98. Woythe, L., Madhikar, P., Feiner-Gracia, N., Storm, C. & Albertazzi, L. A Single-Molecule View at Nanoparticle Targeting Selectivity: Correlating Ligand Functionality and Cell Receptor Density. *ACS Nano* **16**, 3785–3796 (2022).

99. Tenzer, S. *et al.* Rapid formation of plasma protein corona critically affects nanoparticle pathophysiology. *Nat Nanotechnol* **8**, 772–781 (2013).

100. Tweney, R. D. Discovering Discovery: How Faraday Found the First Metallic Colloid. *Perspectives on Science* **14**, 97–121 (2006).

101. Faraday, M. The Bakerian Lecture: Experimental Relations of Gold (and Other Metals) to Light. *Philosophical Transactions of the Royal Society of London Series I* **147**, 145–181 (1857).

102. Kimling, J. *et al.* Turkevich Method for Gold Nanoparticle Synthesis Revisited. *J Phys Chem B* **110**, 15700–15707 (2006).

103. Turkevich, J., Stevenson, P. C. & Hillier, J. A study of the nucleation and growth processes in the synthesis of colloidal gold. *Discuss Faraday Soc* **11**, 55–75 (1951).

104. Piella, J., Bastús, N. G. & Puntes, V. Size-Controlled Synthesis of Sub-10-nanometer Citrate-Stabilized Gold Nanoparticles and Related Optical Properties. *Chemistry of Materials* **28**, 1066–1075 (2016).

105. Poolakkandy, R. R. & Menamparambath, M. M. Soft-template-assisted synthesis: a promising approach for the fabrication of transition metal oxides. *Nanoscale Adv* **2**, 5015–5045 (2020).

106. Liu, Y., Goebl, J. & Yin, Y. Templated synthesis of nanostructured materials. *Chem Soc Rev* **42**, 2610–2653 (2013).

107. Murphy, C. J. *et al.* Anisotropic Metal Nanoparticles: Synthesis, Assembly, and Optical Applications. *J Phys Chem B* **109**, 13857–13870 (2005).

108. Piaskowski, J. & Bourret, G. R. Electrochemical Synthesis of Plasmonic Nanostructures. *Molecules* **27**, (2022).

109. Zijlstra, P., Bullen, C., Chon, J. W. M. & Gu, M. High-Temperature Seedless Synthesis of Gold Nanorods. *J Phys Chem B* **110**, 19315–19318 (2006).

110. Singh, G., Myasnichenko, V. S. & Glomm, W. R. New insights into size-controlled reproducible synthesis of anisotropic Fe3O4 nanoparticles: the importance of the reaction environment. *Mater. Adv.* **1**, 1077–1082 (2020).

111. Hu, X., Lu, C., Wang, Q., Xu, J. & Cui, Y. A high-precision, template-assisted, anisotropic wet etching method for fabricating perovskite microstructure arrays. *RSC Adv.* **10**, 38220–38226 (2020).

112. Sano, K., Ishida, Y. & Aida, T. Synthesis of Anisotropic Hydrogels and Their Applications. *Angewandte Chemie International Edition* **57**, 2532–2543 (2018).

113. Rodriguez-Abreu, C. *et al.* A combination of hard and soft templating for the fabrication of silica hollow microcoils with nanostructured walls. *Nanoscale Res Lett* **6**, (2011).

114. Mdluli, P. S. *et al.* Selective adsorption of PVP on the surface of silver nanoparticles: A molecular dynamics study. *J Mol Struct* **1004**, 131–137 (2011).

115. Kou, X. *et al.* Glutathione- and Cysteine-Induced Transverse Overgrowth on Gold Nanorods. *J Am Chem Soc* **129**, 6402–6404 (2007).

116. Xia, Y., Xiong, Y., Lim, B. & Skrabalak, S. E. Shape-controlled synthesis of metal nanocrystals: Simple chemistry meets complex physics? *Angewandte Chemie - International Edition* vol. 48 60–103 Preprint at https://doi.org/10.1002/anie.200802248 (2009).

117. Smith, D. K. & Korgel, B. A. The Importance of the CTAB Surfactant on the Colloidal Seed-Mediated Synthesis of Gold Nanorods. *Langmuir* **24**, 644–649 (2008).

118. Scarabelli, L., Coronado-Puchau, M., Giner-Casares, J. J., Langer, J. & Liz-Marzán, L. M. Monodisperse Gold Nanotriangles: Size Control, Large-Scale Self-Assembly, and Performance in Surface-Enhanced Raman Scattering. *ACS Nano* **8**, 5833–5842 (2014).

119. Zhang, Q. *et al.* Intertwining Roles of Silver Ions, Surfactants, and Reducing Agents in Gold Nanorod Overgrowth: Pathway Switch between Silver Underpotential Deposition and Gold-Silver Codeposition. *Chemistry of Materials* **28**, 2728–2741 (2016).

120. Ye, W. *et al.* CTAB Stabilizes Silver on Gold Nanorods. *Chemistry of Materials* **32**, 1650–1656 (2020).

121. Scarabelli, L., Sánchez-Iglesias, A., Pérez-Juste, J. & Liz-Marzán, L. M. A 'Tips and Tricks' Practical Guide to the Synthesis of Gold Nanorods. *Journal of Physical Chemistry Letters* **6**, 4270–4279 (2015).

122. Scarabelli, L. & Liz-Marzán, L. M. An Extended Protocol for the Synthesis of Monodisperse Gold Nanotriangles. *ACS Nano* **15**, 18600–18607 (2021).

123. Zhang, X., Fu, Q., Duan, H., Song, J. & Yang, H. Janus Nanoparticles: From Fabrication to (Bio)Applications. *ACS Nano* vol. 15 6147–6191 Preprint at https://doi.org/10.1021/acsnano.1c01146 (2021).

124. Su, H. *et al.* Janus particles: design, preparation, and biomedical applications. *Materials Today Bio* vol. 4 Preprint at https://doi.org/10.1016/j.mtbio.2019.100033 (2019).

125. Lattuada, M. & Hatton, T. A. Synthesis, properties and applications of Janus nanoparticles. *Nano Today* vol. 6 286–308 Preprint at https://doi.org/10.1016/j.nantod.2011.04.008 (2011).

126. Huang, Z., Gong, J. & Nie, Z. Symmetry-Breaking Synthesis of Multicomponent Nanoparticles. *Acc Chem Res* **52**, 1125–1133 (2019).

127. Ghosh Chaudhuri, R. & Paria, S. Core/shell nanoparticles: Classes, properties, synthesis mechanisms, characterization, and applications. *Chemical Reviews* vol. 112 2373–2433 Preprint at https://doi.org/10.1021/cr100449n (2012).

128. Wang, G., Zhang, Y., Liang, X., Takarada, T. & Maeda, M. Regioselective DNA Modification and Directed Self-Assembly of Triangular Gold Nanoplates. *Nanomaterials* vol. 9 Preprint at https://doi.org/10.3390/nano9040581 (2019).

129. Wang, M. *et al.* Programmable Assembly of Nano-architectures through Designing Anisotropic DNA Origami Patches. *Angewandte Chemie* **132**, 6451–6458 (2020).

130. Choueiri, R. M. *et al.* Surface patterning of nanoparticles with polymer patches. *Nature* **538**, 79–83 (2016).

131. Wu, W. & Pauly, M. Chiral plasmonic nanostructures: Recent advances in their synthesis and applications. *Materials Advances* vol. 3 186–215 Preprint at https://doi.org/10.1039/d1ma00915j (2022).

132. Kahn, J. S. & Gang, O. Designer Nanomaterials through Programmable Assembly. *Angewandte Chemie - International Edition* vol. 61 Preprint at https://doi.org/10.1002/anie.202105678 (2022).

133. Sun, M. *et al.* Chirality at nanoscale for bioscience. *Chemical Science* vol. 13 3069–3081 Preprint at https://doi.org/10.1039/d1sc06378b (2022).

134. Kumar, R. *et al.* Determination of the Aspect-ratio Distribution of Gold Nanorods in a Colloidal Solution using UV-visible absorption spectroscopy. *Sci Rep* **9**, 17469 (2019).

135. González-Rubio, G. *et al.* Femtosecond laser reshaping yields gold nanorods with ultranarrow surface plasmon resonances. *Science (1979)* **358**, 640 LP – 644 (2017).

136. Ma, Z., Mohapatra, J., Wei, K., Liu, J. P. & Sun, S. Magnetic Nanoparticles: Synthesis, Anisotropy, and Applications. *Chemical Reviews* Preprint at https://doi.org/10.1021/acs.chemrev.1c00860 (2021).

137. Lisjak, D. & Mertelj, A. Anisotropic magnetic nanoparticles: A review of their properties, syntheses and potential applications. *Progress in Materials Science* vol. 95 286–328 Preprint at https://doi.org/10.1016/j.pmatsci.2018.03.003 (2018).

138. Noh, S. H. *et al.* Nanoscale magnetism control via surface and exchange anisotropy for optimized ferrimagnetic hysteresis. *Nano Lett* **12**, 3716–3721 (2012).

139. Berger, L., Labaye, Y., Tamine, M. & Coey, J. M. D. Ferromagnetic nanoparticles with strong surface anisotropy: Spin structures and magnetization processes. *Phys Rev B Condens Matter Mater Phys* **77**, (2008).

140. Lee, J. S., Cha, J. M., Yoon, H. Y., Lee, J. K. & Kim, Y. K. Magnetic multi-granule nanoclusters: A model system that exhibits universal size effect of magnetic coercivity. *Sci Rep* **5**, (2015).

141. Oehlsen, O., Cervantes-Ramírez, S. I., Cervantes-Avilés, P. & Medina-Velo, I. A. Approaches on Ferrofluid Synthesis and Applications: Current Status and Future Perspectives. *ACS Omega* **7**, 3134–3150 (2022).

142. Zhou, H., Mayorga-Martinez, C. C., Pané, S., Zhang, L. & Pumera, M. Magnetically Driven Micro and Nanorobots. *Chemical Reviews* vol. 121 4999–5041 Preprint at https://doi.org/10.1021/acs.chemrev.0c01234 (2021).

143. Kang, J. H. *et al.* An extracorporeal blood-cleansing device for sepsis therapy. *Nat Med* **20**, 1211–1216 (2014).

144. Wavhale, R. D. *et al.* Water-powered self-propelled magnetic nanobot for rapid and highly efficient capture of circulating tumor cells. *Commun Chem* **4**, (2021).

145. Callaway, J. & Ritchie, R. H. Plasma Losses by Fast Electrons in Thin Films*. *Physical Reviews* **106**, 874–881 (1957).

146. Luther, J. M., Jain, P. K., Ewers, T. & Alivisatos, A. P. Localized surface plasmon resonances arising from free carriers in doped quantum dots. *Nat Mater* **10**, 361–366 (2011).

147. Brazil, R. Plasmonic Color Makes a Comeback. *ACS Cent Sci* **6**, 332–335 (2020).

148. Tan, S. J. *et al.* Plasmonic color palettes for photorealistic printing with aluminum nanostructures. *Nano Lett* **14**, 4023–4029 (2014).

149. Schlather, A. E., Gieri, P., Robinson, M., Centeno, S. A. & Manjavacas, A. Nineteenth-century nanotechnology: The plasmonic properties of daguerreotypes. *Proc Natl Acad Sci U S A* **116**, 13791–13798 (2019).

150. Neubrech, F., Duan, X. & Liu, N. *Dynamic plasmonic color generation enabled by functional materials*. *Sci. Adv* vol. 6 https://www.science.org (2020).

151. Yu, H., Peng, Y., Yang, Y. & Li, Z. Y. Plasmon-enhanced light–matter interactions and applications. *npj Computational Materials* vol. 5 Preprint at https://doi.org/10.1038/s41524-019-0184-1 (2019).

152. Mitra, S. & Basak, M. Diverse bio-sensing and therapeutic applications of plasmon enhanced nanostructures. *Materials Today* vol. 57 225–261 Preprint at https://doi.org/10.1016/j.mattod.2022.05.023 (2022).

153. Altug, H., Oh, S. H., Maier, S. A. & Homola, J. Advances and applications of nanophotonic biosensors. *Nature Nanotechnology* vol. 17 5–16 Preprint at https://doi.org/10.1038/s41565-021-01045-5 (2022).

154. Bai, X. *et al.* The basic properties of gold nanoparticles and their applications in tumor diagnosis and treatment. *International Journal of Molecular Sciences* vol. 21 Preprint at https://doi.org/10.3390/ijms21072480 (2020).

155. Zheng, J. *et al.* Gold Nanorods: The Most Versatile Plasmonic Nanoparticles. *Chemical Reviews* vol. 121 13342–13453 Preprint at https://doi.org/10.1021/acs.chemrev.1c00422 (2021).

156. Kim, M., Lee, J. H. & Nam, J. M. Plasmonic Photothermal Nanoparticles for Biomedical Applications. *Advanced Science* vol. 6 Preprint at https://doi.org/10.1002/advs.201900471 (2019).

157. Lee, S. A. & Link, S. Chemical Interface Damping of Surface Plasmon Resonances. *Acc Chem Res* **54**, 1950–1960 (2021).

158. Zijlstra, P., Paulo, P. M. R. & Orrit, M. Optical detection of single non-absorbing molecules using the surface plasmon resonance of a gold nanorod. *Nat Nanotechnol* **7**, 379–382 (2012).

159. Becker, J., Trügler, A., Jakab, A., Hohenester, U. & Sönnichsen, C. The Optimal Aspect Ratio of Gold Nanorods for Plasmonic Bio-sensing. *Plasmonics* **5**, 161–167 (2010).

160. Beuwer, M. A., Prins, M. W. J. & Zijlstra, P. Stochastic Protein Interactions Monitored by Hundreds of Single-Molecule Plasmonic Biosensors. *Nano Lett* **15**, 3507–3511 (2015).

161. Horáček, M., Armstrong, R. E. & Zijlstra, P. Heterogeneous Kinetics in the Functionalization of Single Plasmonic Nanoparticles. *Langmuir* **34**, 131–138 (2018).

162. Gray, N. Knowing the limit. *Nat Cell Biol* **11**, S8–S8 (2009).

163. Ming, T., Chen, H., Jiang, R., Li, Q. & Wang, J. Plasmon-controlled fluorescence: Beyond the intensity enhancement. *Journal of Physical Chemistry Letters* vol. 3 191–202 Preprint at https://doi.org/10.1021/jz201392k (2012).

164. Pienpinijtham, P., Kitahama, Y. & Ozaki, Y. Progress of tip-enhanced Raman scattering for the last two decades and its challenges in very recent years. *Nanoscale* vol. 14 5265–5288 Preprint at https://doi.org/10.1039/d2nr00274d (2022).

165. Langer, J. *et al.* Present and future of surface-enhanced Raman scattering. *ACS Nano* vol. 14 28–117 Preprint at https://doi.org/10.1021/acsnano.9b04224 (2020).

166. Park, W., Lu, D. & Ahn, S. Plasmon enhancement of luminescence upconversion. *Chem Soc Rev* **44**, 2940–2962 (2015).

167. Jang, Y. H. *et al.* Plasmonic Solar Cells: From Rational Design to Mechanism Overview. *Chemical Reviews* vol. 116 14982–15034 Preprint at https://doi.org/10.1021/acs.chemrev.6b00302 (2016).

168. Mantri, Y. & Jokerst, J. v. Engineering Plasmonic Nanoparticles for Enhanced Photoacoustic Imaging. *ACS Nano* vol. 14 9408–9422 Preprint at https://doi.org/10.1021/acsnano.0c05215 (2020).

169. Verma, R., Belgamwar, R. & Polshettiwar, V. Plasmonic Photocatalysis for CO2Conversion to Chemicals and Fuels. *ACS Mater Lett* **3**, 574–598 (2021).

170. Kauranen, M. & Zayats, A. v. Nonlinear plasmonics. *Nat Photonics* **6**, 737–748 (2012).

171. Li, J. F., Li, C. Y. & Aroca, R. F. Plasmon-enhanced fluorescence spectroscopy. *Chemical Society Reviews* vol. 46 3962–3979 Preprint at https://doi.org/10.1039/c7cs00169j (2017).

172. Semeniak, D., Cruz, D. F., Chilkoti, A. & Mikkelsen, M. H. Plasmonic Fluorescence Enhancement in Diagnostics for Clinical Tests at Point-of-Care: A Review of Recent Technologies. *Advanced Materials* Preprint at https://doi.org/10.1002/adma.202107986 (2022).

173. Li, M., Cushing, S. K. & Wu, N. Plasmon-Enhanced Optical Sensors: A Review. *Analyst* **140**, 386 (2015).

174. Joyce, C., Fothergill, S. M. & Xie, F. Recent advances in gold-based metal enhanced fluorescence platforms for diagnosis and imaging in the near-infrared. *Materials Today Advances* vol. 7 Preprint at https://doi.org/10.1016/j.mtadv.2020.100073 (2020).

175. Liu, S. Y. *et al.* Simultaneous excitation and emission enhancement of fluorescence assisted by double plasmon modes of gold nanorods. *Journal of Physical Chemistry C* **117**, 10636–10642 (2013).

176. Francisco, A. P. *et al.* Extreme Enhancement of Single-Molecule Fluorescence from Porphyrins Induced by Gold Nanodimer Antennas. *Journal of Physical Chemistry Letters* **10**, 1542–1549 (2019).

177. Trofymchuk, K. *et al.* Addressable nanoantennas with cleared hotspots for single-molecule detection on a portable smartphone microscope. *Nat Commun* **12**, (2021).

178. Meskó, B. & Spiegel, B. A Revised Hippocratic Oath for The Era of Digital Health (Preprint). *J Med Internet Res* (2022) doi:10.2196/39177.

179. Tsiompanou, E. & Marketos, S. G. Hippocrates: Timeless still. *J R Soc Med* **106**, 288–292 (2013).

180. Fiala, C., Taher, J. & Diamandis, E. P. P4 Medicine or O4 Medicine? Hippocrates Provides the Answer. *The journal of applied laboratory medicine* vol. 4 108–119 Preprint at https://doi.org/10.1373/jalm.2018.028613 (2019).

181. Pulciani, S., Lonardo, A. di, Fagnani, C. & Taruscio, D. Key words • Human Genome Project • history of medicine • participatory medicine • computational biology P4 Medicine versus Hippocrates. *Ann Ist Super Sanità* **53**, 185–191 (2017).

182. Lunshof, J. E., Chadwick, R. & Church, G. M. Hippocrates revisited? Old ideals and new realities. *Genomic Medicine* vol. 2 1–3 Preprint at https://doi.org/10.1007/s11568-008-9020-2 (2008).

183. Amram, D., Cignoni, A., Banfi, T. & Ciuti, G. From P4 medicine to P5 medicine: transitional times for a more human-centric approach to AI-based tools for hospitals of tomorrow. *Open Research Europe* **2**, 33 (2022).

184. Bensing, J. Bridging the gap.: The separate worlds of evidence-based medicine and patient-centered medicine. *Patient Educ Couns* **39**, 17–25 (2000).

185. Gorini, A. & Pravettoni, G. P5 medicine: A plus for a personalized approach to oncology. *Nature Reviews Clinical Oncology* vol. 8 444 Preprint at https://doi.org/10.1038/nrclinonc.2010.227-c1 (2011).

186. Bragazzi, N. L. From P0 to P6 medicine, a model of highly participatory, narrative, interactive, and 'augmented' medicine: Some considerations on Salvatore Iaconesi's clinical story. *Patient Prefer Adherence* **7**, 353–359 (2013).

187. Flores, M., Glusman, G., Brogaard, K., Price, N. D. & Hood, L. P4 medicine: How systems medicine will transform the healthcare sector and society. *Personalized Medicine* vol. 10 565–576 Preprint at https://doi.org/10.2217/pme.13.57 (2013).

188. Heineman, W. R. & Jensen, W. B. Leland C. Clark Jr. (1918–2005). *Biosens Bioelectron* **21**, 1403–1404 (2006).

189. Clark Jr., L. C. & Lyons, C. ELECTRODE SYSTEMS FOR CONTINUOUS MONITORING IN CARDIOVASCULAR SURGERY. *Ann N Y Acad Sci* **102**, 29–45 (1962).

190. Yoo, E. H. & Lee, S. Y. Glucose biosensors: An overview of use in clinical practice. *Sensors* vol. 10 4558–4576 Preprint at https://doi.org/10.3390/s100504558 (2010).

191. Jang, C., Lee, H. J. & Yook, J. G. Radio-frequency biosensors for real-time and continuous glucose detection. *Sensors* vol. 21 1–21 Preprint at https://doi.org/10.3390/s21051843 (2021).

192. Naresh, V. & Lee, N. A review on biosensors and recent development of nanostructured materials-enabled biosensors. *Sensors (Switzerland)* vol. 21 1–35 Preprint at https://doi.org/10.3390/s21041109 (2021).

193. Davis, K. D. *et al.* Discovery and validation of biomarkers to aid the development of safe and effective pain therapeutics: challenges and opportunities. *Nat Rev Neurol* **16**, 381–400 (2020).

194. Lin, L. L., Huang, H. C. & Juan, H. F. Discovery of biomarkers for gastric cancer: A proteomics approach. *Journal of Proteomics* vol. 75 3081–3097 Preprint at https://doi.org/10.1016/j.jprot.2012.03.046 (2012).

195. Diaz-Uriarte, R. *et al.* Ten quick tips for biomarker discovery and validation analyses using machine learning. *PLoS Comput Biol* **18**, e1010357 (2022).

196. Kraus, V. B. Biomarkers as drug development tools: discovery, validation, qualification and use. *Nat Rev Rheumatol* **14**, 354–362 (2018).

197. Ou, F. S., Michiels, S., Shyr, Y., Adjei, A. A. & Oberg, A. L. Biomarker Discovery and Validation: Statistical Considerations. *Journal of Thoracic Oncology* **16**, 537–545 (2021).

198. Liu, Y., Zhan, L., Qin, Z., Sackrison, J. & Bischof, J. C. Ultrasensitive and Highly Specific Lateral Flow Assays for Point-of-Care Diagnosis. *ACS Nano* vol. 15 3593–3611 Preprint at https://doi.org/10.1021/acsnano.0c10035 (2021).

199. Syu, Y.-C., Hsu, W.-E. & Lin, C.-T. Review—Field-Effect Transistor Biosensing: Devices and Clinical Applications. *ECS Journal of Solid State Science and Technology* **7**, Q3196–Q3207 (2018).

200. Wang, Y., Zhao, Y., Bollas, A., Wang, Y. & Au, K. F. Nanopore sequencing technology, bioinformatics and applications. *Nature Biotechnology* vol. 39 1348–1365 Preprint at https://doi.org/10.1038/s41587-021-01108-x (2021).

201. Guedes, A. F. *et al.* Atomic force microscopy as a tool to evaluate the risk of cardiovascular diseases in patients. *Nat Nanotechnol* **11**, 687–692 (2016).

202. Yeow, N., Tabor, R. F. & Garnier, G. Mapping the distribution of specific antibody interaction forces on individual red blood cells. *Sci Rep* **7**, (2017).

203. Vu, C. A. & Chen, W. Y. Field-effect transistor biosensors for biomedical applications: Recent advances and future prospects. *Sensors (Switzerland)* vol. 19 Preprint at https://doi.org/10.3390/s19194214 (2019).

204. Skedung, L. *et al.* Feeling Small: Exploring the Tactile Perception Limits. *Sci Rep* **3**, 2617 (2013).

205. Reinhold, T. *et al.* Cost analysis of early discharge using combined copeptin/cardiac troponin testing versus serial cardiac troponin testing in patients with suspected acute coronary syndrome. *PLoS One* **13**, (2018).

206. Jaffe, A. S. & White, H. Ruling-In Myocardial Injury and Ruling-Out Myocardial Infarction with the European Society of Cardiology 1-Hour Algorithm. *Circulation* vol. 134 1542–1545 Preprint at https://doi.org/10.1161/CIRCULATIONAHA.116.024687 (2016).

207. Morley, C., Unwin, M., Peterson, G. M., Stankovich, J. & Kinsman, L. Emergency department crowding: A systematic review of causes, consequences and solutions. *PLoS One* **13**, (2018).

208. Oliveira-Silva, R. *et al.* Monitoring Proteolytic Activity in Real Time: A New World of Opportunities for Biosensors. *Trends Biochem Sci* **45**, 604–618 (2020).

209. Prabowo, B. A., Cabral, P. D., Freitas, P. & Fernandes, E. The challenges of developing biosensors for clinical assessment: A review. *Chemosensors* vol. 9 Preprint at https://doi.org/10.3390/chemosensors9110299 (2021).

210. Tetyana, P., Shumbula, M. & Njengele-Tetyana, Z. *Biosensors: Design, Development and Applications*. www.intechopen.com (2020).

211. Tuersun, P. Optimizing the figure of merit of gold nanoshell-based refractive index sensing. *Optik (Stuttg)* **127**, 250–253 (2016).

212. Ong, J. J. *et al.* Optical biosensors - Illuminating the path to personalized drug dosing. *Biosensors and Bioelectronics* vol. 188 Preprint at https://doi.org/10.1016/j.bios.2021.113331 (2021).

213. Slabý, J. & Homola, J. Performance of label-free optical biosensors: What is figure of merit (not) telling us? *Biosens Bioelectron* **212**, (2022).

214. Chamorro-Garcia, A. & Merkoçi, A. Nanobiosensors in diagnostics. *Nanobiomedicine (Rij)* **3**, (2016).

215. Vigneshvar, S., Sudhakumari, C. C., Senthilkumaran, B. & Prakash, H. Recent advances in biosensor technology for potential applications - an overview. *Frontiers in Bioengineering and Biotechnology* vol. 4 Preprint at https://doi.org/10.3389/fbioe.2016.00011 (2016).

216. Mou, L. *et al.* Integrated Biosensors for Monitoring Microphysiological Systems. *Lab Chip* (2022) doi:10.1039/d2lc00262k.

217. Postek, W., Pacocha, N. & Garstecki, P. Microfluidics for antibiotic susceptibility testing. *Lab Chip* (2022) doi:10.1039/D2LC00394E.

218. Choi, J. W. *et al.* Development of an IoT-integrated multiplexed digital PCR system for quantitative detection of infectious diseases. *Lab Chip* (2022) doi:10.1039/d2lc00726f.

219. Dornhof, J. *et al.* Microfluidic organ-on-chip system for multi-analyte monitoring of metabolites in 3D cell cultures. *Lab Chip* **22**, 225–239 (2022).

220. Bruch, R. *et al.* CRISPR-powered electrochemical microfluidic multiplexed biosensor for target amplification-free miRNA diagnostics. *Biosens Bioelectron* **177**, (2021).

221. Tran, T. B., Nguyen, P. D., Baek, C. & Min, J. Electrical dual-sensing method for real-time quantitative monitoring of cell-secreted MMP-9 and cellular morphology during migration process. *Biosens Bioelectron* **77**, 631–637 (2016).

222. Land, K. J., Boeras, D. I., Chen, X. S., Ramsay, A. R. & Peeling, R. W. REASSURED diagnostics to inform disease control strategies, strengthen health systems and improve patient outcomes. *Nature Microbiology* vol. 4 46–54 Preprint at https://doi.org/10.1038/s41564-018-0295-3 (2019).

223. Ho, J. S. & Zhang, Y. Wireless nanomedicine for brain tumors. *Nat Nanotechnol* **17**, 907–908 (2022).

224. Hasselgren, A., Kralevska, K., Gligoroski, D., Pedersen, S. A. & Faxvaag, A. Blockchain in healthcare and health sciences—A scoping review. *Int J Med Inform* **134**, 104040 (2020).

225. Saeed, H. *et al.* Blockchain technology in healthcare: A systematic review. *PLoS One* **17**, (2022).

226. Dilawar, N., Rizwan, M., Ahmad, F. & Akram, S. *Blockchain: Securing Internet of Medical Things (IoMT)*. *IJACSA) International Journal of Advanced Computer Science and Applications* vol. 10 www.ijacsa.thesai.org (2019).

227. Kostick-Quenet, K. *et al.* How NFTs could transform health information exchange. *Science (1979)* **375**, 500–502 (2022).

228. Davenport, T. & Kalakota, R. *DIGITAL TECHNOLOGY The potential for artificial intelligence in healthcare*. *Future Healthcare Journal* vol. 6 (2019).

229. Yu, K. H., Beam, A. L. & Kohane, I. S. Artificial intelligence in healthcare. *Nature Biomedical Engineering* vol. 2 719–731 Preprint at https://doi.org/10.1038/s41551-018-0305-z (2018).

230. Walter, W. *et al.* How artificial intelligence might disrupt diagnostics in hematology in the near future. *Oncogene* vol. 40 4271–4280 Preprint at https://doi.org/10.1038/s41388-021-01861-y (2021).

231. Sato, T., Ishimaru, H., Takata, T., Sasaki, H. & Shikano, M. Application of Internet of Medical/Health Things to Decentralized Clinical Trials: Development Status and Regulatory Considerations. *Front Med (Lausanne)* **9**, (2022).

232. Diamandis, E. P. The failure of protein cancer biomarkers to reach the clinic: why, and what can be done to address the problem? *BMC Medicine* vol. 10 Preprint at https://doi.org/10.1186/1741-7015-10-87 (2012).

233. Schwartz, M. A. The importance of stupidity in scientific research. *Journal of Cell Science* vol. 121 1771 Preprint at https://doi.org/10.1242/jcs.033340 (2008).

234. Ren, A. H., Fiala, C. A., Diamandis, E. P. & Kulasingam, V. Pitfalls in cancer biomarker discovery and validation with emphasis on circulating tumor DNA. *Cancer Epidemiology Biomarkers and Prevention* vol. 29 2568–2574 Preprint at https://doi.org/10.1158/1055-9965.EPI-20-0074 (2020).

235. Diamandis, E. P. Covid-19 and the le chatelier's principle. *Diagnosis* vol. 8 445–446 Preprint at https://doi.org/10.1515/dx-2021-0022 (2021).

236. Duffy, M. J., DIamandis, E. P. & Crown, J. Circulating tumor DNA (ctDNA) as a pan-cancer screening test: Is it finally on the horizon? *Clinical Chemistry and Laboratory Medicine* vol. 59 1353–1361 Preprint at https://doi.org/10.1515/cclm-2021-0171 (2021).

237. Prostate cancer: Send away the PSA? *The Lancet* vol. 380 307 Preprint at https://doi.org/10.1016/S0140-6736(12)61232-X (2012).

238. Fiala, C., Taher, J. & Diamandis, E. P. P4 Medicine or O4 Medicine? Hippocrates Provides the Answer. *The journal of applied laboratory medicine* vol. 4 108–119 Preprint at https://doi.org/10.1373/jalm.2018.028613 (2019).

239. Senior, M. Biotech bubbles during the global recession. *Nature Biotechnology* vol. 39 408–413 Preprint at https://doi.org/10.1038/s41587-021-00876-w (2021).

240. Senior, M. Innovators take cover as market bubble bursts. *Nature Biotechnology* vol. 40 450–457 Preprint at https://doi.org/10.1038/s41587-022-01277-3 (2022).

241. Baird, G. S. If Theranos' Tests Had Actually Worked. *J Appl Lab Med* **4**, 7–10 (2019).

242. Diamandis, E. P., Lackner, K. J. & Plebani, M. Theranos revisited: The trial and lessons learned. *Clinical Chemistry and Laboratory Medicine* vol. 60 4–6 Preprint at https://doi.org/10.1515/cclm-2021-0994 (2022).

243. Amram, D., Cignoni, A., Banfi, T. & Ciuti, G. From P4 medicine to P5 medicine: transitional times for a more human-centric approach to AI-based tools for hospitals of tomorrow. *Open Research Europe* **2**, 33 (2022).

Take the Next Step: here's How!

Before advancing to the next section which comprises the original work developed within the framework of this dissertation a disclaimer must be made. Common sense states that "imitation is the purest form compliment". Hence, like Leland Clark Jr., curiosity, learning and problem-solving were the main driving forces motivating the realization of the works presented next. Therefore, it is important to note that plenty of work still needs to be done until the real-life applications envisioned below become a reality. Nevertheless, recognizing that "slow and steady" wins the race, it is important to keep focus on the end goal and try to understand with what (I believe) I can "bring to the game" and the future I envision. For this reason, specially for the non-specialist audience, a general overview is provided, aiming to integrate the technologies developed herein in socially acknowledged problems.

It's worth noting that the works presented in this dissertation are largely independent of each other and can be read in any order. To make it easier to navigate the content, multimedia links have been provided in the figures or as footnotes at the end of the general overview or near the conclusions of the advanced version. These links will provide further information and context for the reader.[cxxxix]

Gamification, the use of game elements in non-game contexts, has been shown to improve learning and increase productivity, particularly among younger generations. With this in mind, each chapter of this dissertation has been presented in the form of a puzzle-like mind map at the end of the general overview. The keywords for each puzzle piece are provided, along with a few selected examples to serve as starting points. The advanced versions will provide additional "hints" to help complete the puzzle. In the conclusions section, the solutions to all the puzzles will be provided, so be sure not to "sneak peek"!

The decision to present the information in the form of puzzles was driven by two main reasons:

1. It allows for a logical construction pathway that aligns with the experimental design.
2. The puzzle format allows for the presentation of "cause and consequence" type information, as the piece with the "prominence" leads to the consequence contained in the piece with the "hole".

I hope you enjoy. Have fun!

[cxxxix] These sections will be used as scripts for the audio version of the thesis.

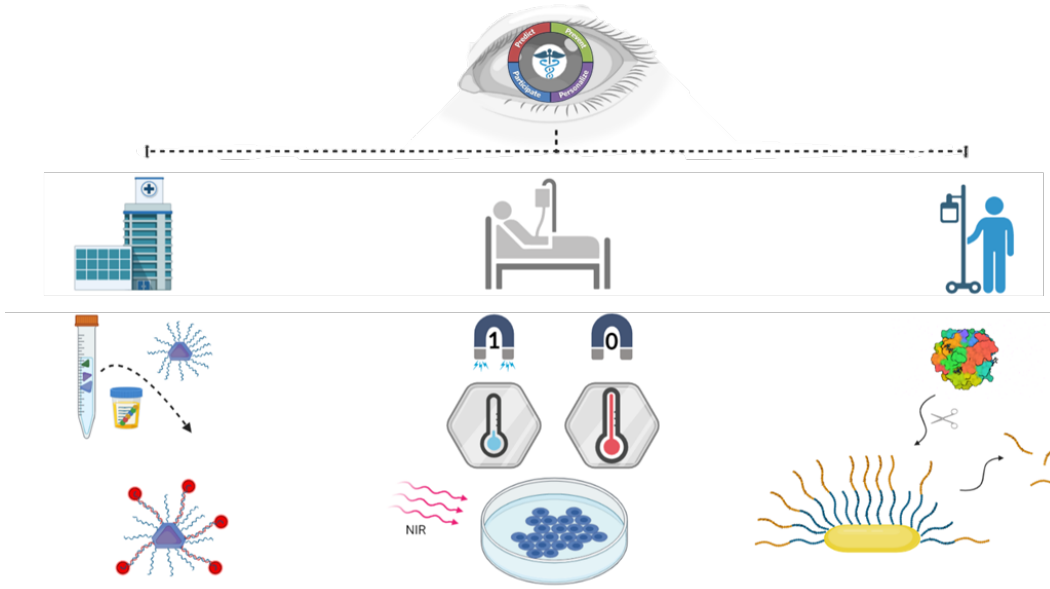

Enhanced Fluorescence | Magnetic Logic-Gate | LSPR sensing

Density Gradient Selection of Colloidal Silver Nanotriangles for Assembling Dye-Particle Plasmophores

General Overview

Nucleotides (C, G, A, T, U) are the fundamental building blocks of nucleic acids such as RNA and DNA that constitute the genetic information of a given entity (genome).[cxl] Organized as genes, during translation in the ribosome, these segments of nucleotides provide the instructions on "how to build" a specific protein.[cxli] Understandably, these sets of instructions vary across species, can be altered over time (i.e. mutations) and their translation can be influenced by the environment (epigenetics). Therefore, assessing the presence or quantity of specific gene sequences is a powerful diagnostic tool.

When it comes to diagnosis of pathophysiological conditions as viral, bacterial infections or cancers, the motto "the sooner the better" is key, as earlier diagnostic could mitigate spreading of infectious diseases or growth/metastasis of cancers. It is estimated that, on average, gold-standard techniques only diagnose cancers when they reach approximately 1 cm^3 which, in many cases, only occurs ten years after its appearance. This constitutes a lost opportunity to tackle the disease and increase survivability and/or mitigate poor outcomes. In many cases, this is the consequence of limited sensitivity of the diagnostic methods available to detect minute amounts of biomarker sequences. To overcome this limitation Polymerase Chain Reaction (PCRs) methods are used as a tool to amplify the signal of the sample. Briefly, nucleotide pairs are specific,[cxlii] thus many copies of the biomarker sequence are created by repeating PCR cycles ($[initial\ biomarker\ concentration] \times 2^{(number\ PCR\ cycles)}$) that can later be detected. However, PCRs demand specialized equipment and trained personnel, use many reactants and are time consuming. These drawbacks critically undermine cost-effectiveness and accessibility. A reliable alternative to PCR will then need to be fast, provide extreme sensitivity and be suitable for implementation in portable and convenient devices such as POCs.

Biosensors based on fluorescence-enhancement can ultimately combine all the relevant features. Such schemes rely on plasmonic nanoparticles that act both as platform for attaching probe molecules and as an antenna to increase the fluorescence[cxliii] when a target molecule is captured. So far, the preparation of these plasmophores (plasmonic particle + probe molecule) still impose many challenges, as these systems critically depend on many aspects:

1. Photophysical properties of the plasmonic nanoparticle – as these are critically dependent on the material, shape and size of the nanoparticle, sample homogeneity is pivotal.

[cxl] Set of genes within and organism. The human genome has approximately 4 billion base pairs (b.p.)
[cxli] Every 3 nucleotides sequence is named "codon" and correspond to an amino acid. i.e. The start codon is "AUG" and eukaryote and archae cells always corresponds to a methionine.
[cxlii] Adenine (A) pairs with Thymine (T) and Cytosine (C) pairs with Guanine (G). Note: Uracile (U) only exists in RNA sequences (single stranded).
[cxliii] Thousands or even million fold fluorescence increases are already reported.

2. Chemical and colloidal stability to enable functionalization with probe molecules and ensure long-term usability.
3. Matching the photophysical properties and distance between the antenna and the fluorescent molecule.

To this end, silver triangular nanoprisms (AgNTs) are exciting candidates. They are easy and fast to produce, their optical properties can be tuned, and the tips act as "hot-spots" to further increase the antenna effect. Overall, silver presents better optical properties when compared to gold. The method to prepare the AgNTs results in polydisperse samples with particles of multiple sizes and aspect ratios. Here, we used "sucrose density gradient centrifugation" [cxliv] to effectively sort AuNTs by size. Another challenge was the fact that during functionalization of the AuNTs with the probing molecule,[cxlv] a quick change in color (from blue to red), was observed, indicating oxidation of the AgNTs to disks. We circumvented this by coating the AgNTs with a thin shell of gold, which originated truncated triangular nanoprisms (Ag@AuNTs). Then, by adjusting the absorption and emission of both the Ag@AuNTs and the fluorophore (Atto-655), a plasmophore was obtained with an emission of over 1000-fold when compared with a single dye molecule.[cxlvi]

Many challenges still arise when it comes to considering the implementation of such strategies into a ready to use POC device. Yet, future work can help improving the potential of the system even further. I suggest, for example:

1. Evaluate the ability of density gradients to purify dimers of nanoparticles and even further constructions.
2. Test fluorophores with lower stand-alone emission to increase the signal-to-noise ratio (background) – better contrast between health-disease conditions resulting in less false-results.
3. Assess the ability to implement plasmophores in different nucleic acid schemes and other biomolecules.
4. After plasmophore optimization, test the system with real samples and evaluate it using benchtop and ultimately POC devices.

Despite other alternatives could also provide a reliable and ultrasensitive alternative for early diagnostics with high precision, due to its intrinsic properties such as simple implementation, versatility and cost effectiveness, fluorescent enhanced biosensors are certainly one of the forefronts worth exploring for diagnostic purposes.[cxlvii]

[cxliv] A standard methodology used Molecular Biology studies to separate biomolecules and organelles.
[cxlv] Single-stranded DNA via Thiol group.
[cxlvi] For comparison this would correspond to a decrease of ~ 10 cycles of PCR - $2^{10} = 1024\ copies$.
[cxlvii] Go to: Magnetic Logic-Gate ; LSPR Prot Act; or Conclusions

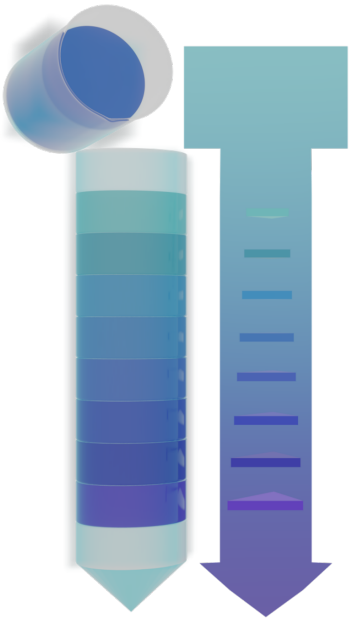

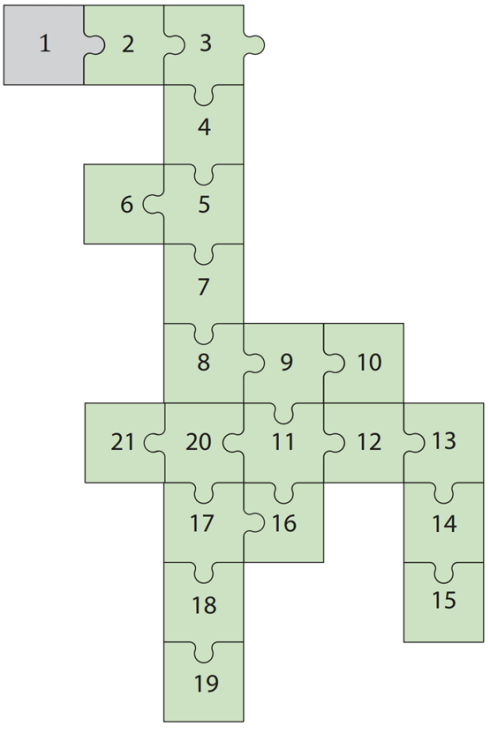

Monodisperse Fractions
H_2O_2 resistant
Nucleic acid detection
Localized Surface Plasmon Resonance (LSPR)
Fluorescence Correlation Spectroscopy (FCS)
Plasmonic Nanoparticles
Oxidation
Plasmonic profile & field-enhancement map
Gold Coating
AgNTs
Uv-Vis
Nanoparticle-based (bio)sensors - **1**
Discrete Dipole Approximation (DDA)
Truncated Ag@AuNTs
Characterization - **11**
STEM
Density Gradient centrifugation ,
AgNTs Fractions
Polydisperse
ssDNA immobilization - **17**
Fluorescence enhancement

Advanced version

Abstract

A simple method based on sucrose density gradient centrifugation is proposed here for the fractionation of colloidal silver nanotriangles. This method afforded particle fractions with surface plasmon resonances spanning the red to infrared spectral ranges, that could be used to tune optical properties for plasmonic applications. This feature was exemplified by selecting silver nanotriangle samples with spectral overlap with Atto-655 dye's absorption and emission, in order to assemble dye-particle plasmophores. The emission brightness of an individual plasmophore, as characterized by fluorescence correlation spectroscopy, is at least 1000-fold more intense than that of a single Atto-655 dye label, which renders them as promising platforms for the development of fluorescence-based nanosensors.

Keywords:

Plasmonic nanoparticles; Density Gradient Centrifugation; Silver Triangular Nanoprisms; Gold Coating; Fluorescence enhancement; Nucleic Acid Detection;

The conjugation of fluorescent dyes onto metal nanoparticles is a promising approach to obtain strongly emitting nanoprobes with emission intensities far superior to their isolated components. The metal nanoparticle can act as an optical antenna through its localized surface plasmon modes, thereby modifying the dye's emission properties by accelerating its excitation and decay rates [1–5]. The overall effect depends on the details of the plasmon near field close to the particle's surface and it may comprise more than intensity changes[6–10]. The role of plasmon-molecule interactions in the emergence of unique emission properties in these systems has been adequately captured in the term plasmophore[11–15].

Several aspects have to be considered in order to achieve substantial emission enhancements from a plasmophore. For instance, the dye-particle separation is crucial, because, at very close distances, quenching by the metal surface mostly overcomes the near field enhancement effects on the dye's excitation and radiative decay rates[1,2]. Typically, there is an optimal location for emission enhancement a few nanometers away from the metal surface. Another key aspect is the spectral dependence of plasmon-coupled emission [5,16,17]. The largest effects occur when the surface plasmon resonance of the nanoparticle is close to the dye's excitation wavelength and, correspondingly, the dye's emission is slightly red-shifted relatively to the plasmon peak wavelength. For a particular dye, the spectral overlap condition can be attained by changing the particle's composition, size and/or shape, in order to tune its surface plasmon resonance.

The development of wet-chemistry methods for the synthesis of colloidal metal nanoparticles offers the possibility of preparing a variety of particle types and therefore to tune its optical properties[18–20]. For the purpose of fluorescence enhancement, gold and silver are the most commonly used metals. The dielectric properties of silver, namely its lower dissipation in the visible range, allow for larger plasmon enhanced fields that yield better antenna effects. However, silver nanoparticles are prone to oxidation and, thus, gold is preferred because of its chemical stability. Elongated particle shapes of gold or silver, such as rods, bipyramids, prisms or stars, display surface plasmon resonances that span from red to infrared spectral ranges, for which dissipation is weak in both metals. This results in surface plasmon resonances with strong

near field enhancements that are mostly concentrated at the sharp features on the particle's surface, which are designated as plasmon hot-spots. Therefore, besides the dye-particle separation and their spectral overlap, it is also important to selectively attach the dye at the plasmon hot-spots to maximize antenna effects in plasmophores' emission.

The colloidal synthesis of elongated metal nanoparticles is usually a sequential process, in which seed particles are first produced and, then grown anisotropically and/or reshaped in the presence of surfactants or other surface agents[18] . This often leads to a mixture of particle sizes and shapes that needs to be purified or processed, in order to yield samples displaying narrow plasmon resonances suitable for plasmonic applications[21–26]. Despite, silver triangular nanoplates being synthetized in a single step, morphological and size heterogeneity are still observed. Therefore, in this contribution, we propose a simple work-up procedure based on nanoparticle centrifugation in a density gradient of aqueous sucrose solutions. The procedure was demonstrated here for the selection of silver nanotriangles, but it could be readily adapted for separating silver nanoparticles of other shapes. The particle selection criterion was the spectral overlap of the plasmon resonance with Atto-655 dye's absorption and emission, in order to develop a red-emitting plasmophore. For this purpose, silver nanotriangles were coated with a thin gold shell to improve their chemical stability and labeled with Atto-655 dye covalently attached on a DNA oligonucleotide sequence with 10-nt and terminated by a thiol group. The strong emission properties of the assembled dye-particle plasmophores were confirmed by fluorescence correlation spectroscopy measurements.

At the beginning of this work, our motivation was to evaluate the performance of silver nanotriangles as plasmonic nanoantennas for fluorescent enhancement. However, the preparation of silver nanotriangles, even if performed by a single-step well-established procedure, it is very dependent on the reagents' quality, such as hydrogen peroxide that is unstable. This aspect can decrease reproducibility and make difficult long-time studies, for which different synthesis need to be prepared. Thus, we believe that a good separation method affording particles with consistent optical properties is important. The silver nanoparticles are easy to prepare, as indicated by the blue color that is promptly observed in the solution, but the resulting samples were too heterogeneous, as inferred from their broad absorption spectrum. With this in mind, we have decided to use Density Gradient Centrifugation (DGC), a procedure well-established in biological sciences, to separate the resulting nanoparticles by size, which could result in narrower optical spectra due to an improved sample homogeneity. The fractionation of the nanotriangle population synthesized was performed by adding the reaction mixture onto the top layer of a sucrose density gradient prepared in a 15 mL centrifuge tube. The centrifugation promotes particle sedimentation under the effect of opposing centrifugal and buoyancy forces. This results in the distribution of nanoparticles according to their size/shape across the density gradient. Fractions of particles with different size can then be obtained by collecting volumes along the centrifuge tube (PEF - Figure 1a).

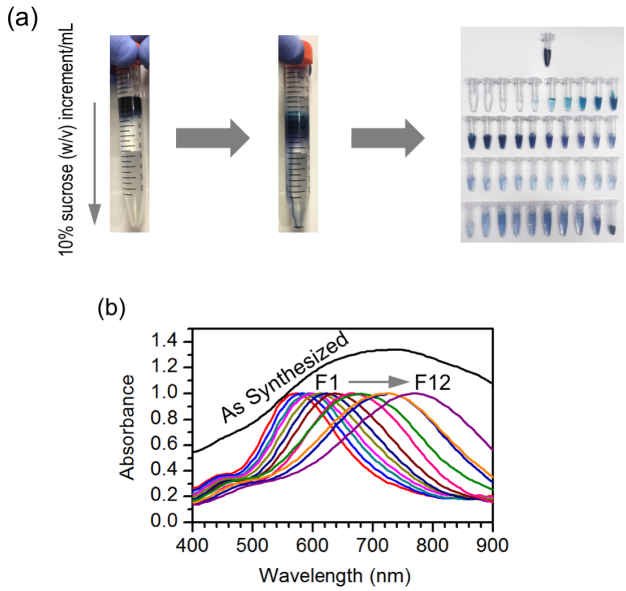

*PEF - Figure 1 - Fractionation and characterization of silver nanotriangles. (**a**) Nanotriangles are fractionated by sucrose density gradient centrifugation. The reaction mixture is placed on top of a sucrose density gradient (100-10% w/v) in a centrifuge tube; following gentle centrifugation (6000 g, 30 minutes), twelve, 500 µL fractions are collected. Separation efficiency can be judged by the color distribution of the resulting fractions. (**b**) Extinction spectrum of the original mixture and spectra of the individual fractions.*

Comparing the extinction spectrum of the original mixture with the spectra of separated fractions (PEF - Figure 1b), it is possible to judge that particle fractionation using DGC was successful. The original mixture displays a broad spectrum that spans a wide wavelength range from 500 to 900 nm. On the other hand, the separated fractions have much narrower spectra and with increasing particle size there is a gradual red-shift of the plasmon resonance peak. In the later spectra, it also becomes possible to distinguish a smaller band or shoulder at lower wavelengths (ca. 450 nm), which is expected for the transverse plasmon mode that is excited perpendicularly to the particle's plane. The in-plane longitudinal modes are responsible for the strong plasmon resonance peak that red-shifts with increasing particle fraction. Although an overall increase of particle size may induce a red shift in the plasmon resonance through the contribution of multipolar modes, it seems more likely that the wide range of peak shifts observed here result from an increase of the particle's aspect ratio. This outcome from particle selection by DGC provides a way to tune the particle's surface plasmon resonance to different dyes across the red to infrared range when developing plasmophores.

Following fractionation, we selected and pooled particle fractions of silver nanotriangles with plasmon resonance peaks at around 550 nm (Ag-1), 620 nm (Ag-2) and 670 nm (Ag-3) (PEF - Figure 2b), which afford a good degree of spectral overlap with the absorption and emission from the Atto-655 dye. The silver nanotriangles in these pooled fractions (Ag-1 to Ag-3) were then coated with a thin gold shell to improve their chemical stability (PEF - Figure 2a), yielding fractions Ag@Au-1 to 3. Indeed, the gold coating rendered these particles' resistant to oxidation by hydrogen peroxide (Fig. S1 of the SI). The extinction spectra of these particle fractions also changed slightly by becoming narrower and with closer peak resonance wavelengths (PEF - Figure 2C). The growth of a gold shell on silver nanotriangles commonly induces a red-shift of the longitudinal plasmon,[27,28] but the spectral changes observed here may have also resulted

from additional washing steps in concentrated CTAB solutions. The spectral narrowing observed in the gold coated particles is nonetheless a beneficial feature for plasmonic applications.

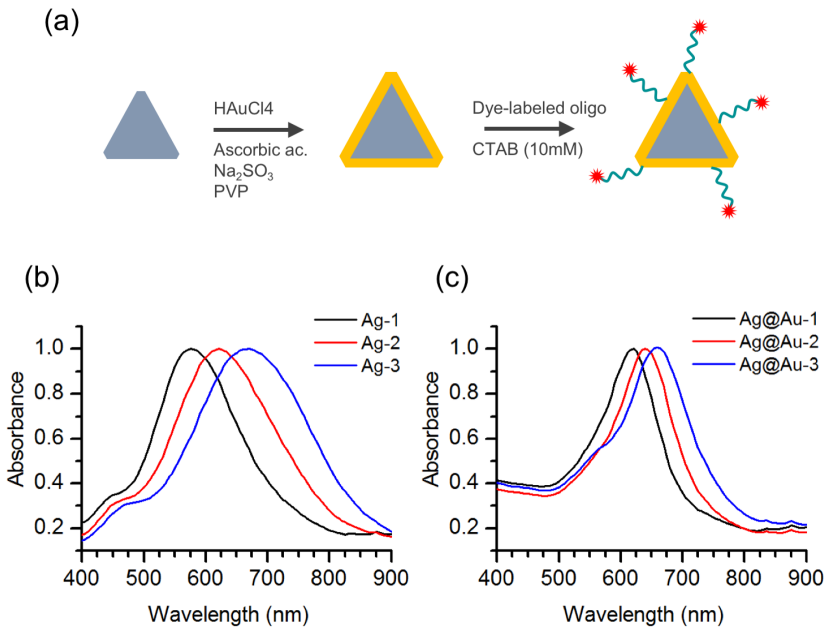

*PEF - Figure 2 - **Gold coating of silver nanotriangles** (**a**) Schematic representation of gold coating of silver nanotriangles and subsequent assembly of dye-particle plasmophores; (**b**) Extinction spectra of silver nanotriangle samples Ag-1 to 3; (**c**) Extinction spectra of gold coated-silver nanotriangle samples Ag@Au-1 to 3*

After successfully obtaining Ag@Au nanoparticles, we tried to evaluate their ability to integrate a plasmophore. The assembly of dye-particle plasmophores from the selected silver nanotriangles coated with gold (Ag@Au-1 to 3) was accomplished by conjugation of Atto-655 dye-labeled oligonucleotides onto these particles. The oligonucleotide sequence is modified at the 3'-end with a thiol group to bind the metal surface, while the Atto-655 dye is attached at the 5'-end. The estimated end-to-end distance of the oligonucleotide spacer is approximately 4.3 nm, but the actual distance is smaller due to conformational freedom of the single strand[29]. The functionalization was performed under an excess of dye-labeled oligonucleotides and in the presence of CTAB surfactant. The use of CTAB surfactant is a well-established strategy to promote tip-selective functionalization of gold nanorods.[30] This tip-preference in the presence of CTAB is attributed to a protective role of the surfactant bilayer on the rods' surface that directs thiol attachment to more sparse regions at the tips. Some evidence that a similar effect of edge-selective thiol attachment could take place for other particle shapes has been reported in the literature.[31] For the dye-particle assembly sought in this work, it would be clearly beneficial to attach the dye-labeled oligonucleotides preferentially at the apex regions of the Ag@Au nanotriangles, which are hot-spots for plasmon-enhanced fluorescence emission.

An approximated view of the plasmon hot-spots on the Ag@Au nanotriangles was obtained from model simulations using discrete dipole approximation. The geometry described in the literature for these particles is that of a triangular shape with truncated apexes, which is claimed to provide six hot-spots at each one of its sharp edges (PEF - Figure 3a).[27,32] The calculated near field maps show that the distribution of the plasmon field is indeed concentrated at the triangle's apexes for the in-plane plasmon modes (PEF - Figure 3b-c). For an excitation

wavelength of 639 nm - used in the FCS measurements - the near field enhancement factors are above 1000-fold in the close proximity of the apexes aligned with the incident field direction. Moreover, the plasmon field extends with enhancement factors of at least 100-fold over a circular region that comprises a significant part of the triangle's side edges. In the perpendicular direction to the triangle's plane, the plasmon field at the apexes gets up to factors of 600-fold enhancement, even if the transverse mode is far from resonance at this excitation wavelength (PEF - Figure 3d). The near field enhancement factors obtained in these simulations are promising for the purpose of plasmon-enhanced fluorescence emission. These factors can be used to estimate the acceleration of the dye's excitation rate on the particles' vicinity. A full theoretical analysis would imply also simulating the particle's effect on the radiative and non-radiative decay rates, in order to estimate the dye-particle emission quantum yield. For a bright dye such as Atto-655, most likely it will not have much implication in the upper limit of the enhancement effect, but it could be important to map surface regions where quenching prevails. It is also for this reason that site-selective approaches for dye attachment at the plasmon hot-spots are important for maximizing emission enhancement toward strong emitting plasmophores.

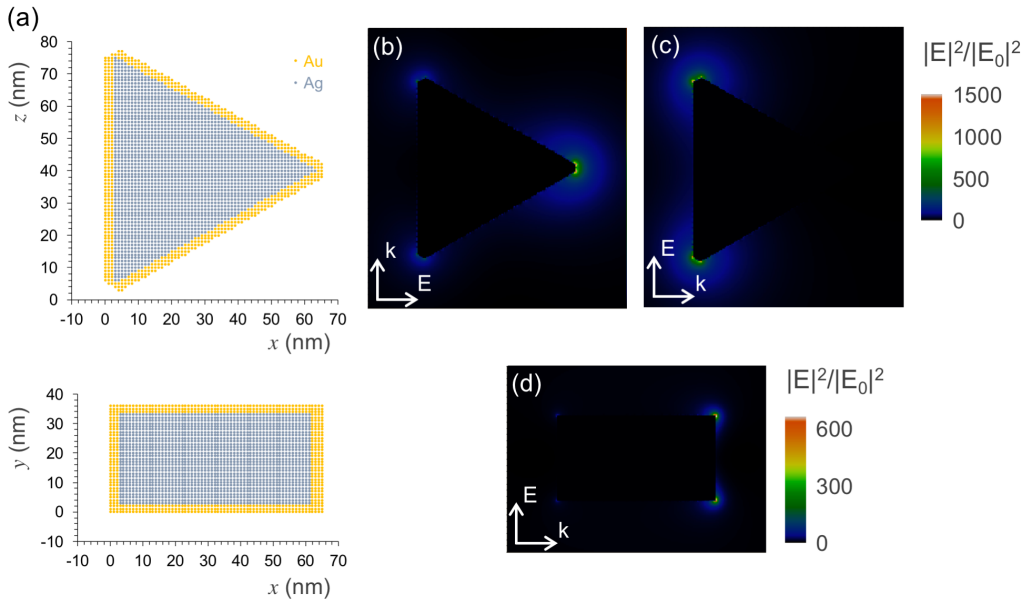

PEF - Figure 3 - ***Plasmon hot-spots on the Ag@Au nanotriangles as obtained by model simulations using discrete dipole approximation.*** *(**a**) Model of the Ag@Au nanotriangles showing particle discretization used in the simulations: (top) longitudinal and (bottom) transverse planes; (**b**) and (**c**) Plasmon near field map excited at a wavelength of 639 nm by an incident field polarized in one longitudinal direction. (**d**) Similar map for an incident field polarized in transverse direction.*

The emission properties of the nanotriangle samples Ag@Au-1 to 3 conjugated to Atto-655 labeled oligonucleotides, hereafter termed plasmophores PPh-1 to 3, were characterized by FCS measurements. The intensity time traces were measured in dilute suspensions for single-particle detection and show intense fluorescence burst events that reach up to hundreds of counts/ms for a low excitation power of 0.044 kW/cm^2 (PEF - Figure 4a). In the same conditions, the emission from the original (non-functionalized) Ag@Au nanotriangles is negligible, as well as the emission from single Atto-655 dye molecules. The conjugation of Atto-655 dye onto Ag@Au nanotriangles resulted in nanohybrid assemblies with single object brightness much larger than

their individual components. The auto-correlation function (ACF) was obtained from each intensity trace of PPh-1 to 3 (PEF - Figure 4b). The ACF curves show two relaxation components with characteristic times of ca. 40 – 50 µs and 7 – 8 ms, that were attributed to rotational and translational Brownian motion of the dye-particle across the confocal volume. A similar behavior of the FCS correlation curves has been previously reported for the emission of dimeric gold nanoparticles conjugated to Atto-647N dye.[33] The ACF's from PPh-1 to 3 were fitted with a two-component model for describing rotational and translational diffusion of the dye-particle assemblies,

$$G(\tau) - 1 = \left(1 - A_s e^{-\tau/t_s}\right) \times \frac{1}{N}\left(1 + \frac{\tau}{t_d}\right)^{-1} \left(1 + \frac{\tau}{\kappa^2 \cdot t_d}\right)^{-1/2} \quad (1)$$

in which, A_s is the amplitude of the rotational correlation, t_s is the rotational diffusion time, N is the number of emitters in the detection volume, t_d is the transverse translational diffusion time, and κ is the ratio between the longitudinal and transverse dimensions of the detection volume. The size parameters of the detection volume were calibrated using free Atto-655 in aqueous solution as a reference dye. Using these parameters, the translational diffusion coefficients determined for PPh-1 to 3 were 8.3, 7.6 and 7.0 µm^2/s, which from Stokes-Einstein equation gave approximate values of hydrodynamic radius of 28, 30 and 33 nm, respectively. The trend observed in these results is in qualitative agreement with the density gradient selection of silver nanotriangles used for assembling PPh-1 to 3 plasmophores. However, the differences observed in diffusion coefficients are close to the experimental uncertainty typically associated with FCS measurements.

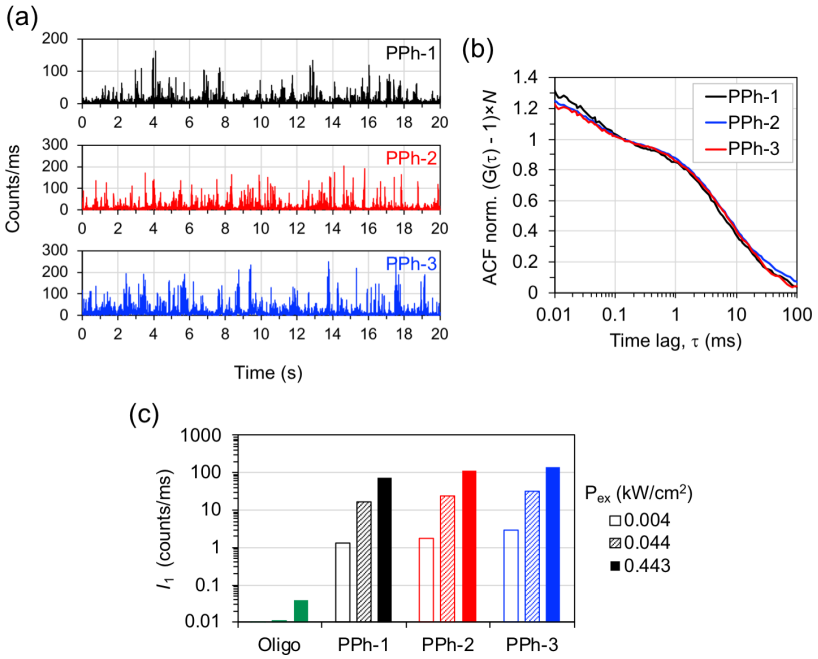

*PEF - Figure 4 - **Fluorescence emission from plasmophores**. (**a**) Emission intensity time traces of plasmophores PPh-1 to 3 measured in colloidal suspension for excitation at 639 nm with a power of 0.044 kW/cm^2; (**b**) Auto-correlation function (ACF) from the previous intensity time traces rescaled by the number N of emitters in the detection volume; (**c**) Individual brightness (I_1) of single dye-labeled oligonucleotide (labeled "Oligo") and of plasmophores PPh-1 to 3 obtained for several excitation powers.*

The average number N of emitters determined from ACF fittings were 0.39, 0.49 and 0.47 for PPh-1 to 3, respectively. The curves shown in PEF - Figure 4b were rescaled by these factors, in order to visually compare the correlation decays of PPh-1 to 3. Also, the individual brightness (I_1) of each dye-particle assembly was estimated by dividing the average emission intensity of the respective time trace by the number N of emitters (PEF - Figure 4c). The values of I_1 obtained for three excitation powers show a proportional increase from approximately 1 to 100 count/ms for the average emission of an individual object. The brightness of a single dye-labeled oligonucleotide was evaluated to be 0.039 count/ms for an excitation power of 0.443 kW/cm^2. These results correspond to ratios of 1900, 2870 and 3400-fold in the individual brightness of PPh-1 to 3 relatively to that of the single dye-labeled oligonucleotide. The remarkable brightness of PPh-1 to 3 is most likely due to the ability of Ag@Au nanotriangles to carry multiple dye-labeled oligonucleotides on its nanometric sized surface combined with the antenna effect on the dye's emission at the hot-spots of these plasmonic particles. In multi-chromophore systems, the contributions of local dye concentration and that of plasmon-coupled emission are strongly convoluted in the average brightness measured. The spatial distribution of plasmon-coupled emission over the particle's surface creates a very heterogeneous picture, in which strong fluorescence enhancement at the plasmon hot-spots is counter-balanced by drastic emission quenching on other surface regions. A detailed analysis on the spatial distribution of plasmon-coupled fluorescence is beyond the scope of this work, but recent studies using super-resolution fluorescence microscopy have contributed with valuable insights in this regard.[34–38] Further studies on the plasmophores demonstrated here will focus on tuning the gold nanoshell thickness and the dye labeling density. It would also be interesting to study Ag@Au nanotriangles with longitudinal plasmon resonances mismatched relatively to the dye's optical spectrum for decoupling the effects of plasmon-enhanced emission and local dye concentration.

In this work, we have demonstrated a simple method for size selection of silver nanotriangles using density gradient centrifugation (DGC) in aqueous sucrose solutions. This method made it possible to resolve a nanotriangle mixture characterized by broad extinction spectrum into twelve particle fractions displaying spectra with narrow plasmon resonances that span the red to infrared wavelength ranges. This very selective separation provides a way to tune the surface plasmon resonance for further applications. We have exemplified this possibility by selecting silver nanotriangles with plasmon resonances that overlap with Atto-655 dye's absorption and emission, in order to produce dye-particle plasmophores. The emission from these plasmophores, as characterized by FCS measurements, is larger by more than 1000-fold when compared to emission from a single dye-labeled oligonucleotide. The remarkable brightness of the assembled plasmophores renders these as promising platforms for the development of fluorescence-based sensing schemes, in view of the large fluorescence signals that can be achieve from a single nano-object.[cxlviii]

[cxlviii] Go to: Magnetic Logic-Gate ; LSPR Prot Act; or Conclusions

Materials and Methods

Reagents

Sodium nitrate ($AgNO_3$) was acquired from Panreac Appliechem, trisodium citrate (99.95%), hydrogen peroxide (H_2O_2, >30%) and sodium hydroxide (NaOH, 99.1%%) from Fisher Scientific, sodium sulfite (Na_2SO_3, 97%) from Acros Organics, sucrose (≥99%) and gold(III) chloride solution ($HAuCl_4$, ≥49% Au bases) from Sigma-Aldrich, polyvinylpyrrolidone (PVP, MW=10 000) and L-(+)-ascorbic acid (L-AA, >99%) from Alfa Aesar by Thermo Fischer Scientific, and sodium borohydride ($NaBH_4$) from Aldrich. DNA oligonucleotide of 10-nt labeled with ATTO-655 dye and purified by HPLC was purchased from STAB Vida (Monte da Caparica, Portugal). The sequence used was the following: (ATTO-655)-5'-GAGTCTGGAC-(C6-SH)-3'. Ultrapure water (18.2 MΩ) was obtained with a Milli-Q purification system (Merck-Millipore) and used in all preparations. All reagents were used as acquired.

Synthesis of silver nanotriangles

The synthesis of colloidal silver nanotriangles has been previously reported in the literature.[39] However, the amount of H_2O_2 was adjusted due to aging effects on the concentration of this reagent. The reaction mixture was prepared from 100 µL of 0.1 M AgNO3, 1.5 mL of 0.1 M trisodium citrate and 900 µL of H_2O_2 that were diluted to a final volume of 100 mL with ultrapure water. The solution was vigorously stirred for 10 min. Then, the stirring speed was decreased and 1 mL of 0.1 M $NaBH_4$ was injected. The stirring was sustained until a color variation was observed. Subsequently, the solution was centrifuged at 9000 g for 30 minutes. The supernatant was discarded and 2 mL of nanotriangles solution was retrieved.

Separation of silver nanotriangles by a sucrose density gradient centrifugation

Nanotriangles in the reaction mixture were fractionated by sucrose density gradient centrifugation. A centrifuge tube was first prepared by successive additions of 1 mL volumes of sucrose aqueous solutions starting from a concentration of 100% (w/v) at the bottom and decreasing in steps of 10% upwards. One mL of the reaction mixture was added at the top of the sucrose density gradient and the separation was promoted by gentle centrifugation (6000 g, 30 minutes). After centrifugation, nanoparticle fractions were collected by carefully pipetting out volumes of 200 µL from the centrifuge tube along the established gradient profile.

Gold coating of silver nanotriangles

The gold coating protocol used was adapted from Ref.[27] with the aim of minimizing the formation of gold nanoparticles. For this procedure, selected fractions of silver nanotriangles were first combined to give three samples: Ag-1 (F2, F3, F4), Ag-2 (F6, F7, F8) and Ag-3 (F9, F10), that after gold coating were labeled: Ag@Au-1 to 3. A growth solution (4.72 mL ultrapure H_2O, 20 µL of 0.25 M $HAuCl_4$, 240 µL of 0.2 M NaOH, 3 mL of 0.01 M Na_2SO_3) was prepared beforehand and incubated overnight at RT. Afterwards, 500 µL of silver nanotriangles solution were added to a solution containing 637.5 µL of ultrapure H_2O, 250 µL of 5% (w/w) PVP, 50 µL of 0.5 M ascorbic acid, 50 µL of 0.5 M NaOH, 12.5 µL of 0.1 M Na_2SO_3 and 1 mL of growth solution. The mixture was kept under stirring at RT for 10 h. The resulting nanoparticles were then centrifuged at 6000g for 30min.

Functionalization with Atto-655 labelled oligonucleotide

The plasmophores were prepared by incubating 50 µL of gold coated silver nanotriangles with 250 nM of the oligonucleotide labeled with Atto-655 in 10 mM CTAB during 1 hour at room temperature. The resulting particles were centrifuged 3 times at 6000g for 15 mins against a solution of 1 mM CTAB.

Equipment

Extinction spectra were measured with an UV/Vis spectrophotometer from PerkinElmer, model Lambda 35. Corrected fluorescence emission spectra were recorded with a FluoroLog-3 spectrofluorimeter (Horiba Jobin Yvon). Fluorescence correlation spectroscopy (FCS) measurements were performed on a time-resolved confocal fluorescence microscope (MicroTime 200, PicoQuant GmbH). The microscope setup details were previously described. Briefly, the excitation source is a pulsed diode laser emitting at 639 nm with a repetition rate set to 20MHz. The excitation light is coupled into an inverted microscope (Olympus IX 71) through a water immersion objective (UPLSAPO 60×, N.A. 1.2, Olympus) and the emitted light is collected in the reverse pathway and is cleaned by an emission filter (Chroma 695AF55 with a transmission window of 667-725 nm) and a 50 µM pinhole that rejects out-of-focus light. Then, the re-collimated beam is divided by means of a 50/50 polarizing beam splitter cube and is detected by two single-photon avalanche diode detectors (SPAD, SPCM-AQR-13, Perkin Elmer). The signal is processed by TimeHarp 200 TC-SPC PC- board (PicoQuant GmbH) working in the time-tagged time-resolved (TTTR) operation mode. Data acquisition and analysis were performed in SymPhoTime software (PicoQuant GmbH).

References - PEF

[1] L. N. P. Anger, P. Bharadwaj, *Phys. Rev. Lett.* **2006**, *96*, 113002.

[2] S. Kühn, U. Håkanson, L. Rogobete, V. Sandoghdar, *Phys. Rev. Lett.* **2006**, *97*, 17402.

[3] T. H. Taminiau, F. D. Stefani, N. F. van Hulst, *New J. Phys.* **2008**, *10*, 105005.

[4] A. Kinkhabwala, Z. Yu, S. Fan, Y. Avlasevich, K. Müllen, W. E. Moerner, *Nat. Photonics* **2009**, *3*, 654–657.

[5] S. Khatua, P. M. R. Paulo, H. Yuan, A. Gupta, P. Zijlstra, M. Orrit, *ACS Nano* **2014**, *8*, 4440–4449.

[6] M. Ringler, A. Schwemer, M. Wunderlich, A. Nichtl, K. Kürzinger, T. A. Klar, J. Feldmann, *Phys. Rev. Lett.* **2008**, *100*, 203002.

[7] T. Kosako, Y. Kadoya, H. F. Hofmann, *Nat. Photonics* **2010**, *4*, 312–315.

[8] P. K. Jain, D. Ghosh, R. Baer, E. Rabani, A. P. Alivisatos, *Proc. Natl. Acad. Sci.* **2012**, *109*, 8016 LP – 8019.

[9] J. V Pellegrotti, G. P. Acuna, A. Puchkova, P. Holzmeister, A. Gietl, B. Lalkens, F. D. Stefani, P. Tinnefeld, *Nano Lett.* **2014**, *14*, 2831–2836.

[10] T. Ming, H. Chen, R. Jiang, Q. Li, J. Wang, *J. Phys. Chem. Lett.* **2012**, *3*, 191–202.

[11] J. R. Lakowicz, K. Ray, M. Chowdhury, H. Szmacinski, Y. Fu, J. Zhang, K. Nowaczyk, *Analyst* **2008**, *133*, 1308–1346.

[12] T. Ming, L. Zhao, H. Chen, K. C. Woo, J. Wang, H.-Q. Lin, *Nano Lett.* **2011**, *11*, 2296–2303.

[13] G. R. Bourret, T. Ozel, M. Blaber, C. M. Shade, G. C. Schatz, C. A. Mirkin, *Nano Lett.* **2013**, *13*, 2270–2275.

[14] Q. Zhu, S. Zheng, S. Lin, T.-R. Liu, C. Jin, *Nanoscale* **2014**, *6*, 7237–7242.

[15] A. Hakonen, N. Strömberg, *Chem. Commun.* **2011**, *47*, 3433–3435.

[16] P. Bharadwaj, L. Novotny, *Opt. Express* **2007**, *15*, 14266–14274.

[17] S. Vukovic, S. Corni, B. Mennucci, *J. Phys. Chem. C* **2009**, *113*, 121–133.

[18] C. J. Murphy, T. K. Sau, A. M. Gole, C. J. Orendorff, J. Gao, L. Gou, S. E. Hunyadi, T. Li, *J. Phys. Chem. B* **2005**, *109*, 13857–13870.

[19] P. Zijlstra, M. Orrit, *Reports Prog. Phys.* **2011**, *74*, 106401.

[20] Y. Xia, X. Xia, H.-C. Peng, *J. Am. Chem. Soc.* **2015**, *137*, 7947–7966.

[21] L. Scarabelli, M. Coronado-Puchau, J. J. Giner-Casares, J. Langer, L. M. Liz-Marzán, *ACS Nano* **2014**, *8*, 5833–5842.

[22] J.-H. Lee, K. J. Gibson, G. Chen, Y. Weizmann, *Nat. Commun.* **2015**, *6*, 7571.

[23] G. González-Rubio, P. Díaz-Núñez, A. Rivera, A. Prada, G. Tardajos, J. González-Izquierdo, L. Bañares, P. Llombart, L. G. Macdowell, M. Alcolea Palafox, et al., *Science (80-.).* **2017**, *358*, 640 LP – 644.

[24] G. Chen, Y. Wang, L. H. Tan, M. Yang, L. S. Tan, Y. Chen, H. Chen, *J. Am. Chem. Soc.* **2009**, *131*, 4218–4219.

[25] K. Chandra, V. Kumar, S. E. Werner, T. W. Odom, *ACS Omega* **2017**, *2*, 4878–4884.

[26] M. J. Eller, K. Chandra, E. E. Coughlin, T. W. Odom, E. A. Schweikert, *Anal. Chem.* **2019**, *91*, 5566–5572.

[27] H. Liu, T. Liu, L. Zhang, L. Han, C. Gao, Y. Yin, *Adv. Funct. Mater.* **2015**, *25*, 5435–5443.

[28] C. Gao, Z. Lu, Y. Liu, Q. Zhang, M. Chi, Q. Cheng, Y. Yin, *Angew. Chemie Int. Ed.* **2012**, *51*, 5629–5633.

[29] A. M. M. Rosa, D. M. F. Prazeres, P. M. R. Paulo, *Phys. Chem. Chem. Phys.* **2017**, *19*, 16606–16614.

[30] J. G. Hinman, J. R. Eller, W. Lin, J. Li, J. Li, C. J. Murphy, *J. Am. Chem. Soc.* **2017**, *139*, 9851–9854.

[31] Z. Guan, S. Li, P. B. S. Cheng, N. Zhou, N. Gao, Q.-H. Xu, *ACS Appl. Mater. Interfaces* **2012**, *4*, 5711–5716.

[32] B. Xue, D. Wang, J. Zuo, X. Kong, Y. Zhang, X. Liu, L. Tu, Y. Chang, C. Li, F. Wu, et al., *Nanoscale* **2015**, *7*, 8048–8057.

[33] M. P. Busson, B. Rolly, B. Stout, N. Bonod, J. Wenger, S. Bidault, *Angew. Chemie Int. Ed.* **2012**, *51*, 11083–11087.

[34] E. Wertz, B. P. Isaacoff, J. D. Flynn, J. S. Biteen, *Nano Lett.* **2015**, *15*, 2662–2670.

[35] K. L. Blythe, K. A. Willets, *J. Phys. Chem. C* **2016**, *120*, 803–815.

[36] D. L. Mack, E. Cortés, V. Giannini, P. Török, T. Roschuk, S. A. Maier, *Nat. Commun.* **2017**, *8*, 14513.

[37] K. A. Willets, A. J. Wilson, V. Sundaresan, P. B. Joshi, *Chem. Rev.* **2017**, *117*, 7538–7582.

[38] A. Taylor, R. Verhoef, M. Beuwer, Y. Wang, P. Zijlstra, *J. Phys. Chem. C* **2018**, *122*, 2336–2342.

[39] Q. Zhang, N. Li, J. Goebl, Z. Lu, Y. Yin, *J. Am. Chem. Soc.* **2011**, *133*, 18931–18939.

Supporting information

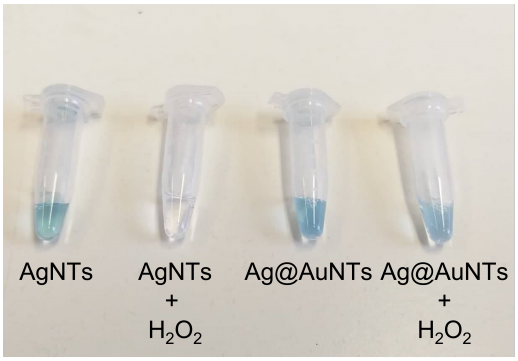

PEF (SI) - Figure 1 - Confirmation of gold coating on Ag@Au nanotriangles by testing their resistance to oxidation by hydrogen peroxide. The original silver nanotriangles ("Ag NTs") when exposed to hydrogen peroxide are oxidized, which is indicated by the color loss ("Ag NTs + H_2O_2"). On the other hand, the gold coated Ag@Au nanotriangles ("Ag@Au") are resistant to oxidation ("Ag@Au + H_2O_2").

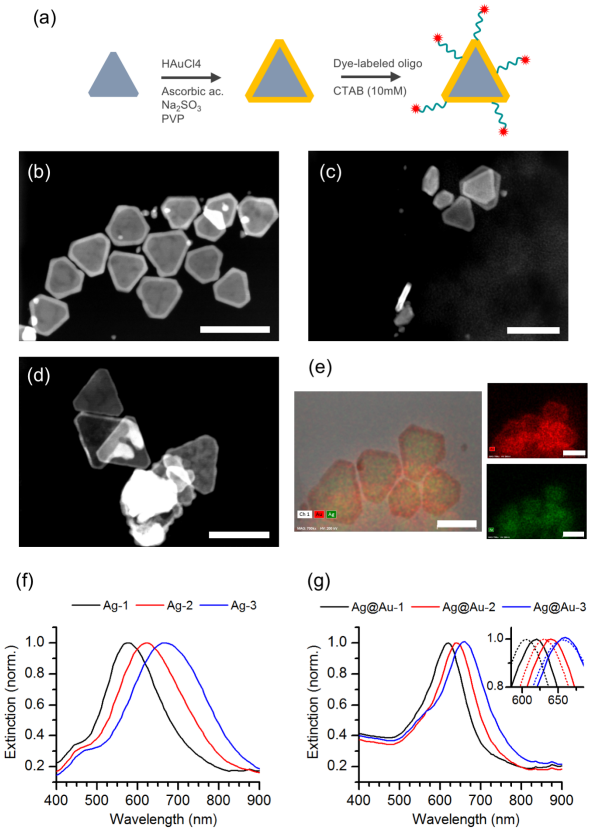

*PEF (SI) - Figure 2 - Normalized extinction spectra of: (**a**) silver nanotriangle samples Ag-S1 to S3, and (**b**) gold-coated silver nanotriangles prepared from the same samples Ag@Au-S1 to S3. STEM images measured in high-angle annular dark-field imaging mode of (**c**) silver nanotriangle sample Ag-S3 and (**d**) of the same sample after gold coating, i.e. sample Ag@Au-S3. The yellow arrows in part (**d**) illustrate the height of the silver core measured along the triangle bisector (L) and the thickness of the gold coating layer (δ), that are reported below in Table S1. (**e**) Elemental analysis mapping obtained by EDX of the gold-coated silver nanotriangles in sample Ag@Au-S3 (green and red represents silver and gold, respectively). The scale bar corresponds to 80 nm for all images shown here.*

*PEF (SI) - Table 1 - Geometrical parameters of gold-coated silver nanotriangles measured from STEM images of samples Ag@Au-S1 to S3. The height of the silver core measured along the triangle bisector (L) and the thickness of the gold coating layer (δ) were measured as illustrated in figure S2(**d**). The uncertainty interval corresponds to the standard deviation of the sample.*

	L (nm)	δ (nm)
Ag@Au-S1	36 ± 5	5.1 ± 0.7
Ag@Au-S2	42 ± 6	4.6 ± 0.7
Ag@Au-S3	66 ± 9	3.1 ± 0.5

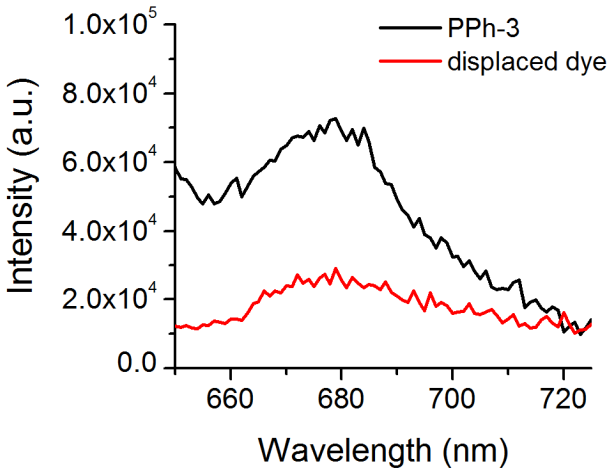

PEF (SI) - Figure 3 - Emission spectrum of plasmophore PPh-3 measured in dilute suspension for excitation at 620 nm (black line) and emission of the same sample after displacing the dye-labeled oligonucleotides from the particles' surface into solution by using 2-mercaptoethanol and separating the particles by centrifugation (red line). The comparison between the emission of dye-particle nano-assemblies and that of the dye displaced in solution affords an average enhancement factor of about 3-fold for excitation of PPh-3 at 620 nm.

Temperature-responsive nanomagnetic logic gates for cellular hyperthermia

General Overview

Cancer is a leading cause of death and morbidity worldwide. Thie dreadfull disease is characterized by an uncontrolled cellular growth with potential to spread to other parts of the body through a process called metastasis. According to the World Health Organization (WHO), 10 million deaths are estimated to occur annually due to cancer, representing costs that surpass 1 trillion dollars. Known to be an age-related disease, the impact of cancer is becoming greater because of the tendency of aging population worldwide. Along with reliable diagnostic methods, effective and controlled treatments are imperative.

With chances of surging in any part of the body, cancer treatments must be adjusted according to the organ or tissue affected. Currently, chemo- and radiotherapy are the gold-standard methods used to shrink and eradicate cancer. However, these strategies aren't always effective, and side-effects are often severe. To alleviate these drawbacks new approaches and implementations are being tested. Among these, hyperthermia treatments are already being used in specialized hospitals as a co-adjuvant treatment along with chemo- or radiotherapies. Hyperthermia is characterized by a sudden increase in the temperature (~43°C) [cxlix] ideally at the location of the tumour. The treatment effectiveness is based on the premise that cancerous cells are more susceptible to high temperature than their healthy counterparts[cl]. However, a dangerous downside of hyperthermia is the lack of temperature control/assessment. Temperature undershoots are not always effective and can promote EMT(ransition)[cli] and induce nefarious side-effects, including death.

The lack of feedback during the procedure is currently one of the Achilles-heels of hyperthermia treatment, as commonly it resorts to the insertion of probes to locally heat the tissue. These perfusion techniques are invasive, have limited accessibility and can cause swelling, clotting and other side-effects in the impacted region. On the other hand, whole-body hyperthermia lacks specificity and cause severe effects, including heart problems. Alternatively, nanoparticle-based treatments can tackle these limitations as they can be locally injected or administered via blood stream. Intuitively, targeted strategies present less side-effects than untargeted. Hence, specific nanoparticle accumulation at the target-site is promoted either by the EPR effect[clii] or via decoration of the nanoparticles with tumor homing peptides or antibodies.[cliii] Magnetic, metallic and carbon-nanoparticles are the most promising and studied materials as power sources to induce the local heating. These materials usually rely on electromagnetic radiation or alternated magnetic fields. Nanoparticle-based hyperthermia improves accessibility and precision, is versatile and ultimately implementable as theranostic tool. However, a reliable method to

[cxlix] Target temperature is often organ-dependent.
[cl] "Those who cannot be cured by medicine can be cured by surgery; Those who cannot be cured by surgery can be cured by heat; Those who cannot be cured by heat are to be considered incurable" – Hippocrates (460-370 BC).
[cli] Epithelial-mesenchymal transition (EMT) grants cells migratory and invasive capabilities that can promote metastasis (see glossary for detailed information).
[clii] Molecules of certain sizes tend to accumulate in tumor tissue much more than they do in normal tissues due to increased vascularization.
[cliii] Neutral-charge molecules are usually attached to the nanoparticles to avoid macrophage clearance from the body.

assess the temperature at which the system was subjected during the treatment procedure is still lacking.

As mentioned, magnetic nanoparticles (MNPs) are one of the forefront materials being tested in hyperthermia treatments. Until now, their usage concerns the usage of soft-magnetic[cliv] materials and as MRI contrast agents, carriers, and as local heaters when exposed to high-frequency alternated magnetic fields. So far, the magnetic properties of the MNPs used in hyperthermia treatments are constant across biologically relevant temperatures, thus, undermining their potential for nanothermometry purposes. Alternatively, nanosized hard magnets (Fe_3Se_4) present a bistable behavior with a sharp magnetic transition (T_C) near biological relevant temperatures (~42°C). Succinctly, this implies that Fe_3Se_4 MNPs can be recorded using a magnetic field and the magnetic moment will be retained until the T_C is crossed. This implies that during the hyperthermia treatment, if temperature overshoot occurs (T_C is crossed), Fe_3Se_4 MNPs become demagnetized. This is valid until both the temperature decreases below the T_C, and an external magnetic field is reapplied. By being a physical property of such MNPs these nanothermometric logic-gates operate as non-volatile logic-gates, which boosts their potential.[clv] The major hurdle during these materials' preparation was to ensure phase purity and monodispersity (morphology and size ~5-10% std) since magnetic properties and temperature response are intimately related with that. As proof of concept, we aimed to assess temperature overshoots during an *in vitro* hyperthermia treatment using a fluxgate sensor, an 808nm wavelength NIR-laser and a prostate cancer cell-line (PC-3). By regulating the laser potency (four were tested in independent experiments) different temperatures were achieved during the hyperthermia experiments. As expected, our sensor was able to accurately distinguish the occurrence of undershoots, when intermediate temperatures were achieved, and overshoots. A tight correlation between cell death and temperature was also observed.

To the best of my knowledge this was the first time a bioapplication directly relying on hard-magnets was described. For this reason, the potential of materials with such properties is still dawning with immense unexplored potential. Future work on nanothermometry-associated hyperthermia should encompass a precise control and optimization of magnetic properties, a biocompatibility study, and the evaluation of synergies with other materials through construction of hybrid materials. Hopefully in the future hyperthermia can be proven to be an effective tool in fighting cancer and other diseases and temperature can be monitored and controlled by a simple PID[clvi]-like device.[clvii]

[cliv] Soft-magnets become magnetized when subjected to an external magnetic field and lose their magnetization (almost entirely or entirely in superparamagnetic materials) when the external field is removed (detailed in the glossary).
[clv] Doesn't rely on the usage of an energy source.
[clvi] Proportional integral derivative devices are the most accurate and stable devices. They rely on feedback mechanisms to automatically control process variables (i.e. temperature) over time.
[clvii] Go to: PEF Nucleic acid Detection; LSPR Prot Act; or Conclusions

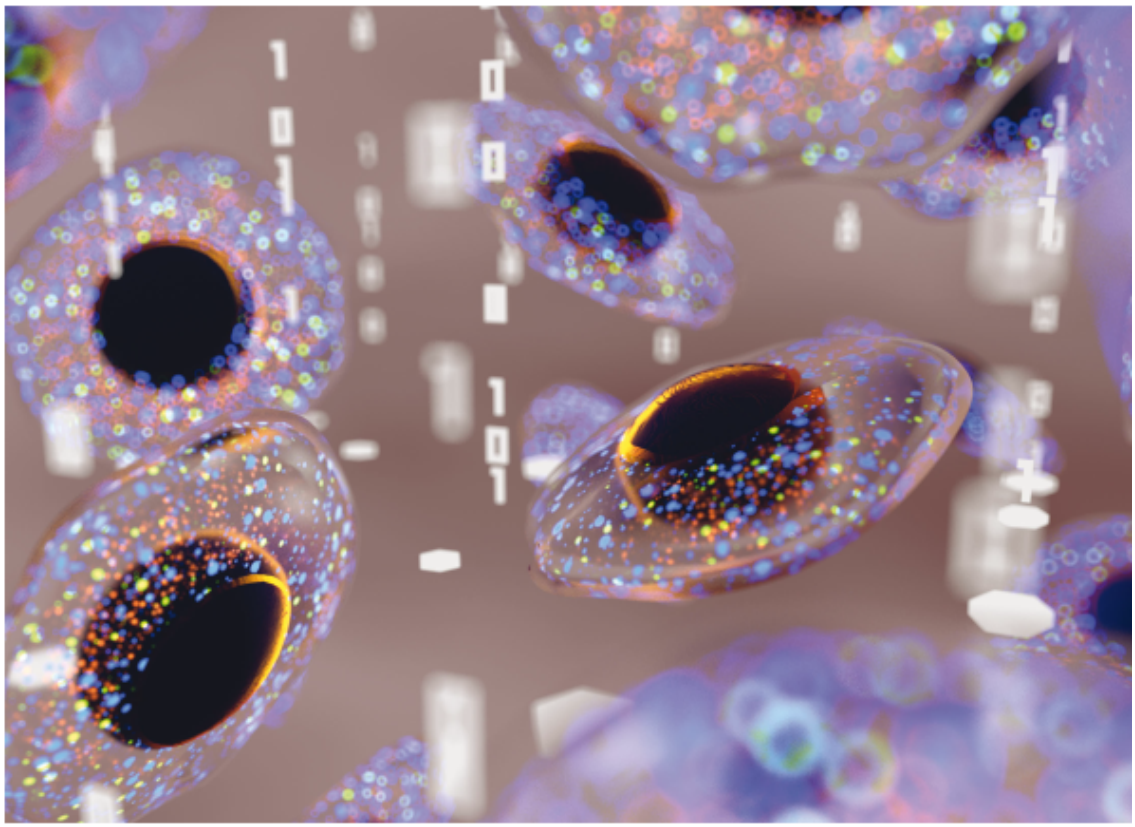

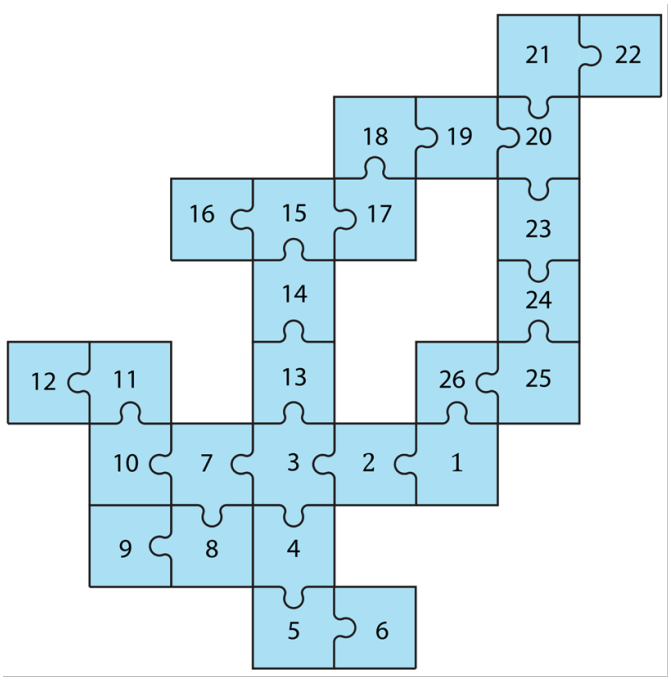

Nanoplatelets
Phase Purity
Nanoparticle-based (Bio)sensors - **1**
Logic-gate
Monodisperse
Atomic Composition
XRD
NIR
SQUID
Hyperthermia Treatment - **20**
Crystal Size
Temperature Overshoot?
Yes(0) No(1)
TC near RT
Fluxgate
Fe_3Se_4
Morphology
Bistable
SR-Latch
Magnetic properties
Characterization - **7**
PC-3 cell line
Hard Magnet - **15**
Cell Culture
Laser Heating
STEM
EDX

Advanced Version

Gaining insight into temperature at the micro- and nanoscales is currently addressed using nanothermometers based on the well-defined temperature dependence of a given property (e.g. luminescence, spin transitions). This approach is challenged when the temperature range of interest and the timescale are short, such as in cellular hyperthermia, since space, time and temperature resolutions are entangled. Here we propose the use of nanosized logic gates recording temperature overshoots for such a demanding application, i.e. we propose the use of materials with a temperature-switch behaviour (recording the occurrence of a switch) instead of materials with a smooth temperature response. The materials used here are magnetically hard nanoparticles losing order at a transition temperature TC tunable around room temperature. Nanomagnets with such behaviour are usually disregarded for applications including biomedical and biosensing where nanomagnets with a high TC (4300 ˚C) are explored. We expect that the logic gates based on these nanomagnets will give valuable insights into temperature in cellular hyperthermia and other demanding applications such as subtle temperature changes during (abnormal) metabolism, heat/laser-triggered release of drugs/genes and ultra-fast PCRs, contributing to their accuracy and development. We further expect that the switching behaviour of the nanomagnets developed here can inspire biosensing in general, exploring concepts such as the temperature-selective detection, tagging and separation of ‘‘hot’’ and ‘‘cold’’ analytes.

Abstract

While a continuous monitoring of temperature at the micro- and nano-scales is clearly of interest in many contexts, in many others a yes or no answer to the question ‘‘did the system locally exceed a certain temperature threshold?’’ can be more accurate and useful. This is the case of hard-to-detect events, such as those where temperature fluctuations above a defined threshold are shorter than the typical integration time of micro/nanothermometers and systems where fluctuations are rare events in a wide time frame. Herein we present the synthesis of iron selenide magnetic nano-platelets and their use as non-volatile logic gates recording the near infrared (NIR) dose that triggers a temperature increase above a critical temperature around 42 8C in prostate cancer cell cultures. This use is based on the bistable behaviour shown by the nanoplatelets below a magnetic phase transition at a tuneable temperature TC and on their photothermal response under NIR light. The obtained results indicate that the synthesized nanomagnets may be employed in the future as both local heaters and temperature monitoring tools in a wide range of contexts involving systems which, as cells, are temperature-sensitive around the tunable T_C

Temperature control is a key aspect in many areas of daily life, where devices, food, organisms and molecules are designed to function and preserve their properties within well-defined temperature limits. Devices that can signal a temperature exceeding these limits are vital in all these areas. In other contexts, the crossing of temperature limits is used intentionally, as in the case of hyperthermia therapy;[1] in this case the critical question is, ‘‘what is the radiation dose that causes a local temperature overshoot?’’ The answer to this question can be given by a set/reset flip-flop logic gate (SR-latch) responding to temperature as one of the inputs, as shown below. A SR-latch changes state as soon as the temperature increases above a well-defined threshold and keeps memory of that state even when the temperature decreases below the threshold. Resetting the original memory state can be performed by a second kind of input. During the last decade, different non-volatile SR-latches based on molecules[2] and nanoparticles[3,4] have been developed, mainly exploring photochromic and electrochromic bistable responses. Such gates are able to record information about local pH and redox

conditions, including those occurring in living cells.[5] Easy integration into biosystems, access to local properties, output detection at a distance and no need for external power are major advantages of molecular and nano SR-latch gates and the main driving forces for their development. Hard magnetic nanoparticles display the bistable non-volatile response shown by the SR-latches. A magnetic material is termed ''hard'' when the direction of its net magnetic moment is difficult to change with an external field, in opposition to ''soft'' magnetic materials where the net magnetic moment can easily follow the external field. The development of hard magnetic nanoparticles is focused almost exclusively on enhancing and maintaining magnetic hardness up to temperatures well above room temperature. While in contexts such as hard disk recording this is a basic requirement, in a context like biomedical applications, the use of nanoparticles with a dramatic change in magnetic behaviour around room temperature represents an unexplored opportunity.

The hard magnetic nanoparticles presented here are iron selenides (Fe_3Se_4), which have a dramatic change in their magnetic properties at a transition temperature TC close to room temperature (between 40 ˚C and 47 ˚C in the bulk form),[6,7] being hard magnets (i.e. being able to record information) below TC and losing this ability above this temperature. This behaviour is quite unique and contrasts with the magnetic nanoparticles explored so far (including magnetite, for instance), where the magnetic properties are almost constant around room temperature and TC is well above room temperature (around 580 ˚C in the case of magnetite). Iron selenides are a family of compounds with a wide range of magnetic properties and compositions, including the diamagnetic $FeSe_2$, the ferrimagnetic Fe_3Se_4 and Fe_7Se_8 and the antiferromagnetic (and superconductor) FeSe.[6–8] The iron/selenium phase diagram shows that the Se-rich phase ($FeSe_2$) and $FeSe_2$/ Fe_3Se_4 mixtures are formed at lower temperatures, the phases approaching the 1 : 1 stoichiometry are formed at higher temperatures, while Fe_3Se_4 forms at intermediate temperatures.[9] With this rich phase diagram, phase purity was the first hurdle to overcome in the design of a successful chemical route for the synthesis of Fe_3Se_4 nanocrystals. The current approach to prepare phase pure Fe_3Se_4 nanoparticles is based on the thermal decomposition of iron and selenium precursors at intermediate temperatures (300 to 340 ˚C),[10,11] where $FeSe_2$ nuclei formed during the heating ramp are transformed into Fe_3Se_4. However, without exceptions, this approach leads to nanoparticles and nanostructures with poor control over size, shape and the aggregation state,[10–14] leading to poor control over the magnetic properties and stability of colloidal dispersions of Fe_3Se_4 nanoparticles. This poor control is the present hurdle to overcome.

Our approach to synthesize Fe_3Se_4 nanoparticles focused on the use of ligands that could control the reactivity of selenide and iron precursors during the thermal decomposition process, in a strategy to have a low amount of Fe^{2+} and Se^{1-} available to react in the (lower) temperature range where $FeSe_2$ can be formed. The best results in terms of phase, size and shape control are obtained when iron oleate and selenium-octadecene are used as cation and anion sources and tetradecylphosphonic acid (TDPA) and 1-dodecanethiol (DDT) as ligands (see the Experimental section and detailed microscopy, diffraction and spectroscopy data comparing nanoplatelets and a reference sample [15] in the SI). Within well-defined windows of concentrations, reaction temperatures and ramp slopes, a dramatic improvement in the control over size, shape homogeneity and distribution is obtained, exceeding those of state-of-the-art methods. [10–14] Within these windows, quasi-hexagonal nanoplatelets with lateral average diameters ranging

from 90 to 300 nm and thicknesses between 40 and 60 nm are obtained (M LG - Figure 1 and M LG (SI) - Figure 1). The key parameters that control the average size of the nanoplatelets are the ramp rate, the structure of iron oleate and its content in free oleic acid. In fact, iron oleate with a larger amount of free oleic acid and unidentate Fe–carboxylate coordination leads to wider nanoplatelets, while purer iron-oleate leads to smaller ones. A relevant influence of these iron-oleate properties was already reported for the case of iron oxide nanoparticles.[16] The nanoplatelets are obtained at temperatures between 200 ˚C and 220 ˚C, lower than those previously reported (300–340 ˚C). [10–14]

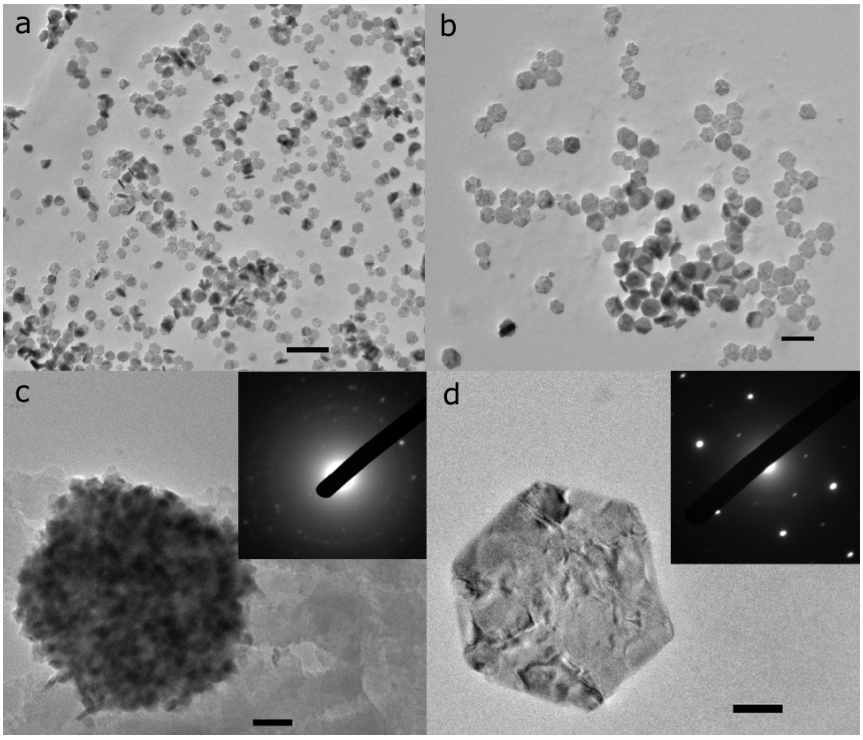

M LG - Figure 1 - Electron microscopy images of the Fe_3Se_4 nanoplatelets with an average diameter of 250 nm. (a) Low magnification image (scale bar 1 mm); (b) medium magnification image (scale bar 500 nm); (c) an Fe_3Se_4 nanoplatelet under formation by coherent attachment and an electron diffraction image showing diffraction rings together with spots (scale bar 100 nm); and (d) an Fe_3Se_4 nanoplatelet and an electron diffraction image showing a [001] zone axis with 6 {200} ''inner'' spots associated with a threefold twinning (scale bar 100 nm). Images of nanoplatelets with other average sizes are presented in the ESI.

Having ensured control over phase, shape, size and size distribution using organic media, phase transfer of the nanoplatelets to aqueous media is the last hurdle before their use in biomedical applications. Our approach focused on the use of a catechol acid, as reported in ref. [17] for the phase transfer of magnetite. Colloidal suspensions of Fe_3Se_4 nanoplatelets, stable over a wide pH range (from 3 to 12) in concentrations up to 2 mg mL-1, are obtained using caffeic acid as the coating molecule (see the dynamic light scattering analysis of suspensions in M LG (SI) - Figure 2). As shown in ref. [17], the carboxylate group of the acid is free to react, allowing further functionalization.

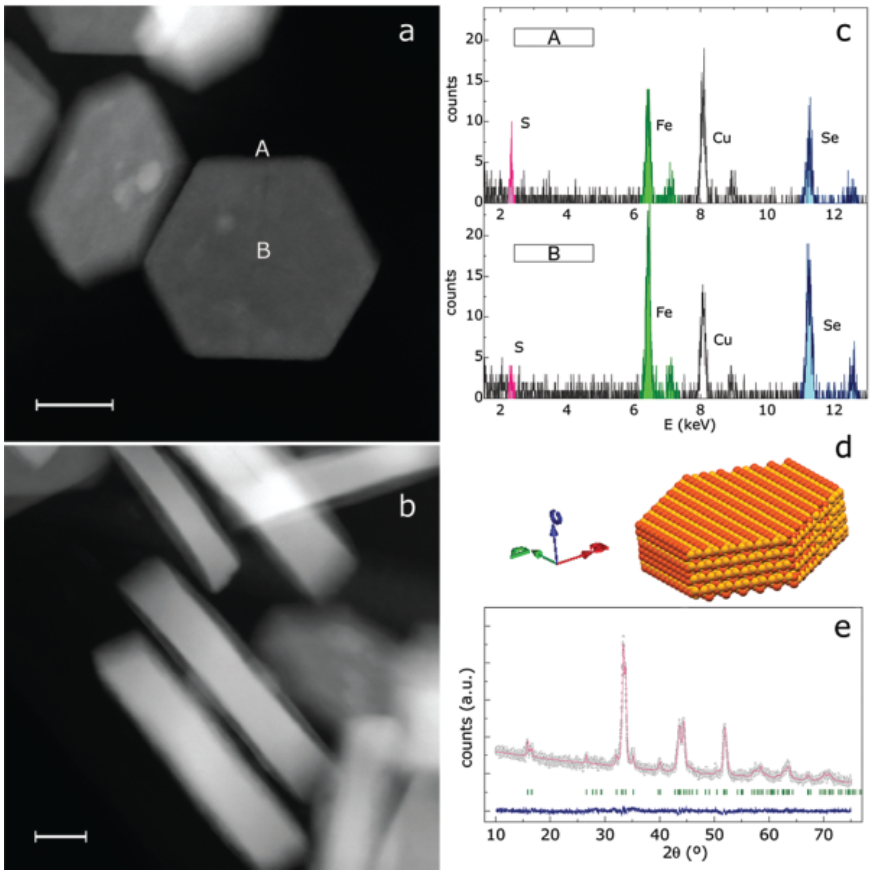

M LG - Figure 2 - Electron microscopy images, chemical information and structure of the Fe_3Se_4 nanoplatelets with an average diameter of 250 nm. (a and b) High-angle annular dark-field (HAADF) images of Fe_3Se_4 nanoplatelets (top-view, scale bar 100 nm; and side-view, scale bar 50 nm); (c) EDX spectra at the surface (A) and top (B) of the Fe_3Se_4 nanoplatelets; (d) ball-stick representation of an Fe_3Se_4 nanoplatelet and (e) X-ray diffraction pattern of the Fe_3Se_4 nanoplatelets. The continuous (red) line represents a Rietveld refinement of the XRD data considering space group P2/m and cell parameters a = 6.1160(5) Å, b = 3.5025(4) Å, c = 11.144(1) Å, b = 91.495(4)1, average apparent (crystallite) size 31 nm and average maximum strain 12%. Vertical (green) lines represent the positions of the allowed Bragg reflections, and continuous (blue, noise-like) lines represent fit residues. XRD data and refinement of nanoplatelets with other average sizes are shown in the ESI.

Fe_3Se_4 has a monoclinic quasi-hexagonal crystal structure and the nanoplatelets replicate this structure, growing in thickness along the c-axis such that the top and bottom surfaces correspond to the {001} family of planes and the lateral surfaces to {100} and {110} families. Interestingly, all these 3 families generate surfaces composed of ‘‘all-Fe’’ or ‘‘all-Se’’ atoms, while families having mixed Fe and Se atoms (like {010}) are generally absent as surfaces of the nanoplatelets. This is compatible with a scenario of shape control by preferential surface coordination of the capping ligands. In fact, the nanoplatelets observed on the electron microscope after typical centrifugation and washing techniques are still coated by an organic layer containing sulfur, suggesting the active role of DDT in controlling the formation of the nanoplatelets (M LG - Figure 2). The nanoplatelets present ripples (M LG - Figure 1) and a relatively high degree of strain, as shown by Rietveld refinement to X-ray diffraction (XRD) data (M LG - Figure 2). This high degree of strain is associated with the existence of a 3-fold twinning observed in the electron diffraction patterns of individual nanoplatelets, where the (-200) and (200) inner spots appear 3 times, rotated by 120˚. During the intermediate states of the synthesis, we found proto-nanoplatelets composed of nanocrystals (M LG - Figure 1C). These proto-nanoplatelets display electron diffraction patterns composed of both rings and well-

defined spots, suggesting that the growth of the nanoplatelets occurs by the coherent attachment of Fe_3Se_4 nanocrystals, being thus particle-mediated rather than atom-mediated.[18] At the intermediate state shown in M LG - Figure 1C, the nanoplatelet is close to its final size and shape, while the crystallinity is still quite low. The crystallinity, average size and size dispersion evolve until the end of the synthesis procedure. At this end point, chosen to minimize size dispersion, the nanoplatelets are still polycrystalline, being at different stages of crystallization depending on their average sizes. This means that, for each average size, minimizing dispersion leaves the nanoplatelets at different degrees of crystallization, such that the relation between size and crystallite size is not monotonic (see M LG (SI) - Table 1).

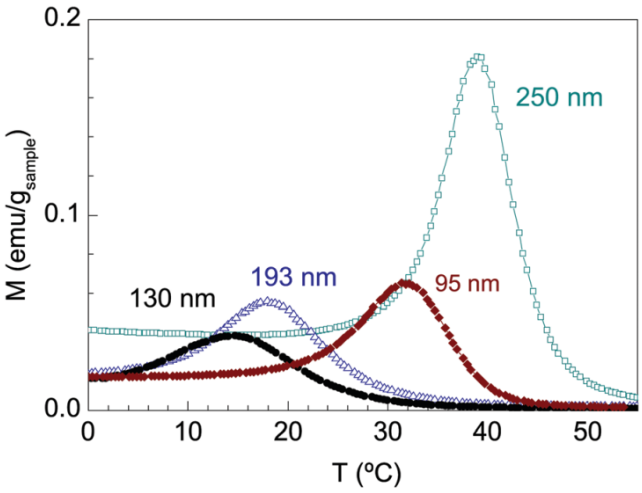

M LG - Figure 3- Magnetization of Fe_3Se_4 nanoplatelets with different average lateral diameters (shown in the legend) as a function of temperature. Magnetization was recorded on heating after cooling from 60 ˚C down to 0 ˚C in the absence of an external field. TC is the temperature where the derivative of magnetization is minimum, i.e., slightly above the maximum. T_C increases monotonically with the increase of the crystallite size and not with the increase of the diameter of the nanoplatelets.

While in the micro- and nano-particles reported so far TC is between 47 ˚C and 67 ˚C, [10–14] the nanoplatelets reported here have a T_C tunable from 18 ˚C to 42 ˚C, increasing with the increase of the crystallite size determined by XRD (M LG - Figure 3, and M LG (SI) - Figure 4 and M LG (SI) - Figure 6), as usually found in finite-size systems.[19] Below T_C, the nanoplatelets behave as hard ferrimagnets presenting a spontaneous (remanent) magnetization in the absence of an external field (Mr, M LG (SI) - Figure 8). The coercive field (H_C, M LG (SI) - Figure 8) corresponds to the field needed to bring this remanent magnetization down to zero. As the temperature decreases across T_C, H_C has a pronounced increase up to values of the order of 4 kOe, which is high enough to prevent demagnetization under normal conditions and small enough to be overcome using a strong permanent magnet.

Hard magnetic nanocrystals with TC close to room temperature, like the Fe_3Se_4 nanoplatelets presented here, are useless in traditional magnetic recording, where temperature-sensitive recording is a problem. However, this sensitivity can give valuable insight into materials and systems which are sensitive in the same temperature range, such as tissues, cells, biomolecules and soft materials in general. For instance, Fe_3Se_4 nanoplatelets with a TC close to 42 ˚C can record information of an event of temperature increase above the normal cell temperature. Below T_C, i.e. in the normal temperature range, the nanoplatelets may have a stable high or a

stable low value of Mr (with the difference between both being at least an order of magnitude), depending on which stimuli was applied last: a magnetic field or a temperature above T_C, respectively (M LG - Figure 4 and M LG (SI) - Figure 9 and M LG (SI) - Figure 15, for further details).

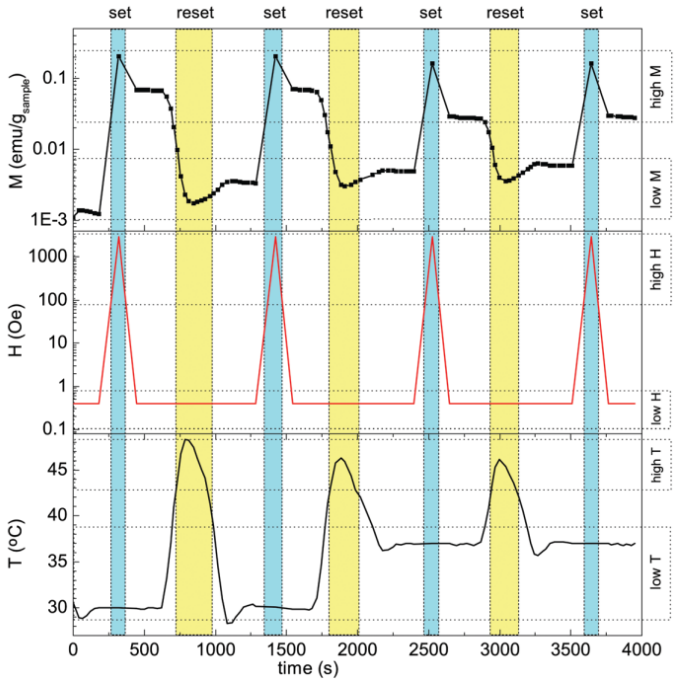

M(t)	H	T	M(t+1)
0	0	0	0
0	0	1	0
0	1	0	1
0	1	1	RC
1	1	1	RC
1	0	0	1
1	0	1	0
1	1	0	1

M LG - Figure 4- Example of the time diagram of the bistable gate. Basic operations of the gate based on the change in the magnetization M (output) response of the Fe_3Se_4 nanoplatelets (average diameter 250 nm) to the field H (set) and temperature T (reset) inputs. Time diagrams obtained for the remaining samples are shown in M LG (SI) - Figure 9. Stability tests on field temperature cycling and the stability of the magnetization response over time are shown in M LG (SI) - Figure 18 and M LG (SI) - Figure 19. For a given initial output sate M(t) (which can be high 1 or low 0), the states of the two inputs H and T will determine the final state M(t + 1) as shown in the table. If both H and T are high, the final state M(t + 1) is ill-defined and will depend on which H or T turns back to a low state first, in a so-called race condition (RC).

After setting the Fe_3Se_4 nanoplatelets into a high state by the application of a magnetic field, a temperature increase above the threshold defined by TC will reset Mr into a low state, thus recording information about that increase. After reading this information, the nanoplatelets can be set again in a state of high Mr, which can be easily performed with an external magnetic field. This corresponds to a SR-latch where temperature and the field are the input stimuli and (remanent) magnetization is the output, with this gate being able to answer the question ‘‘did the temperature exceed the threshold defined by TC since the last time an external field was applied?’’.

In the context of cells, this question arises, for instance, after the application of targeted hyperthermia, where heat sources placed close to or inside cells are triggered at distance. SR-latches are basic memory elements with one output having two possible stable states (high and low) and two inputs: one having the role of setting the output high and the other having the role of setting the output low. In electronics, inputs are voltage levels connected by two NOR gates to one output and its negation (M LG (SI) - Figure 9). In the present implementation of a SR-latch using magnetic nanoplatelets, the output is magnetization, which can be set high using a magnetic field as an input and reset low using temperature as the second input. Since the nanoplatelets are hard magnets, high and low magnetization states remain stable without

energy consumption until the temperature (or field) is changed, responding to temperature in the timeframe of the spin–lattice relaxation (typically between 10^{-7} and 10^{-4} s).[20]

In order to illustrate the use of the Fe_3Se_4 nanoplatelets as SR-latches in cells during hyperthermia, we used a layer of nanoplatelets with TC = 42 ˚C embedded in a layer of Matrigel® where prostate cancer cells were seeded (see M LG - Figure 5 schematics and experimental details are found in SI). The layered system was designed to keep the expected maximum temperature drop between the nanoplatelets and cells below B 0.5 ˚C in a compromise between an accurate temperature assessment and being as less intrusive as possible (see M LG (SI) - Figure 10). The layered system was then heated at a distance using a near infrared (NIR – 850 nm) LED. In this setup, the nanoplatelets act as both logic gates and the main NIR light absorbers, i.e., the main heat sources.

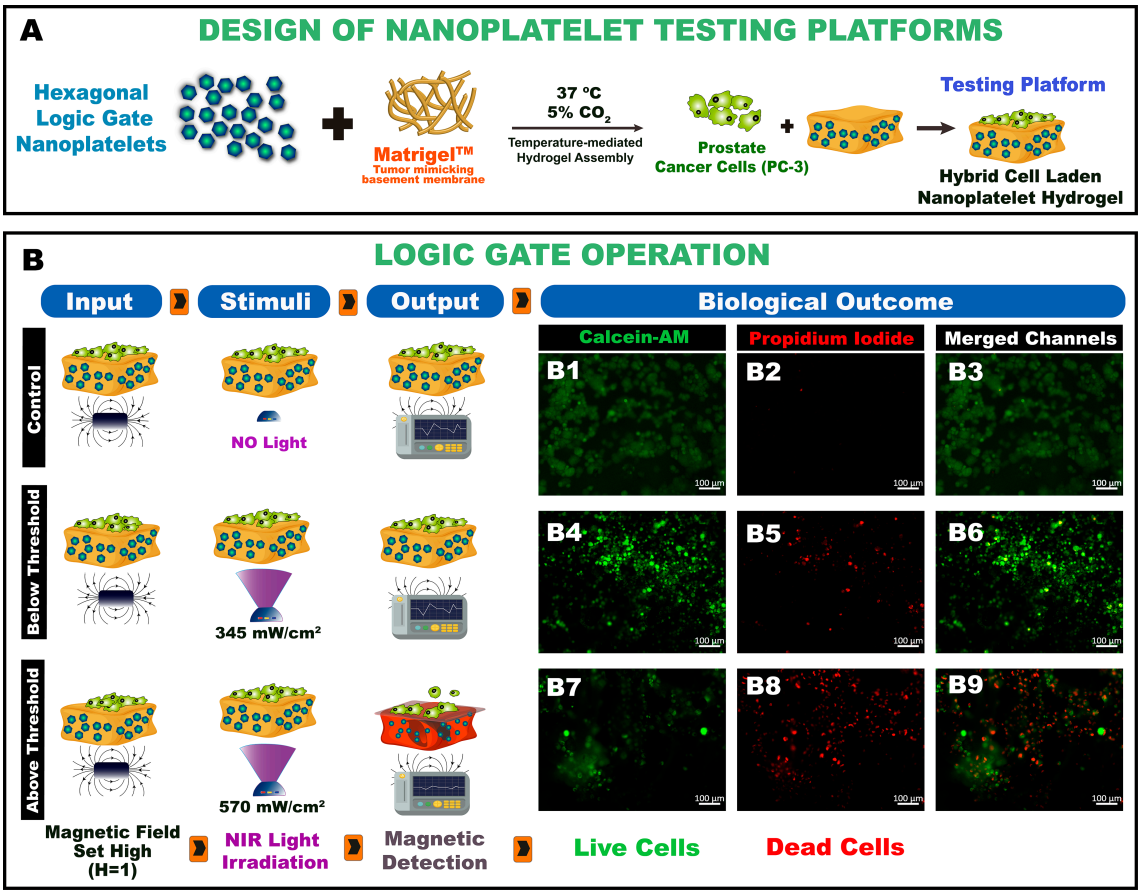

M LG - Figure 5- (A) Scheme showing the assembly of the nanoplatelets with the Matrigel® and Cells, giving rise to the testing platform for logic gate nanoplatelet operation under temperature and field stimuli. (B) Scheme showing the use of the logic gates to record a possible surpassing of the 42 1C threshold temperature during irradiation and fluorescence microscopy micrographs of irradiated PC-3 cells: first, the nanoplatelets are set in a high state; second, the cells are irradiated with different NIR doses; third, the state of the nanoplatelets is evaluated after irradiation. The state of the cells is evaluated after 24 h using a live-dead assay: (B1 to B3) non-irradiated PC-3 cells, control; (B4 to B6) NIR irradiated PC-3 cells with the recorded temperature below the set threshold (345 mW cm2, 5 min); (B7 to B9) NIR irradiated PC-3 cells with the temperature above the threshold (570 mW cm2, 5 min). Green channel: calcein-AM, red-channel: propidium iodide.

The temperature increase was manipulated by changing the intensity of the LED and the irradiation time. For a total irradiation time of 5 min, the logic gates indicated that the temperature threshold of 42 ˚C is surpassed at a power density between 456 and 570 mW cm^{-2}

(see the M LG (SI) - Figure 11). This result shows a good correlation with the binary indication given by the live/dead assay: in the non-irradiated control and for LED powers below the threshold determined by the logic gates (M LG - Figure 5B1–B6), the assay shows that the great majority of cells are viable 24 h after irradiation, while above that power threshold the opposite is observed (M LG - Figure 5 B7–B9). These results highlight the use of the Fe_3Se_4 nanoplatelets to simultaneously gain insight as a quality control technology for temperature thresholds during treatments, while acting as NIR light absorbers in anti-cancer hyperthermia.

The nanoplatelets reported here represent a landmark in the size control of Fe_3Se_4 nanoparticles, leading to good control over their magnetic properties and stability in water. Such control of properties opens the way to new applications exploring the unique characteristics of Fe_3Se_4 nanoparticles: ability to record information and inability to keep that information above a critical temperature TC tunable in a range around room temperature. In other words, Fe_3Se_4 nanoparticles are not suitable for long-term data storage but are valuable for monitoring materials having also some sort of critical change in their behaviour at a temperature close to TC, such as tissues, cells, biomolecules and soft matter in general. A noteworthy example is the combination of Fe_3Se_4 nanomagnets and cells sharing a critical temperature, with this combination being explored to keep track of threshold temperatures in the context of hyperthermia, as shown here. This proof of concept opens the pathway to other noteworthy applications such as monitoring temperature thresholds in heat-triggered release of drugs or genetic therapy and monitoring temperature thresholds in ultrafast local increase of temperature in polymerase chain reaction.[21] In addition, the ultrafast response to temperature and the nanometer size of the Fe_3Se_4 platelets allow them to be further explored in limit situations where both high temporal and high space resolution are required, avoiding the typical constraints of nanoscale thermometers.[22][clviii]

Experimental section

Fe_3Se_4 nanoplatelets were synthesized by the thermal decomposition of Fe–oleate in the presence of a Se–octadecene complex, tetradecylphosphonic acid (TDPA) and 1-dodecanethiol (DDT). Typical amounts used were 210 mg of Fe–oleate, 10 g of Se–octadecene, 150 mg of DDT and 30 mg of TDPA. The mixture was allowed to purge at low pressure and 120 1C for 30 min, and ramped at 5 ˚C min^{-1} up to 210 ˚C, where it remained for 1 h. Fe–oleate was prepared and washed using standard procedures.16 The Se–octadecene complex was also prepared using standard procedures[23] by the reaction of 434 mg of metallic Se powder with 75.3 g of 1-octadecene for 30 min at 180 ˚C.

Phase transfer of the Fe_3Se_4 nanoplatelets was performed by exchanging the DDT/TDPA molecules on the nanoplatelets' surfaces for molecules of caffeic acid. 10 mg of nanoplatelets were dispersed in THF, along with 50 mg of caffeic acid. The mixture was left at 50 1C for 4 h under stirring to promote the exchange of molecules. 100 mL of a 0.5 M solution of NaOH were added to the mixtures and the particles were centrifuged and separated from the THF, which were dispersed in about 2 mL of distilled water without further washing. A water suspension of Fe_3Se_4 nanoplatelets was cast in µ-slide angiogenesis Ibidi imaging chambers until a uniform

[clviii] Go to: PEF Nucleic acid Detection; LSPR Prot Act; or Conclusions

layer was formed. Matrigel® was then deposited and allowed to crosslink with the nanoplatelets at 37 ˚C for 2 h. This dual deposition strategy allowed for the formation of a cell adhesive substrate for PC-3 cell proliferation. Prostate cancer cells were then seeded at a density of 1.3 x 10^5 cells per cm^2 and allowed to proliferate for 24 h. Before irradiation, the Fe_3Se_4 nanoplatelets were magnetized (i.e. set in a high state M = 1, by applying a high field H = 1) using a cylindrical neodymium–iron–boron magnet (diameter 8 mm, height 30 mm, N42). Irradiation was then performed using an 850 NIR LED (Oslon PowerStar) with power densities between 285 and 570 mW cm^{-2} (according to specifications) for 5 min.

This irradiation may lead (or not) to a change in temperature state from low to high and it may thus change (or not) the magnetization state from high to low. This possible change in the magnetization state after the irradiation procedure was measured using a fluxgate magnetometer (FL1-100 Stefan Mayer Instruments) embedded in a permalloy foil to decrease the ambient magnetic field and noise at the fluxgate. At last, on the following day, cells were incubated with Calcein-AM/PI for 30 min at 37 ˚C. The cells were then washed 3 times with PBS and imaged using a Zeiss Imager M2 fluorescence microscope.

References – M LG

(1) Gordon, R. T.; Hines, J. R.; Gordon, D. Intracellular Hyperthermia a Biophysical Approach to Cancer Treatment via Intracellular Temperature and Biophysical Alterations. *Medical Hypotheses* **1979**, *5* (1), 83–102. https://doi.org/https://doi.org/10.1016/0306-9877(79)90063-X.

(2) Silva, A. P. de. *Molecular Logic-Based Computation, Mono- Graphs in Supramolecular Chemistry*; Royal Society of Chemistry, 2016. https://doi.org/9781782626237.

(3) Medalsy, I.; Klein, M.; Heyman, A.; Shoseyov, O.; Remacle, F.; Levine, R. D.; Porath, D. Logic Implementations Using a Single Nanoparticle–Protein Hybrid. *Nature Nanotechnology* **2010**, *5* (6), 451–457. https://doi.org/10.1038/nnano.2010.62.

(4) Mu, L. X.; Shi, W. S.; Zhang, T. P.; Zhang, H. Y.; Wang, Y.; She, G. W.; Gao, Y. H.; Wang, P. F.; Chang, J. C.; Lee, S. T. ZnO Nanowire-Based All-Optical Switch with Reset-Set Flip-Flop Function. *Applied Physics Letters* **2011**, *98* (16), 163101. https://doi.org/10.1063/1.3581884.

(5) Miller, E. W.; Bian, S. X.; Chang, C. J. A Fluorescent Sensor for Imaging Reversible Redox Cycles in Living Cells. *Journal of the American Chemical Society* **2007**, *129* (12), 3458–3459. https://doi.org/10.1021/ja0668973.

(6) Hirone, T.; Chiba, S. The Magnetic Properties of FeSex with the NiAs Structure. *Journal of the Physical Society of Japan* **1956**, *11* (6), 666–670. https://doi.org/10.1143/JPSJ.11.666.

(7) Peter Terzieff, K. L. K. The Antiferromagnetic and Ferrimagnetic Properties of Iron Selenides With NiAs-Type Structure. *Monatshefte für Chemie/Chemical Monthly* **1978**, *109*, 1037–1047. https://doi.org/10.1007/BF00913006.

(8) Dutrizac, J. E.; Janjua, M. B. I.; Toguri, J. M. Phase Studies on the Iron–Selenium System. *Canadian Journal of Chemistry* **1968**, *46* (8), 1171–1174. https://doi.org/10.1139/v68-200.

(9) Schuster, W.; Mikler, H.; Komarek, K. L. Transition Metal-Chalcogen Systems, VII.: The Iron-Selenium Phase Diagram. *Monatshefte für Chemie / Chemical Monthly* **1979**, *110* (5), 1153–1170. https://doi.org/10.1007/BF00910963.

(10) Zhang, H.; Long, G.; Li, D.; Sabirianov, R.; Zeng, H. Fe3Se4 Nanostructures with Giant Coercivity Synthesized by Solution Chemistry. *Chemistry of Materials* **2011**, *23* (16), 3769–3774. https://doi.org/10.1021/cm201610k.

(11) Lyubutin, I. S.; Lin, C.-R.; Funtov, K. O.; Dmitrieva, T. V; Starchikov, S. S.; Siao, Y.-J.; Chen, M.-L. Structural, Magnetic, and Electronic Properties of Iron Selenide Fe6-7Se8 Nanoparticles Obtained by Thermal Decomposition in High-Temperature Organic Solvents. *The Journal of Chemical Physics* **2014**, *141* (4), 44704. https://doi.org/10.1063/1.4887356.

(12) He, X.; Li, T.; Wang, L.; Wang, J.; Jiang, J.; Yang, G.; Meng, F.; Wu, Q. Electrically Tunable Terahertz Wave Modulator Based on Complementary Metamaterial and Graphene. *Journal of Applied Physics* **2014**, *115* (17), 17B903. https://doi.org/10.1063/1.4866079.

(13) Sen Bishwas, M.; Das, R.; Poddar, P. Large Increase in the Energy Product of Fe3Se4 by Fe-Site Doping. *The Journal of Physical Chemistry C* **2014**, *118* (8), 4016–4022. https://doi.org/10.1021/jp411956q.

(14) Li, S.; Li, D.; Liu, W.; Zhang, Z. High Curie Temperature and Coercivity Performance of Fe3−xCrxSe4 Nanostructures. *Nanoscale* **2015**, *7* (12), 5395–5402. https://doi.org/10.1039/C4NR07287A.

(15) Pohjonen, R.; Mustonen, O.; Karppinen, M.; Lindén, J. Mössbauer Study of Magnetism in Fe3Se4. *Journal of Alloys and Compounds* **2018**, *746*, 135–139. https://doi.org/https://doi.org/10.1016/j.jallcom.2018.02.257.

(16) Bronstein, L. M.; Huang, X.; Retrum, J.; Schmucker, A.; Pink, M.; Stein, B. D.; Dragnea, B. Influence of Iron Oleate Complex Structure on Iron Oxide Nanoparticle Formation. *Chemistry of Materials* **2007**, *19* (15), 3624–3632. https://doi.org/10.1021/cm062948j.

(17) Liu, Y.; Chen, T.; Wu, C.; Qiu, L.; Hu, R.; Li, J.; Cansiz, S.; Zhang, L.; Cui, C.; Zhu, G.; You, M.; Zhang, T.; Tan, W. Facile Surface Functionalization of Hydrophobic Magnetic Nanoparticles. *Journal of the American Chemical Society* **2014**, *136* (36), 12552–12555. https://doi.org/10.1021/ja5060324.

(18) You, H.; Fang, J. Particle-Mediated Nucleation and Growth of Solution-Synthesized Metal Nanocrystals: A New Story beyond the LaMer Curve. *Nano Today* **2016**, *11* (2), 145–167. https://doi.org/https://doi.org/10.1016/j.nantod.2016.04.003.

(19) Fisher, M. E.; Barber, M. N. Scaling Theory for Finite-Size Effects in the Critical Region. *Physical Review Letters* **1972**, *28* (23), 1516–1519. https://doi.org/10.1103/PhysRevLett.28.1516.

(20) Abrahams, E. Relaxation Processes in Ferromagnetism; Marton, L. B. T.-A. in E. and E. P., Ed.; Academic Press, 1954; Vol. 6, pp 47–68. https://doi.org/https://doi.org/10.1016/S0065-2539(08)60131-6.

(21) Lee, J.-H.; Cheglakov, Z.; Yi, J.; Cronin, T. M.; Gibson, K. J.; Tian, B.; Weizmann, Y. Plasmonic Photothermal Gold Bipyramid Nanoreactors for Ultrafast Real-Time Bioassays. *Journal of the American Chemical Society* **2017**, *139* (24), 8054–8057. https://doi.org/10.1021/jacs.7b01779.

(22) Brites, C. D. S.; Lima, P. P.; Silva, N. J. O.; Millan, A.; Amaral, V. S.; Palacio, F.; Carlos, L. D. Thermometry at the Nanoscale. *Nanoscale* **2012**, *4* (16), 4799–4829. https://doi.org/10.1039/C2NR30663H.

(23) Bullen, C.; van Embden, J.; Jasieniak, J.; Cosgriff, J. E.; Mulder, R. J.; Rizzardo, E.; Gu, M.; Raston, C. L. High Activity Phosphine-Free Selenium Precursor Solution for Semiconductor Nanocrystal Growth. *Chemistry of Materials* **2010**, *22* (14), 4135–4143. https://doi.org/10.1021/cm903813r.

Supplementary Information

Detailed experimental description

Here we detail the synthesis and experiments performed in four samples of Fe_3Se_4 nanoplatelets, whose general procedure is given in the manuscript. Specific conditions and selected properties are given in table 1.

Synthesis of precursors

Fe-oleate was prepared and washed using standard procedures .1 Washing processes included an extraction with a mixture of ethanol acetone and a redispersion with hexane followed by an evaporation step at room temperature. These steps were repeated for 2 to 4 times, resulting in brown Fe-oleates spanning from a slightly viscous behaviour to a solid darker wax, used to produce smaller and larger nanoplatelets, respectively. The Se-octadecene complex was also prepared using standard procedures2 by the reaction of 434 mg of metallic Se powder with 75.3 g of 1-octadecene during 30 min at 180 ˚C.

Microscopy

Transmission electron microscopy (TEM) on the nanoparticles was performed using a HitachiH9000 microscope, working at 300 kV. Scanning Transmission Electron Microscopy – High Angle Annular Dark Field (STEM-HAADF) images were obtained in a probe-corrected Titan (FEI) at a working voltage of 300 kV, coupled with a HAADF detector (Fischione). In order to analyse the chemical composition of the materials, X-ray Energy Dispersive Spectra (EDS) were obtained with an EDAX detector. Samples for TEM observations of the NPs dispersed in the ferrofluids were prepared by dip coating of carbon coated copper grids. Prostate cancer cells were washed 3 times with PBS and imaged in a Zeiss Imager M2 fluorescence microscope (Carl Zeiss Microscopy GmbH, Germany), equipped with a 10x/0.25 Plan Apochromat air objective. All the data was processed in the Zeiss Zen software (v 2.3).

X-ray diffraction

X-ray diffraction (XRD) measurements were performed at room temperature with a PANalytical Empyrean powder diffractometer using monochromated CuKα radiation (λ = 1.541 ˚A) in the 10 - 80◦ 2θ range at 0.02◦ resolution, and 4000 acquisition points per step. Theincident beam optics included a Soller slit of 0.04 rad, a 10 mm fixed mask, a divergence fixed slit of 1/4 and an anti-scatter slit of 1/8. The diffracted beam optics included a Soller slit of 0.04 rad and anti-scatter slit of 7.5 mm. The analysis of the diffraction patterns was performed by Rietveld refinement using the F ullProf package.3 The size effects were treated with the integral breadth method using the Voigt model for both the instrumental and intrinsic diffraction peak shape considering a Thompson-Cox-Hastings pseudo-Voigt convoluted with Axial divergence asymmetry function to describe the peak shape. The contribution of the instrument to the peaks broadening was determined by the refinement of the XRD pattern of a LaB6 standard sample (NIST ref. 660a).

Magnetic data

Magnetic measurements were performed in a superconducting quantum interference device (SQUID) magnetometeres model MPMS-XL and MPMS3, from Quantum Design Inc, under helium atmosphere and under controlled magnetic field and temperature. The field is provided

by a superconducting magnet and temperature is controlled in feedback using a cold helium flow and a heater acting on the flow

X-ray photoelectron spectroscopy

The X-ray photoelectron spectroscopy (XPS) analysis was carried out using a Kratos Axis SUPRA spectrometer employing a monochromatic Al Kα (1486.6 eV) 15 mA, 15 kV) X-ray source and a power of 225 W.

Cell culture

Prostate cancer cells (PC-3) were routinely cultured in RPMI-1640 medium supplemented with 10% FBS and 1% antibiotic/antimycotic. PC-3 cells were grown in cell culture treated t flasks in a temperature-controlled incubator at 37◦, 5% CO2 and in a humidified atmosphere. Upon reaching confluency cells were detached by using TripLETMXpress and subcultured.

Hyperthermia studies on cells

The normal use of the nanoplatelets as logic gates, to know if a temperature threshold during irradiation is crossed, involves setting them in a high magnetization state (M=1) by the application of a (high) magnetic field (H=1), followed by the irradiation procedure and followed by measuring the final magnetization state, which may or may not have changed to zero due to irradiation). Although less useful in practice, the use of the SR latch gate can be reversed and used to detect any magnetic field going above a threshold during a period of time where temperature is known to be always below TC. In this case, temperature is turned first such that magnetization is reset low (M=0) and any possible field during a given period of time will set magnetization in a high state (Q=1).

Simulations

Thermal simulations were performed using the finite element analysis software QuickFieldTMProfessional 6.3. We considered a axial symmetric geometry with hot spots representing the nanoplatelets at a constant temperature (42 ◦C) embedded in a 780 ➪m thick Matrigel^{TM} layer with thermal conductivity 0.5 W/Km and a 20 ➪m thick cell layer with the same conductivity. The top cell layer exchanges heat with the cell medium by convection, simulated using a surface convection boundary condition with h = 500 W/Km2 and ambient temperature 37 ◦C.4 The remaining Matrigel^{TM} and cell surfaces exchange heat by conduction with a plastic frame (thermal conductivity 0.4 W/Km), which in turn exchanges heat with air by convection (h = 10 W/Km2 and ambient temperature 37 ◦C). This simulation provides an estimation of the maximum expected temperature difference between the nanoplatelets and the cells due to the chosen geometry. Additional temperature drops may occur at the micro/nano interfaces and are presently a matter of debate (see, for instance, Ref.5). Such additional temperature drops would be present even if the nanoplatelets were mixed together will cells.

Tables and figures

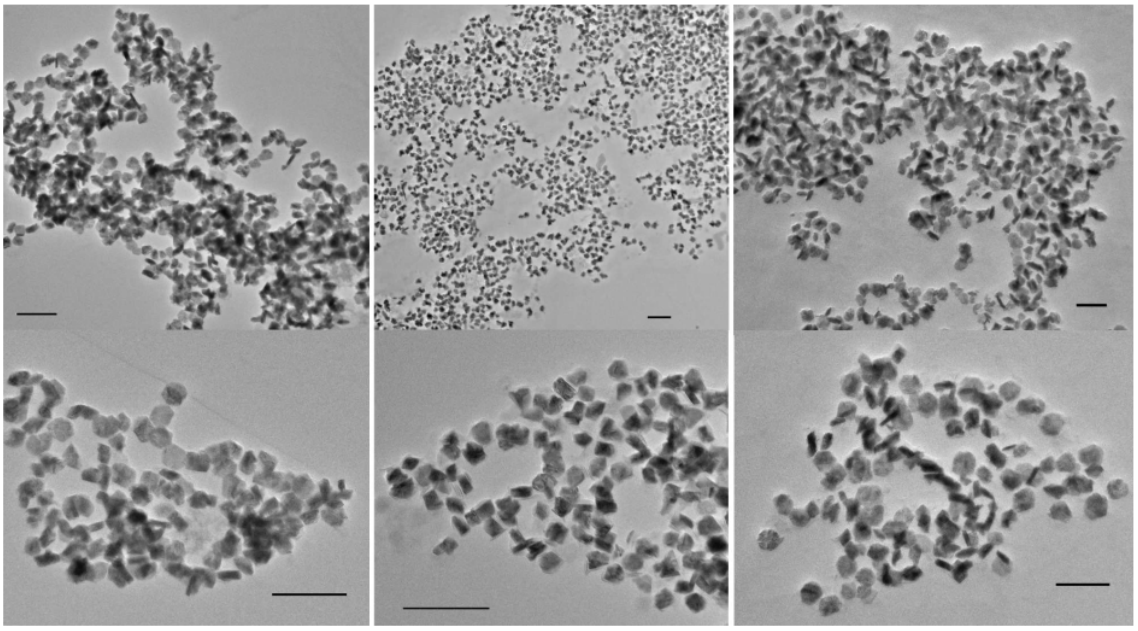

M LG (SI) - Figure 1 - ***Electron microscope images of Fe_3Se_4 nanoplatelets****. Left column shows images of sample with average lateral diameters of 130 nm, central column 95 nm and right column 193 nm. All scale bars correspond to 500 nm.*

M LG (SI) - Table 1 - Relevant parameters of synthesis conditions, morphology, and magnetic properties of the four samples of Fe_3Se_4 nanoplatelets presented in the manuscript. The diameter of the nanoplatelets is estimated as the distance across two parallel edges. D_g is calculated using the average diameter and thickness considering that the nanoplatelets are flat cylinders.

Synthesis conditions			Characteristic sizes and magnetic phase transition				
Ramp rate (˚C/min)	T_{max} (˚C)	time@ T_{max} (h)	Diameter (nm)	Thickness (nm)	XRD size (nm)	D_g (nm)	T_C (˚C)
7.5	210	1	130	43	18	95	18
5	210	1	95	36	26	70	36
18	210	0.75	193	46	21	137	22
18	210	1	250	60	31	180	42

M LG (SI) - Table 2- True table of the SR latch as usually presented, showing the output of the logic circuit at a time t (Q(t)), the subsequent action on S, R, or both and the resulting output at a time t + 1 (Q(t + 1)). RC stands for 'race condition', where the state Q(t + 1) is ill-defined and depend on which S or R is set low in first place. In the present case, Q corresponds to the magnetization M, S corresponds to the field H and R corresponds to temperature T.

Q(t)	S	R	Q(t + 1)
0	0	0	0

0	0	1	0
0	1	0	1
0	1	1	RC
1	1	1	RC
1	0	1	0
1	1	0	1

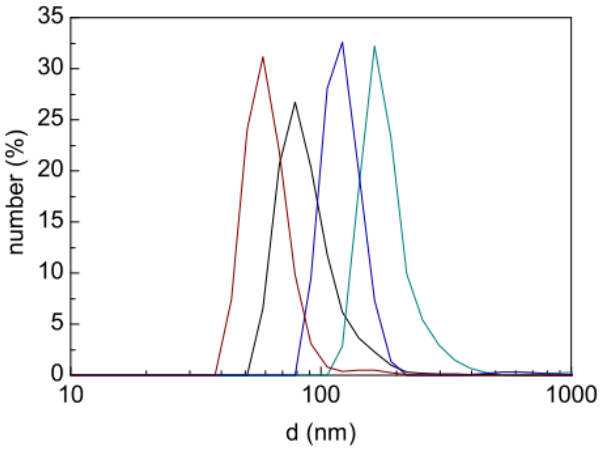

M LG (SI) - Figure 2 - ***Diameter size distributions of the colloidal suspensions of the Fe_3Se_4 nanoplatelets.*** *Hydrodynamic size distribution obtained with dynamic light scattering. The average hydrodynamic sizes are compatible with suspensions of isolated Fe_3Se_4 nanoplatelets. In fact, these sizes are systematically smaller than the average diameter obtained from electron microscopy and close to the average gyration diameter (D_g) obtained for flat cylinders (gyration radius $R_g^2 = (a^2/2) + (t^2/12)$ where R_g is half of the gyration diameter, a is half of the average diameter and t is the thickness of the nanoplatelets).*

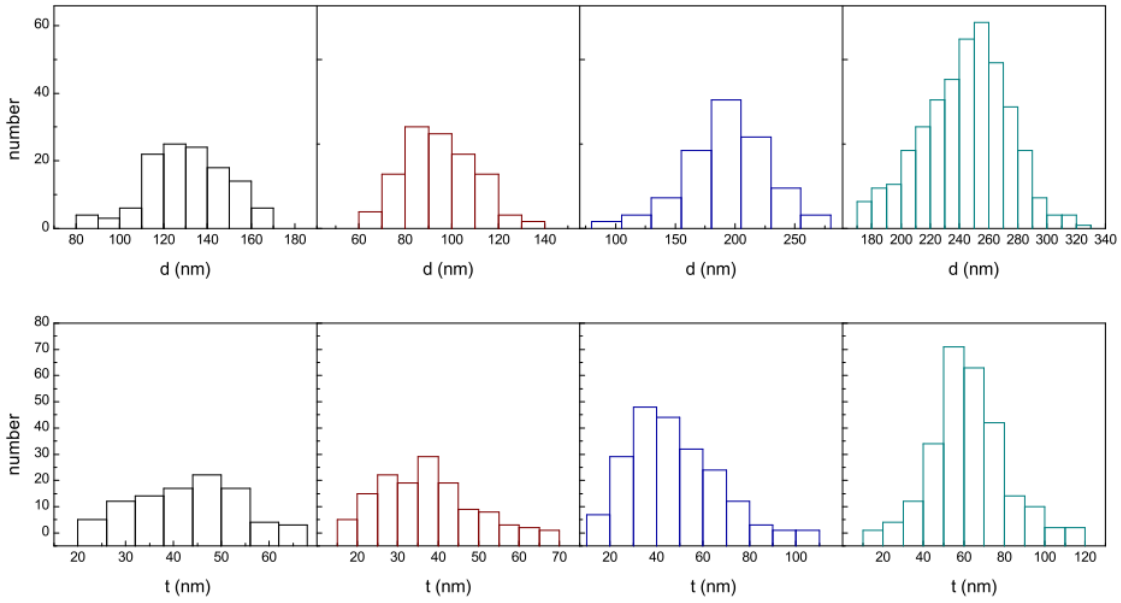

M LG (SI) - Figure 3 - ***Diameter and thickness distributions of the Fe_3Se_4 nanoplatelets.***

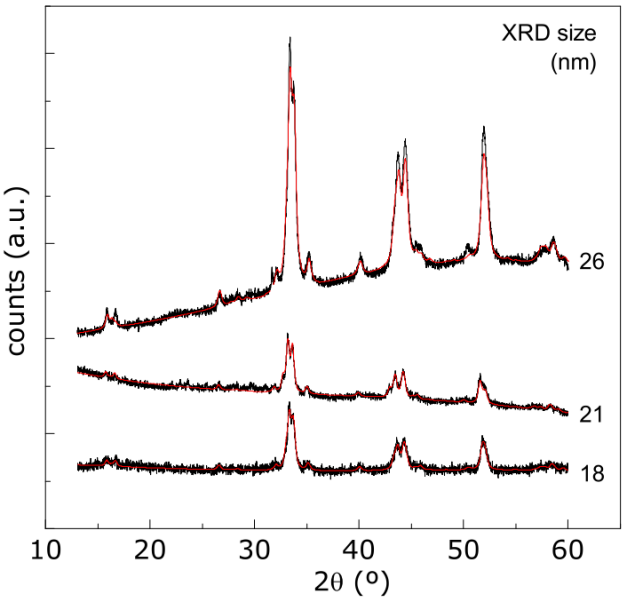

M LG (SI) - Figure 4- ***X-ray diffraction patterns of Fe_3Se_4 nanoplatelets****. Continuous (red) line represents Rietveld refinement to the XRD data. Average apparent sizes are shown in the right side of the plot.*

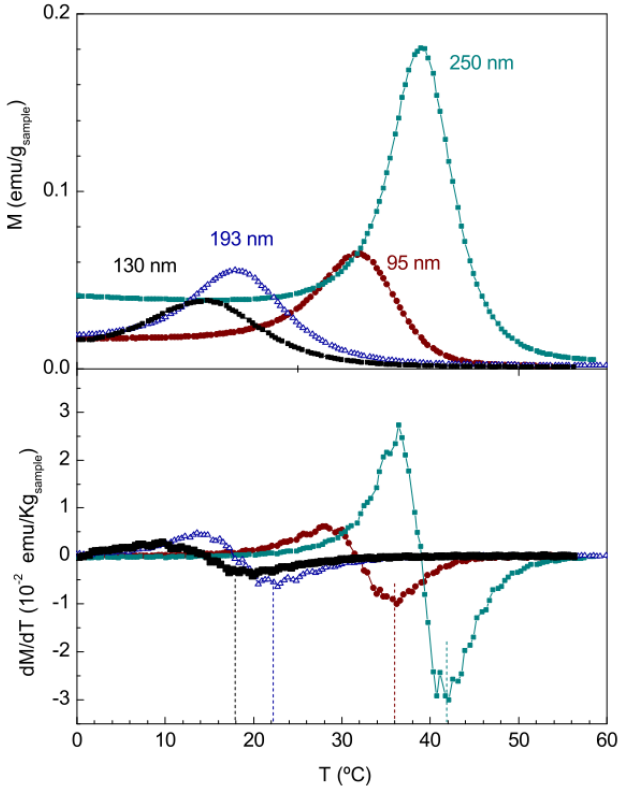

M LG (SI) - Figure 5 - ***Magnetization of Fe_3Se_4 nanoplatelets with different average lateral diameter as a function of temperature and associated derivative. T_C is taken as the minimum of that derivative, i. e., the inflexion point of the M(T) data****.*

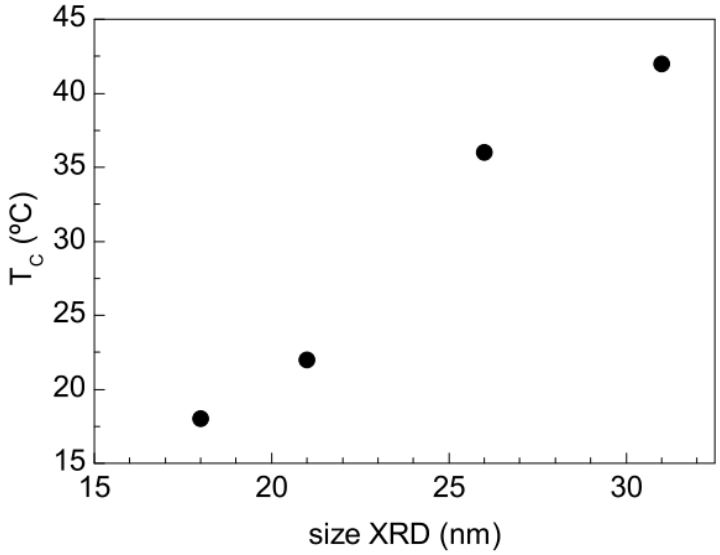

M LG (SI) - Figure 6 - Average apparent sizes obtained from Rietveld refinement as a function of the transition temperature T_C.

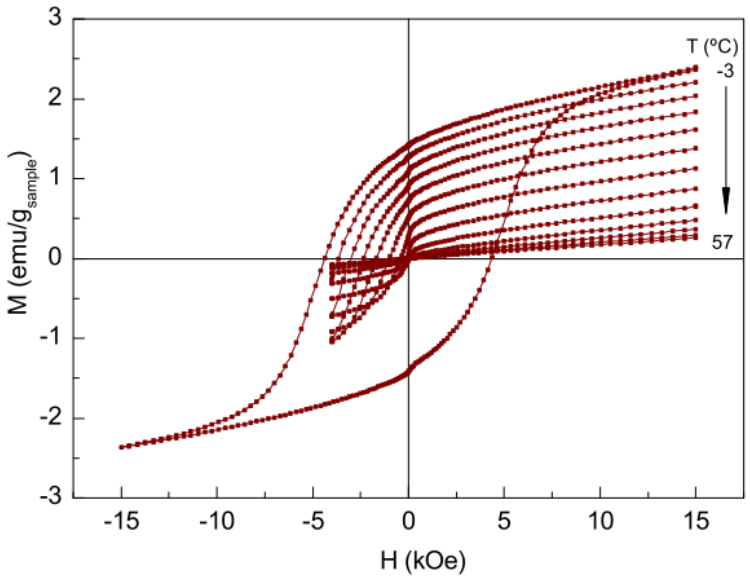

M LG (SI) - Figure 7 - ***Dependence of magnetization with the external magnetic field.*** *Curves were recorded at selected temperatures around room temperature in the Fe_3Se_4 nanoplatelets with an average diameter of 95 nm.*

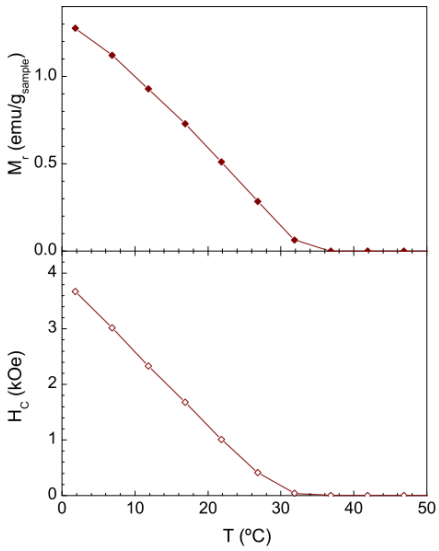

M LG (SI) - Figure 8 - ***Remanent magnetization, susceptibility and coercive field of the Fe_3Se_4 nanoplatelets with average diameter/thickness of 95 nm.*** *All data shown was taken from the hysteresis cycles shown in the previous figure.*

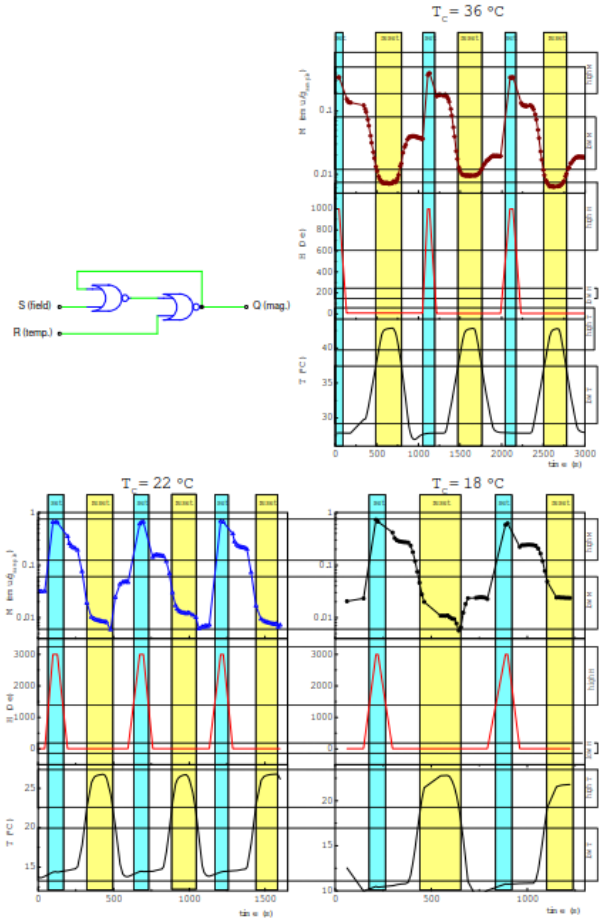

M LG (SI) - Figure 9 - ***Logic element representation of the bistable gate (SR latch) and examples of the time diagram of the gate.*** *The gate can be represented by two NOR elements in feedback, with two possible inputs, a set (S) and a reset (R), and one output (Q). Example of functioning of the logic gate as a function of time in samples with different T_C, showing the basic operations of the gate based on the response of magnetization (Q) to the field (S) and temperature (R) inputs.*

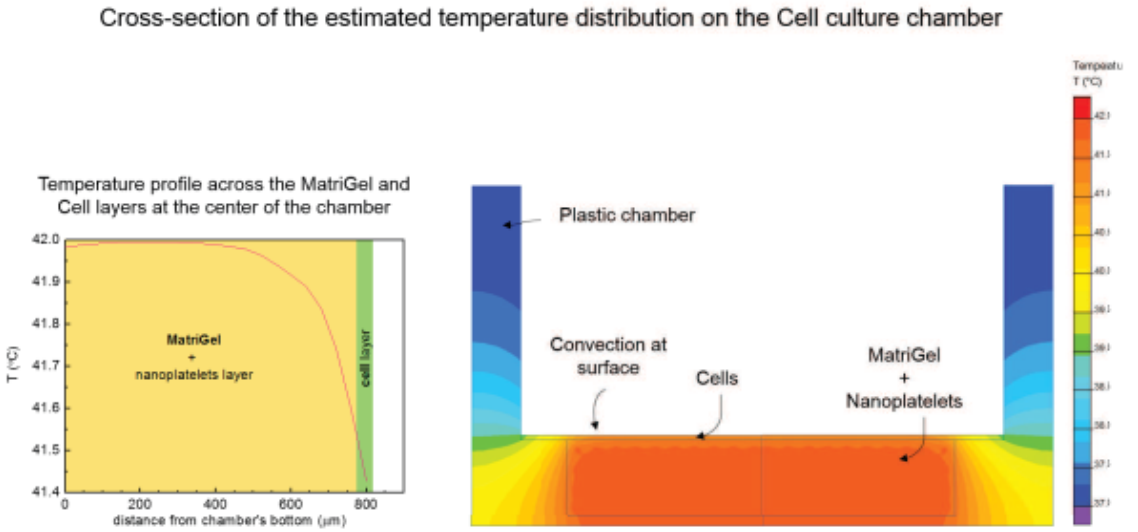

M LG (SI) - Figure 10 - ***Simulated temperature distribution at equilibrium of the cell culture.*** *Estimation of the temperature distribution on the cell culture chambers containing the Matrigel™, nanoplatelets, cells and cell medium when the nanoplatelets are at 42 °C and the total heat flux generated by the nanoplatelets is 0.045 W across a 0.12 cm² surface. The layered system used in the cell hyperthermia experiments introduces per se a maximum temperature drop between nanoplatelets and cells of ~0.5 °C and any additional temperature drop will be due to intrinsically lower thermal conductivity at the micro and interfaces which would be present even in a non-layered geometry where cells and nanoplatelets were mixed without internalization.*

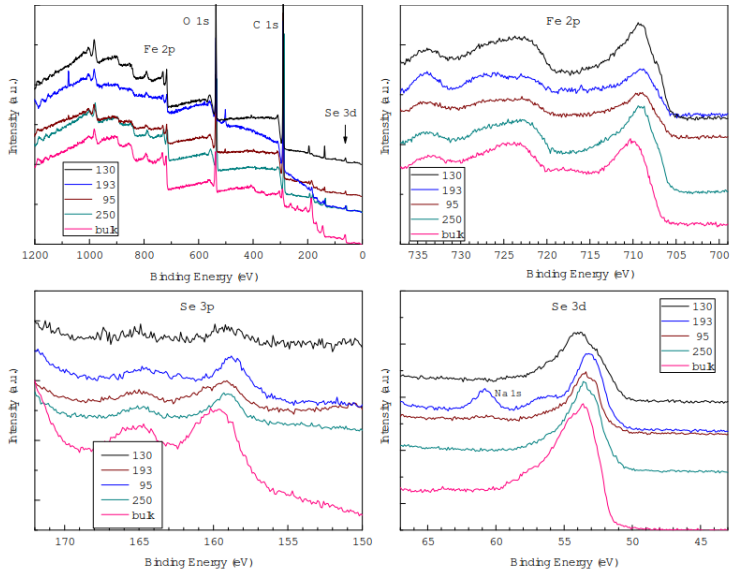

M LG (SI) - Figure 11 - ***XPS data of the Fe3Se4 nanoplatelets (with different average sizes) and reference (bulk) sample.*** *The panels show the full spectra and the high-resolution Fe 2p, Se 3p and Se 3d spectra. The spectra show small differences among the nanoplatelets with different average sizes and shifts to lower energy values when compared to the microcrystalline sample. This shift is of the order of the uncertain associated to the C 1s peak used to correct the effect of the charge neutralizer and therefore it can be an intrinsic effect (associated to different Fe and Se environments/oxidation states) or a spurious effect since the C 1s found in the nanoplatelets is probably different from that found in the microcrystalline sample. Apart this shift, the most noticeable difference between spectra is a satellite peak near 717.6 eV found only in the microcrystalline sample and the broadening/deconvolution around the 725 eV region. One of the samples shows a contamination with Na.*

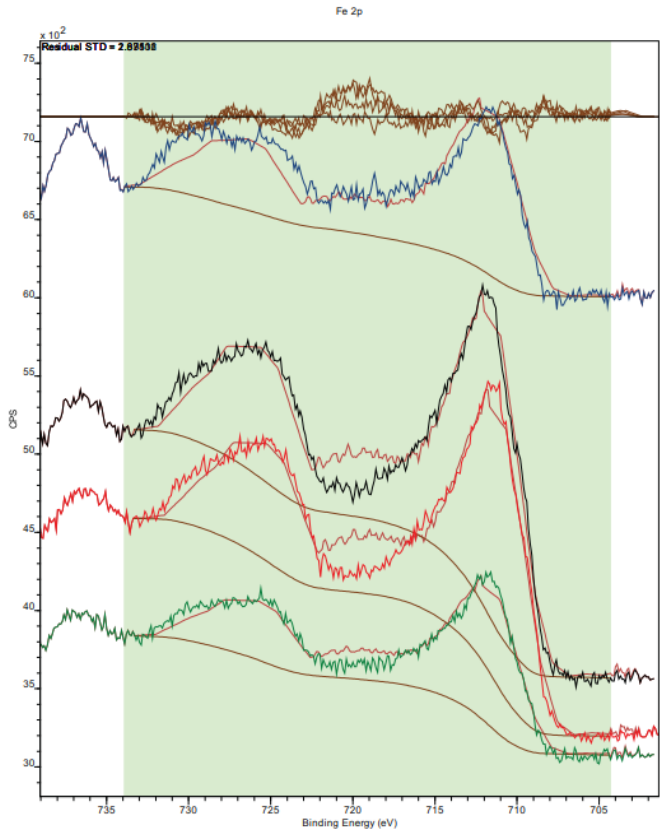

M LG (SI) - Figure 12 - ***High resolution XPS Fe 2p spectra of the nanoplatelets fitted to that of the microcrystalline sample, allowing an energy shift.***

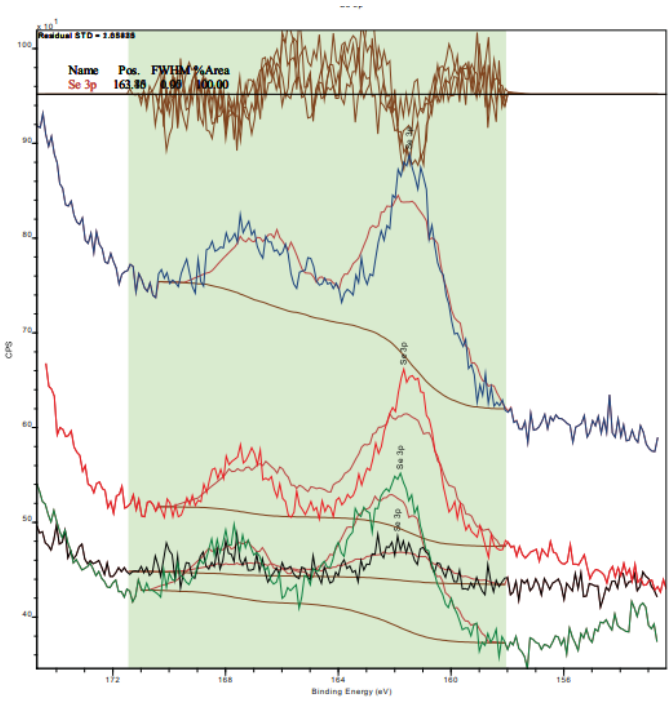

M LG (SI) - Figure 13 - ***High resolution XPS Se 3p spectra of the nanoplatelets fitted to that of the microcrystalline sample, allowing an energy shift.***

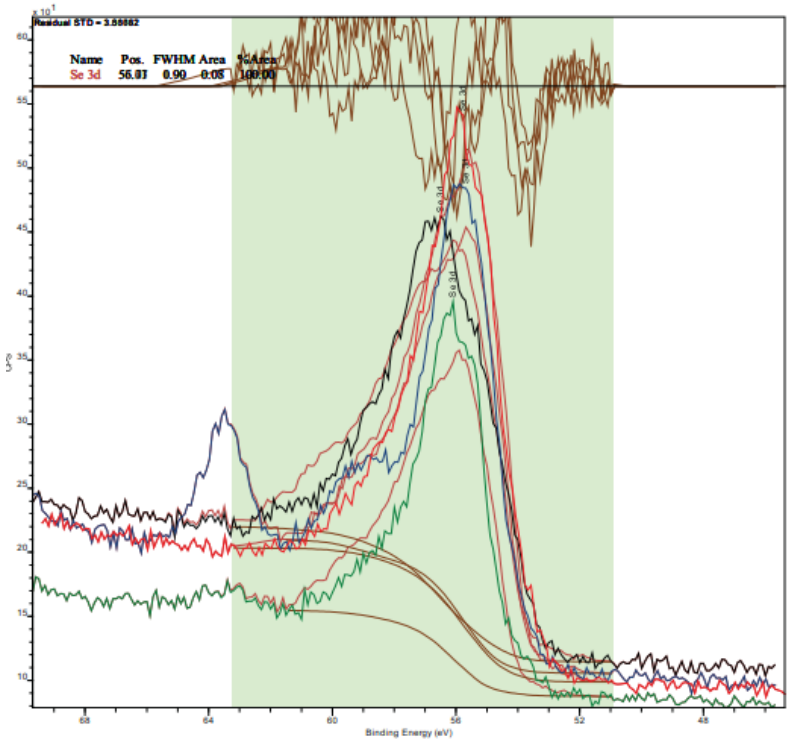

M LG (SI) - Figure 14 - ***High resolution XPS Se 3d spectra of the nanoplatelets fitted to that of the microcrystalline sample, allowing an energy shift****.*

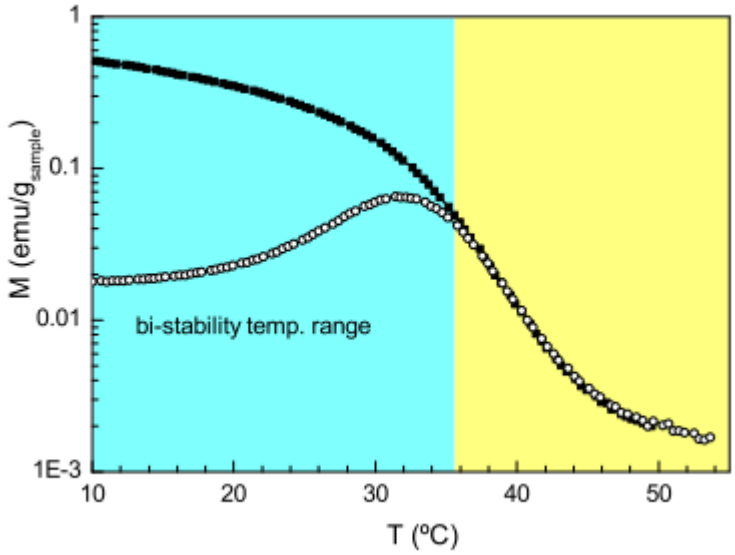

M LG (SI) - Figure 15 - ***Standard zero-field cooling (ZFC) and field cooling curves (FC).*** *Magnetization was recorded as a function of temperature around room temperature at a low applied field (H_{app} = 50 Oe) after cooling from 60 ◦C under zero field (ZFC, open circles) and after cooling under H_{app} (FC, filled squares). Data was recorded on Fe_3Se_4 nanoplatelets with average diameter of 95 nm. Below ∼ 35 ◦C the curves diverge, and the system can be in a high or a low state. Above that temperature the system can be reset.*

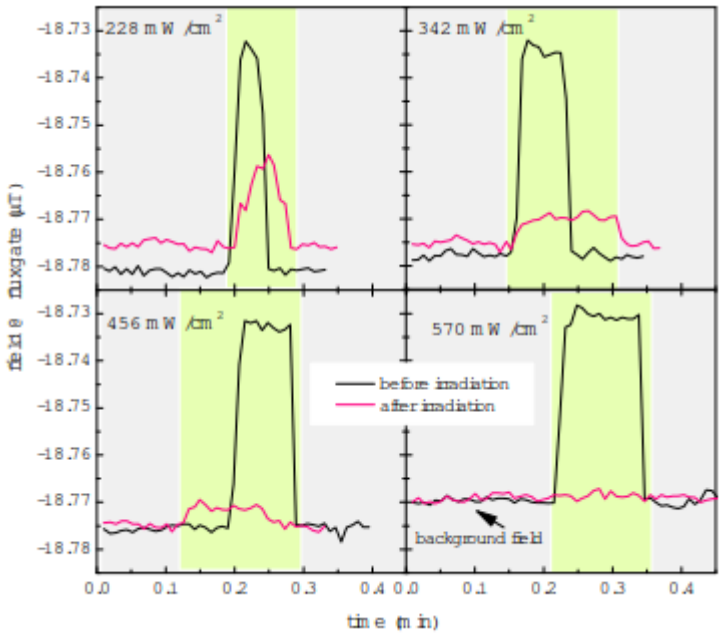

M LG (SI) - Figure 16 ***- Remanent magnetization M_r measured by the fluxgate magnetometer on the cell wells before and after irradiation with a given power during 5 minutes****. The nanoplatelets were set in a high state before irradiation and then approached to the fluxgate magnetometer that senses an increase of magnetic field of the order of 0.05 μT due to dipolar magnetic field created by the M_r of the nanoplatelets (black curves). The curves show the ambient background field (grey areas) and the field created by the nanoplatelets plus background (green areas). After irradiation, the nanoplatelets were again approached to the fluxgate to measure again the dipolar magnetic field (red curves, green area); this field decreases as the power increases, vanishing into the background noise for a power between 456 and 570 mW/cm².*

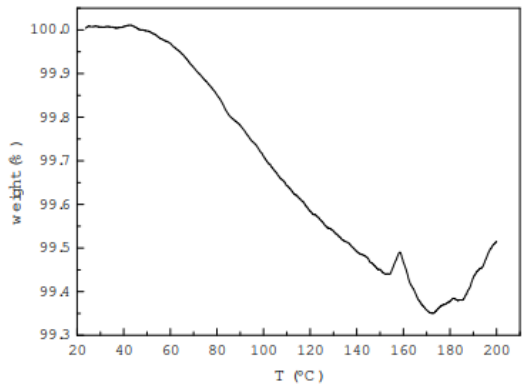

M LG (SI) - Figure 17 - ***Thermogravimetric analysis on the Fe_3Se_4 nanoplatelets before phase transfer****. Analysis was performed on a Shimadzu TGA-50 thermogravimetric analyzer, using a heating rate of 5 °C/min under air atmosphere, with a flow rate of 20 mL/min. The sample holder was a 5 mm diameter platinum plate and the sample mass was 4.03 mg.*

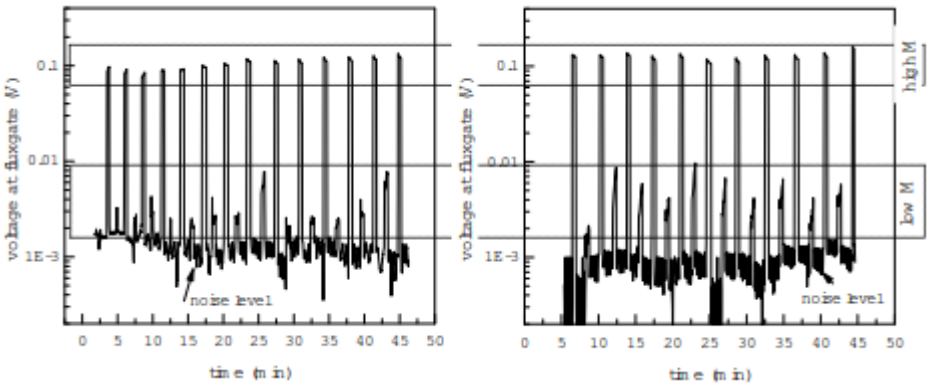

M LG (SI) - Figure 18 - ***Reproducibility tests.*** *Repetition of set/reset cycles measuring the output voltage at the fluxgate magnetometer induced by the high and low magnetization states of the logic gates. The high and low states are clearly separated by an order of magnitude of signal difference. The oscillations from cycle to cycle are much smaller than this difference. We present 2 groups of measurements performed on different days.*

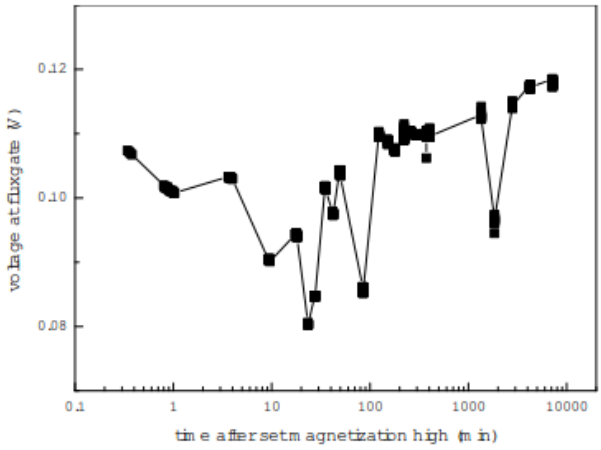

M LG (SI) - Figure 19 - ***Stability tests****. Stability over time of the output voltage at the fluxgate magnetometer after setting magnetization in the high state. The fluctuation of the response is quite low compared to the difference between the high and low magnetization levels. A long stability means that the logic gates can test a possible temperature threshold surpass occurring in a wide time frame.*

A single-particle plasmon sensor to monitor proteolytic activity in real-time.

General Overview

Homeostasis is the thin line that often separates health from disease. To ensure this fine balance, metabolic processes that are mainly regulated by enzymes, dynamically adapt to the environment through a set of chemical reactions. Proteolytic enzymes or proteases are essential to many metabolic pathways, such as tissue regeneration, digestion, blood coagulation. Deregulation of proteases may result in pathophysiological conditions as mood disorders, neurodegenerative and cardiorespiratory diseases, cancer… Consequently, proteases have some peculiarities such as the need of post-translational activation and are tightly regulated by feedback-loop mechanisms and/or embedded in complex enzymatic cascades. Furthermore, their activity is conditioned by environmental factors such as temperature, pH and presence of co-factors. For this reason, correlating protease concentration with an outcome is challenging and often erroneous/misleading. Conversely, monitoring the activity of a protease is more informative and can render valuable and precise understanding of a metabolic process and its evolution.

Proteases like thrombin and Prostate Specific Antigen (PSA) are already well-established biomarkers for diagnostic purposes. However, a transition towards activity-based assays such as coagulation tests or thrombin generation assays (TGAs) that provide more insightful and accurate information is gaining momentum. Other examples include probes to determine gelatinolytic activity of MMP-2/9 proteases, for sensitive and precise determination of tumor margins in breast cancer.[clix] Beyond diagnostic purposes, and due to their dynamic and adaptative nature, protease activity holds the potential to be a valuable tool to track the efficiency of a treatment and follow-up on the evolution of a disease. This gain increasing relevance in the context of in P4 medicine, where a deep understanding of the individual characteristics of biological processes and precise tracking of responses to enable feedback-based therapies is essential. Therefore, it is crucial to develop technologies that can measure proteolytic activity in a stable and reliable manner.

Optical molecular-rulers, generally based on FRET,[clx] which present detection limits in the nanomolar range and enable real-time measurements, are the gold-standard methods for proteolytic monitorization. Although, by relying of organic fluorophores their performance and stability is affected in complex environments by parameters such as pH, ionic strength, and the presence of redox species. Additionally, photobleaching[clxi] is likely to occur during long-term measurements, undermining the performance of the sensor and its capabilities. Alternative non-optical methods such as nanopores and IDAMs[clxii] are also interesting especially due to increased sensitivity and multiplexing capabilities. However, these systems are complex to fabricate, can

[clix] AVB-620 from Avelas Biosciences
[clx] FRET - Förster Resonance Energy Transfer from Henrik's Lab
[clxi] Is often considered a spurious effect resulting in lost of fluorescence
[clxii] 3D demonstration of the diffusion phenomenon for interdigitated array (IDA) electrodes from Andrew Lai

be unreliable in complex media such as biofluids and information about enzyme kinetics are unattainable.

Plasmonic nanoparticles are a trustworthy alternative to surpass these restrictions as they are versatile, chemically inert and exhibit long-lasting and robust photostability. The Localized Surface Plasmon Resonance (LSPR) of AuNRs is sensitive to refractive index changes of its surroundings, thus enabling the detection of alterations of its environment in real-time by tracking intensity variations due shifts in their "color spectrum" induced by variations of the refractive index.[clxiii] Due to its clinical relevance in evaluating coagulopathies and potential to understand vascularization, cancer, and other diseases thrombin was selected as a model protease.[clxiv] In our strategy relies on dark-field microscopy using prism-based Total Internal Reflection (TIR) illumination which renders single particle detection with milliseconds time resolution. Resorting to a single-particle detection, hundreds of particles are tracked simultaneously and insights on the kinetics of the enzyme were obtained. The reaction half-time ($t_{1/2}$) enabled the discernment of a sublinear dependence, and the time required for the first enzyme to reach a given particle (t_0) allowed the estimation of the affinity constant between the enzyme and the peptide. Interestingly, both values agreed with predictions obtained with a simplified kinetic model established herein. A major limitation of this label-free and substrate-based assay is the generation of a non-trivial response of the (bio)sensor [clxv]. This occurs because the peptide cleavage induces a blue-shift, while thrombin adsorption (predominant in higher concentrations) induces a red-shift. Acknowledging this, this behavior was exploited to make the sensor quantitative over >2 orders of magnitude (3-300nM) within the biologically relevant window for thrombin by normalizing the response of the sensor against the amount of peptide immobilized.[clxvi]

Many aspects of this LSPR-based sensor still merit further understanding and optimization. Hopefully, this groundwork will encourage the development of single-particle sensors to monitor the activity of hydrolytic enzymes. Future work may explore testing in real and dynamic samples, and testing other proteases, multiplexing, and mapping. Furthermore, the kinetic model described can be improved and merged with bioinformatic tools enabling machine learning algorithms to predict the response of the sensor to many other proteases and speed up the adaptation of the sensor to meet the desired need.[clxvii] The proteolytic sensor exposed above offers many advantages for fundamental studies, quality control of food, follow-up treatments and recoveries. Ultimately, this will deliver an interesting foundation for bedside or POC devices.[clxviii]

[clxiii] Single-Molecule Detection using Plasmons in Metal Nanoparticles from ICMS
[clxiv] Target-peptide can be designed for detect activity of other proteases
[clxv] In this case it means that more than one solution is possible and often depends on other parameters such as time and temperature (for example)
[clxvi] The recovery ratio between of the signal is proportional to the peptide originally immobilized and the amount of enzyme adsorbed after assay.
[clxvii] This is important because of enzymes have different kinetic profiles, they are inhibited by different molecules, sensitive to the environment…
[clxviii] Go to: PEF Nucleic acid Detection; Magnetic Logic-Gate; or Conclusions

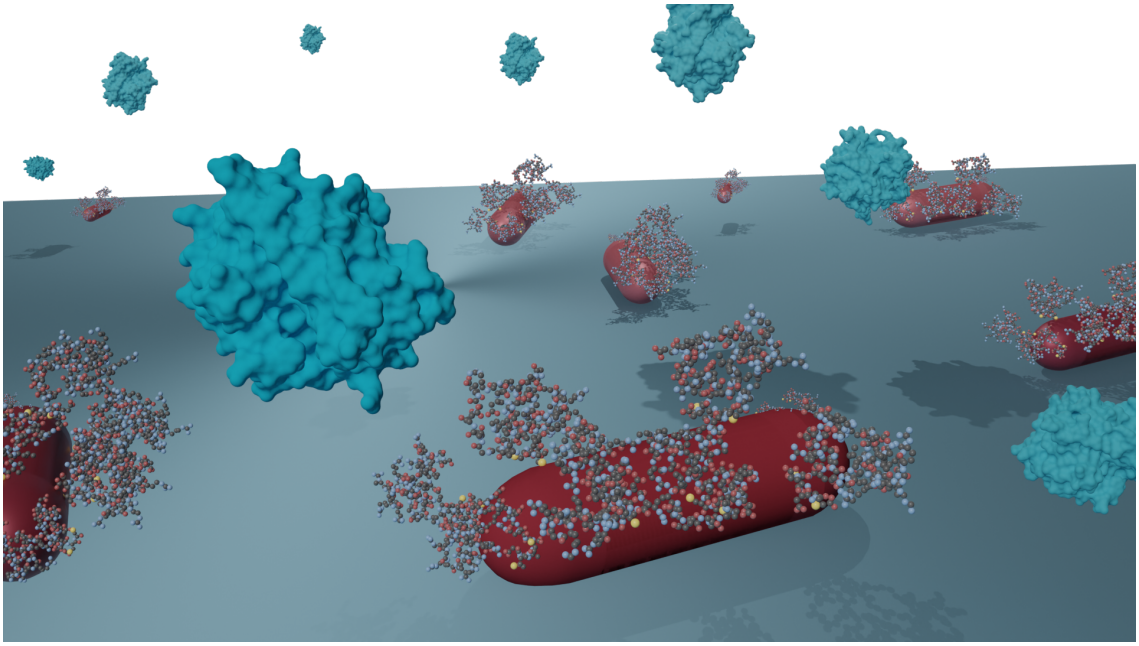

Sub-linear Dependence - **19**
Characterization - **5**
Red-shift
Step 4: THRB adsorption or diffusion to the solution;
Thrombin assays - **12**
Plasmonic Nanoparticles (metallic)
Dark-field Microscopy (DFM)
Blue shift
Single NP LSPR spectrum
Single Wavelength probing
Step 1:Enzime diffusion to NP
Time of arrival (t_0)
AuNRs
Kinetics evaluation
Peptide immobilization
Concentration Dependence
Affinity constant
HyperSpectral Microscopy (HSM)
Step 3: Peptide cleavage
Pseudo 1st-order
Nanoparticle-based (Bio)sensors - **1**
Modelling
Half-time reaction (t1/2)
Localized Surface Plasmon Resonance (LSPR) - **3**
Step 2:THRB rotation

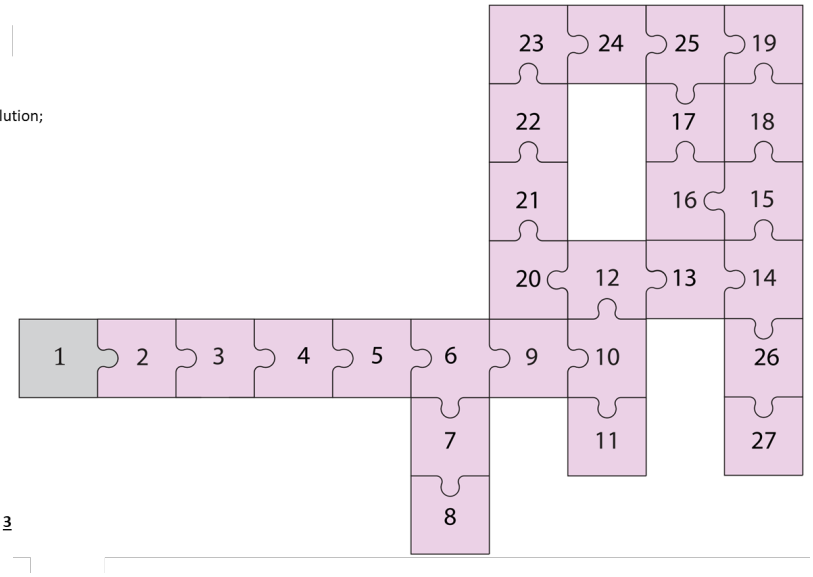

Advanced Version

ABSTRACT

We have established a label-free plasmonic platform that monitors proteolytic activity in real-time. The sensor consists of a random array of gold nanorods that are functionalized with a design peptide that is specifically cleaved by thrombin resulting in a blue-shift of the longitudinal plasmon. By monitoring the plasmon of many individual nanorods we determined thrombin's proteolytic activity in real-time and inferred relevant kinetic parameters. Furthermore, comparison to a kinetic model revealed that the plasmon shift is dictated by a competition between peptide cleavage and thrombin binding, which have opposing effects on the measured plasmon shift. The sensor presents a dynamic range of >2 orders of magnitude with a physiologically relevant detection limit of 3 nM. We expect these plasmon-mediated label-free sensors open the window to a range of applications stretching from the diagnostics of bleeding disorders to fundamental proteolytic and pharmacological studies.

KEYWORDS:
Plasmonic nanoparticles, monitoring, proteolytic sensor, single-particle spectroscopy, thrombin, modelling, and kinetics

The plasmon resonance of metallic nanoparticles depends not only on the shape, size and material of the particle, but also on the local refractive index in its immediate environment. This has sparked the usage of plasmonic nanoparticles as biosensors because changes in the local refractive index due to molecular binding are transduced to shifts of the plasmon resonance.[1] In addition, plasmonic nanoparticles are chemically inert and exhibit long-lasting photostability which is highly beneficial in the monitoring of molecular interactions or processes. Plasmon sensors have been developed for a large range of analytes[2] and with large range of particle shapes and sizes.[3] The majority of these sensors are based on suspensions of particles and essentially monitor the ensemble-averaged optical spectrum in a spectrometer. One drawback

of this approach is that the optical spectrum is inhomogeneously broadened because even the best nanoparticle synthesis methods yield size distributions of ~5%.[4,5]

Recently, sensors based on single immobilized particles, rather than particle suspensions, have proven their advantage as they exhibit a higher sensitivity due to the absence of inhomogeneous broadening.[6] The sensitivity of plasmon sensors is often quantified by a figure-of-merit (FoM),[7] which is most often defined as the ratio between the refractive-index sensitivity (in eV/refractive-index-unit) and resonance linewidth (in eV). Previous single-particle studies reported the FoM for isolated gold spheres and found values ranging from 0.5-1.[8] Simulations of gold nanoshells reported a slightly higher FoM of 2.5.[9] In general, elongated gold structures profit from an increased sensitivity as their tips get sharper, and combined with a narrow SPR away from the interband transitions in gold results in improved sensing performance. Indeed, FoMs of ~5-10 are typical for individual nanorods and bipyramids, which has led to the first demonstrations of plasmon biosensors with single-molecule sensitivity.[10–12]

To enable the tracking of the plasmon resonance of a single particle over time, the particles are usually immobilized on a substrate at low density to prevent their diffusion out of the focal plane of the microscope. An added advantage of this implementation is that it circumvents potential problems related to colloidal stability due to salt-induced aggregation which may also induce plasmon shifts. Combined with shot-noise limited dark-field microscopy[12] these platforms have been used to measure the concentration of biomolecules by quantifying the time-dependent red-shift of the plasmon resonance.[13]

For enzymes however, gene expression and affinity-based approaches have demonstrated that it is not the concentration of enzyme but rather the enzymatic activity that is crucial in its function.[14] Colorimetric[15] and mass-spectrometry techniques[16,17] are commonly used to determine proteolytic activity. However, these strategies often present limited sensitivity and specificity and do not enable real-time measurements. This has sparked developments in assays based on Förster Resonance Energy Transfer (FRET) that demonstrated detection limits in the

nanomolar range and enabled real-time measurements. However, the photostability of organic fluorophores is often affected by environmental parameters such as pH, ionic strength, and the presence of redox species.

Here we demonstrate a plasmonic platform that enables the real-time monitoring of proteolytic activity in a label-free manner. Compared to previous plasmonic sensors the ability to monitor in real-time is achieved by a combination of two approaches: the use of AuNRs provides 5-fold higher sensitivity compared to nanospheres,[18] while sensing at the single-particle level eliminates inhomogeneous broadening further boosting the signal.[19] The sensor optically probes the plasmon shift of hundreds of gold nanorods simultaneously achieving a dynamic range of >2 orders of magnitude with a physiologically relevant detection limit of 3 nM. We present a kinetic model that describes the plasmon shift as a competition between peptide cleavage and thrombin binding, which have opposing effects on the measured plasmon shift. The use of a peptide-based substrate enables the generalization to other enzymes and to the (multiplexed) detection of a panel of proteases or even hydrolases from other families.

We use thrombin as a model protease due to its central role in the coagulation cascade and key role in clotting diseases.[20–23] Also, its involvement in the homeostasis of the gut and central nervous system has been recently suggested[24–27] indicating its potential as biomarker for other pathological conditions. Hence, biosensing assays to quantify thrombin's activity are much needed in both fundamental biochemistry studies and in the future in clinical settings.

The underlying principle of our single-particle proteolytic biosensor is schematically presented in LSPR PA - Figure 1. Gold nanorods (AuNRs) are immobilized on a coverslip by spin coating and then functionalized with a thiolated peptide that contains a thrombin-specific cleavage site in the middle of the sequence. The evanescent tail of the electromagnetic near-field associated with the plasmon decays on length scales of tens of nanometers.[28]

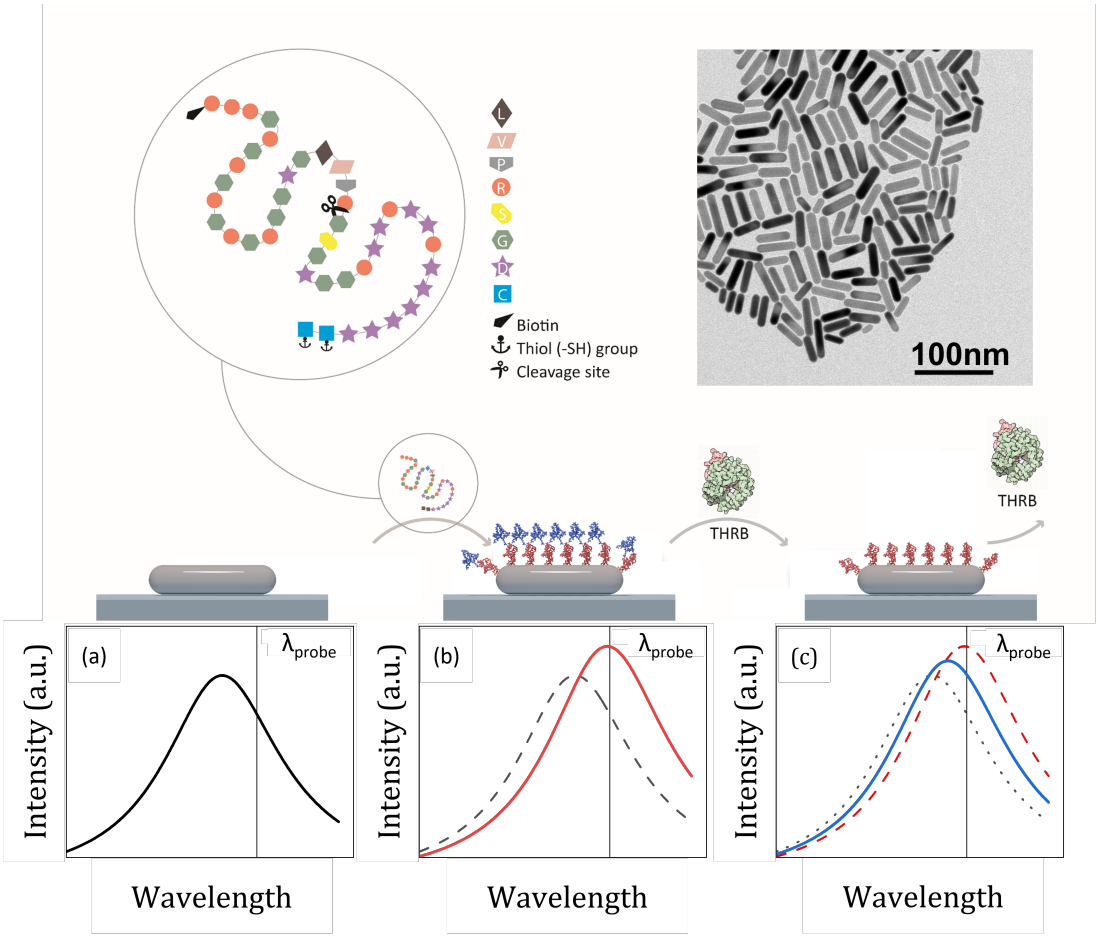

LSPR PA - Figure 1 -. Schematic working principle of the plasmonic proteolytic sensor. The thrombin-specific peptide with the cleavage site is depicted, together with an electron microscopy image of a dried drop of the gold nanorods on a carbon coated grid. The bottom diagram illustrates the workflow of the sensor involving the peptide immobilization step and the sequential peptide cleavage by thrombin (THRB) along with the induced plasmon red- and blueshifts. The plasmon shifts are probed in real-time at the single-particle level.

Refractive index changes in this near-field are transduced to shifts of the plasmon resonance.[12,29] Upon coating the particle with the peptide (b), the plasmon resonance will therefore red-shift, whereas subsequent introduction of active thrombin will result in a gradual blue-shift of the plasmon due to cleavage of the conjugated peptide (c). These processes are probed in an optical microscope by monitoring the scattering signal of many individual particles in real-time in a wide-field geometry.[12,30]

A schematic representation of the dark-field scattering setup used (based on earlier reports[12]) is depicted in LSPR PA - Figure 2a. In short, sample illumination is achieved using total-internal-reflection and the scattered light from the AuNRs is collected by the objective. An exemplary image is shown in LSPR PA - Figure 2b where individual particles are revealed as diffraction

limited point spread functions. To determine the LSPR-related spectroscopic properties of each AuNR we resorted to hyperspectral microscopy (HSM) using white-light illumination. The resulting spectrum is fitted with a Lorentzian profile to get the plasmon peak position and its linewidth. Only particles with Lorentzian linewidth < 200 meV were included in the analysis, as broader linewidths often indicate particle clustering. We find that ~20 % of the spots represent dimers or higher-order clusters, as indicated by a broad linewidth or the appearance of a double peak. We discard such spots from further analysis.

To probe plasmon shifts in real-time we use a superluminescent diode, centered at 793 nm wavelength, as illumination source. In this configuration plasmon shifts are conveyed to changes in scattered intensity because the spectral overlap between the plasmon resonance and the light source changes. The advantage of this approach is that plasmon shifts can be probed on millisecond timescales because the need for broadband spectroscopy is circumvented. Using the plasmon wavelength and linewidth from the single-particle scattering spectra of the same particles we convert intensity to a plasmon shift (see LSPR PA - Figure 2c and SI). This procedure is automatically performed for several hundred nanoparticles in the field-of-view, allowing for statistical analysis of the plasmon shifts as shown in LSPR PA - Figure 2d.

The peptide functionalization of the particle (red line in Figure2c) induces a large red-shift of 13 ± 4 nm indicating that the particles were effectively functionalized. The spread in measured plasmon shift is caused by particle-to-particle differences in the peptide density and refractive-index sensitivity.[31] Then, after immobilizing the peptide onto the AuNRs, we performed the proteolytic assay by injecting thrombin into the flowcell. A typical timetrace is shown as the blue line in Figure 2c, recorded on one of the particles in the field of view for 50 nM of thrombin. The plasmon resonance remains stable until the enzyme enters the reaction chamber after which a rapid blue-shift is observed.

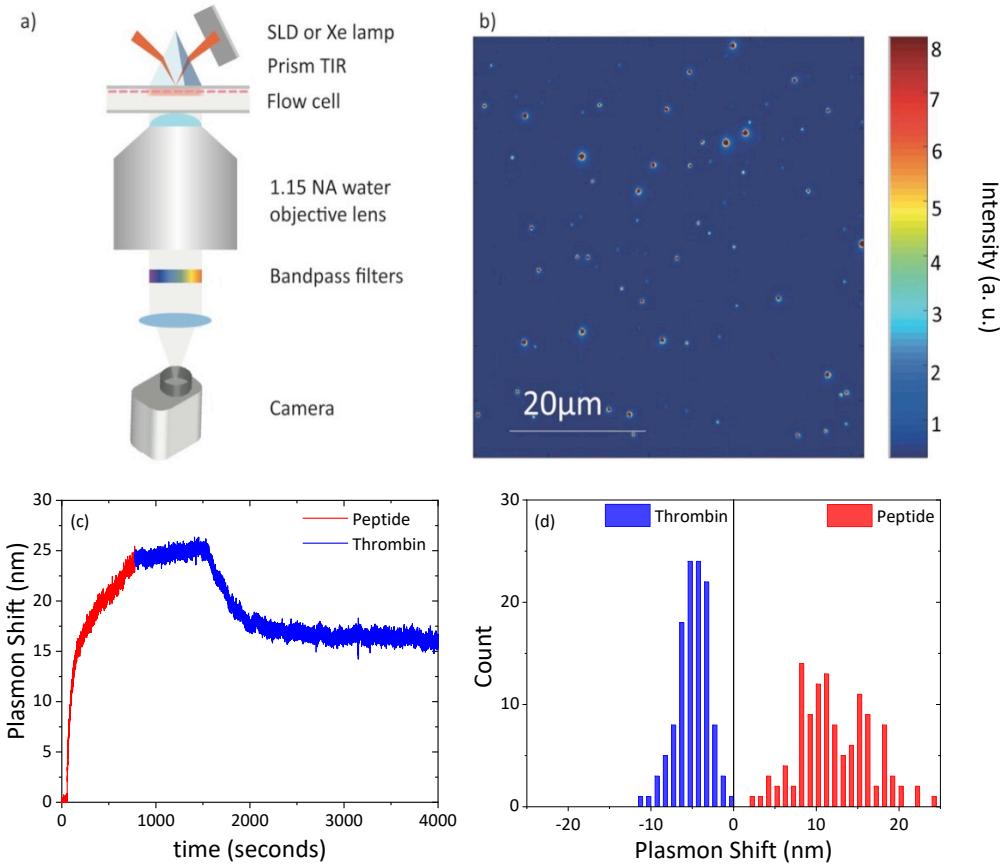

LSPR PA - Figure 2 -(a) Schematic representation of the dark-field microscope setup. (b) Dark-field scattering microscopy image of the AUNRs on the sample. Each spot represents light scattered by a single AuNR. (c) Representative single particle timetraces showing the plasmon shifts during the peptide immobilization at a peptide concentration of 10 µM and the enzymatic cleavage at a thrombin concentration of 50 nM. (d) Distribution of single-particle plasmon shifts measured across one field-of-view of the microscope during peptide immobilization (10 µM peptide concentration, in red) and cleavage (50 nM thrombin concentration, in blue).

As expected, this blue-shift is less pronounced than the red-shift due to peptide functionalization, indicating that only part of the peptide is removed by the cleavage. The peptide cleavage resulted in an average blue-shift of 5 ± 2 nm, indicating that approximately 40% of the plasmon red-shift is recovered due to enzymatic cleavage. This is reasonable since the peptide was designed such that approximately half its length is cleaved off by thrombin. In all assays we observed a strong correlation between the plasmon shifts of both the peptide immobilization and the enzymatic reaction (see SI Figure1), indicating that particles with high peptide density are on average also more responsive to the peptide cleavage.

We then compared the kinetics of cleavage across different active enzyme concentrations. Characteristic timetraces from three different thrombin concentrations (3 nM, 50 nM, and 300 nM) are presented in LSPR PA - Figure 3a. To facilitate comparison among the kinetic profiles, we chose particles with similar LSPR (~825 nm) while the time-axis was adjusted to assure that the enzymatic reaction starts simultaneously for all the particles (at t ≈ 200 s, see vertical line).

At first glance, we perceive a non-trivial behavior as the concentration of active enzyme increases (LSPR PA - Figure 3a). At low concentrations of thrombin (3 nM, blue), we observe slow kinetics as the plasmon shift continuously evolves. For intermediate concentrations (50 nM, green), the cleavage rate increases, as well as the plasmon shift, that reaches a limit value before the endpoint. In contrast, at large concentrations (300 nM, purple) even faster kinetics are observed, however, the average plasmon shift for all particles in the field-of-view is significantly smaller when compared to 3 and 50 nM thrombin. We attribute this to a competing mechanism where thrombin absorbs non-specifically to the particle surface. This results in a red-shift of the plasmon resonance that competes with the cleavage-induced blue-shift in a concentration-dependent manner.

To better understand the effect of these two competing mechanisms we construct a simplified kinetic model (detailed in SI) that assumes a 3-stage process: (I) first, the enzyme at concentration c_0 adsorbs onto the peptide layer with a rate $k_a c_0$; (II) it reorients until it binds a peptide and cleaves it at a rate k_b; and (III) peptide cleavage exposes regions where later an enzyme may non-specifically interact with rate constants $k_c c_0$ for association and k_d for dissociation, respectively.

It was further assumed that the plasmon shift associated with stage I is negligible because the enzyme binds on the thick peptide layer, and that the magnitudes of blue- and red-shift from stages II and III, respectively, are similar. This assumption implies that only peptides that are exposed to solvent (i.e. without non-specifically bound thrombin) result in a blue-shift.

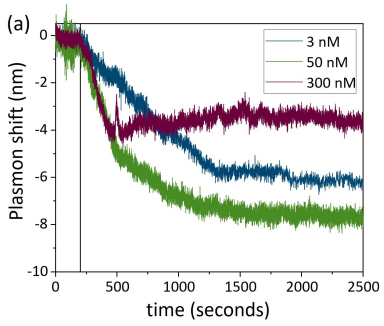

(c)

Kinetics / [THRB]	Plasmon Shift	Velocity (rate)
3nM	+	-
50nM	+	+
300nM	-	+

LSPR PA - Figure 3 - (a) Representative timetraces collected during cleavage with different concentrations of thrombin. The starting point (t = 0 s) of the timetraces was aligned to enable comparison. (b) Kinetic curves simulated from eq. 1 using $k_a = 2 \times 10^5\ M^{-1}s^{-1}$; $k_b = 0.01\ s^{-1}$; $k_c = 2.5 \times 10^4\ M^{-1}s^{-1}$; $k_d = 0.005\ s^{-1}$; $p_T = 100$ and an average shift of 0.08 nm per peptide.

As detailed in the SI, the time-dependent plasmon shift $\Delta SP(t)$ is then given by:

$$\Delta SP(t) \propto \frac{p_1(t)}{p_T} = A_1 e^{-k_a c_0 t} + A_2 e^{-k_b t} - A_3 e^{-(k_c c_0 + k_d)t} + \frac{k_d}{k_c c_0 + k_d} \qquad (1)$$

where p_T is the total number of peptides per particle and p_1 is the number of cleaved peptides that are solvent exposed. The solution concentration of active thrombin c_0 is assumed time-independent. The pre-exponential factors A_i depend only on the rate constants previously described and are omitted here for the sake of brevity (see full details in SI). The last term in eq. 1 makes it explicit that at long times the overall plasmon shift is determined by the adsorption/desorption equilibrium on the peptide cleaved regions.

The kinetic curves shown in LSPR PA - Figure 3b were extracted from eq. 1 where the rate constants were adjusted to match the experimental data. Despite the model's simplicity and ensemble chemical kinetics it accounts very well for the main features observed in the experimental timetraces. The model predicts $k_b \sim 0.01\ s^{-1}$ which is significantly slower than solution-phase rates presumably due to steric hindrance from peptide crowding on the particle surface.

At low enzyme concentrations, the reaction-rate is limited by adsorption in stage I because $k_a c_0 \ll k_b$. At $c_0 > 10$ nM the non-specific adsorption in stage III starts competing with peptide cleavage, thereby decreasing the end-point plasmon shift. The model nicely accounts for a local maximum observed at $t \sim 500\ s$ in the experimental data for 300 nM, which occurs because the

peptide cleavage rate is faster than the rate of non-specific interactions. The best correspondence between model and experimental results was found for $k_c \ll k_a$, which indicates that non-specific adsorption in stage III is less efficient than specific adsorption in stage I. This is expected because cleaved regions form an adsorption site only if their dimensions are large enough to host an enzyme.

The model fits to the data indicate an enzyme binding rate of $k_a = 2 \times 10^5\ M^{-1}s^{-1}$, which we independently verify by analyzing the variability in the time t_0 at which the cleavage starts: the diffusion of thrombin toward the NPs' surface is dictated by mass transport and thus, it is stochastic. This results in particle-to-particle differences in t_0, which we extracted from the intercept between two linear fits to the data, see LSPR PA - Figure 4a. Because the absolute value of t_0 depends on the exact time at which the thrombin solution enters the flowcell we instead consider the standard deviation of the distribution of t_0. As shown in LSPR PA - Figure 4b and 4c the standard deviation of t_0 is reduced for higher thrombin concentrations, indicating that the time at which the first enzyme binds become less heterogeneous at increasing concentrations. This can be understood by considering that the rate of mass transport increases at higher concentrations, thereby decreasing the absolute waiting time until the first binding event and thus also decreasing the standard deviation of the waiting times.

The waiting time for the first enzyme to bind to a particle is dictated by the association rate k_a and the thrombin concentration c_0 . The average waiting time is given by $\tau_w = (k_a c_0)^{-1}$ with a standard deviation of $\sigma = \sqrt{\tau_w} = (k_a c_0)^{-1/2}$ due to the stochastic (Poissonian) nature of the mass transport. The standard deviation σ was fitted to the measurements as shown in Figure4c, where we have allowed for an additional uncertainty of 20 seconds in determining the starting time t_0 due to the limited signal-to-noise ratio. We found a very good agreement between the assumption of Poisson statistics and our experimental data for an association rate of $k_a = 1 \times 10^5\ M^{-1}s^{-1}$. This value is in good agreement with the value found from the kinetic model fits in LSPR PA - Figure 3.

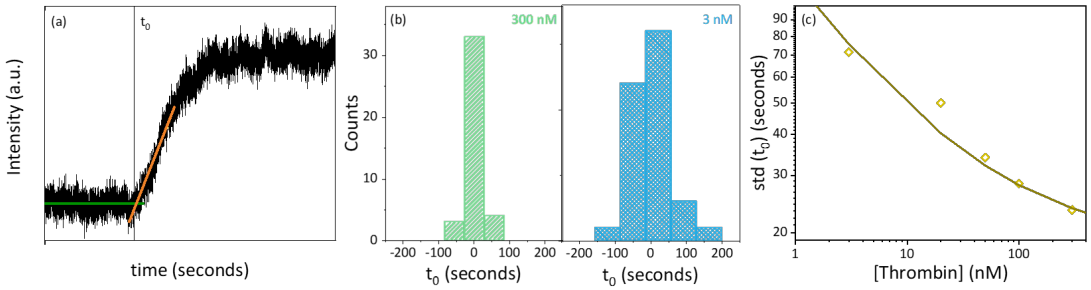

LSPR PA - Figure 4 - Kinetic parameters extracted from the timetraces. a) Illustration of the determination of the start-time t_0, determined from the intercept between the two indicated linear fits. b) Histogram of t_0 for two thrombin concentrations; c) Concentration dependence of t_0. The solid line indicates a fit to the datapoints further explained in the main text (fit parameter k_a = 1 x 10^5 M^{-1} s^{-1}).

We now turn to the analysis of the cleavage rate. We observe kinetics that cannot be described by a simple single-exponential (Langmuir) model, so to extract kinetic constants we use the reaction half-time $t_{1/2}$. This represents the time at which the plasmon shift has evolved to half of its final value (see LSPR PA (SI) - Figure 4a) and is model-independent. We find that at each thrombin concentration the single-particle half times are distributed normally (see LSPR PA (SI) - Figure 4b), so in LSPR PA - Figure 5a we only plot their average value as a function of concentration. We find a sub-linear dependence of half-time on thrombin concentration that scales approximately as $t_{1/2} \propto c_0^{-n}$ with $n = 0.24$. The kinetic model also predicts a sub-linear dependence due to the competition between peptide cleavage and non-specific enzyme interactions, albeit with an exponent $n = 0.67$ that is closer to linearity. A sub-linear sensor response was also observed in previous literature reports where end-point plasmon shifts were measured,[32] which was attributed to crowding, steric hinderance, or enzyme depletion by non-specific interactions that are not captured in the rate models.

After evaluation of the real-time kinetic data, we now shift our attention to the end-point plasmon shift for different concentrations of active enzyme. Because of the particle-to-particle differences in peptide loading as discussed above we normalized the plasmon blue-shift to the red-shift due to peptide conjugation (see LSPR PA (SI) - Figure 5). Indeed, the concentration dependence of the maximum plasmon shift recovery correlates strongly with the thrombin concentration, see LSPR PA - Figure 5b. As expected, the scaling is not linear due to the

competition between peptide cleavage and non-specific adsorption as discussed above. In addition, at low concentrations of active enzyme (1 nM) the maximum contrast is not reached because a considerable portion of the peptide remains uncleaved during the measurement time. These observations are in good agreement with ensemble-averaged results using gold spheres obtained by Svärd et al.[32]

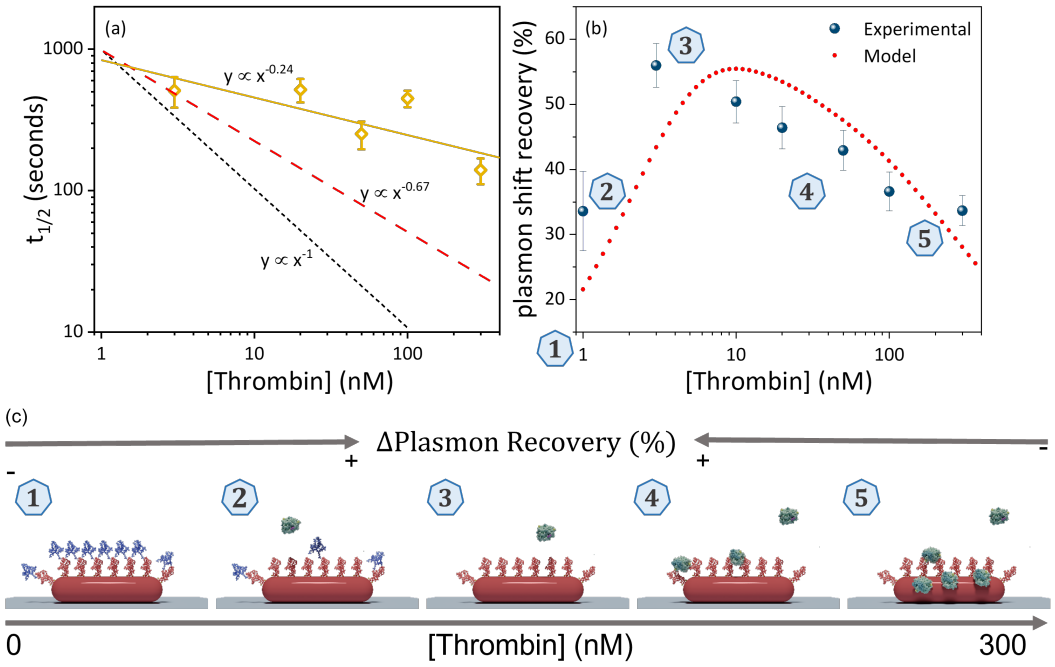

LSPR PA - Figure 5 - Concentration dependence results a) Reaction half-time of $t_{1/2}$. The error bars indicate the standard deviation of the distribution in SI Figure 4, whereas the dashed line indicates the expected linear dependence on thrombin concentration in case mass-transport dictates the cleavage rate; b) Normalized Plasmon shift vs concentration of active enzyme results – experimental and modeled results.

Moreover, the trend shown by our kinetic model – discussed above – matches the experimental results (LSPR PA - Figure 5b). This indicates that the mechanisms underlying sensor response is properly explained by a competition between peptide cleavage and non-specific enzyme binding. We speculate that these non-specific interactions may be a consequence of the affinity of the exosite II (one of thrombin's active sites) towards negatively charged surfaces,[33] which become exposed upon peptide cleavage.

The presented proteolytic sensor provides a versatile plasmonic platform to study and measure proteolytic activity in real-time. Thrombin activity monitoring has biological and clinical

relevance in the study of coagulopathies and other diseases. To evaluate this, we benchmark the performance and the features of our sensor against Thrombin generation assays (TGAs). The working range of our sensor at low nanomolar concentrations matches the relevant thrombin concentrations and its equivalent activity in pathophysiological conditions.[34] Ultimately, other key parameters such as the lag-time and endogenous thrombin potential (ETP)[3536] also have the potential to be determined using our plasmonic proteolytic biosensor.[37] The presented plasmonic platform paves the way to the exploitation of the promising features of plasmonic-based proteolytic sensors in biochemical research as well as diagnostics.

A single particle plasmonic biosensor to determine proteolytic activity in real-time was developed using thrombin as model protease. Cleavage of a thrombin-specific peptide immobilized on gold nanorods enabled the label-free and real-time measurement of cleavage kinetics at the level of single particles. We found that the total amount of cleaved peptide only depends weakly on thrombin concentration, indicating a substrate-limited reaction in which all peptide eventually gets cleaved irrespective of the thrombin concentration. The sensor exhibits a dynamic range of >2 orders of magnitude with a detection limit of 3 nM while providing a stable readout over long timescales. Furthermore, by monitoring the process we were able to extract kinetic parameters such as the binding time of the 1st active enzyme (t_0) and the reaction half-time ($t_{1/2}$). The kinetics of the sensor are in good agreement with a kinetic model that reproduces the temporal evolution of the plasmon shift as well as the end-point shift after the reaction has completed.

Regarding thrombin, subsequent work should include the effects of external factors such as temperature, pH and biological media on the kinetic parameters and the sensor's potential to be used in complex samples and as thrombin generation assay (TGA). Lastly, the sensor concept is easily expanded to multiplexed detection by using particles with a different LSPR. The ability to measure cleavage kinetics on each particle opens the window to spatial mapping of protease

activity in the vicinity of cells and tissue, which may lead to a deeper comprehension of metabolic processes involving proteases.[clxix]

MATERIALS AND METHODS

Materials

AuNRs with a plasmon resonance at 780 nm and stabilized in a solution containing cetyltrimethylammonium bromide (CTAB) were acquired from Nanoseedz (product #NR 10-780). The average size of the AuNRs was 39 nm x 10 nm. Figure1 shows an electron microscope image of a dried drop of the AuNRs on a carbon coated grid.

The peptide was acquired from Caslo ApS (Denmark) and it has the following sequence: (Biotin)-RRRGRGRGRGRGGDGLVPR|GSGDGGRDDRDDRDDDDDCC-NH2. In detail, the sequence comprises a biotin at the N-terminal (not used in this work), two spacer regions, a target sequence (denoted with the "|" symbol) and two cysteines to ensure strong particle-peptide conjugation via sulfur-gold adsorption.

AuNR Immobilization

The stock solution of AuNRs (optical density 1) was diluted 50x in a 1 mM CTAB solution and subsequently centrifuged at 1500 rpm for 3 minutes to precipitate potential clusters. The supernatant was collected for further use.

To prepare the thiol (-SH) functionalized coverslips, we started by cleansing the surface by sonicating them in methanol for 15 minutes and dried using a N_2 flow. Then, the surface was activated using an O_2 plasma cleaner for 1 minute or UV/Ozone cleaning for 90 minutes. Grafting of the thiol groups was achieved by immersion of the coverslips in a 5% v/v solution of mercaptopropyltrimethoxysilane (MPTMS) in absolute ethanol for 3 minutes and consequent rinsing with ethanol and methanol removed excess MPTMS. Lastly, sonication in methanol for 20 minutes and drying in a N_2 flow was repeated.

[clxix] Go to: PEF Nucleic acid Detection; Magnetic Logic-Gate; or Conclusions

Immediately after, to immobilize the AuNRs onto the coverslip, ~100uL of AuNR solution (prepared above) was drop casted and spin coated at 2000 rpm for 90 seconds. The remaining CTAB was removed by rinsing with phosphate buffered saline (PBS) -> Milli-Q water -> Methanol, and dried using a N_2 flow. Lastly, the sample was assembled into a flow cell (Warner instruments) and mounted under the microscope. This procedure results in well-isolated particles with ~100-200 individual spots in the field-of-view of our microscope. Samples were used within two weeks after preparation.

Optical Microscopy

A schematic representation of the dark-field scattering setup (based on earlier reports[30]) equipped with an autofocus system is depicted in Figure2a. In short, the setup uses total-internal-reflection illumination through a prism. The light scattered by the particles is collected by the water immersion objective lens (Nikon 1.15 NA CFI Apochromat LWD Lambda S 40XC) and directed to the camera (Andor Ixon 885+ EMCCD). An exemplary image is shown in Figure2b where individual particles are revealed as diffraction limited point spread functions.

White-light scattering spectra of the individual particles were collected using hyperspectral microscopy (HSM) using white-light illumination (Energetiq EQ-99X) through the prism.[30] A range of bandpass filters with a 10 nm passband are introduced in the detection path and the scattered intensity at each wavelength band is determined by a 2D Gaussian fit to the point-spread function (PSF). The resulting spectrum is fitted with a Lorentzian profile to get the plasmon peak position and its linewidth. Only particles with Lorentzian linewidth < 200 meV were included in the analysis, as broader linewidths often indicate particle clustering.[44] We find that ~20 % of the spots represent dimers or higher-order clusters, as indicated by a broad linewidth or the appearance of a double peak. We discard such spots from further analysis.

To probe plasmon shifts in real-time we use a superluminescent diode (Superlum SLD-38-HP, center wavelength 793 nm, emission bandwidth 15 nm) as illumination source. In this configuration plasmon shifts are conveyed to changes in scattered intensity because the spectral

overlap between the plasmon resonance and the light source changes. These changes in scattered intensity are extracted by a 2D Gaussian fit of the PSF, yielding an integrated scattered intensity that is normalized to the initial intensity. Using the plasmon wavelength and linewidth from the single-particle scattering spectra of the same particles we convert intensity to a plasmon shift (see Figure 2c and SI). This procedure is automatically performed for several hundred nanoparticles in the field-of-view, allowing for statistical analysis of the plasmon shifts as shown in Figure2d.

Peptide Functionalization

Peptide aliquots with 100 µM concentration were prepared by resuspending the dried peptide in 25 mM citrate buffer with pH 6.5 and 50 mM NaCl. The aliquots were kept at -20˚C until use. Peptides were conjugated to the particles by first diluting the aliquots to 10 µM in a buffer containing 50 mM citric acid and 1.5 M NaCl at pH 3. A 100 µL/min flow rate was used to inject the peptide into the flowcell. The flow was continued for 10 minutes until the plasmon shift saturated. After this the remaining unbound peptide was removed from the flowcell by flushing with 1.5 mL of incubation buffer.

Thrombin Activity Assays

Active thrombin was acquired from Abcam (ab62452) and re-dispersed into 1 µM aliquots using an incubation buffer composed of 50 mM Tris-HCl, 10 mM $CaCl_2$ and 150 mM NaCl at pH 8.4. Thus, aliquots with different concentrations of active thrombin (1, 3, 20, 50, 100, 300 nM) were prepared and frozen until usage. During our experiments thrombin's solution was injected using a 5 µL/min flowrate and maintained throughout the measurement.

REFERENCES – LSPR PA

(1) Mayer, K. M.; Hafner, J. H. Localized Surface Plasmon Resonance Sensors. *Chem Rev* **2011**, *111* (6), 3828–3857. https://doi.org/10.1021/cr100313v.

(2) Altug, H.; Oh, S. H.; Maier, S. A.; Homola, J. Advances and Applications of Nanophotonic Biosensors. *Nature Nanotechnology*. Nature Research January 1, 2022, pp 5–16. https://doi.org/10.1038/s41565-021-01045-5.

(3) Mitra, S.; Basak, M. Diverse Bio-Sensing and Therapeutic Applications of Plasmon Enhanced Nanostructures. *Materials Today*. Elsevier B.V. July 1, 2022, pp 225–261. https://doi.org/10.1016/j.mattod.2022.05.023.

(4) Khanal, B. P.; Zubarev, E. R. Gram-Scale Synthesis of Isolated Monodisperse Gold Nanorods. *Chemistry - A European Journal* **2019**, *25* (6), 1595–1600. https://doi.org/10.1002/chem.201805571.

(5) Dheyab, M. A.; Aziz, A. A.; Khaniabadi, P. M.; Jameel, M. S.; Oladzadabbasabadi, N.; Mohammed, S. A.; Abdullah, R. S.; Mehrdel, B. Monodisperse Gold Nanoparticles: A Review on Synthesis and Their Application in Modern Medicine. *International Journal of Molecular Sciences*. MDPI July 1, 2022. https://doi.org/10.3390/ijms23137400.

(6) Paulo, P. M. R.; Zijlstra, P.; Orrit, M.; Garcia-Fernandez, E.; Pace, T. C. S.; Viana, A. S.; Costa, S. M. B. Tip-Specific Functionalization of Gold Nanorods for Plasmonic Biosensing: Effect of Linker Chain Length. *Langmuir* **2017**, *33* (26), 6503–6510. https://doi.org/10.1021/acs.langmuir.7b00422.

(7) Slabý, J.; Homola, J. Performance of Label-Free Optical Biosensors: What Is Figure of Merit (Not) Telling Us? *Biosens Bioelectron* **2022**, *212*. https://doi.org/10.1016/j.bios.2022.114426.

(8) Offermans, P.; Schaafsma, M. C.; Rodriguez, S. R. K.; Zhang, Y.; Crego-Calama, M.; Brongersma, S. H.; Gómez Rivas, J. Universal Scaling of the Figure of Merit of Plasmonic Sensors. *ACS Nano* **2011**, *5* (6), 5151–5157. https://doi.org/10.1021/nn201227b.

(9) Tuersun, P. Optimizing the Figure of Merit of Gold Nanoshell-Based Refractive Index Sensing. *Optik (Stuttg)* **2016**, *127* (1), 250–253. https://doi.org/10.1016/j.ijleo.2015.10.069.

(10) Ament, I.; Prasad, J.; Henkel, A.; Schmachtel, S.; Sönnichsen, C. Single Unlabeled Protein Detection on Individual Plasmonic Nanoparticles. *Nano Lett* **2012**, *12* (2), 1092–1095. https://doi.org/10.1021/nl204496g.

(11) Zijlstra, P.; Paulo, P. M. R.; Orrit, M. Optical Detection of Single Non-Absorbing Molecules Using the Surface Plasmon Resonance of a Gold Nanorod. *Nat Nanotechnol* **2012**, *7* (6), 379–382. https://doi.org/10.1038/nnano.2012.51.

(12) Beuwer, M. A.; Prins, M. W. J.; Zijlstra, P. Stochastic Protein Interactions Monitored by Hundreds of Single-Molecule Plasmonic Biosensors. *Nano Lett* **2015**, *15* (5), 3507–3511. https://doi.org/10.1021/acs.nanolett.5b00872.

(13) Beuwer, M. A.; van Hoof, B.; Zijlstra, P. Spatially Resolved Sensitivity of Single-Particle Plasmon Sensors. *The Journal of Physical Chemistry C* **2018**, *122* (8), 4615–4621. https://doi.org/10.1021/acs.jpcc.8b00849.

(14) Oliveira-Silva, R.; Sousa-Jerónimo, M.; Botequim, D.; Silva, N. J. O.; Paulo, P. M. R.; Prazeres, D. M. F. Monitoring Proteolytic Activity in Real Time: A New World of Opportunities for Biosensors. *Trends Biochem Sci* **2020**, *45* (7), 604–618. https://doi.org/10.1016/j.tibs.2020.03.011.

(15) Odintsova, E. S.; Buneva, V. N.; Nevinsky, G. A. Casein-Hydrolyzing Activity of SIgA Antibodies from Human Milk. *Journal of Molecular Recognition* **2005**, *18* (5), 413–421. https://doi.org/https://doi.org/10.1002/jmr.743.

(16) Trindade, F.; Amado, F.; Oliveira-Silva, R. P.; Daniel-da-Silva, A. L.; Ferreira, R.; Klein, J.; Faria-Almeida, R.; Gomes, P. S.; Vitorino, R. Toward the Definition of a Peptidome Signature and Protease Profile in Chronic Periodontitis. *Proteomics Clin Appl* **2015**, *9* (9–10), 917–927. https://doi.org/10.1002/prca.201400191.

(17) Oliveira-Silva, R.; Pinto da Costa, J.; Vitorino, R.; Daniel-da-Silva, A. L. Magnetic Chelating Nanoprobes for Enrichment and Selective Recovery of Metalloproteases from Human Saliva. *J Mater Chem B* **2015**, *3* (2), 238–249. https://doi.org/10.1039/C4TB01189A.

(18) Becker, J.; Trügler, A.; Jakab, A.; Hohenester, U.; Sönnichsen, C. The Optimal Aspect Ratio of Gold Nanorods for Plasmonic Bio-Sensing. *Plasmonics* **2010**, *5* (2), 161–167. https://doi.org/10.1007/s11468-010-9130-2.

(19) Zijlstra, P.; Paulo, P. M. R.; Yu, K.; Xu, Q.-H.; Orrit, M. Chemical Interface Damping in Single Gold Nanorods and Its Near Elimination by Tip-Specific Functionalization. *Angewandte Chemie International Edition* **2012**, *51* (33), 8352–8355. https://doi.org/https://doi.org/10.1002/anie.201202318.

(20) Chang, W. C.; Jackson, J. W.; Machlus, K. R.; Wolberg, A. S.; Ovanesov, M. v. Fluorescence Artifact Correction in the Thrombin Generation Assay: Necessity for Correction Algorithms in Procoagulant Samples. *Res Pract Thromb Haemost* **2021**, *5* (3), 447–455. https://doi.org/https://doi.org/10.1002/rth2.12499.

(21) ten Cate, H.; Hemker, H. C. Thrombin Generation and Atherothrombosis: What Does the Evidence Indicate? *J Am Heart Assoc* **2016**, *5* (8), e003553. https://doi.org/10.1161/JAHA.116.003553.

(22) Loeffen, R.; Winckers, K.; Ford, I.; Jukema, J. W.; Robertson, M.; Stott, D. J.; Spronk, H. M.; ten Cate, H.; Lowe, G. D.; Group, on behalf of the P. S. Associations Between Thrombin Generation and the Risk of Cardiovascular Disease in Elderly Patients: Results From the PROSPER Study . *The Journals of Gerontology: Series A* **2015**, *70* (8), 982–988. https://doi.org/10.1093/gerona/glu228.

(23) Chambers, R. C.; Laurent, G. J. Coagulation Cascade Proteases and Tissue Fibrosis. *Biochem Soc Trans* **2002**, *30* (2), 194 LP – 200.

(24) Campello, E.; Bulato, C.; Spiezia, L.; Boscolo, A.; Poletto, F.; Cola, M.; Gavasso, S.; Simion, C.; Radu, C. M.; Cattelan, A.; Tiberio, I.; Vettor, R.; Navalesi, P.; Simioni, P. Thrombin Generation in Patients with COVID-19 with and without Thromboprophylaxis. *Clinical Chemistry and Laboratory Medicine (CCLM)* **2021**, *59* (7), 1323–1330. https://doi.org/doi:10.1515/cclm-2021-0108.

(25) Ebrahimi, S.; Jaberi, N.; Avan, A.; Ryzhikov, M.; Keramati, M. R.; Parizadeh, M. R.; Hassanian, S. M. Role of Thrombin in the Pathogenesis of Central Nervous System Inflammatory Diseases. *J Cell Physiol* **2017**, *232* (3), 482–485. https://doi.org/10.1002/jcp.25501.

(26) Krenzlin, H.; Lorenz, V.; Danckwardt, S.; Kempski, O.; Alessandri, B. The Importance of Thrombin in Cerebral Injury and Disease. *Int J Mol Sci* **2016**, *17* (1), 84. https://doi.org/10.3390/ijms17010084.

(27) Denadai-Souza, A.; Bonnart, C.; Tapias, N. S.; Marcellin, M.; Gilmore, B.; Alric, L.; Bonnet, D.; Burlet-Schiltz, O.; Hollenberg, M. D.; Vergnolle, N.; Deraison, C. Functional Proteomic Profiling of Secreted Serine Proteases in Health and Inflammatory Bowel Disease. *Sci Rep* **2018**, *8* (1), 7834. https://doi.org/10.1038/s41598-018-26282-y.

(28) Mazzotta, F.; Johnson, T. W.; Dahlin, A. B.; Shaver, J.; Oh, S.-H.; Höök, F. Influence of the Evanescent Field Decay Length on the Sensitivity of Plasmonic Nanodisks and Nanoholes. *ACS Photonics* **2015**, *2* (2), 256–262. https://doi.org/10.1021/ph500360d.

(29) Ye, W.; Götz, M.; Celiksoy, S.; Tüting, L.; Ratzke, C.; Prasad, J.; Ricken, J.; Wegner, S. v; Ahijado-Guzmán, R.; Hugel, T.; Sönnichsen, C. Conformational Dynamics of a Single Protein Monitored for 24 h at Video Rate. *Nano Lett* **2018**, *18* (10), 6633–6637. https://doi.org/10.1021/acs.nanolett.8b03342.

(30) Celiksoy, S.; Ye, W.; Wandner, K.; Kaefer, K.; Sönnichsen, C. Intensity-Based Single Particle Plasmon Sensing. *Nano Lett* **2021**, *21* (5), 2053–2058. https://doi.org/10.1021/acs.nanolett.0c04702.

(31) Horáček, M.; Armstrong, R. E.; Zijlstra, P. Heterogeneous Kinetics in the Functionalization of Single Plasmonic Nanoparticles. *Langmuir* **2018**, *34* (1), 131–138. https://doi.org/10.1021/acs.langmuir.7b04027.

(32) Svärd, A.; Neilands, J.; Palm, E.; Svensäter, G.; Bengtsson, T.; Aili, D. Protein-Functionalized Gold Nanoparticles as Refractometric Nanoplasmonic Sensors for the Detection of Proteolytic Activity of Porphyromonas Gingivalis. *ACS Appl Nano Mater* **2020**, *3* (10), 9822–9830. https://doi.org/10.1021/acsanm.0c01899.

(33) Troisi, R.; Balasco, N.; Autiero, I.; Vitagliano, L.; Sica, F. Exosite Binding in Thrombin: A Global Structural/Dynamic Overview of Complexes with Aptamers and Other Ligands. *Int J Mol Sci* **2021**, *22* (19), 1422–0067. https://doi.org/10.3390/ijms221910803.

(34) de Laat-Kremers, R. M. W.; Yan, Q.; Ninivaggi, M.; de Maat, M.; de Laat, B. Deciphering the Coagulation Profile through the Dynamics of Thrombin Activity. *Sci Rep* **2020**, *10* (1), 12544. https://doi.org/10.1038/s41598-020-69415-y.

(35) Kintigh, J.; Monagle, P.; Ignjatovic, V. A Review of Commercially Available Thrombin Generation Assays. *Res Pract Thromb Haemost* **2017**, *2* (1), 42–48. https://doi.org/10.1002/rth2.12048.

(36) Tripodi, A. Thrombin Generation Assay and Its Application in the Clinical Laboratory. *Clin Chem* **2016**, *62* (5), 699–707. https://doi.org/10.1373/clinchem.2015.248625.

(37) Verhagen, M. J. A.; Valke, L. L. F. G.; Schols, S. E. M. Thrombin Generation for Monitoring Hemostatic Therapy in Hemophilia A: A Narrative Review. *Journal of Thrombosis and Haemostasis* **2022**, *20* (4), 794–805. https://doi.org/https://doi.org/10.1111/jth.15640.

Supplementary Information

Single-particle correlation between peptide loading and response to proteolytic activity

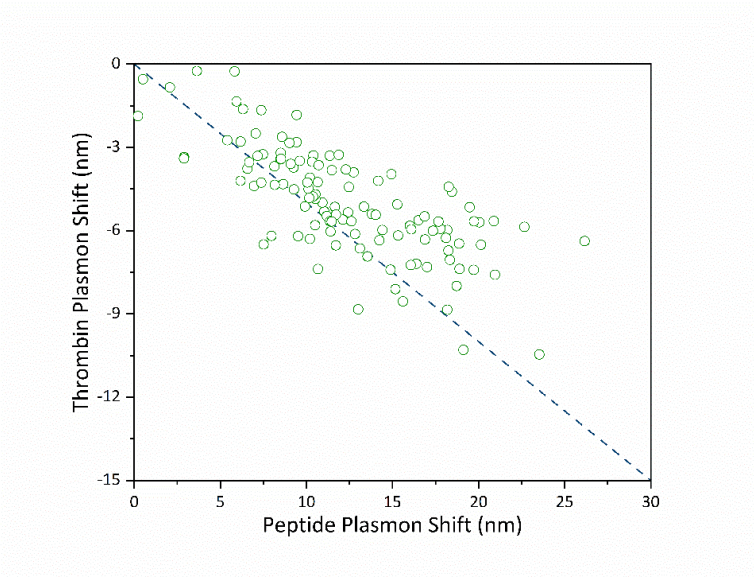

LSPR PA (SI) - Figure 1 - Correlation between the plasmons shifts induced by the peptide immobilization and the consequent enzymatic cleavage (20nM thrombin). Dash line represents a reference line (y = -0.5x).

Intensity-based plasmon sensing

We will derive equations to convert changes in the intensity scattered by a single nanoparticle into a plasmon shift. We assume that the plasmon resonance can be approximated by a Lorentzian function given by

$$I(E) = \frac{\Gamma}{2\pi}\frac{1}{\left(E-E_{sp}\right)^2+\left(\frac{1}{2}\Gamma\right)^2} \quad (1)$$

Where $\boldsymbol{E}$ is the incident photon energy, $\boldsymbol{E_{sp}}$ and $\boldsymbol{\Gamma}$ are the plasmon energy and linewidth (measured from the scattered spectrum). Note that all units are in eV. In a biosensing experiment this spectrum becomes time dependent due to a time-dependent shift of the plasmon resonance. This can be taken into account by considering $\boldsymbol{E_{sp}}$ to be time-dependent due to a shift $\boldsymbol{\Delta E_{sp}(t)}$. The plasmon resonance is then given by

$$I(E,t) = \frac{\Gamma}{2\pi}\frac{1+A\Delta E_{sp}(t)}{\left(E-[E_{sp}+\Delta E_{sp}(t)]\right)^2+\left(\frac{1}{2}\Gamma\right)^2}. \quad (2)$$

Herein the factor $\boldsymbol{A}$ has a negative value and describes the increase in scattering cross section in response to a plasmon redshift (i.e. a decrease in cross section with an increase in plasmon energy). The contrast in an intensity-based experiment is probed using a light source with a center energy $\boldsymbol{E_p}$. We assume that the linewidth of the source is much narrower than $\boldsymbol{\Gamma}$. The contrast is then given by:

$$contrast\ (t) = \frac{I(E_p,t)}{I(E_p,0)} = \frac{\left[1+A\Delta E_{sp}(t)\right]\left[\left(E_p-E_{sp}\right)^2+\left(\frac{1}{2}\Gamma\right)^2\right]}{\left(E_p-\left[E_{sp}+\Delta E_{sp}(t)\right]\right)^2+\left(\frac{1}{2}\Gamma\right)^2}. \quad (3)$$

Provided the value of A is known (either estimated from the asymmetric shape of a typical s-curve or estimated from a numerical model of the scattering spectrum) this approach can be used to solve analytically for $\Delta E_{sp}(t)$. For $A = 0$ we can extract $\Delta E_{sp}(t)$ directly:

$$\Delta E_{sp}(t) = E_p - E_{sp} \pm \sqrt{\frac{\left(E_p-E_{sp}\right)^2+\left(\frac{1}{2}\Gamma\right)^2}{contrast(t)} - \left(\frac{1}{2}\Gamma\right)^2}, \quad (4)$$

Where the plus sign holds when $E_p < E_{sp}$ and the minus sign when $E_p > E_{sp}$.

For $A \neq 0$ we first need to rewrite the equation into:

$$p_2\Delta E_{sp}(t)^2 + p_1\Delta E_{sp}(t) + p_0 = 0, \quad (5)$$

Where,

$$p_2 = contrast(t), p_1 = 2 * contrast(t)\left[E_{sp} - E_p\right] - A\left[\left(E_p - E_{sp}\right)^2 + \left(\frac{1}{2}\Gamma\right)^2\right], \quad (6)$$

$$p_2 = [contrast(t) - 1]\left[\left(E_p - E_{sp}\right)^2 + \left(\frac{1}{2}\Gamma\right)^2\right]. \quad (7)$$

From here $\Delta E_{sp}(t)$ is easily calculated:

$$\Delta E_{sp}(t) = \frac{-p_1 \pm \sqrt{(p_1^2 - 4p_2p_0)}}{2p_2}, \quad (8)$$

Where the plus sign holds when $E_p < E_{sp}$ and the minus sign when $E_p > E_{sp}$.

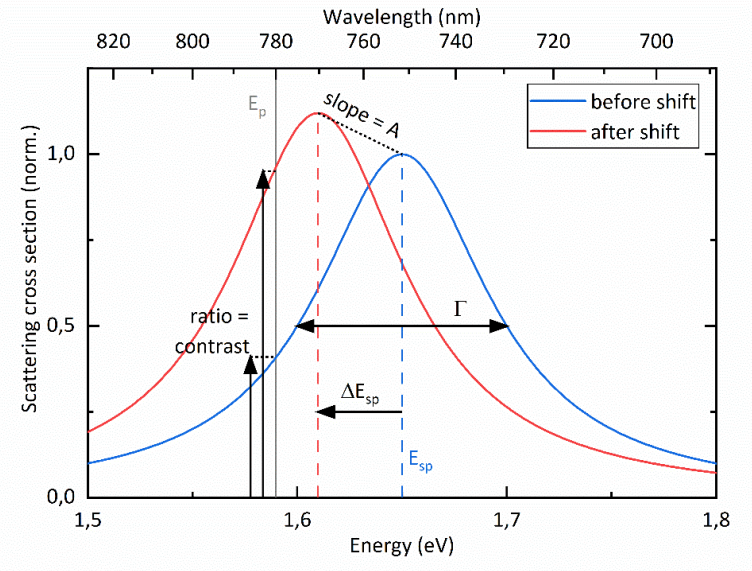

LSPR PA (SI) - Figure 2 - Illustration of the quantities used in this derivation.

A pseudo-first order kinetic model for protease adsorption and cleavage

The kinetic model described in the main text comprises 3 stages: (I) the enzyme adsorption onto the peptide layer; (II) the enzyme binding to the cleavage site and peptide cutting; (III) the enzyme adsorption onto cleaved regions in the peptide layer. The first and third stages are modeled as pseudo-first order reversible reactions for the adsorption/desorption equilibrium, whereas the second stage is modeled as two consecutive irreversible steps,

$$p_0 \underset{k_e}{\overset{k_a c_0}{\rightleftarrows}} p_{0a} \xrightarrow{k_b} p_{0b} \xrightarrow{k_{cat}} p_1 \underset{k_d}{\overset{k_c c_0}{\rightleftarrows}} p_{1a} \tag{9}$$

where p_0 and p_{0a} represent the intact peptide before and after enzyme adsorption, respectively; p_{0b} is the peptide with an enzyme specifically bound to its cleavage site, and; p_1 and p_{1a} are the cleaved peptide before and after enzyme adsorption, respectively. The pseudo-first order rate constants are indicated in the reaction scheme of eq. 9, where c_0 is the protease bulk concentration. When solving the kinetic equations, it was assumed that the peptide cutting rate constant k_{cat} is much larger than the binding rate constant k_b, so that p_{0b} converts almost instantaneously into p_1. The typically large values of k_{cat} for thrombin make this assumption reasonable, and, while enzyme binding rates should also be large in bulk solution because the species involved are freely diffusing, the same does not necessarily apply at the particle's surface

due to molecular crowding in the peptide layer. Under these assumptions, the set of differential equations from the reaction scheme of eq. 9 give the following solution for the time evolution of cleaved peptide,

$$p_1(t) = p_T \frac{k_a c_0 k_b}{\lambda_+ - \lambda_-} \times \left\{ \left(1 + \frac{k_d}{\lambda_+}\right) \times \frac{e^{\lambda_+ t} - e^{-k_+ t}}{\lambda_+ + k_+} - \left(1 + \frac{k_d}{\lambda_-}\right) \times \frac{e^{\lambda_- t} - e^{-k_+ t}}{\lambda_- + k_+} + \frac{k_d}{k_+} \frac{\lambda_+ - \lambda_-}{\lambda_+ \lambda_-} \times \left(1 - e^{-k_+ t}\right) \right\} \tag{10}$$

where p_T is the average number of peptides per particle and the following definitions were introduced for grouping the rate constants,

$$k_- = k_a c_0 + k_e + k_b \quad , \quad k_+ = k_c c_0 + k_d \tag{11}$$

$$\lambda_\pm = -k_-/2 \pm \sqrt{(k_-/2)^2 - k_a c_0 k_b} \tag{12}$$

The plasmon shift is roughly proportional to the number of cleaved peptides that are solvent exposed (p_1), because it was assumed that the plasmon shift associated with stage I is negligible and that the magnitudes of blue- and red-shift from stages II and III are comparable to each other. The kinetic law of eq. 1 in the main text was derived from eq. 10 by further assuming that $k_e \ll k_a c_0, k_b$, which, despite the loss of generality, still affords a good description of our experimental results. The pre-exponential factors of eq. 1 from the main text (A_i) are then given by,

$$A_1 = \frac{k_b}{k_a c_0 - k_b} \times \frac{k_d - k_a c_0}{k_+ - k_a c_0} \tag{12}$$

$$A_2 = \frac{k_a c_0}{k_b - k_a c_0} \times \frac{k_d - k_b}{k_+ - k_b} \tag{13}$$

$$A_3 = A_1 + A_2 + \frac{k_d}{k_c c_0 + k_d} \tag{14}$$

Using this simplified model, a set of kinetic curves were simulated for the values of thrombin concentration used in the experiments, as shown in fig. S1.

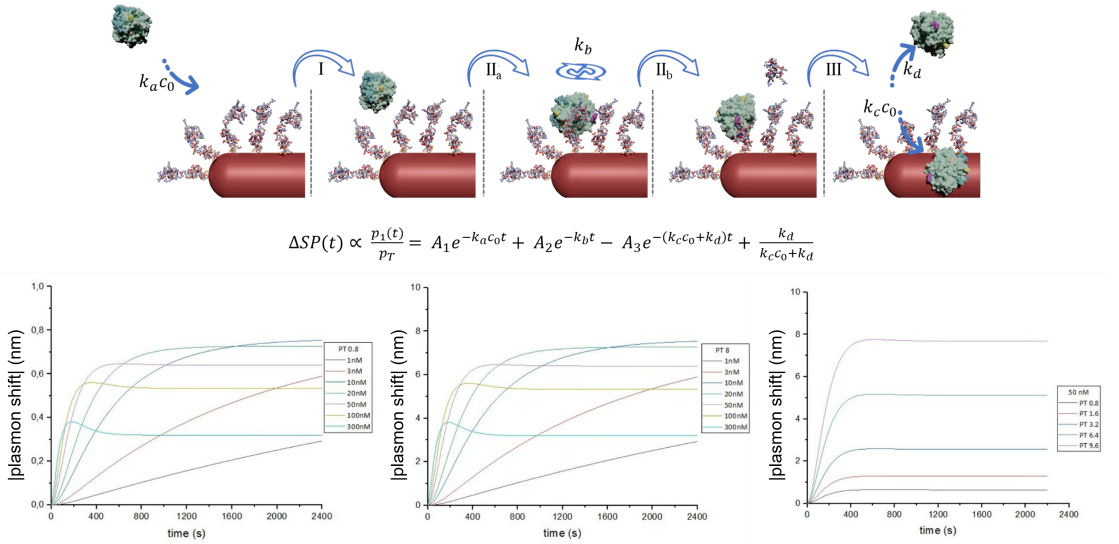

LSPR PA (SI) - Figure 3 - Kinetic curves simulated from eq. 1 of the main text using $\boldsymbol{k_a}$= 2 2×10^5 M^{-1}s^{-1}, $\boldsymbol{k_b}$= 0.01 s^{-1}, $\boldsymbol{k_c}$= 2.5×10^4 M^{-1}s^{-1}, $\boldsymbol{k_d}$= 0.005 s^{-1}, $\boldsymbol{p_T}$= 100 and an average shift of 0.08 nm per peptide.

Above some concentration c_0, the simulated kinetic curves display a local maximum, which is also observed in the experimental time traces. The instant $t_{\max}$ at which this local maximum occurs can be approximately found from,

$$\left.\frac{dp_1(t)}{dt}\right|_{t_{max}} = 0 \quad \xrightarrow{|\lambda_-| \gg |\lambda_+|\,,\ k_+} \quad \ldots$$

$$t_{max} \approx \frac{1}{\lambda_- + k_+} \times ln\left\{\frac{k_+}{\lambda_-} \times \frac{\lambda_- + k_d}{\lambda_- + k_+} - \frac{k_+}{\lambda_+} \times \frac{\lambda_+ + k_d}{\lambda_+ + k_+} - k_d \frac{\lambda_+ - \lambda_-}{\lambda_+ \lambda_-}\right\} \tag{15}$$

which has only physical meaning for positive values of $t_{\max}$, and this sets a minimum concentration value needed to verify this condition,

$$c_0^* = \frac{k_d}{|k_a - k_b|} \tag{16}$$

In the example of LSPR PA (SI) - Figure 3, this concentration limit is c_0^* = 28.6 nM. Instead of using the approximation of eq. 16, the values of $t_{\max}$ were numerically calculated using the method of Newton-Raphson. In order to replicate the experimental results, the model estimates of plasmon shift were calculated from $p_1(t_{\max})$, when $t_{\max} < t_w$, when $t_{\max}$ occurs before the end point of the measurement window which was set at $t_w = 2400$ s. Otherwise at low c_0 values, when a local maximum is not observed, the plasmon shifts were calculated at the end point of kinetic curves, i.e. from $p_1(t_w)$. This calculation afforded the model curve shown below in S1

Figure 5, from which it was calculated the normalized plasmon shift shown in Figure 5 of the main text (red dashed curve).

Another parameter from the kinetic curves that was assessed both experimentally and theoretically was the reaction half-time $t_{1/2}$, which is defined as,

$$p_1(t_{1/2}) = p_1(t_w)/2 \tag{17}$$

When using eq. 10 to express the condition of eq. 18, it yields an equation that does not have an exact algebraic solution, so it was again numerically calculated using the method of Newton-Raphson. The main result is shown as a dashed red curve in Figure 5a of the main text.

Reaction half-time determination

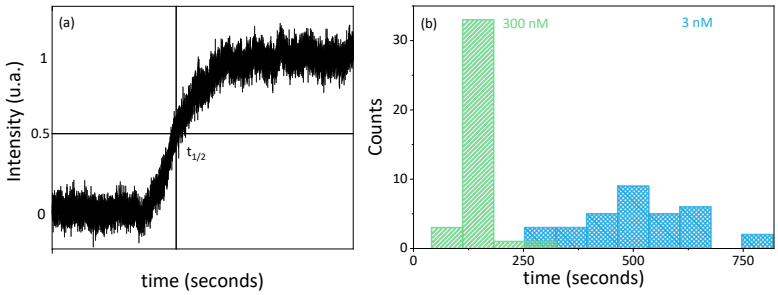

LSPR PA (SI) - Figure 4 - Reaction Half-time determination a) Illustration of the determination of the half-time $t_{1/2}$; b) Histogram of $t_{1/2}$ for two thrombin concentrations.

Lorentzian derivate fitting results vs concentration of active enzyme

LSPR PA (SI) - Table 1 - Fitting results overview. Comparison of the estimated plasmon shifts and respective errors from different THRB concentrations. The average reaction time for each experiment was the following: 1nM ~80min; 3, 10 and 20nM ~50 min; 50nM ~15 min; 100nM ~20 min; 300 nM ~5min.

[THRB]	Peptide Plasmon Shift (nm)	Fitting R^2	THRB Plasmon Shift (nm)	Fitting R^2	Plasmon shift recovery (%)	Ratio uncertainty (%)
1	13.4 ± 1	0.95	4.4 ± 0.8	0.77	32.8	6.4
3	13.4 ± 0.7	0.94	7.5 ± 0.5	0.96	56.0	4.7
10	12.3 ± 0.8	0.93	6.2 ± 0.4	0.95	50.4	4.6
20	15.3 ± 1.2	0.9	7.1 ± 0.5	0.95	46.4	4.9
50	13.0 ± 0.8	0.93	5.8 ± 0.5	0.88	44.6	4.2
100	13.3 ± 0.8	0.94	5.4 ± 0.2	0.97	40.6	2.9
300	14.7 ± 0.9	0.96	5.0 ± 0.4	0.94	34.0	3.4

Non-trivial response of the plasmonic sensor

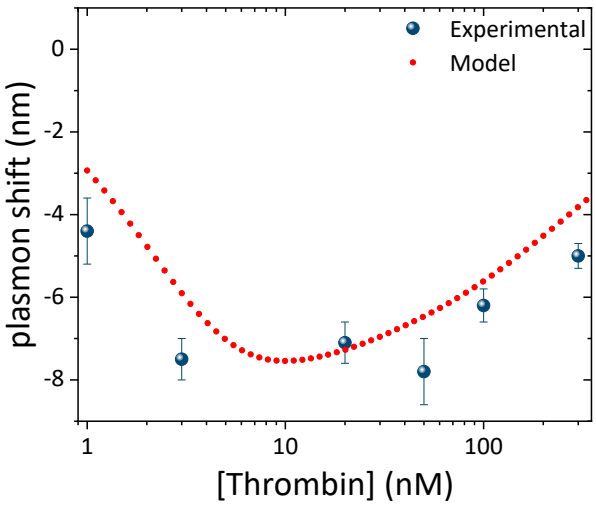

LSPR PA (SI) - Figure 5 - Quantification of active enzyme. Non-trivial response from plasmon shift vs concentration of active enzyme – experimental and modeled results.

Conclusions and Remarks: Building the Pieces of the Puzzle

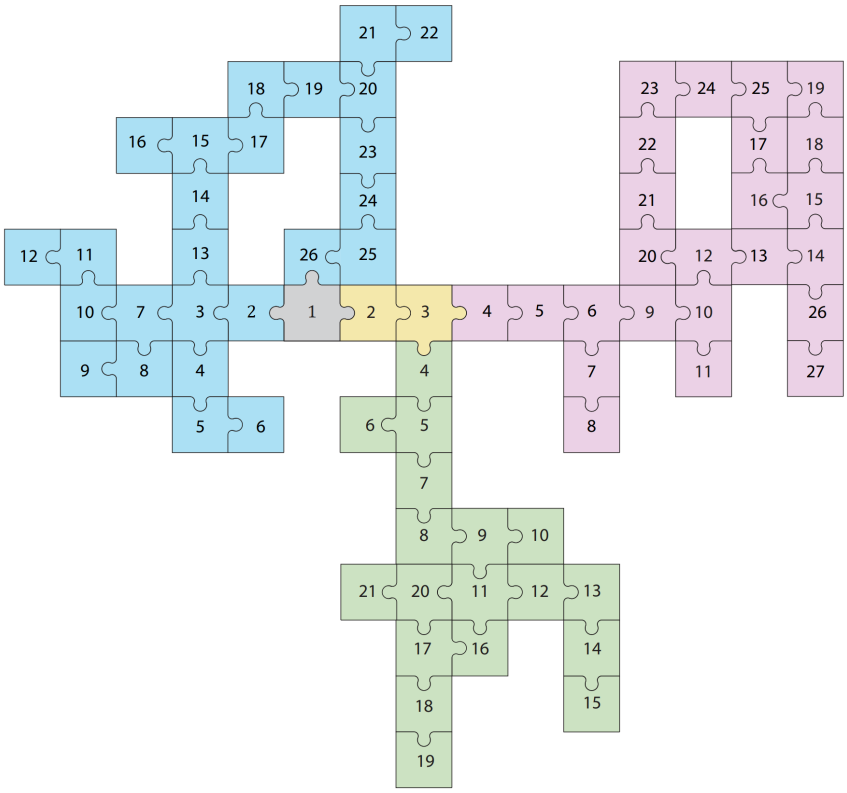

Piece of the Puzzle	*M LG*	*PEF*	*LSPR PA*
1	Nanoparticle-based (Bio)sensors		
2	Fe_3Se_4	Plasmonic Nanoparticles	
3	Characterization	LSPR	
4	XRD	AgNTs	AuNRs
5	Phase Purity	Polydisperse	Characterization
6	Crystal Size	Oxidation	Dark-field Microscopy (DFM)
7	STEM	Density Gradient Centrifugation	Hyperspectral Microscopy (HSM)
8	EDX	AgNTs Fractions	Single NP LSPR Spectrum
9	Atomic Composition	Gold Coating	Single wavelength probing
10	Morphology	H_2O_2 Resistant	Peptide immobilization
11	Nanoplatelets	Characterization	Red shift
12	Monodisperse	STEM	Concentration Dependence
13	SQUID	Truncated Ag@AuNTs	Kinetic evaluation
14	Magnetic Properties	Discrete Dipole Approximation (DDA)	Time of arrival (t_0)
15	Hard Magnet	Plasmonic profile and enhancement map	Affinity constant
16	T_C Near Room T	FCS	Half-time reaction ($t_{1/2}$)
17	Bistable	ssDNA immobilization	Sub-linear dependence
18	Logic-Gate	Fluorescence enhancement	Modelling
19	SR-Latch	Nucleic Acid detection	Pseudo-1st order
20	Hyperthermia Treatment	Uv-Vis characterization	Step 1: Enzyme diffusion to the NP
21	Laser Heating	Monodisperse Fractions	Step 2: THRB rotation
22	Near-IR		Step 3: Peptide Cleavage
23	Cell Culture		Step 4: THRB adsorption or diffusion back to solution
24	PC-3 Cell Line		
25	Flux Gate		
26	Temperature Overshoot? Yes (0) No(1)		

Life is the keyword of biology. However, the concept of life is not as trivially defined as we may initially expect. According to Erwin Schrodinger, "living things avoid decay into disorder and equilibrium" and cells are the fundamental units of life. In essence, cells are perceivable as protein-based robots physically delimited from their environment. Despite being pivotal in homeostasis, none of the building blocks composing cells are considered alive. These premises provide the foundation for the question "where can the line between living and non-living entities be drawn?". The answer to this question can be long and extend beyond the scope of this thesis. However, it seems irrefutable that information is a pivotal asset for life to occur and that both concepts are intrinsically intertwine. This is inferred by our innate biological mission to generate offspring. Ultimately storing and passing genetic information is nature's instrument to maintain life itself, keeping a proof of history while providing the basis for adaptation through evolution. Interestingly, acknowledging Symbiogenesis and the endosymbiotic theory,[clxx] organelles like the mitochondria and the ribosome gave up on life for the sake of evolution and genetic information prevalence.

We can all agree that biology gifts us with marvelous sources of inspiration enclosing billions of years of persistent optimization through trial and error. Taking the interaction between genetic information and the ribosome as an example, it becomes evident that information storage and translational are pivotal to evolution and adaptation. Therefore, to understand biology and consequently predict or act on its flaws, we followed nature's example and pursued the development of novel ways to store and decipher information regarding biological events.

Cancer is arguably the biggest health-related challenge afflicting modern societies. Many strategies have been developed to tame such a huge burden. Approaches reaching the forefront of cancer therapies are temperature-based treatments like hyperthermia treatments. Unfortunately, the real temperature experienced by cancerous cells and/or healthy tissues is only estimated or not assessed. This is especially valid when using remote sources of heating, such as lasers. The fact that temperature under- or overshoots can impose major side effects while mitigating treatment efficiency constitutes an important Achilles heel when conceiving or performing hyperthermia therapies. To tackle this limitation, the synthesis and preparation of magnetic nanoparticles with a sharp magnetic transition near biologically relevant temperatures was optimized. The Fe_3Se_4 nanoparticles were monodisperse and their Curie temperature was mainly determined by its crystallinity. After characterization, the ability of a batch of particles, which presented a magnetic transition around ~42 °C, to behave as thermometric logic gates was evaluated. Using prostate cancer cell cultures and a NIR laser to induce heating, temperature overshoots were accurately assessed. To the best of my knowledge this was the first time a permanent magnet (hard magnet) was employed directly in a biological application. Hopefully, this proof-of-concept design will inspire researchers to explore the properties of hard-magnets and magnetic nanothermometry in a range variety of bio-applications and ultimately pushing it towards multi-sensing, theranostic and smart self-regulated platforms.

Furthermore, I migrate from magnetic thermometers to optical detection of nucleic acids using metallic fluorescence-enhancement biosensors. Despite already pivotal in many diagnostic contexts, the current pandemic (COVID-19) caused by the virus SARS-CoV-2 popularized nucleic

[clxx] Endosymbiotic Theory From Amoeba Sisters

acid testing. To control the unrestrained spreading and nefarious consequences of the virus, antibody (LFAIs) and PCR testing were developed and deployed with urgency. This educated the population about the need for immediate, reliable, and accessible results. Contrary to LFIAs, PCR testing depends on nucleic acid amplification prior to detection. Despite increasing the sensitivity of the test, PCR procedures are morous and depend on specialized facilities and personnel for collection and analysis. Not exclusive in the context of diagnostic of infectious diseases, strategies enabling fast signal amplification and potential for integration with POC devices are enticing. In this regard, Plasmon-enhanced fluorescence (PEF) biosensors fill both these boxes. Plasmophores operate holistically and thus overall fluorescence emitted by the nanohybrid can vastly exceed its individual counterparts. Intelligibly, this critically improves detection limits while being POC-suited. In the third chapter, sucrose-density gradient (SDC) was applied for size selection of silver triangular nanoprisms. The hot-spots from anisotropic plasmonic nanoparticles stimulate fluorescence thus responsible for signal amplification. While the synthesis of such nanoprisms is simple and fast, the resulting particles are heterogenous with poorly defined optical properties, and present low shelf life due to Oswald Ripening. Since these limitations are inherently size dependent, by using SDC the optical properties of the antenna can be selected and matched with the fluorophore enabling to optimize plasmophore efficiency. Also, to prevent oxidation of tips during DNA anchoring, which is indicated by a quick color change, particles were coated with a gold layer. The plasmophore composed by truncated triangular nanoprisms (Ag@AuNTPs) and Atto-655 presented 1000-fold higher emission than individual fluorophore. Many aspects can mitigate direct application of such approach in the clinical setup, as for example the cost of SDC in an industrial scale. Nevertheless, I believe that our approach can help shedding light to PEF and swift optimization of its framing by contributing to many fundamental studies in the fields of materials science, biophysics, and others.

Metaphorically speaking, nucleic acids provide the instructions to cells on “how to build the biological machinery”. Yet, in some specific cases, after assembling this machinery needs to be finely tuned and orchestrated with peer components to guarantee proper metabolic functioning. In this metaphor we can easily perceive enzymes, such as proteases, as highly skilled engineers and/or robots embedded within this “Toyotistic”[clxxi] production line. With this in mind and acknowledging the central influence of proteases in metabolic processes, chapter 4 describes an LSPR proteolytic activity sensor in real-time. Despite its underlying versatility by means of peptide designing, herein we decided to use thrombin as enzyme model due to its central role in coagulation and clinic relevance. Our single particle strategy is stable for longtime scales monitoring and provided real-time information with hundreds of milliseconds time resolution. Also, information about kinetic parameters like time of arrival of the first enzyme (t_0) and reaction half-time (t1/2) were attained. Furthermore, we were able to quantify the concentration of active thrombin over 2 orders of magnitude within the clinically relevant range – 3 to 300nM. Our experimental results were parallelly compared to a theoretic model and mirroring tendencies were observed. I believe this strategy can set the foundation for further development in a research topic that is currently fairly unexplored and technologically limited with inherent merits. The intrinsic features of our strategy can provide advantageous capabilities like mapping, multiplexing and others over long periods of timescales which can be detrimental

[clxxi] How Toyota Changed The Way We Make Things From Bloomberg Quicktake

in molecular biologic studies, drug development, be clinically relevant ultimately in POCs and theranostics, and many others.

Wrapping-up, through the course of this thesis, the challenges, limitations, and merits of three distinct (Bio)sensors to determine environmental conditions, genetic expression and metabolic processes were addressed. Contrary to a laser focus approach, this amalgam of concepts and designs aims to address 3 of the underlying segments critically influencing biology and homeostasis and bring them under a cloud covering-up the fields of (Bio)sensors and P4 Medicine.

This thesis aimed to explore the synergy between nanotechnology and (Bio)sensors and to endow its reader with the fundamental picks and shovels underlying the development of innovative detection systems. With the support of adjuvant technologies like machine learning, and others, or even by simple conceptual merging, we will ultimately achieve smart multiparametric sensors and actuators. One may wonder if we will ever reach the holy grail and the word medicine will be a synonym of “kryptonite” for diseases. Nonetheless, hopefully, by the end of the day, the technological increments and concepts exposed here will shed some light and support the dawn of a wellness-oriented medicine where the word “sick” becomes obsolete.

Appendixes and other outcomes

Outputs from this dissertation

- 3 published papers in peer reviewed scientific journals as 1st author (1, 2, 3) and one under revision (4) from which 2 of them I am also the corresponding author;
- Co-author of 4 papers in peer reviewed scientific journals (1, 2, 3, 4)
- Co-writing an approved nationally funded project "On2Off" and mild contribution in the recently funded project "A Gold Nanosensor for Single-Molecule Detection of RNA Biomarkers in a Miniaturized Microscope"….
- Field trips to the University of Zaragoza (Angel Millan Group) and University of Groningen (Romana Schirhagl group)
- Supervision of 7 students:
    - 3 students: preparation and analysis of Carbon dots in catalysis and metal sensing,
    - 1 student: Polyoxo-metalates (POMs) preparation, encapsulation, and functionalization for paper-based LFIA assays.
    - 1 student: Synthesis and functionalization of gold nanoparticles for paper-based LFIA assays.
    - 1 student: Correlative microscopy of Gold triangular nanoprisms using dark-field microscopy and AFM. From sample preparation to BEM calculations.
    - 1 student: Involved with the "On2Off" project - Preparation of nanomaterials, functionalization's and thereof
- 1 international Patent written and submitted: "N/Ref: PTI-US 2019/48011 - PROBE ELEMENT AND METHODS FOR SEPARATION"
- 4 conferences participation: 2 Travel Awards and 3 oral presentations: NanoSpain; Nano Today; NanoPT and S_3IC;
- Intimate involvement with Student Organizations to restructure the lab experiences for "open science weeks"

And probably the most important of them all, a panoply of (un)told stories that enabled me to learn an essential skill set from the conceptualization to the experimental design and problem solving.

*Appendix - Table 1 – **Suggested videos evoking the potential and/or features of Nanotechnology** (available on Youtube).*

	Title	Duration (min)	Channel	Year
General	Nanotechnology: A New Frontier	13	Aperture	2020
	Nanotechnology Expert Explains One Concept in 5 Levels of Difficulty	24	Wired	
	Age of GRAPHENE	8	Genius Engineering	
	Scientists Create the FIRST Living Robot!	11	ColdFusion	
	Quantum Computers, Explained With Quantum Physics	10	Quanta Magazine	2021
	How Two Physicists Unlocked the Secrets of Two Dimensions	8		2022
Materials	Conductive Polymers	6	SciToons	2013
	How To Make Colour With Holes	6	Veritasium	
	Tiny treasure: The future of nano-gold	4	Nature Video	2015
	What is molecular self-assembly?	4	SciToons	2018
	World's Lightest Solid!	12	Veritasium	2019
	Magnetic Micro-Robots	8		
	Two-dimensional (2D) materials and atomic scale "Lego set"	4	Scitoons	2020
	March of the microscopic robots	3	Nature Video	
	How Carbon Nanotubes Will Change the World	20	Real Engineering	2021
	Nanocrystal Assemblies: Gaining Power in Numbers	7	SciToons	2022
BioMedicine	Cancer Killing Nanobots	12	ColdFusion	2019
	Nanoparticle Eats Plaque Responsible for Heart Attacks	12		2020

An example for a 2-min Pitch[clxxii]

1 - If you've ever asked yourself what information is, you probably realized that a simple definition doesn't come to mind. However, the importance of information is undeniable.

2 - From our genetic information to history books and the universe around us, information exists in many forms and can be obtained in many ways.

3 - Naturally, we are endowed with a set of built-in sensors. That's why you can see me and hear me as I am standing here.

4 - Fast-forwarding to our fight against diseases, biosensors can act as our "white hat" spies providing information about a given system, thus enabling us to choose an appropriate response.

5 - In my thesis, I developed sensors with the following in mind;

6 - A patient arrives at the hospital and needs a diagnostic. I developed a fluorescence-enhanced biosensor to detect nucleic acids.

7 - After diagnosis, the patient needs treatment. So, we developed magnetic nanothermometers to assess temperature during hyperthermia treatments, for example.

8 - After treatment, we developed a metabolic sensor to monitor proteolytic activity and its kinetics.

9 - Hopefully, everything goes well and we were able to mitigate poor outcomes and the "patient" can go home to live happily ever after…

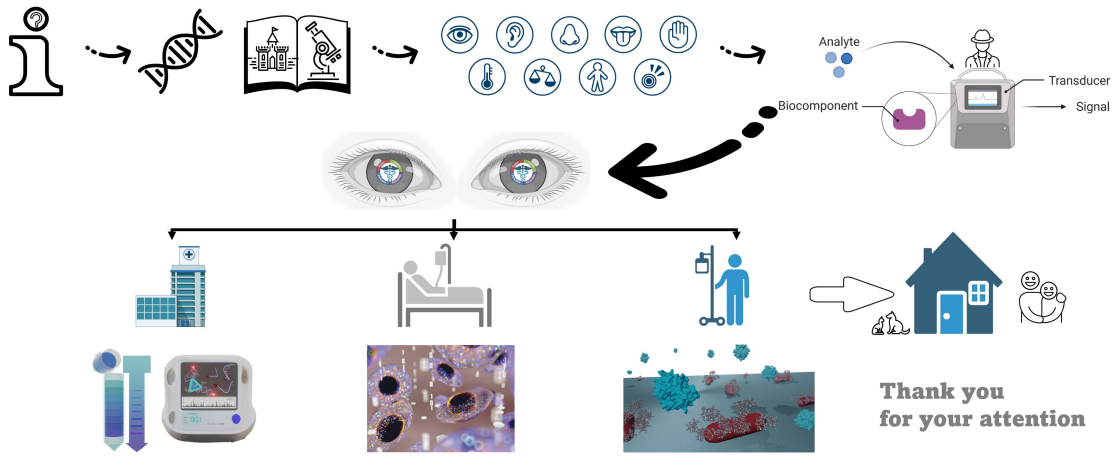

[clxxii] 6ª Conferência Anual da redeSAÚDE - A. Oncology and Precision Medicine from ULisboa and it can be seen from 1:54:15 onwards.

Extended Abstract

Powered by technological advancements, the Anthropocene[clxxiii] era defines humanity's ability to skew the course of its environment. The constant appearance of novel technologies along with globalization has marked the beginning of the XXI century, leading to a deep change in our life paradigms. A clear showcase of such transformation is the Big data companies, which nourish on the ability to gather data from its users, reaching market valuations up to trillions of dollars. However, it is interest to note that the value of information per se is often intangible[clxxiv] and thus difficult to assess in most real-life scenarios like health-related circumstances. Often, in diagnostics, treatments, quality control of processes and/or products, and many other examples, information can set the border between a positive and a negative outcome.

Acknowledging the holistic[clxxv] nature of metabolic processes, Biology-based fields such as medicine abandoned the reductionist[clxxvi] view and heavily invested in deep evaluation and monitorization of cell signaling and metabolic processes to comprehend its dynamics. In this framework and taking advantage of the maturation of the nanotechnology field and related technologies, this thesis will focus on the development of nanoparticle-based magnetic and optical (bio)sensors. This document will mainly uncover three independent designs of (bio)sensors. For simplicity, despite the versatility of the presented concepts, only health and biology-related applications are explored. Thereby, I will showcase designs of (bio)sensors to assess temperature-related events, nucleic acid detection and to monitor proteolytic activity. To note, all the sensors presented here possess the fundamental capabilities for real-time[clxxvii] monitorization. However, in given circumstances, this feature is cumbersome, complicates implementation or is not required at all. Hence, real-time measurements will only be investigated when pertinent.

In the introductory section, I overview topics, theories and the underlying concepts to reason about our motivation and grasp the relevance of the developed concepts. Then, the proposed (bio)sensors are elucidated in technologic focused chapters. In the first example, the usage of magnetic non-volatile logic gates to determine temperature-related events is shown. This apparatus was used to assess temperature overshoots during hyperthermia treatments in cell cultures. Hyperthermia therapy is trending as a cancer co-treatment alongside with chemo- and radiotherapy, already being a reality in the clinical context throughout hospitals worldwide. Despite its potential, both temperature under- and overshoot can cause negative side effects such as epithelial-to-mesenchymal-like transition (EMT)[clxxviii] that increase likability of metastasis. Also, the premise behind hyperthermia treatment is that cancerous cells are prone to damage or being killed at lower temperatures (41-45°C) when compared to its healthy

[clxxiii] Denotes the current global age during which human's activity play a dominant influence over natural phenomena

[clxxiv] Something that exists but that cannot be touched, exactly described, or given an exact value

[clxxv] characterized by the belief that the parts of something are intimately interconnected and explicable only by reference to the whole.

[clxxvi] analyzing and describing a complex phenomenon in terms of its simple or fundamental constituents

[clxxvii] (author' definition) assays that have an immediate response that is proportional to proteolytic activity and can be rapidly read by a sensor, but not necessarily as a continuous measurement

[clxxviii] epithelial cells lose their cell polarity and cell–cell adhesion, thus gaining migratory and invasive properties to become mesenchymal stem cells

counterparts. However, if an abrupt temperature overshoot occurs, necrotic[clxxix] events can be triggered, and ultimately leading to the unwanted damage of healthy tissues. This clarifies the relevance of temperature assessment as a tool to avoid therapeutic side effects of hyperthermia. Recognizing the potential and aiming to circumvent the limitations of hyperthermia procedures, monodisperse nano-sized Hard-magnets of iron selenide (Fe_3Se_4) were synthesized. To characterize the physical properties of the nano-magnets, we used XRD, STEM, XPS and SQUID techniques. Afterwards, COMSOL simulations enabled to estimate the temperature gap between the sensor's surface (Fe_3Se_4NPs) and the exact temperature experienced by the cells. Lastly, the ability of these novel nanoparticles to be used as temperature-responsive logic-gates was assessed with a commercial fluxgate to measure temperature overshoots during an *in vitro* hyperthermia treatment using a prostate cancer (PC-3) cell line as a model. Results showed the ability of the nanoparticles to function as logic-gates to determine temperature overshoots (above approximately 42°C) during hyperthermia treatments.

The following chapter comprises an enhanced fluorescence biosensor based on plasmonic nanoparticles, namely gold-coated silver triangular nanoprisms (Ag@AuNTPs), and its potential for nucleic acid detection. Biosensor technologies that enable fast and reliable detection of nucleic acids are crucial in many contexts of our daily lives, with applications ranging from quality control of food to diagnostic of diseases such as Covid-19. Therefore, a sensitive and portable technology to determine the presence of nucleic acids — either RNA or DNA — can have a major impact on contemporary societies. Due to their intrinsic features, optical properties, easy preparation and versatility, anisotropic Gold-coated silver (Ag@AuNTPs) nanoparticles are a viable tool as nano-antenna platforms, thus increasing the performance of such Biosensors. However, the prospective application of such nanostructures is still limited by size polydispersity, which results in broad spectral features, low shelf-life and susceptibility of silver to oxidation. To overcome these issues, a highly reproducible and simple purification method based on sucrose density-gradient separation was developed to enable the size selection of nanoparticles and isolation of purified fractions with narrow Localized Surface Plasmon Resonance (LSPR) profiles. Further than mitigating Oswald ripening phenomena, this tactic enabled to tailor and precisely match fluorophore's emission with the NPs LSPR and optimize plasmophore properties. Because of the instability of the nanoprisms' tips during the functionalization with thiol-derivatized DNA probes, the fractionated silver nanoprisms were coated with a gold layer resulting in truncated Ag@Au NTPs. These bimetallic particles were characterized using confocal microscopy either in Fluorescence Lifetime Imaging (FLIM) and Fluorescence Correlation Spectroscopy (FCS), Scanning Transmission Electron Microscopy (STEM) and UV-Vis-NIR spectroscopy. Discrete Dipole Approximation (DDA) simulations were performed to predict the theoretically expected near field enhancements at the particle's surface. The selected samples of Ag@Au NPs were functionalized with an oligonucleotide marked with a fluorophore – SH-DNA-ATTO-655 – and we used FCS to evaluate the performance of the plasmophores. The enhanced performance from the composite particles was proven by its superior emission (~1000-fold) intensity when compared to a single dye-labeled oligonucleotide.

[clxxix] Irreversible cell injury and eventual cell death due to pathological processes

Lastly, a single particle LSPR-based metabolic biosensor was developed to monitor proteolytic activity. As model enzyme, we selected thrombin due to its clinical relevance and intricate regulation mechanisms entangled within complex cascades and feedback-loops composed by activators and inhibitors. Unfortunately, this implies that resorting to protease quantification is often misleading. Hence, direct measurement of proteolytic activity provides valuable information about the physiological state and the prospective outcomes of a system. Consequently, rationalizations and distinctions between healthy and disease situations can be established and correlations between proteolytic activity and diseases' extension or its severity are reliable. To this end, activity of thrombin was assessed using gold nanorods (AuNRs) immobilized onto a glass coverslip and functionalized with a peptide rationally designed. Within its structure the peptide pertains an anchor group (a thiol; -SH), a specific target sequence for thrombin recognition, and a biotin unit. Furthermore, the N-terminal side of the peptide was mainly positively charged contrarily to the C-terminal region. The overall structure of the peptide can be written as: biotin – positive spacer – target sequence – negative spacer – cysteine C. Resorting to a widefield microscope with a prism-based dark-field illumination the sensor was characterized. Our sensor displayed a dynamic range >2 orders of magnitude – from 3nM to 300nM – and thrombin's cleavage kinetics were obtained and compared with a theoretical model.

The future impact of the research summarized above in the context of (bio)sensors field is broadly discussed in this thesis and is open to speculation. Besides knowledge expansion and other potential applications, my expectations are to pertinently contribute to the implementation of "P4 Medicine" – from (P)articipatory, (P)reventive, (P)redictive and (P)ersonalized. Understandably, this emerging concept is swiftly grabbing the attention of the scientific community engaged with the development of (bio)sensors and monitoring technologies. This is particularly relevant as biology and metabolic processes tendentially behave as "chaotic systems", as popularized in the "butterfly effect", where a small change in an "initial state" can result in large differences in the "later state". Case examples of this can range from an individual cancerous cell evolving into metastatic terminal cancer, a zoonotic virus turning into a global pandemic in just a couple of months – as we are currently experiencing with the Covid-19 pandemic caused by the virus SARS-CoV2 - or even a small deregulation of a cascade mechanism, such as blood coagulation, often leading thromboembolic conditions, which are the most common cause of death and debilitation nowadays. By giving us access to previously inaccessible information – both by increasing sensitivity or by the ability to reach new nanosized dimensions – or by enabling monitorization throughout a process, magnetic and optical nanosensors will make an undeniable contribution to the intrinsic value of (bio)sensors in our contemporary societies.

The concept of a "Biomolecular Big Brother" seems closer than ever, although in a different sense from that originally described by George Orwell, of an entity that is able to track and manipulate an entire population, into the positive societal role encompassed in the goal of this thesis.

Resumo Alargado

A era do Antropoceno veio, acima de muitas outras coisas, demonstrar a capacidade da humanidade alterar, redesenhar e redirecionar o seu ambiente. Impulsionadas pelo método científico, invenções como a "internet das coisas" (do inglês "Internet Of Things" - IOT) que é hoje subjacente à indústria 4.0, algoritmos de aprendizagem de máquina (do inglês "Machine Learning") e inteligência artificial, a par do fenómeno de globalização, têm originado rápidas e profundas mudanças de paradigma nas nossas vidas. Um exemplo claro desta revolução são as empresas de análise massiva de dados (Big Data Companies), cujo modelo assenta na ~~sua~~ capacidade de obter informação/dados, catapultando frequentemente o seu valor de mercado para os milhares de milhão ou até mesmo biliões de dólares. Curiosamente, em grande parte dos casos o valor da informação, é intangível e por isso difícil de determinar em muitos casos da nossa vida quotidiana. Isto é particularmente verdade em assuntos relacionados com saúde, seja no diagnóstico de uma doença, no controlo e monitorização da qualidade dos nossos produtos ou até nos tratamentos. Consequentemente, este progresso contínuo e exponencial tem levado à consolidação, integração e combinação de novas tecnologias que tendem também a alimentar mudanças de paradigma na área da medicina, nomeadamente, uma transição da medicina moderna, partindo de uma visão "reducionista" para um ponto de vista mais integrativo e holístico, que implica monitorização e compreensão profunda dos processos metabólicos e dos sistemas de sinalização celular e metabólica.

Com base nesta premissa, o papel dos biossensores no diagnóstico e/ou prognóstico, devido à sua capacidade de reportar sobre a condição de um paciente e até de avaliar a resposta terapêutica, é crucial na tomada de decisões informadas. Estes sensores são fundamentais para garantir a qualidade de produtos relacionados com a saúde. Reconhecendo o potencial desta realidade e tirando partido do desenvolvimento rápido que ocorre simultaneamente na área da nanotecnologia, esta tese focar-se-á essencialmente no desenvolvimento de nano-construções e na aplicação subsequente em (bio)ssensores magnéticos ou óticos. Neste contexto, vários tipos de sensores foram desenvolvidos, incluindo nanotermómetros magnéticos, sistemas de deteção amplificada de ácidos nucleicos e sistemas de determinação de atividade proteolítica. Apesar de todos os sensores aqui desenvolvidos terem potencialmente capacidade para serem integrados em sistemas de monitorização, em alguns casos a obtenção da informação em tempo-real não é necessária levando apenas a uma sobre-complicação do sensor e comprometendo assim a sua implementação prática. Deste modo, tanto aplicações de sensores com leituras em tempo-real como de medição pontual serão apresentados.

No primeiro capítulo de resultados experimentais uma porta lógica magnética não volátil é apresentada para determinação da ocorrência de eventos de sobreaquecimento térmico durante tratamentos de hipertermia em cultura de células. A terapia por hipertermia tem vindo a ganhar popularidade como adjuvante de químio- ou radioterapia no tratamento de cancros, estando já a ser testada e aplicada, dependendo do tipo e localização da doença, em vários hospitais no mundo. Apesar do seu potencial, esta estratégia terapêutica está ainda sob algum escrutínio, muitas vezes instigado por limitações tecnológicas. Isto ocorre essencialmente porque tanto o sub- como o sobreaquecimento podem dar origem a efeitos nefastos como a transição epitelial para mesenquimal (do inglês Epithelial-to-mesenchymal-like) que aumenta a

probabilidade de ocorrência de metástases. Ainda, a premissa subjacente aos tratamentos por hipertermia é de que as células cancerígenas são mais suscetíveis a sofrerem danos ou até mesmo morrerem quando expostas a temperaturas mais baixas (41-45°C) que as células saudáveis homólogas. Contudo, se um sobreaquecimento abrupto ocorrer durante o processo de tratamento, as células saudáveis irão também ser afetadas, e, no limite, morrer. A verificação da ocorrência de sobreaquecimentos durante tratamentos de hipertermia pode ser uma ferramenta fulcral para mitigar potenciais efeitos negativos. Motivado pelo potencial da hipertermia enquanto estratégia terapêutica e de forma a tentar contornar as limitações tecnológicas atuais, a síntese de nanopartículas de seleneto de ferro (Fe_3Se_4) monodispersas foi desenvolvida. A escolha desta fase deve-se às suas propriedades magnéticas, uma vez que são consideradas magnetos "duros" e com uma transição magnética (T_c) abrupta em torno das temperaturas de interesse. As propriedades físicas das nanopartículas sintetizadas foram avaliadas utilizando diversas técnicas de caracterização de materiais, nomeadamente XRD, STEM, XPS e SQUID. Por forma a estimar a diferença de temperatura entre a superfície do sensor (Fe_3Se_4NPs) e a temperatura real à qual as células foram submetidas, foram realizadas simulações utilizando o software COMSOL. Após caracterização exaustiva dos nanomateriais obtidos e da resposta do sensor com a temperatura, a aptidão destas nanopartículas de atuarem como portas lógicas térmicas para determinação de eventos de sobreaquecimento durante tratamentos de hipertermia *in vitro* foi avaliada. Para tal, foi utilizado um fluxgate comercial como sensor magnético e uma linha celular de cancro da próstata (PC-3) como modelo. Os resultados obtidos demonstraram que eventos de sobreaquecimento poderiam ser determinados utilizando portas-lógicas não voláteis.

Seguidamente, um biossensor de fluorescência intensificada baseado em partículas plasmónicas, nomeadamente nanoprismas triangulares de prata revestidos a ouro (Ag@AuNTPs) foi desenvolvido e aplicado para potencial deteção de ácidos nucleicos. Tecnologias como biossensores podem permitir uma determinação rápida e confiável de ácidos nucleicos em diversas situações, desde o controlo de qualidade de alimentos até ao diagnóstico de doenças infeciosas como o Covid-19. Este método de elevada sensibilidade e adaptabilidade a sistemas portáteis para determinar a presença – e idealmente quantificação – de ácidos nucleicos (DNA e RNA) pode ter elevado impacto no nosso quotidiano. Devido à sua forma anisotrópica, partículas plasmónicas como as Ag@AuNTPs são de síntese e funcionalização simples e as suas propriedades óticas conferem-lhes aptidão para atuar como nano-antenas. Prospectivamente, a aplicação sistemática destas nanoestruturas é limitada pela polidispersão obtida durante o processo de síntese, resultando em propriedades óticas mal definidas, e pela suscetibilidade da prata a sofrer oxidação. De forma a superar estas limitações, foi concebido um método simples e de elevada reprodutibilidade baseado em centrifugação com gradientes de sacarose que permite selecionar e purificar as nanopartículas com base no seu tamanho, resultando em frações com propriedades óticas bem definidas (LSPRs estreitos). Este atributo é benéfico para o desenvolvimento de plasmóforos (partícula plasmónica + fluoróforo) pois permite a otimização do acoplamento ótico entre as duas entidades. Como referido, devido à instabilidade das pontas do nanoprisma durante a funcionalização com sondas de ADN derivatizadas com um grupo tiol, as frações de nanoprismas de prata foram revestidas com uma camada de ouro, resultando em nanoprismas truncados - Ag@AuNTPs. Estas partículas bimetálicas foram caracterizadas recorrendo a microscopia confocal utilizando os modos FLIM

e FCS, também por STEM e espectroscopia UV-Vis-NIR. Simulações em DDA foram feitas de forma a prever/estimar os fatores de intensificação obtidos pelo "campo próximo" à superfície das partículas. As amostras selecionadas de Ag@AuNTPs foram funcionalizadas com uma molécula de ADN contendo um fluoróforo na extremidade – SH-DNA-ATTO-655 – e a sua eficiência enquanto plasmóforo foi avaliada recorrendo à espectroscopia de correlação de fluorescência (do inglês Fluorescence Correlation Spectroscopy – FCS). Os nanocompósitos resultantes apresentaram intensidade de emissão aproximadamente 1000x superior quando comparados aos oligonucleótidos marcados com um único fluoróforo.

Por fim, foi desenhado um biossensor de partícula plasmónica individual para deteção metabólica e determinação da atividade proteolítica da trombina em tempo real. A atividade da trombina é estritamente regulada por mecanismos complexos de atuação em cascata de respostas retroativas baseadas em ativadores e inibidores. Infelizmente, isto implica que recorrer à quantificação de protéases pode ser erróneo. Assim, a informação obtida através da medição da atividade proteolítica traduz de maneira mais viável o estado fisiológico e o potencial acesso longitudinal à resposta terapêutica. Consequentemente, podemos passar a tirar ilações e distinguir entre estados de saúde e doença possibilitando correlações entre a atividade proteolítica e a extensão da doença. Para determinar a atividade da trombina foram imobilizados nanobastonetes de ouro (AuNRs) numa superfície de vidro e, posteriormente, funcionalizados com um péptido de estrutura planeada, composto por um grupo de ancoramento (tiol), uma sequência-alvo para deteção da trombina, espaçadores e uma biotina. Aqui, utilizámos microscopia de "campo largo" com recurso a um prisma para iluminação (tanto luz branca como 793nm SLD) em modo de campo escuro por reflexão interna total para caracterização espectroscópica das NPs, acompanhamento do processo de imobilização do péptido-alvo e, também, avaliação cinética da atividade trombinolítica. O limite de deteção para concentrações de enzima ativa observado está na gama dos nM e a gama de trabalho do sensor é de pelo menos 3 ordens de grandeza. Apesar de alguma variabilidade durante a imobilização do péptido, os ensaios enzimáticos demonstraram grande sensibilidade e capacidade de determinação de atividade proteolítica em tempo-real.

O impacto futuro da investigação sumarizada acima no contexto dos (bio)ssensores é discutido em várias frentes e está aberto a especulação. Particularmente, os princípios subjacentes aos trabalhos desenvolvidos podem contribuir significativamente para a implementação de conceitos como o de "Medicina P4" – de (P)articipativa, (P)reventiva, (P)redictiva e (P)ersonalizada – que têm vindo rapidamente a cativar a atenção da comunidade científica para a necessidade de desenvolvimento de (bio)ssensores e tecnologias de monitorização. Isto é particularmente importante pois a biologia tende a comportar-se como um sistema caótico e, por isso, suscetível ao "efeito borboleta", na qual uma pequena variação num momento inicial pode originar diferenças abismais entre os possíveis estados finais resultantes. Exemplos notórios de tal efeito podem ser: a formação e proliferação de uma única célula tumoral num cancro terminal metastizado; outro, um vírus zoonótico causar uma pandemia global que nos obriga a reajustar o nosso estilo de vida e com consequências ~~quase~~ imprevisíveis a todos os níveis da sociedade em apenas alguns meses – como é o caso da pandemia causada pelo vírus SARS-CoV2; ou então, uma pequena desregulação num mecanismo de atuação em cascata, como a coagulação sanguínea, que pode resultar numa condição de tromboembolismo e que é atualmente a maior causa de morte e debilitação no mundo.

Os nanossensores magnéticos e óticos permitem-nos aceder a informação previamente indisponível – quer seja por recurso a novos mecanismos de gravação de informação, aumento da sensibilidade ou até mesmo diminuição de escala – quer seja através da monitorização constante ao longo do processo. Indiscutivelmente, estas contribuições podem trazer valor intrínseco ao ramo dos biossensores e à sociedade contemporânea.

Assim, o conceito de "Big Brother Biomolecular" parece, cada vez mais, estar iminente, com a diferença que contrariamente ao originalmente descrito por George Orwell, aqui, a entidade capaz de rastrear e manipular uma população/sistema tem na sua origem um objetivo benéfico para a sociedade.

Monitoring Proteolytic Activity in Real Time: A New World of Opportunities for Biosensors

Highlights

Proteases are widespread in nature and play a pivotal role in many biological processes in life forms and viruses.

Deregulation of protease metabolism can result in several pathological conditions (i.e., cancer, neurodegenerative disorders, and others).

Assays and biosensors that measure proteolytic activity in real time can provide a wealth of information contributing to the rapid evaluation of individual health conditions.

Protease biosensors are mostly based on molecular rulers and usually rely on optical, electrical, or magnetic detection.

Novel and improved protease sensing systems are rapidly emerging with the potential to impact healthcare, drug development, and fundamental studies in biology and biochemistry.

Abstract

Proteases play a pivotal role in several biological processes, from digestion, cell proliferation, and differentiation to fertility. Deregulation of protease metabolism can result in several pathological conditions (i.e., cancer, neurodegenerative disorders, and others). Therefore, monitoring proteolytic activity in real time could have a fundamental role in the early diagnosis of these diseases. Herein, the main approaches used to develop biosensors for monitoring proteolytic activity are reviewed. A comparison of the advantages and disadvantages of each approach is provided along with a discussion of their importance and promising opportunities for the early diagnosis of severe diseases. This new era of biosensors can be characterized by the ability to control and monitor biological processes, ultimately improving the potential of personalized medicine.

Biosensing in Personalized Medicine: The Emergence of Protease Biomarkers

A deep understanding of the individual characteristics of biological processes and precise control of responses and feedback to therapies are essential in a world that is running towards personalized medicine (see Glossary). Recent reports predict that this market will grow at a compound annual growth rate (CAGR) of over 11% from US$92.4 billion dollars in 2017 to US$194.4 billion in 2024 (https://www.researchandmarkets.com/research/n5kqz7/global?w=5), with oncology responsible for 30% of the revenues generated. Biosensors are one of the underlying technologies of personalized medicine, giving support to the highly informed decisions that are critical to obtain better clinical outcomes and to decrease undesired side-effects. Compared with the personalized medicine market, a similar tendency is observed for the biosensors market where growth from US$18.6 billion dollars in 2018 to US$31.5 billion in 2025 (8% CAGR) is expected (https://www.gminsights.com/industry-analysis/biosensors-market).

The role and idiosyncrasies of proteases: why monitor proteolytic activity?

Proteases are a widely explored research topic as illustrated by more than 487 000 entries registered in PUBMED. However, it was only recently that proteases emerged as an analyte of interest for biosensing.[1] These hydrolytic enzymes (EC 3.4) play a pivotal role in several biological processes, such as digestion, cell proliferation, and differentiation,[2] as well as apoptosis,[3] coagulation,[4] immunity,[5] and fertility.[6] The deregulation of protease metabolism can result in numerous pathological conditions (i.e., cancers,[7] neurodegenerative disorders,[8] and others).[9] For this reason, the pharmaceutical industry is actively evaluating the potential of proteases as drug targets or as biomarkers for diagnosis and prognosis. In this regard, thrombin and prostate-specific antigen (PSA) can be highlighted as two of the most common protease targets in clinical biochemistry.[10,11] And, one notable example of a protease-targeted therapy is the administration of HIV-1 protease inhibitors (i.e., lopinavir/ritonavir branded as Kaletra from Abbott Laboratories) in the context of AIDS.[12] Lopinavir is a specific inhibitor of HIV proteases, which prevents maturation of the virus, hindering its ability to infect new cells and replicate. However, lopinavir is quickly degraded within the human body by cytochrome P450 3A4 enzyme (CYP3A4).[13] To overcome this and increase the lifetime of lopinavir, a potent CYP3A4 inhibitor (ritonavir) is included in the formulation. During the preparation of this manuscript (March 27,2020), the world is facing an unprecedented pandemic due to the outbreak of the coronavirus disease, COVID-19, caused by the virus SARS-CoV-2. Similar to HIV, proteases are pivotal during viral maturation, affecting the ability of the virus to infect new host cells.[14] Likewise, protease-targeted therapies with protease inhibitors are one of the forefront strategies being pursued to fight the outbreak. Several drugs are undergoing testing and clinical trials (https://www.sciencemag.org/news/2020/03/who-launches-global-megatrial-four-most-promising-coronavirus-treatments#), with mild results,[15,16] notably lopinavir/ritonavir and arbidol (https://clinicaltrials.gov/ct2/show/NCT04252885). In this regard, the ability to monitor proteolytic activity in real-time can play a pivotal role in screening potential protease inhibitors for therapeutic purposes.[17] The spread of COVID-19 caught most countries off-guard, with their health-care systems being unable to restrain transmission before adequate testing to allow controlled isolation and tracking.[18] This may due to the fact that the 'gold-standard' RT-PCR test is time-consuming and expensive, among other limitations (https://www.fda.gov/media/136151/download; ttps://www.iaea.org/newscenter/news/how-is-the-covid-19-virus-detected-using-real-time-rt-pcr). Alternative, less expensive and easier to use serological tests also have limitations.[19] Both tests may also provide non-definitive results (https://www.politico.eu/article/spanish-government-under-fire-after-defective-testing-kits-fiasco). Although to our knowledge diagnosis of viral infections by proteolytic activity monitoring is unavailable in health care, experimental studies on viral proteolytic maturation should clarify the potential of proteases as drug targets and as diagnostic tools.[20]

In view of its biological and therapeutic relevance, understanding and evaluation of proteolytic activity, both in vitro and in vivo, is extremely informative. However, determining protease concentration in serum, tissues, and other samples without correlation with its activity can give limited or erroneous information due to particular features of these enzymes, as described below. Despite the disadvantages of measuring protease concentration instead of

proteolytic activity, this is still performed due to the simple adaptation of gold-standard procedures to these enzymes. The presence of proteases is usually established indirectly by measuring genetic expression via RNA quantification or by using immunoassays. A good example of this approach is the use of reverse transcription PCR (RT-PCR) to infer the presence of matrix metalloproteases (MMPs) in rheumatoid arthritis.[21] However, in these studies immunosensing and mRNA quantification can be misleading because proteases are naturally synthetized in an inactive pro-form, which is activated post-expression. Unfortunately, most immunoassays cannot distinguish between the two forms and the detection of mRNA cannot be taken as a guarantee of the presence of proteolytic activity. Additionally, enzymes are sensitive to disease-related environmental conditions (e.g., pH is often lower in cancerous cells) and thus genetic expression does not necessarily correlate with activity.[21,22]

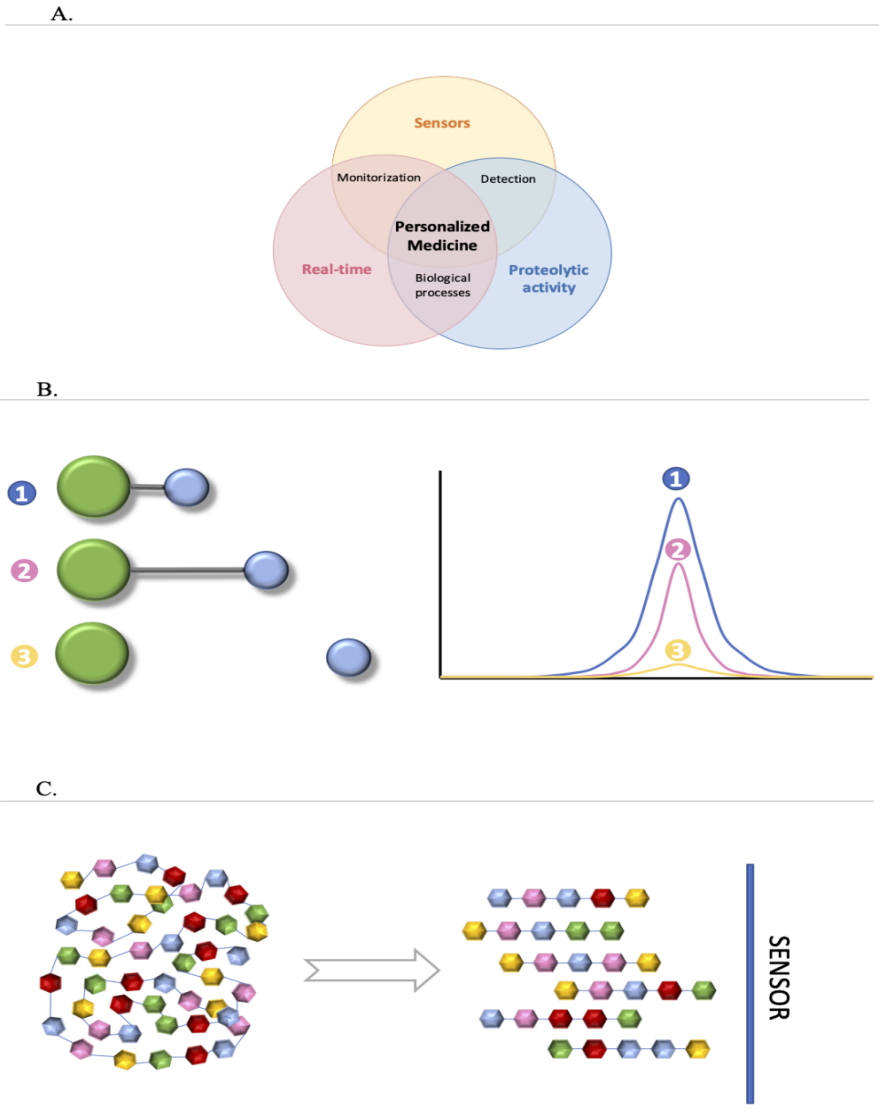

M PA RT - Figure 1 - ***Real-Time Proteolytic-Activity Biosensors and Personalized Medicine****. (A) Triangulation of proteolytic-activity sensors in real time onto personalized medicine. (B) Generalized scheme illustrating the working principle of a molecular ruler'. Here, the interaction between two or more entities is distance dependent; thus, the signal detected by the sensor is strictly dependent on the distance. In proteolytic sensors, molecular-rulers operate to differentiate the signal of the intact molecule (absence of target protease) and that of a cleaved molecule (presence of target protease) in which the interaction between the entities cannot occur. (C) Schematic of proteolytic sensor based on the fragmentation of an original target molecule. In such systems, the cleavage of the original molecule induces a change of a given property, which will provide a sensor reading that is proportional to the proteolytic activity.*

Also, proteases are characterized by a high catalytic constant (10^8–10^9 $M^{-1}s^{-1}$), which means that even a very small variation in genetic expression can have a major outcome difference. Finally, these enzymes are often regulated by endogenous inhibitors, such as tissue inhibitors of metalloproteinase (TIMPs), which are responsible for restraining the activity of MMPs, and a disintegrin and metalloproteinases (ADAMs) within the homeostatic range.[23] For the reasons mentioned above, concentration is not always correlated with activity. Alternatively, by measuring the proteolytic activity one is directly evaluating the function of the protease at physiological conditions and not merely its presence. This creates several opportunities, as described next.

Monitoring proteolytic activity in real-time: What are the advantages?

Given the involvement of proteases in many metabolic and cellular processes, the determination of proteolytic activity is important to understand the role of specific proteases and of proteolytic cascades in cellular events/pathways. For example: caspases play essential roles in programmed cell death and inflammation;[24] MMPs are key to the degradation of most extracellular matrix proteins during organogenesis, growth, and tissue turnover;[25] and the HIV-1 viral protease is critical for the budding of virions from host cells.[26] In real-time detection, more data points are obtained, allowing the correlation between an occurring event and its influence on proteolytic activity.

In healthcare, determination of the protease biomarkers thrombin and PSA is considered the gold standard in the diagnosis of blood disorders and prostate cancer, respectively. More specifically, recent studies have shown the importance of prothrombin/thrombin regulation and its involvement in neurological diseases.[27,28] Here, it is critical to understand and correlate inactive/active thrombin to predict potential outcomes.[29] Therefore, measuring proteolytic activity in real time can overcome limitations of standard biomarkers while potentially leading to new protease-focused biomarkers, which will greatly contribute to optimize healthcare procedures.

Most current proteolytic activity assays are neither real-time measurements nor suitable for in vivo studies (i.e., zymography assays or protocols that use azo dye-marked substrates such as casein).[30,31] Changing the paradigm to real-time detection, where the sensor gives an immediate response proportional to the proteolytic activity, would be extremely interesting in drug development, fundamental studies, and healthcare. From the perspective of the development of protease-targeted drugs/therapies, measuring enzyme kinetics over time using the same sample and without the need for suicidal experiments decreases the number of assays needed for each test.[32] Usually, proteases and pharmaceutical compounds, especially those of clinical relevance, can be expensive and, by decreasing the number of performed tests, the development costs can diminish significantly. Additionally, in assays that determine the concentration of a given analyte, usually one molecule produces one output signal. When measuring enzyme activity, however, a single enzyme can be responsible for multiple events of substrate cleavage thus leading to multiple readout signals, which ultimately produce signal amplification with a concomitant increase of the signal-to-noise ratio (SNR).

Looking for activity in real-time: How is it done?

Proteases are hydrolases responsible for cleaving peptide bonds in proteins/peptides. In general, real-time proteolytic assays exploit the molecular-ruler principle,[33] whereby a sensor molecule is used that contains two labels bridged by the target peptide sequence (M PA RT - Figure 1B). The distance between the two components should change only due to the proteolytic activity of the target protease – as result of cleavage of the target sequence – thus producing a signal readout, while in control samples this bridging sequence remains intact and, in this case, no readout is produced. Other real time sensors, on the other hand, explore the fact that the cleavage of the original protein target generates smaller fragments and often induces a change in a given property (impedance, diffusion), which will influence the sensor readings proportionally to the proteolytic activity (M PA RT - Figure 1).

Different approaches to different needs: which designs are implemented?

Several strategies are currently being explored in real-time proteolytic sensors, as highlighted in the next section and listed in Table 1.

Optical Biosensors: from organic molecules to inorganic particles

Energy-transfer (ET)-based biosensors are, by far, the most commonly used for proteolytic activity determination in real-time. These systems are wash-free, allow for low-depth *in vivo* imaging, and are very sensitive, and the readout is easily obtained. In most designs, ET occurs through long-range dipole–dipole interactions [Förster mechanism or FRET], in which one entity works as an energy donor and another as an energy acceptor. Herein, the fluorophore properties critically affect the detection limit and the dynamic range of the method; a good fluorophore should possess a high molar absorption coefficient, high quantum yield (QY), chemical and photochemical stability, and, ideally, no or low toxicity.[34] The advantage of organic fluorophores is illustrated by the fact that tailormade proteolytic sensors using cyanine and Atto dyes are commercially available.[35] Furthermore, being molecular-sized entities, these organic dye labels exhibit almost no steric effects, which can be critical in enzymatic assays. Despite these advantages, organic fluorophores, especially near-IR (NIR) dyes, have limiting photophysical properties, such as photobleaching and low QY, which hampers their potential for in vivo applications.[35]

M PA RT - Table 1 - Highlights of Proteolytic Activity in Real-Time Biosensors and Their Features

Type of biosensor	Target Protease	Method of detection	Limit of detection	Suitable for *in vivo*	Advantages	Drawbacks	Ref.
Optical	MMP-14	Förster Resonance Energy Transfer (FRET)	ND	✓	- versatile - spectral properties and brightness - ↓ background	- may have misleading results - ↓ in-depth penetration imaging	36*
			ND	✓		- genetic modification is needed	37
	Micro PA + MMP-9		ND	✓	- multiplexing measurements - ↑ SNR - ↓ false positives interference	- ↓ in-depth penetration imaging - ↑ photobleaching	38*
	Caspase-9		ND	✓			39,40*
	Caspase-3/-8/-9		ND	✓			40*
	Trypsin, Chymotrysin	double FRET	1 nM	✗	- double validation - multiplexing measurements - can be used as logic gates	- limited by spectra overlapping	41*
	MMP-2	FRET, NIR-II optical imaging	ND	✓	- versatile to use for several proteases - ↑ spatial resolution through deep tissues - photostability and brightness	- may have misleading results - limited for long-term studies - laborious manufacture	42*
	Caspase-3/-8/-9	Bioluminescence Resonance Energy Transfer	12.5 pM	✓	- does not need an excitation light source - easy manufacturing - comparing to FRET, ↓ photobleaching and ↓ light scattering	- may have misleading results - conditioned by surrounding medium	43
			12.0 pM		- ↑ sensitivity		44

	Caspase-3	Nano Surface Energy Transfer		✓	- ↓ photobleaching - ↑ SNR	- ↓ in depth penetration imaging	
	Trypsin	**Surface-Enhanced Raman Spectroscopy (SERS)**	8.6 nM	✗	- multiplexing measurements	- cannot be used for a wide range of proteases - complex equipment needed - complex manufacture of the nanodomes	45
	PSA	Nanoplasmonic resonator, Raman	6.0 pM	✗	- ↑ sensitivity - multiplexing measurements	- complex equipment needed	46
	MMP-2	Multispectral Photoacoustic Imaging	ND	✓	- spatial resolution - optical contrast without ionizing radiation	- ↑ scattering level - ↓ in depth penetration imaging	47
		Photoacoustic Imaging	0.52 ng/mL	✓	- non-invasive - ↑ depth imaging - ↑ spatial resolution	- ↑ scattering level - ↓ in depth penetration imaging	48
	Caspase-3	Optical imaging of plasmon rulers	ND	✓	- ↓ photobleaching - stable over time - ↑ enhanced signal intensity	- complex equipment is needed - prone to interference	49*
	MMP-2/-9	Evanescent Wave Spectroscopy	32 nM/ 256 nM	✗	- cheap design - portable - constant measurements	- difficult to adapt - ↓ sensitivity - ↓ detection limits	50
Combining techniques	Thrombin	NIR Fluorescence/Positron Emission Tomography (PET)	ND	✓	- ↑ spatial resolution - ↑ sensitivity - ↑ accurate results - whole body imaging	- complex equipment is needed - complexity	51
	MMP-2/-9/-13		ND	✓			52

	Catepsin B	NIR Fluorescence/Computed Tomography (CT)	ND	✓	- ↑ spatial resolution - rapid imaging	- ↓ in depth - some interference	53
	MMP-2/-9	FRET/ Single-Photon Emission Computed Tomography(SPECT)	4.8 ng/mL	✓	- non-radioactive probe	- complex equipment is needed	54
	Caspase-3/-7	FRET/PET	ND	✓	- ↑ spatial resolution	- unstable PET probe	55
	MMP-2	FRET/Magnetic Resonance Imaging (MRI)	0.64 pM	✓	- ↑ time/spatial resolution - ↑ in-depth imaging - ↑ SNR	- complex equipment is needed	56*
Non-optical	MMP-9	Interdigitated array microelectrodes (IDAMs)	10.0 pM to 10.0 nM	✘	- ↑ versatility - suitable for complex cause/effect studies	- limited to "2D systems"	57*
	HIV-1 protease	Nanopore	47.0 pM	✘	- stable over time - multiplexing - unambiguous response - ↑ sensitive	- steric hindrance - specific equipment is required - limited to "2D systems"	58*
	Caspase-3/-7	Magnetic Resonance Imaging	ND	✔	- ↑ time/spatial resolution - ↑ in depth imaging - ↑ SNR	- complex equipment is needed - very expensive - multiplexing can be difficult	59*

Inorganic emitters such as quantum dots (QDs) can be an alternative to surpass such limitations. These nanocrystals have enhanced optical properties such as high photostability, spectral tunability, and a broad excitation wavelength range, while allowing surface functionalization for biomolecule immobilization.[35] For example, Jeong et al. developed a QD-

based ET biosensor in the second NIR region to determine the proteolytic activities of MMP-2 and -9 in real time (M PA RT - Figure 2A).[42] In this work, a multifunctional peptide was used to bridge a QD to an acceptor that quenches its emission in the absence of MMPs. On breaking the peptide bond, the acceptor is released, and the donor brightness increases proportionally to the presence of the active protease. Compared with other NIR dyes, this QD-based sensor displayed better performance for in-depth in vivo imaging. Despite these improvements, the application of QDs in these systems can still be hindered by toxicity, photoblinking phenomena, and size-related issues.

As an alternative to luminescence-based sensors, a system based on the scattering of light from plasmonic nanoparticles was develop by Jun et al.[49] to detect Caspase-3 and -7 inside cells using an adenocarcinoma (SW 620) cell line. In their design, the authors used a crown nanoparticle assembly comprising a core 40-nm plasmonic gold particle coupled to several gold nanoparticles by a target sequence for caspase detection (M PA RT - Figure 2B). Using this plasmon ruler, the authors were able to optically probe caspase activity by measuring the scattered light from the nanoassembly and to follow cell-signaling pathways in vivo at a single-molecule level during a period of over 2 h (continuous measuring). The crown nanoassemblies were crucial to obtain a good SNR in such a highly scattering environment, because two or more particles display a scattering signal 44× greater than individual particles. Additionally, the nanoassembly was functionalized with a cell-penetrating peptide (TAT) allowing intracellular/cytosolic sensing of Caspase-3 and -7 activity in real time. The movement of the particles was minimal during experiments due to constriction from the network of cytoskeleton filaments, although after cleavage the resulting particles were able to freely diffuse away from the region of interest. This system proved to be a powerful tool to determine single proteolytic events in real time inside living cells and allowed the researchers to characterize biochemical parameters, such as lag time, and to determine cell heterogeneity in the same sample. The main disadvantage of the strategy appeared to be the difficulty in preparing the nanocrown systems and their inherent heterogeneity.

As shown in several reported works,[44,60] gold nanoparticles are valuable optical labels in the field of proteolytic sensors. However, most of the strategies used to conjugate gold nanoparticles and peptides rely on the establishment of sulfur–gold bonds, which can be compromised by interference from other thiol-containing molecules that may be present in the medium. This may result in the effective displacement of the thiol-bonded peptide and thus lead to false-positive results. As a strategy to overcome this problem, Tang and coworkers evaluated the stability of selenol (–SeH)-containing peptides as functionalizing groups in cell cultures [39]. The authors demonstrated that R–SeH-functionalized particles exhibit higher performance and increased stability when exposed to high concentrations of glutathione (GSH) (5 mM) and to high temperatures, relative to their R–SH counterparts. The selenium-functionalized systems showed increased SNR during in vitro tests in MCF-7 cells and serum, showing the potential of this strategy in the development of highly stable and reproducible gold-based nanosensors. Furthermore, the authors developed a multiplexing sensing system to study protease cascades in vitro that was able to discriminate between the activity of Caspase-3 (executioner) and that of -8 and -9 (initiators) with minimal background and nonspecific signal in real time.[38,40]

Combining techniques: what can be done to surpass optical sensors' limitations?

A next generation of proteolytic sensors is emerging with the expansion to multiplex-modality systems with activatable probes for in vivo detection/imaging, where optically based sensors are conjugated with other techniques, such as photoacoustic imaging, to improve imaging resolution. So far, the performance of fluorescence-based sensors has been improved and tested using tumor models. For example, Matthias et al. [53] and Yin et al.[54] have combined optical detection with computational tomography (CT). Also, Elvas et al.[55] and Lee et al.[52] have developed probe systems for, respectively, photoacoustic imaging and *positron emission tomography (PET)* to expand the information provided by their proteolytic sensors. One notable example is the system recently reported by Shi et al., which includes various techniques to enhance the diagnosis and to kill gastric tumor cells in vivo (M PA RT - Figure 2C).[56] The authors developed a tumor-targeted and MMP-2-activatable nanoprobe, denoted T-MAN, through an engineered nanoparticle that combined fluorescence/magnetic resonance (MR) bimodal imaging with photothermal therapy (PTT) capabilities. Succinctly, tumor margins are determined using fluorescence imaging activated by the proteolytic activity of MMP-2. After cleavage from MMP-2, a ligand (cRGD) becomes accessible and leads to preferential accumulation and internalization of T-MAN on tumor cells. Consequently, an MR image with enhanced contrast can be acquired due to the presence of Gd-doped CuS nanoparticles in the T-MAN nanohybrids. Additionally, CuS nanodisks exhibit high photothermal conversion efficiency under NIR irradiation, which allows the killing of gastric tumor cells in vitro and in vivo in a mouse model. The potential of these nanoprobes for theranostics of gastric tumors was demonstrated and it was proposed they may also be easily adaptable for other malignant tumors.[56]

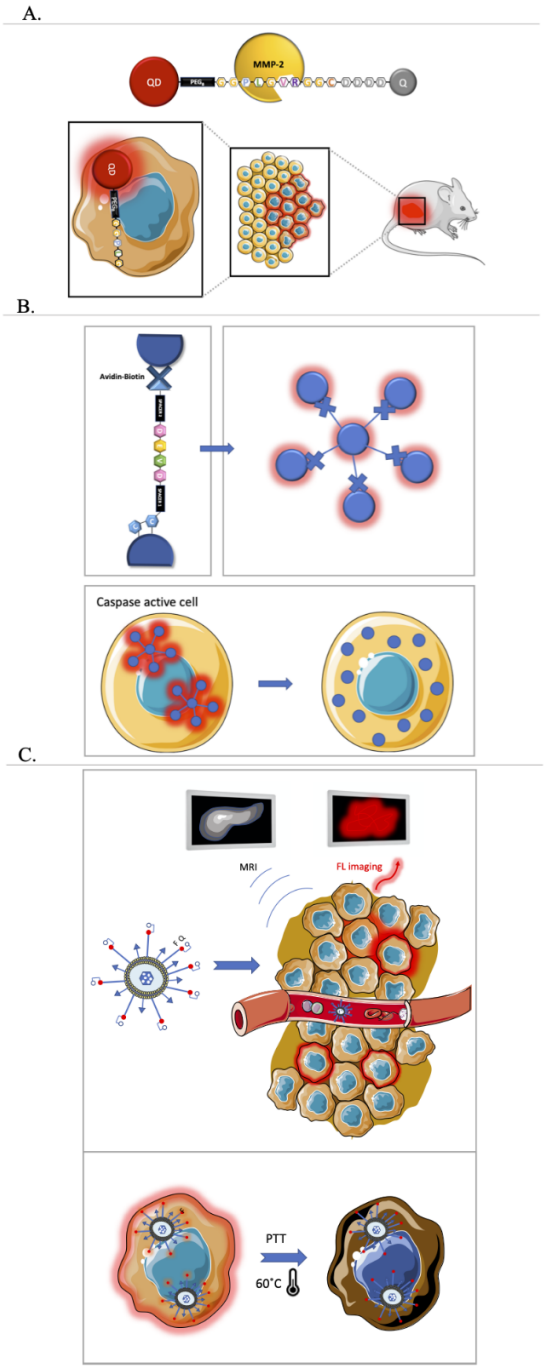

M PA RT - Figure 2 - ***Optically Based Sensors****. (A) Matrix metalloprotease (MMP)-2/9 detection using a near-IR (NIR-II)-emitting quantum dot (QD) and a quencher (Q). When the enzymes are active, fluorescence (FL) increases and nearby cells are marked. This system was able to detect colon cancer in mouse models. Adapted from* [42]*.(B) Crown-shaped assembly of 40-nm plasmonic gold nanoparticles bridged by a peptide sequence for Caspase-3/7 detection. Scattered light from the plasmonic assembly is proportional to proteolytic activity, and particles can freely diffuse within the cell after cleavage. Adapted from* [49]*. (C) Multifunctional nanohybrid comprising Gd-doped CuS nanodisks, a fluorescent probe for MMP-2 activity determination and tumor cell-targeting peptide. After proteolytic cleavage of the activatable probe, tumor margins are determined by FL imaging. Thus, the nanohybrids accumulate on tumor cells allowing MRI with increased spatiotemporal resolution and subsequent photothermal therapy (PTT). Adapted from* [56]*.*

In the examples above, a map of a metabolic process (proteolytic activity) was acquired using fluorescence imaging and complementary techniques with increased spatial resolution and/or in-depth imaging. Moreover, as demonstrated by the last example, therapeutic agents can be included in the formulation to render theranostic features. For these reasons, we believe

that multimodal imaging systems complemented with drug delivery mechanisms are a pathway full of potential to be exploited in the future.

Non-optical Biosensors

Nanopore-based sensors are an interesting alternative to optical sensors since they allow an immediate clear readout and have become less expensive in recent years. In work by Wang et al., [58] HIV-1 protease activity is monitored in vitro by the translocation of substrate degradation products through a nanopore sensor in real time and in a label-free fashion (M PA RT - Figure 3A).

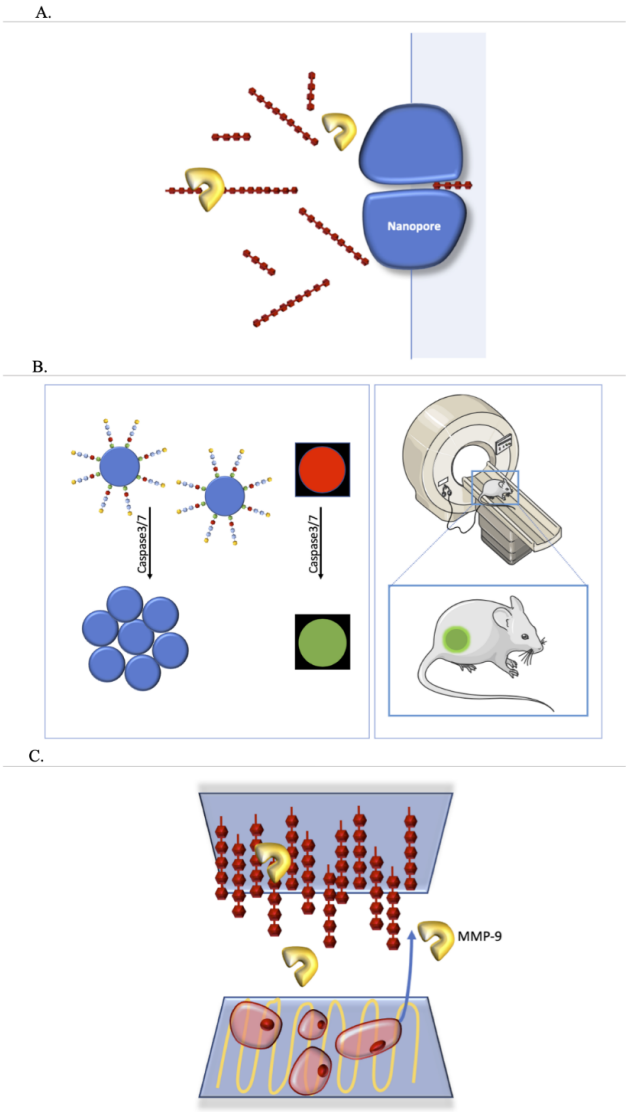

*M PA RT - Figure 3 - **Non-optical Biosensors**. (A) Real-time detection of HIV-1 protease activity using a nanopore. Here, a molecule crossing through the nanopore induces current modulation events. The cleaved peptide rises in two differently sized fragments, which results in different residence times and amplitudes. Adapted from [58]. (B) MRI detection of proteolytic activity from Caspase-3/7 in real time. Peptide-stabilized iron oxide (Fe3O4) nanoparticles lose their colloidal stability and aggregate near apoptotic cells. T2-weighted images were obtained from subcutaneously xenografted HepG2 tumors in nude mice. Adapted from [59]. (C) Simultaneous detection of matrix metalloprotease (MMP)-9 activity and evaluation of cellular behavior using interdigitated-array microelectrodes (IDAMs). Here, the bottom layer detects the cells' morphology change by differences in resistance while the upper layer detects the presence of secreted MMP-2/9 by the change in electrode capacitance. Adapted from [57]*

In this design, the peptide substrate that crosses the nanopore-containing membrane produces only one major type of current modulation event. When the target protease is present or active, however, the substrate is cleaved in two differently sized fragments, producing two new types of blockage events with smaller residence times and/or amplitudes relative to the original substrate. Given the high sensitivity of the method and its potential to discriminate the target protease from false positives, this strategy is potentially useful in diagnosis, prognosis, and the development of drugs. The major disadvantage of nanopore systems is that these are not suitable to be used in vivo and in complex media.

MRI is a noninvasive and well-established technique for in vivo analysis/diagnosis that allows time and spatial resolution with reasonably high sensitivity and in-depth tissue penetration. In view of these advantages, Yuan et al.[59] developed an MRI proteolytic sensor in real time based on iron oxide (Fe_3O_4) nanoparticles, which aggregate after proteolytic activity in a process induced by Caspase-3 and/or -7 and concomitantly increase T2 contrast (M PA RT - Figure 3B). This design was tested in nude mice with subcutaneously xenografted HepG2 tumor. These in vivo tumor MRI measurements suggested specificity for T2-enhanced imaging in tumor apoptosis, demonstrating that MRI can be efficiently applied to evaluate chemotherapeutic efficiency, or other treatments, in routine preclinical studies.

Electrochemical-based sensors provide time resolution and render clear readouts with multiplexing capabilities. For example, Tran et al.[57] developed an on-chip dual-sensing device for the detection of cell-secreted MMP-9 that simultaneously monitors cellular resistance and correlates it with the secretome and morphological analysis. The device comprises two independent sensing platforms featuring interdigitated-array microelectrodes (IDAMs) in one common fluidic chamber (M PA RT - Figure 3C). The goal of the device is to detect MMP-9 activity and understand cellular behavior during motility. On migration, cells tend to change morphology by extending their shape (i.e., lamellipodium formation)[61] and that increases resistance to the flow of electrical current between electrodes. The faster cells extend, the higher the value of the electrical resistance measured. During the migration process, MMP-9 was simultaneously secreted and diffused upwards from the cell binding site.[57] The substrate peptides at the upper site were proteolytically cleaved, causing a change in electrode capacitance. We believe that this dual-sensing method is interesting since it affords high versatility and could be applicable to a wide range of cell-secreted proteases by choosing the appropriate target proteins or peptides. Despite not being suitable for in vivo studies, this approach could deliver promising insights on the relation between the cellular secretome and morphological analysis in real time; for example, in the context of bioengineering approaches used for cellular differentiation.

From the bench to clinical trials

Currently, there are at least two clinical trials registered on the National Institutes of Health (NIH) ClinicalTrials.gov database involving the use of in vivo sensors to determine proteolytic activity in real time.[62–64] These sensors were developed to determine the activity of MMPs (AVB-620 from Avelasbio) and cathepsins (LUM015 from Lumicell) in breast cancer. In breast surgery, surgeons rely on physical examination, tissue texture, and correlation with radiographic data to determine tumor margins. By using such sensors, surgeons can precisely

differentiate between tumorous tissue and nontumorous with precision with no tissue destruction or processing. [65]

Although the target proteases differ, the working principles underlying AVB-620 and LUM015 are similar. For this reason, only AVB-620 is detailed herein. AVB-620 is a fluorescence-based sensor that is currently undergoing Phase III trials for breast cancer and entering Phase I trials for multiple cancers (M PA RT - Figure 4).[62] In this hairpin sensor design, two fluorophores (Cy-5 and Cy-7) are in close proximity due to electrostatic interactions between two oppositely charged domains of the sensor molecule, which are bridged by a specifically targeted peptide sequence. In the absence of tumor-associated enzymes such as MMP-2 and -9, the two fluorophores are close to each other, with Cy-5 acting as an energy donor to Cy-7, which then emits brightly. In the presence of MMP-2/9, the target sequence is cleaved and the two fluorophores are separated, leading to a decrease in Cy-7 emission that is dependent on the protease activity as detected by fluorescence cameras, allowing intraoperative imaging in real time. Additionally, the presence of an activated cell penetration peptide (positively charged) in the resulting Cy-5-containing peptide fragment allows the fluorophore to be internalized by nearby cells, precisely delimiting tumor margins. The system did not exhibit significant side effects and showed improved performance in defining tumor margins. If the AVB-620 sensor is able to pass through the whole validation process, it will potentially encourage the development of protease-based theranostic systems.

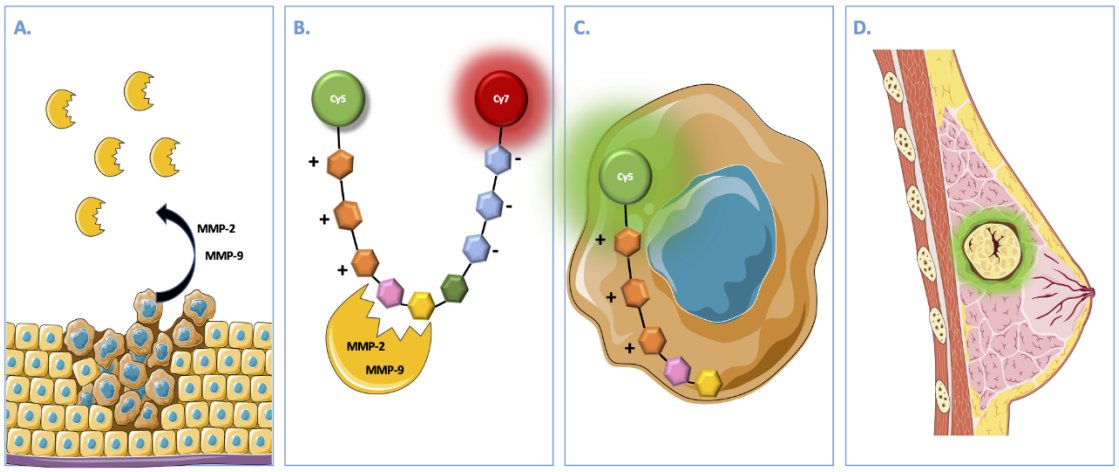

*M PA RT - Figure 4 - **Workflow for AVB-620 Detection System**. (A) Breast cancer cells producing matrix metalloprotease (MMP)-2/9. (B) The AVB-620 molecule is U-shaped due to electrostatic interactions, which increases the proximity between the Förster resonance energy transfer (FRET) pair (Cy-5 and Cy-7). (C) After cleavage, the pair dissociates and the positively charged side of the peptide is internalized by nearby cells. Consequently, Cy-5 emission increases preferentially in breast cancer cells. (D) Doctors are able to determine tumor margins with high precision.*

Proteolytic activity in real-time biosensors: where to?

Throughout this review, we highlighted the advantages of measuring proteolytic activity in real-time and the reasons why they can provide a wealth of information about biological

processes. Despite the fast pace of development of novel and improved detection systems, the field has plenty of space to grow. In our perspective, there are several opportunities and challenges that can and should be addressed in the future. For instance, to the best of our knowledge, multiplexing systems are so far based on optical methods only. New strategies for multiplexing can overcome the current limitations, increase diagnostic precision, and be helpful in correlating metabolic information between different enzymes. Within the same rational multiparametric systems, the work of Zhao et al.,[60] in which proteolytic activity and pH are simultaneously evaluated in real time, also seems promising (M PA RT - Figure 5A).

Another important issue is specificity. Despite most proteases tested as potential biomarkers being specific towards a target peptide sequence, often it is not possible to discriminate between two or more family-related proteases (i.e., MMP-2/9 and Cas-3/7). One possible strategy to achieve this goal was developed by Bainbridge et al.,[66] who exchanged L-amino acids for their D- counterparts in the peptide structure when designing a fibroblast activation protein (FAP)-specific substrate. Although the kinetic parameters of the target protease were slightly influenced in a negative way, a specific target peptide without dipeptidyl peptidase-4 (DPPIV) interference was obtained (M PA RT - Figure 5B).

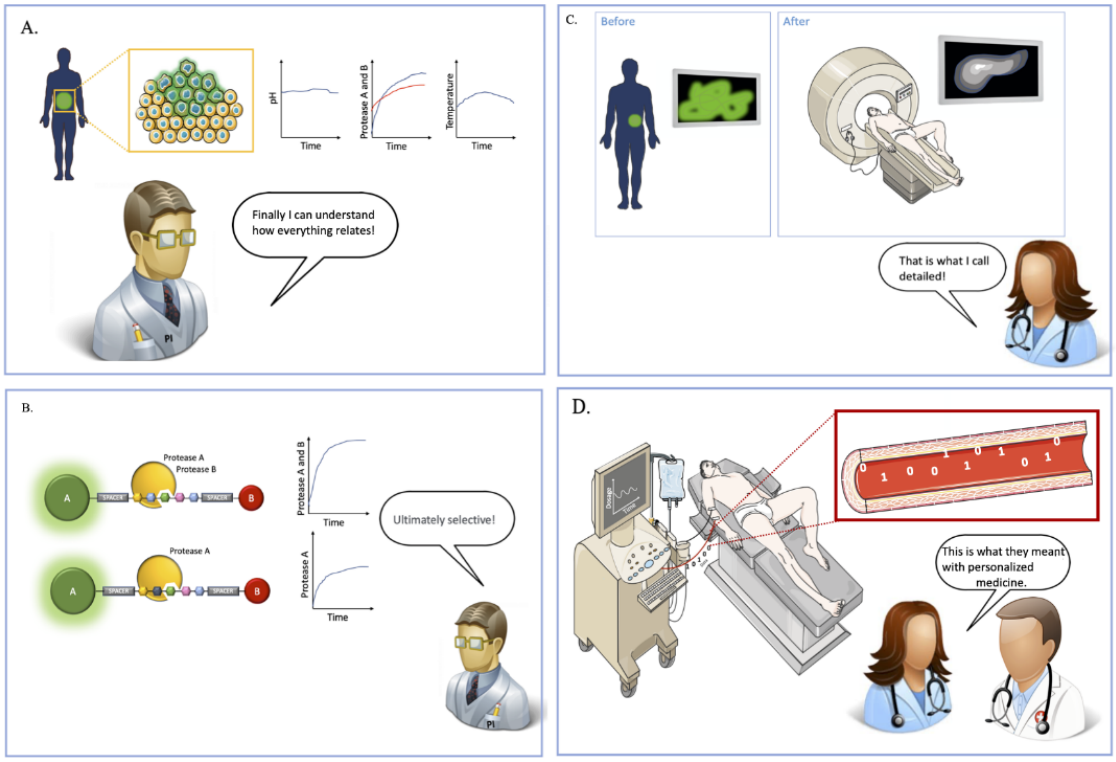

M PA RT - Figure 5 - ***Real-Time Biosensors in the Foreseeable Future****. (A) Multiplex proteolytic activity and multiparametric sensors in real time. (B) Specific target peptide sequence for single protease detection. (C) Imaging of 'in-depth' tissues with high resolution. (D) Programmable medicine representation comprising a real-time feedback system based on proteolytic-activity logic gates.*

The lack of in-depth imaging is one of the major pitfalls of optical sensors. Magnetic sensors, however, can reliably provide good 3D reconstruction and high in-depth abilities with almost no background signal (M PA RT - Figure 5C). Another interesting vision for proteolytic sensors in real time suggests their integration in logic gates.[41] Also, Kwong et al. [67,68] used nonreal-time proteolytic activity as biologic bits and integrated them in the field of

programmable medicine. By merging these concepts, one can imagine a machine analyzing the readout in real time and giving an immediate and proper response – for example, to stop/start the administration of a drug – in a feedback scheme and without the constant supervision of a healthcare professional. Also, this approach has the potential to decrease the amount of drug administered and to avoid drug spikes in the patient's body, since the drug can be delivered through microdosing (M PA RT - Figure 5D).

In summary, a wealth of research is being dedicated to the field of protease sensing with adversity of purposes, such as drug development, tumor imaging, and others. Although these types of biosensors are already under development, we strongly believe that there are plenty of unexplored concepts that can arise in the future. We cannot predict the pathways that are going to be pursued henceforth in real-time proteolytic-activity biosensors. Nevertheless, we hope that platforms for general use and the accessibility of these sensors will accelerate protease-based research and intensively propel the field. Undoubtedly, optimized systems to monitor and control biological processes will play a role in improving healthcare and moving towards a better version of personalized medicine.

References - M PA RT

(1) López-Otín, C.; Bond, J. S. Proteases: Multifunctional Enzymes in Life and Disease. *J Biol Chem* **2008**, *283* (45), 30433–30437. https://doi.org/10.1074/jbc.R800035200.

(2) Scher, W. The Role of Extracellular Proteases in Cell Proliferation and Differentiation BT - Pathology Reviews · 1989; Rubin, E., Damjanov, I., Eds.; Humana Press: Totowa, NJ, 1989; pp 187–213. https://doi.org/10.1007/978-1-4612-4502-5_11.

(3) Li, J.; Yuan, J. Caspases in Apoptosis and Beyond. *Oncogene* **2008**, *27* (48), 6194–6206. https://doi.org/10.1038/onc.2008.297.

(4) Narayanan, S. Multifunctional Roles of Thrombin. *Ann Clin Lab Sci* **1999**, *29* (4), 275–280.

(5) Heutinck, K. M.; ten Berge, I. J. M.; Hack, C. E.; Hamann, J.; Rowshani, A. T. Serine Proteases of the Human Immune System in Health and Disease. *Mol Immunol* **2010**, *47* (11), 1943–1955. https://doi.org/https://doi.org/10.1016/j.molimm.2010.04.020.

(6) Haley, S. A.; Wessel, G. M. Regulated Proteolysis by Cortical Granule Serine Protease 1 at Fertilization. *Mol Biol Cell* **2004**, *15* (5), 2084–2092. https://doi.org/10.1091/mbc.e03-11-0843.

(7) Koblinski, J. E.; Ahram, M.; Sloane, B. F. Unraveling the Role of Proteases in Cancer. *Clinica Chimica Acta* **2000**, *291* (2), 113–135. https://doi.org/https://doi.org/10.1016/S0009-8981(99)00224-7.

(8) Krenzlin, H.; Lorenz, V.; Danckwardt, S.; Kempski, O.; Alessandri, B. The Importance of Thrombin in Cerebral Injury and Disease. *Int J Mol Sci* **2016**, *17* (1), 84. https://doi.org/10.3390/ijms17010084.

(9) Cao, B.; Yu, Q.; Zhao, W.; Tang, Z.; Cong, B.; Du, J.; Lu, J.; Zhu, X.; Ni, X. Kallikrein-Related Peptidase 8 Is Expressed in Myocardium and Induces Cardiac Hypertrophy. *Sci Rep* **2016**, *6*, 20024.

(10) Danforth, C. M.; Orfeo, T.; Everse, S. J.; Mann, K. G.; Brummel-Ziedins, K. E. Defining the Boundaries of Normal Thrombin Generation: Investigations into Hemostasis. *PLoS One* **2012**, *7* (2), e30385–e30385. https://doi.org/10.1371/journal.pone.0030385.

(11) Cabarkapa, S.; Perera, M.; McGrath, S.; Lawrentschuk, N. Prostate Cancer Screening with Prostate-Specific Antigen: A Guide to the Guidelines. *Prostate Int* **2016**, *4* (4), 125–129. https://doi.org/10.1016/j.prnil.2016.09.002.

(12) Lv, Z.; Chu, Y.; Wang, Y. HIV Protease Inhibitors: A Review of Molecular Selectivity and Toxicity. *HIV AIDS (Auckl)* **2015**, *7*, 95–104. https://doi.org/10.2147/HIV.S79956.

(13) Mangum, E. M.; Graham, K. K. Lopinavir-Ritonavir: A New Protease Inhibitor. *Pharmacotherapy: The Journal of Human Pharmacology and Drug Therapy* **2001**, *21* (11), 1352–1363. https://doi.org/10.1592/phco.21.17.1352.34419.

(14) Liu, C.; Zhou, Q.; Li, Y.; Garner, L. v; Watkins, S. P.; Carter, L. J.; Smoot, J.; Gregg, A. C.; Daniels, A. D.; Jervey, S.; Albaiu, D. Research and Development on Therapeutic Agents and Vaccines for COVID-19 and Related Human Coronavirus Diseases. *ACS Cent Sci* **2020**, *6* (3), 315–331. https://doi.org/10.1021/acscentsci.0c00272.

(15) Baden, L. R.; Rubin, E. J. Covid-19 — The Search for Effective Therapy. *New England Journal of Medicine* **2020**. https://doi.org/10.1056/NEJMe2005477.

(16) Cao, B.; Wang, Y.; Wen, D.; Liu, W.; Wang, J.; Fan, G.; Ruan, L.; Song, B.; Cai, Y.; Wei, M.; Li, X.; Xia, J.; Chen, N.; Xiang, J.; Yu, T.; Bai, T.; Xie, X.; Zhang, L.; Li, C.; Yuan, Y.; Chen, H.; Li, H.; Huang, H.; Tu, S.; Gong, F.; Liu, Y.; Wei, Y.; Dong, C.; Zhou, F.; Gu, X.; Xu, J.; Liu, Z.; Zhang, Y.; Li, H.; Shang, L.; Wang, K.; Li, K.; Zhou, X.; Dong, X.; Qu, Z.; Lu, S.; Hu, X.; Ruan, S.; Luo, S.; Wu, J.; Peng, L.; Cheng, F.; Pan, L.; Zou, J.; Jia, C.; Wang, J.; Liu, X.; Wang, S.; Wu, X.; Ge, Q.; He, J.; Zhan, H.; Qiu, F.; Guo, L.; Huang, C.; Jaki, T.; Hayden, F. G.; Horby, P. W.; Zhang, D.; Wang, C. A Trial of Lopinavir–Ritonavir in Adults Hospitalized with Severe Covid-19. *New England Journal of Medicine* **2020**. https://doi.org/10.1056/NEJMoa2001282.

(17) Zhang, L.; Lin, D.; Sun, X.; Curth, U.; Drosten, C.; Sauerhering, L.; Becker, S.; Rox, K.; Hilgenfeld, R. Crystal Structure of SARS-CoV-2 Main Protease Provides a Basis for Design of Improved α-Ketoamide Inhibitors. *Science (1979)* **2020**, eabb3405. https://doi.org/10.1126/science.abb3405.

(18) Sheridan, C. Fast, Portable Tests Come Online to Curb Coronavirus Pandemic. *Nat Biotechnol* **2020**. https://doi.org/10.1038/d41587-020-00010-2.

(19) Nair, P. QnAs with Sangeeta N. Bhatia. *Proceedings of the National Academy of Sciences* **2020**, *117* (3), 1243 LP – 1245. https://doi.org/10.1073/pnas.1922176117.

(20) Burrage, P. S.; Mix, K. S.; Brinckerhoff, C. E. Matrix Metalloproteinases: Role in Arthritis. *Front Biosci* **2006**, *11* (1), 529–543.

(21) Salganik, M.; Venkatakrishnan, B.; Bennett, A.; Lins, B.; Yarbrough, J.; Muzyczka, N.; Agbandje-McKenna, M.; McKenna, R. Evidence for PH-Dependent Protease Activity in the Adeno-Associated Virus Capsid. *J Virol* **2012**, *86* (21), 11877 LP – 11885. https://doi.org/10.1128/JVI.01717-12.

(22) Mason, S. D.; Joyce, J. A. Proteolytic Networks in Cancer. *Trends Cell Biol* **2011**, *21* (4), 228–237. https://doi.org/https://doi.org/10.1016/j.tcb.2010.12.002.

(23) Brew, K.; Nagase, H. The Tissue Inhibitors of Metalloproteinases (TIMPs): An Ancient Family with Structural and Functional Diversity. *Biochim Biophys Acta* **2010**, *1803* (1), 55–71. https://doi.org/10.1016/j.bbamcr.2010.01.003.

(24) McIlwain, D. R.; Berger, T.; Mak, T. W. Caspase Functions in Cell Death and Disease. *Cold Spring Harb Perspect Biol* **2013**, *5* (4), 1–28. https://doi.org/10.1101/cshperspect.a008656.

(25) Almalki, S. G.; Agrawal, D. K. Effects of Matrix Metalloproteinases on the Fate of Mesenchymal Stem Cells. *Stem Cell Res Ther* **2016**, *7* (1), 129. https://doi.org/10.1186/s13287-016-0393-1.

(26) Hanne, J.; Göttfert, F.; Schimer, J.; Anders-Össwein, M.; Konvalinka, J.; Engelhardt, J.; Müller, B.; Hell, S. W.; Kräusslich, H.-G. Stimulated Emission Depletion Nanoscopy Reveals Time-Course of Human Immunodeficiency Virus Proteolytic Maturation. *ACS Nano* **2016**, *10* (9), 8215–8222. https://doi.org/10.1021/acsnano.6b03850.

(27) Lorenzano, S.; Inglese, M.; Koudriavtseva, T. Editorial: Role of Coagulation Pathways in Neurological Diseases . *Frontiers in Neurology* . 2019, p 791.

(28) Ebrahimi, S.; Jaberi, N.; Avan, A.; Ryzhikov, M.; Keramati, M. R.; Parizadeh, M. R.; Hassanian, S. M. Role of Thrombin in the Pathogenesis of Central Nervous System Inflammatory Diseases. *J Cell Physiol* **2017**, *232* (3), 482–485. https://doi.org/10.1002/jcp.25501.

(29) Ta, H. T.; Arndt, N.; Wu, Y.; Lim, H. J.; Landeen, S.; Zhang, R.; Kamato, D.; Little, P. J.; Whittaker, A. K.; Xu, Z. P. Activatable Magnetic Resonance Nanosensor as a Potential Imaging Agent for Detecting and Discriminating Thrombosis. *Nanoscale* **2018**, *10* (31), 15103–15115. https://doi.org/10.1039/C8NR05095C.

(30) Leber, T. M.; Balkwill, F. R. Zymography: A Single-Step Staining Method for Quantitation of Proteolytic Activity on Substrate Gels. *Anal Biochem* **1997**, *249* (1), 24–28. https://doi.org/https://doi.org/10.1006/abio.1997.2170.

(31) Caldas, C.; Cherqui, A.; Pereira, A.; Simões, N. Purification and Characterization of an Extracellular Protease from <Em>Xenorhabdus Nematophila</Em> Involved in Insect Immunosuppression. *Appl Environ Microbiol* **2002**, *68* (3), 1297 LP – 1304. https://doi.org/10.1128/AEM.68.3.1297-1304.2002.

(32) Son, J.; Kalafatovic, D.; Kumar, M.; Yoo, B.; Cornejo, M. A.; Contel, M.; Ulijn, R. v. Customizing Morphology, Size, and Response Kinetics of Matrix Metalloproteinase-Responsive Nanostructures by Systematic Peptide Design. *ACS Nano* **2019**, *13* (2), 1555–1562. https://doi.org/10.1021/acsnano.8b07401.

(33) Mathew-Fenn, R. S.; Das, R.; Silverman, J. A.; Walker, P. A.; Harbury, P. A. B. A Molecular Ruler for Measuring Quantitative Distance Distributions. *PLoS One* **2008**, *3* (10), e3229.

(34) Lavis, L. D.; Raines, R. T. Bright Ideas for Chemical Biology. *ACS Chem Biol* **2008**, *3* (3), 142–155. https://doi.org/10.1021/cb700248m.

(35) Resch-Genger, U.; Grabolle, M.; Cavaliere-Jaricot, S.; Nitschke, R.; Nann, T. Quantum Dots versus Organic Dyes as Fluorescent Labels. *Nat Methods* **2008**, *5* (9), 763–775. https://doi.org/10.1038/nmeth.1248.

(36) Chung, E. Y.; Ochs, C. J.; Wang, Y.; Lei, L.; Qin, Q.; Smith, A. M.; Strongin, A. Y.; Kamm, R.; Qi, Y.-X.; Lu, S.; Wang, Y. Activatable and Cell-Penetrable Multiplex FRET Nanosensor for Profiling MT1-MMP Activity in Single Cancer Cells. *Nano Lett* **2015**, *15* (8), 5025–5032. https://doi.org/10.1021/acs.nanolett.5b01047.

(37) Braun, A.; Farber, M. J.; Klase, Z. A.; Berget, P. B.; Myers, K. A. A Cell Surface Display Fluorescent Biosensor for Measuring MMP14 Activity in Real-Time. *Sci Rep* **2018**, *8* (1). https://doi.org/10.1038/s41598-018-24080-0.

(38) Luan, M.; Shi, M.; Pan, W.; Li, N.; Tang, B. A Gold–Selenium-Bonded Nanoprobe for Real-Time in Situ Imaging of the Upstream and Downstream Relationship between UPA and MMP-9 in Cancer Cells. *Chemical Communications* **2019**, *55* (41), 5817–5820. https://doi.org/10.1039/C9CC01454C.

(39) Hu, B.; Kong, F.; Gao, X.; Jiang, L.; Li, X.; Gao, W.; Xu, K.; Tang, B. Avoiding Thiol Compound Interference: A Nanoplatform Based on High-Fidelity Au–Se Bonds for Biological Applications. *Angewandte Chemie International Edition* **2018**, *57* (19), 5306–5309. https://doi.org/10.1002/anie.201712921.

(40) Liu, X.; Song, X.; Luan, D.; Hu, B.; Xu, K.; Tang, B. Real-Time in Situ Visualizing of the Sequential Activation of Caspase Cascade Using a Multicolor Gold–Selenium Bonding Fluorescent Nanoprobe. *Anal Chem* **2019**, *91* (9), 5994–6002. https://doi.org/10.1021/acs.analchem.9b00452.

(41) Bui, H.; Brown III, C. W.; Buckhout-White, S.; Díaz, S. A.; Stewart, M. H.; Susumu, K.; Oh, E.; Ancona, M. G.; Goldman, E. R.; Medintz, I. L. Transducing Protease Activity into DNA Output for Developing Smart Bionanosensors. *Small* **2019**, *15* (14), 1805384. https://doi.org/10.1002/smll.201805384.

(42) Jeong, S.; Song, J.; Lee, W.; Ryu, Y. M.; Jung, Y.; Kim, S.-Y.; Kim, K.; Hong, S. C.; Myung, S. J.; Kim, S. Cancer-Microenvironment-Sensitive Activatable Quantum Dot Probe in the Second Near-Infrared Window. *Nano Lett* **2017**, *17* (3), 1378–1386. https://doi.org/10.1021/acs.nanolett.6b04261.

(43) den Hamer, A.; Dierickx, P.; Arts, R.; de Vries, J. S. P. M.; Brunsveld, L.; Merkx, M. Bright Bioluminescent BRET Sensor Proteins for Measuring Intracellular Caspase Activity. *ACS Sens* **2017**, *2* (6), 729–734. https://doi.org/10.1021/acssensors.7b00239.

(44) Li, Y.; Li, P.; Zhu, R.; Luo, C.; Li, H.; Hu, S.; Nie, Z.; Huang, Y.; Yao, S. Multifunctional Gold Nanoclusters-Based Nanosurface Energy Transfer Probe for Real-Time Monitoring of Cell Apoptosis and Self-Evaluating of Pro-Apoptotic Theranostics. *Anal Chem* **2016**, *88* (22), 11184–11192. https://doi.org/10.1021/acs.analchem.6b03389.

(45) Wuytens, P. C.; Demol, H.; Turk, N.; Gevaert, K.; Skirtach, A. G.; Lamkanfi, M.; Baets, R. Gold Nanodome SERS Platform for Label-Free Detection of Protease Activity. *Faraday Discuss* **2017**, *205* (0), 345–361. https://doi.org/10.1039/C7FD00124J.

(46) Sun, C.; Su, K.-H.; Valentine, J.; Rosa-Bauza, Y. T.; Ellman, J. A.; Elboudwarej, O.; Mukherjee, B.; Craik, C. S.; Shuman, M. A.; Chen, F. F.; Zhang, X. Time-Resolved Single-Step Protease Activity Quantification Using Nanoplasmonic Resonator Sensors. *ACS Nano* **2010**, *4* (2), 978–984. https://doi.org/10.1021/nn900757p.

(47) Liu, C.; Li, S.; Gu, Y.; Xiong, H.; Wong, W.; Sun, L. Multispectral Photoacoustic Imaging of Tumor Protease Activity with a Gold Nanocage-Based Activatable Probe. *Mol Imaging Biol* **2018**, *20* (6), 919–929. https://doi.org/10.1007/s11307-018-1203-1.

(48) Yin, L.; Sun, H.; Zhang, H.; He, L.; Qiu, L.; Lin, J.; Xia, H.; Zhang, Y.; Ji, S.; Shi, H.; Gao, M. Quantitatively Visualizing Tumor-Related Protease Activity in Vivo Using a Ratiometric Photoacoustic Probe. *J Am Chem Soc* **2019**, *141* (7), 3265–3273. https://doi.org/10.1021/jacs.8b13628.

(49) Jun, Y.; Sheikholeslami, S.; Hostetter, D. R.; Tajon, C.; Craik, C. S.; Alivisatos, A. P. Continuous Imaging of Plasmon Rulers in Live Cells Reveals Early-Stage Caspase-3 Activation at the Single-Molecule Level. *Proceedings of the National Academy of Sciences* **2009**, *106* (42), 17735 LP – 17740. https://doi.org/10.1073/pnas.0907367106.

(50) Schyrr, B.; Boder-Pasche, S.; Ischer, R.; Smajda, R.; Voirin, G. Fiber-Optic Protease Sensor Based on the Degradation of Thin Gelatin Films. *Sens Biosensing Res* **2015**, *3*, 65–73. https://doi.org/https://doi.org/10.1016/j.sbsr.2014.12.004.

(51) Page, M. J.; Lourenço, A. L.; David, T.; LeBeau, A. M.; Cattaruzza, F.; Castro, H. C.; VanBrocklin, H. F.; Coughlin, S. R.; Craik, C. S. Non-Invasive Imaging and Cellular Tracking of Pulmonary Emboli by near-Infrared Fluorescence and Positron-Emission Tomography. *Nat Commun* **2015**, *6*, 8448.

(52) Lee, S.; Kang, S.-W.; Ryu, J. H.; Na, J. H.; Lee, D.-E.; Han, S. J.; Kang, C. M.; Choe, Y. S.; Lee, K. C.; Leary, J. F.; Choi, K.; Lee, K.-H.; Kim, K. Tumor-Homing Glycol Chitosan-Based Optical/PET Dual Imaging Nanoprobe for Cancer Diagnosis. *Bioconjug Chem* **2014**, *25* (3), 601–610. https://doi.org/10.1021/bc500020g.

(53) Matthias, N.; Peter, W.; Greg, T.; Kevin, G.; Milind, R.; Peter, P.; Brett, M.; Elena, A.; J., P. M.; K., S. F.; Ralph, W. Hybrid In Vivo FMT-CT Imaging of Protease Activity in Atherosclerosis With Customized Nanosensors. *Arterioscler Thromb Vasc Biol* **2009**, *29* (10), 1444–1451. https://doi.org/10.1161/ATVBAHA.109.193086.

(54) Yin, L.; Sun, H.; Zhao, M.; Wang, A.; Qiu, S.; Gao, Y.; Ding, J.; Ji, S.-J.; Shi, H.; Gao, M. Rational Design and Synthesis of a Metalloproteinase-Activatable Probe for Dual-Modality Imaging of

Metastatic Lymph Nodes in Vivo. *J Org Chem* **2019**, *84* (10), 6126–6133. https://doi.org/10.1021/acs.joc.9b00331.

(55) Elvas, F.; vanden Berghe, T.; Adriaenssens, Y.; Vandenabeele, P.; Augustyns, K.; Staelens, S.; Stroobants, S.; van der Veken, P.; wyffels, L. Caspase-3 Probes for PET Imaging of Apoptotic Tumor Response to Anticancer Therapy. *Org Biomol Chem* **2019**, *17* (19), 4801–4824. https://doi.org/10.1039/C9OB00657E.

(56) Shi, H.; Sun, Y.; Yan, R.; Liu, S.; Zhu, L.; Liu, S.; Feng, Y.; Wang, P.; He, J.; Zhou, Z.; Ye, D. Magnetic Semiconductor Gd-Doping CuS Nanoparticles as Activatable Nanoprobes for Bimodal Imaging and Targeted Photothermal Therapy of Gastric Tumors. *Nano Lett* **2019**, *19* (2), 937–947. https://doi.org/10.1021/acs.nanolett.8b04179.

(57) Tran, T. B.; Nguyen, P. D.; Baek, C.; Min, J. Electrical Dual-Sensing Method for Real-Time Quantitative Monitoring of Cell-Secreted MMP-9 and Cellular Morphology during Migration Process. *Biosens Bioelectron* **2016**, *77*, 631–637. https://doi.org/https://doi.org/10.1016/j.bios.2015.10.030.

(58) Wang, L.; Han, Y.; Zhou, S.; Guan, X. Real-Time Label-Free Measurement of HIV-1 Protease Activity by Nanopore Analysis. *Biosens Bioelectron* **2014**, *62*, 158–162. https://doi.org/https://doi.org/10.1016/j.bios.2014.06.041.

(59) Yuan, Y.; Ding, Z.; Qian, J.; Zhang, J.; Xu, J.; Dong, X.; Han, T.; Ge, S.; Luo, Y.; Wang, Y.; Zhong, K.; Liang, G. Casp3/7-Instructed Intracellular Aggregation of Fe3O4 Nanoparticles Enhances T2 MR Imaging of Tumor Apoptosis. *Nano Lett* **2016**, *16* (4), 2686–2691. https://doi.org/10.1021/acs.nanolett.6b00331.

(60) Zhao, X.; Yang, C.-X.; Chen, L.-G.; Yan, X.-P. Dual-Stimuli Responsive and Reversibly Activatable Theranostic Nanoprobe for Precision Tumor-Targeting and Fluorescence-Guided Photothermal Therapy. *Nat Commun* **2017**, *8* (1), 14998. https://doi.org/10.1038/ncomms14998.

(61) Innocenti, M. New Insights into the Formation and the Function of Lamellipodia and Ruffles in Mesenchymal Cell Migration. *Cell Adh Migr* **2018**, *12* (5), 401–416. https://doi.org/10.1080/19336918.2018.1448352.

(62) Avelas Biosciences, Inc.; RRD International, Inc.; Clinipace Worldwide. *Study of AVB-620 in Women With Primary, Nonrecurrent Breast Cancer Undergoing Surgery*. https://clinicaltrials.gov/ct2/show/NCT03113825.

(63) David Kirsch; American Society of Clinical Oncology; Lumicell. *Cathepsin Activatable Fluorescent Probe (LUM015)*. https://clinicaltrials.gov/ct2/show/NCT01626066.

(64) Smith, B. L.; Lanahan, C. R.; Specht, M. C.; Kelly, B. N.; Brown, C.; Strasfeld, D. B.; Ferrer, J. M.; Rai, U.; Tang, R.; Rice-Stitt, T.; Biernacka, A.; Brachtel, E. F.; Gadd, M. A. Feasibility Study of a Novel Protease-Activated Fluorescent Imaging System for Real-Time, Intraoperative Detection of Residual Breast Cancer in Breast Conserving Surgery. *Ann Surg Oncol* **2020**, *27* (6), 1854–1861. https://doi.org/10.1245/s10434-019-08158-1.

(65) Unkart, J. T.; Chen, S. L.; Wapnir, I. L.; González, J. E.; Harootunian, A.; Wallace, A. M. Intraoperative Tumor Detection Using a Ratiometric Activatable Fluorescent Peptide: A First-in-Human Phase 1 Study. *Ann Surg Oncol* **2017**, *24* (11), 3167–3173. https://doi.org/10.1245/s10434-017-5991-3.

(66) Bainbridge, T. W.; Dunshee, D. R.; Kljavin, N. M.; Skelton, N. J.; Sonoda, J.; Ernst, J. A. Selective Homogeneous Assay for Circulating Endopeptidase Fibroblast Activation Protein (FAP). *Sci Rep* **2017**, *7* (1), 12524. https://doi.org/10.1038/s41598-017-12900-8.

(67) Holt, B. A.; Kwong, G. A. Protease Circuits for Processing Biological Information. *Nat Commun* **2020**, *11* (1), 5021. https://doi.org/10.1038/s41467-020-18840-8.

(68) Mac, Q. D.; Mathews, D. v; Kahla, J. A.; Stoffers, C. M.; Delmas, O. M.; Holt, B. A.; Adams, A. B.; Kwong, G. A. Non-Invasive Early Detection of Acute Transplant Rejection via Nanosensors of Granzyme B Activity. *Nat Biomed Eng* **2019**, *3* (4), 281–291. https://doi.org/10.1038/s41551-019-0358-7.

Glossary

Biosensors: analytical devices used for detection and/or measurement of a specific analyte, biometric parameters and body conditions.

Caspases: a family of intracellular cysteine-aspartic proteases that are pivotal in programmed cell death such as apoptosis, pyroptosis and necrosis.

Compound annual growth rate (CAGR): rate of return required for an investment to grow from its beginning balance to its ending balance, assuming the profits were reinvested at the end of each year of the investment's lifespan.

Energy transfer-based (ET): are systems in which energy transfer can occur from an electronically excited-state of a donor to an acceptor entity. In biosensors the efficiency of this process can be influenced by a target analyte thus signalling its presence by means of a spectroscopic observable (emission spectrum, intensity or lifetime of donor/acceptor).

Logic-gate: a device that performs logical operations to convert the signal from the sensor onto a binary output ("0" or "1"). Logic gates based on proteolytic activity operate by differentiating "low-activity" from "high-activity" states and further address them as "0" and "1", respectively.

Matrix Metalloproteases (MMPs): metal-dependent endopeptidases found in the extracellular matrix, which are responsible for degrading several proteins and bioactive products.

Multiplex modality systems: combine two or more complementary techniques enabling imaging of metabolic processes, such as proteolytic activity, with increased resolution when compared with their individual counterparts.

Personalized Medicine is a new paradigm in Medicine that views patients not as members of a group of individuals but rather as unique individuals with intrinsic characteristics that must be diagnosed, evaluated and used to inform therapeutic decisions.

Photothermal therapy (PTT): uses electromagnetic radiation – commonly infrared wavelengths – which is absorbed by a molecule/particle (photosensitizer). This activation brings the sensitizer to an excited state further releasing heat. The resulting heat increases the Temperature locally killing the targeted cells.

Plasmonic nanoparticles: display strong interactions with light– scattering, absorption and coupling - being critically dependent on the particle's material, size, geometry and interparticle distances.

Positron Emission Tomography (PET): is a nuclear medical imaging technique based on the detection of radioactivity emitted by a delivered radioactive tracer to an individual in order to monitor physiological functions.

Programmable medicine: current medical practice and based on the analysis of the symptomatology and the medical examination results. Programmable medicine does not consider the phenotypic and genotypic characterization, sociodemographic, environmental, and lifestyle of an individual and does not include disease preventive strategies. M PA RT - Table 1. Highlights of proteolytic activity in real-time Biosensors and their features. Some of these examples are detailed in the main text and are marked in the reference column with a *.

Real-time assays: (in the authors definition) assays that have an immediate response that is proportional to proteolytic activity and can be rapidly read by a sensor, but not necessarily as a continuous measurement.

Signal-to-noise ratio (SNR): defined as the ratio between the intensity of a specific-signal generated during the measurement and the intensity or standard deviation of a signal generated from unspecific sources (noise). A high SNR corresponds to a bigger difference between the signal generated from an occurring event and the background noise, increasing the confidence/sensitivity.

Suicidal Experiments: experiments which can only be used once to determine a specific parameter at a given time. Therefore, an experiment needs to be done for each desired time point.

Patent - Probe element and methods for separation and sensing of analytes controlled by temperature.[clxxx]

Technical field

This application relates to a probe element for separation and sensing of analytes, a device comprising at least one probe element, a process of analyte determination and a process for selective separation of analytes.

Background art

Magnetic particles, nanoparticles and beads are currently used as probes for magnetic detection of a wide range of analytes, as described, for instance in patents US7906345, WO/2005/010542, US20090104707, US7696548, US6844202, US9121887, references therein[1–6] and in the literature.[7–10] Almost all references consider the use of paramagnetic, superparamagnetic or any other kind of magnetic particles, nanoparticles and beads that appear "non-magnetic" in the absence of a magnetic field.[1, 3-6] The reason is that particles that appear "magnetic" in the absence of an external magnetic field (in other words particles with a remanent magnetization, i. e. particles able to create a magnetic field in the absence of an external magnetic field) tend to agglomerate, which makes their use in assays difficult and less reliable.[1, 3-6] The exceptions that consider possible the use of particles that appear "magnetic" in the absence of an external magnetic field just ignore the problem of agglomeration and do not present a solution for it. [2]

The use of particles that appear "non-magnetic" does not mean that agglomeration will not occur. In fact, "non- magnetic" particles, nanoparticles and beads stable in normal conditions have sometimes tendency to aggregate when in the presence of an external field. The presence of such field is mandatory during detection, since in its absence the particles appear "non-magnetic". The state of art mitigates this problem of in-field aggregation by using smaller external fields during the assay and by improving surface modification.[3] This mitigation comes at the expense of signal to noise ratio since at smaller fields the magnetization induced in the particles is (proportionally) smaller and better stabilization implies bulky ligands and larger distances between particles and sensors.

The use of an external field during reading is, by itself, a source of errors. As this field sums to the field created by the particles, extra design is needed. This extra design typically includes the use of an alternating (perpendicular) magnetic field [1-3] or the use of multiple readers. [11]

Therefore, the state of the art present the following problems and constrains:

Aggregation of nanoparticles possessing a permanent magnetic field:

Magnetic nanoparticles able to create a permanent magnetic field (nanoparticles with a remanent magnetization) are systematically excluded from sensing and separation devices due

[clxxx] WO2018215970; PT110107; EP3631455; US20200232946

to their tendency to aggregate. Aggregation impacts negatively their rheology, their interaction with analytes and their signal, since the magnetic field can be enclosed in loops of particles making the detectable signal low. In this sense, superparamagnetic nanoparticles and beads (i.e. nanoparticles creating a zero magnetic field in the absence of an external field) are considered the best choice for sensing and separation and have been developed to that aim.

Lack of a permanent magnetic field (permanent remanent magnetization or moment) in superparamagnetic beads:

Although applied in sensing, superparamagnetic nanoparticles and beads need the presence of an external field to be detected. This external field, however, interacts with the reader, decreasing the sensitivity of the device. Perpendicular geometries and multiple readers are used to mitigate this problem.[11] However, cross-talking between different directions in the magnetic field readers always take place, leading to inaccuracy and errors. Also, by using perpendicular geometries, the whole field created by the nanoparticle is not detected but just a smaller weaker component, a fringe field,[7] meaning that the full potential of the magnetic signal is not explored.

One analyte magnetic separation per step:

Separation using magnetic nanoparticles and beads explores the force exerted by a magnetic field gradient on the nanoparticles/beads. This force depends mainly on viscosity, magnetic susceptibility, and volume. Separation is often used as a way to concentrate an analyte of interest before its detection. Concentrate should be understood as the selective capture of the analyte of interest or selective elimination of non-wanted materials or media, resulting in a product where the analyte of interest has an enhanced concentration. In practice, a batch of homogeneous nanoparticles/beads is used and a complete separation process includes an incubation step, where chemically selective attachment between nanoparticles/beads and an analyte of interest occurs, followed by the application of a magnetic field gradient to separate and concentrate said analyte. Such concentration step assumes a special relevance in ultra-sensitive microfluidic-based devices, as most of point-of-care devices being developed, due to the low diffusion of molecules. Consequently, one must choose to use high volume of sample or wait a longer period of time in order to achieve the equilibrium specially in high diluted analytes (below nanomolar range) Both the amount of sample and time are crucial elements in point-of-care devices, being the absence of a concentration step (such as that provided by magnetic separation) a major drawback in these devices.

However, current magnetic separation methods and devices are useful to separate one analyte per incubation step and multiple incubation/separation steps are needed in the case where several analytes are being detected in the same device.

In this view, it would be desirable to have probe elements that (i) do not need an external field bias or tickling field to be detected, (ii) do not aggregate, and (iii) multiple analytes could be separated and concentrated after one incubation step. Suda et al., JACS 129(17), 5538-5543 (2007), Solano et al., J. Nanoparticle Res. 14(8), 1-15 (2012), Sharma et al., J. Colloid Interface Sc. 351(2), 323-329 (2010) and Zhang et al., Nanotechnology 16(10), 2288-2294 (2005) disclose nanoparticles comprising magnetic crystals which provide controllable remanent magnetic fields.

Summary

The present application relates to a probe element for separation and sensing of analytes, comprising at least one magnetic crystal composed of one of more nanoparticles with a composition including at least one transition metal or ion and with size ranging from 5 to 500 nm and at least one type of capping agent that is either gallic acid, caffeic acid, levodopamine, wherein the magnetic crystal is Fe_3Se_4, wherein the magnetic crystal produces a magnetic field in the absence of an external field at a temperature of use between -80 and 100°C and the intensity of the magnetic field produced by the magnetic crystal changes by a temperature change.

The present application also relates to a device comprising at least one probe element, at least one analyte of interest, at least one temperature controller, at least one magnetic field reader, and at least one minute magnetic field source, wherein said source does not interact with the said reader; and wherein the temperature controller comprises a heating element, a temperature sensor, and a feedback and/or feedforward controller.

The present application also relates to a process of analyte determination, comprising an inlet stage, a stage of manipulation of the magnetic field of the crystal of the probe element, a reading stage and an outlet stage wherein the manipulation stage is assisted by the temperature controller and the minute magnetic field source; wherein the reading stage comprises the determination of the remanent magnetic field created by the magnetic crystal of the probe element by a magnetic field reader.

The present application also relates to a process for selective separation of analytes comprising:

- the capture of analytes using probe elements;
- the application of a magnetic field gradient using the magnetic field source at a well-defined temperature;

wherein the probe elements have temperature dependent remanent magnetization and magnetic susceptibility that controls the separation velocity.

Disclosure

The present application discloses a probe element that can be used for separation and sensing of analytes of interest in the absence of an external field, without aggregation of the probe element. This is the probe elements and the analyte can be anchored together and the probe elements can carry a permanent field that can be sensed by a magnetic field reader. The intensity of the permanent field of the probe element is controlled by temperature and therefore, aggregation and sensitivity are also controlled by temperature.

The probe elements provided herein include at least one magnetic crystal and at least one type of capping agent.

Brief description of drawings

For an easier understanding of this application, figures are attached in the annex that represent the preferred forms of implementation which nevertheless are not intended to limit the technique disclosed herein.

Figure 1A depicts one embodiment of a probe element, composed of a magnetic crystal (101) and capping agents (120).

Figure 1B depicts one embodiment of a probe element, composed of a magnetic crystal (101), capping agents behaving as stabilizers (121), capping agents behaving as anchors (122) and an analyte of interest (150).

Figure 1C depicts one embodiment of a probe element, where the magnetic crystal (101) provides a permanent magnetic field in the up (131) or down (141) direction, whose intensity is changeable with temperature.

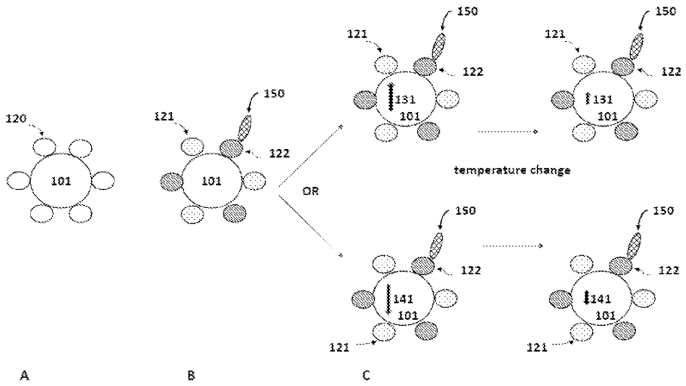

Patent - Figure 1A-C – ***Probe embodiment***

Figure 1D depicts the permanent (remanent) magnetization created by the magnetic crystal FeSe in the up (131) and down (141) direction as a function of temperature.

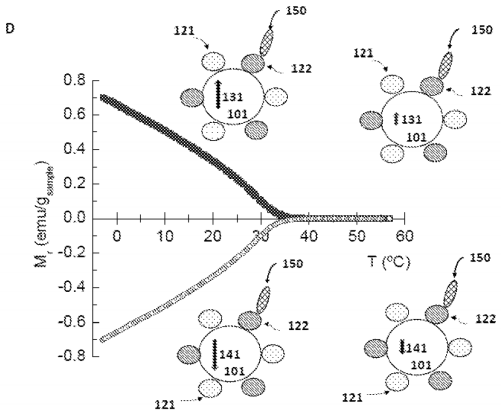

Patent - Figure 1D – ***Magnetic Properties of FeSe vs Temperature***

Figure 1E depicts the permanent (remanent) magnetization of two different magnetic crystals designed to work in two complementary temperature regions (one from -200 °C to 40 °C) and the other from -75 °C to 90°C).

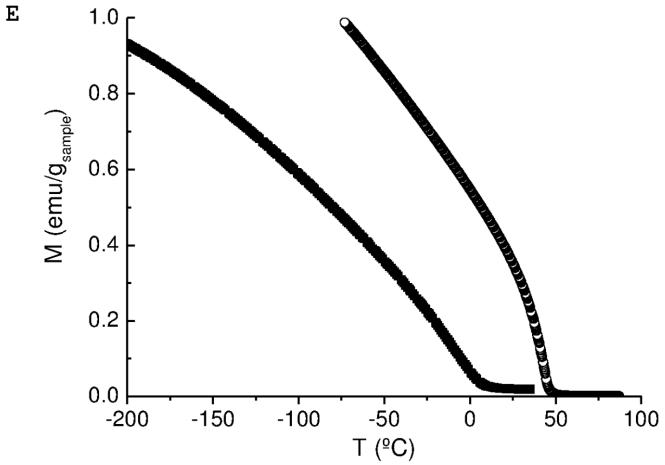

Patent - Figure 1E – ***Magnetic Properties vs Temperature of 2 distinct magnetic crystals with different magnetic transitions***

Figures 1F and 1G depict electron microscope images of magnetic crystals of Fe3Se4 with sizes ranging from 5 nm to 500 nm.

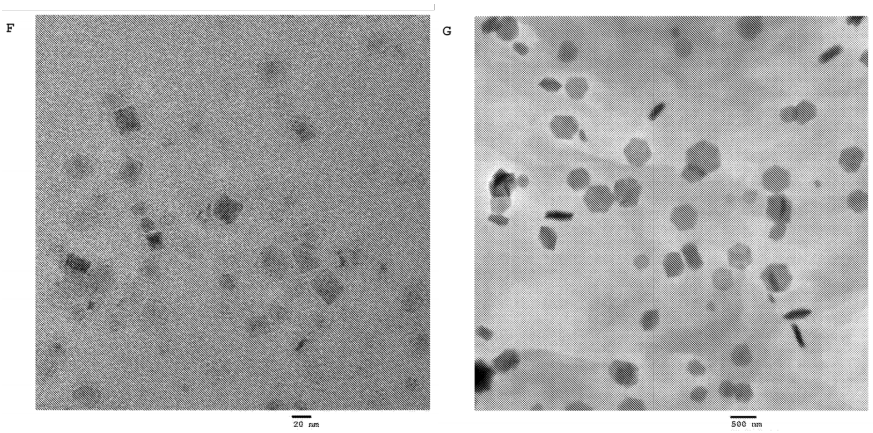

Patent - Figure 1F and G – ***Electron Microscopy of Fe_3Se_4 with different sizes (5 and 500nm)***

Figure 2 depicts one embodiment of a device, where temperature control is provided by a Proportional-integral (PI) or a Proportional-integral-derivative (PID) controller (210), a temperature sensor (211), a peltier (or heater) unit (212), a magnetic field source composed of permanent magnets (220), a (fluxgate) magnetic field sensor (230), an inlet (241) and an outlet (242).

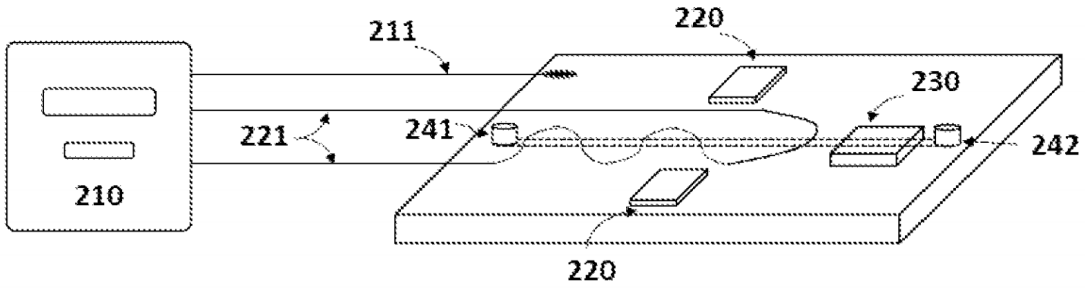

Patent - Figure 2 – ***Embodiment of a device***

Figure 3 depicts one embodiment of a part of the device, where separation and/or concentration occurs at different outlet systems (342), after entering at inlet (341), being exposed to a magnetic field source (320) and to a controlled temperature environment.

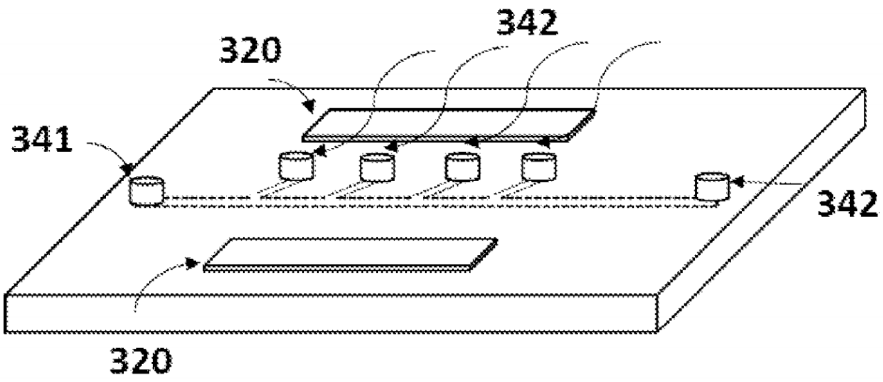

Patent - Figure 3 – ***Alternative embodiment of a device***

Figure 4A depicts one embodiment of a part of the device, in a first stage of operation where separation and/or concentration and/or detection is mediated by a positioning/temperature control system (460) with a tip (461) where the probe element (401) is permanently attached to the tip or enters the inlet system (441) and attaches to the tip by magnetic forces, due to the remanent moment (471). The magnetic field source (430) is used to control the direction of magnetization of the probe element (401) and/or tip (461).

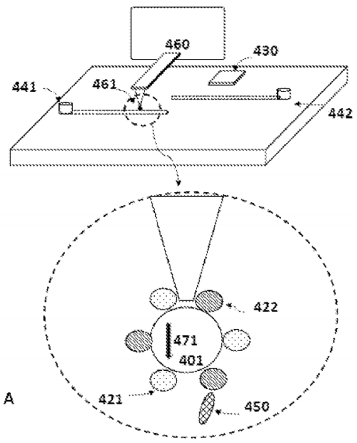

Patent - Figure 4A – ***Embodiment of a tip-based device***

Figure 4B depicts the same second stage of operation and/or analyte of interest embodiment of **Figure 4A** in a where the probe element (401) (450) is detached from the tip (461) by a change in temperature and consequent reduction of remanent magnetization (471). Element (421) depicts capping agents and element (122) depicts capping agents behaving as anchors.

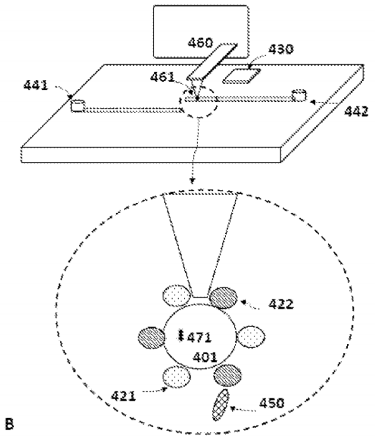

Patent - Figure 4B – ***Alternative embodiment of a tip-based device***

Description of embodiments

Now, preferred embodiments of the present application will be described in detail with reference to the annexed drawings. However, they are not intended to limit the scope of this application.

The magnetic crystal (101) is designed as such that the permanent magnetic field that it is able to create is controlled by temperature, within a temperature range compatible with the integrity of the analyte of interest. Within this temperature range, two distinct situations can be achieved: one, at a given temperature, the permanent field of the magnetic crystal is small enough to avoid aggregation and to avoid separation by a magnetic field gradient and two, at another given temperature, the permanent field of the magnetic crystal is high enough to be detected and separated by a magnetic field gradient.

The analytes of interest are molecules that maintain their integrity and reversibility of all their relevant properties within a temperature range between 4 and 100 °C. In other embodiments this temperature range is 4 to 60 °C.

In an embodiment, the magnetic crystal is composed of at least one nanoparticles with a composition and structure chosen such that its remanent magnetization decreases sufficiently within the temperature range between 5 and 60 °C. The composition includes at least one transition metal atom or ion. The composition includes at least one lanthanide atom or ion. The composition includes at least one of the previous ions and one ion of group 16 or 17 of the periodic table. In an embodiment, the composition includes iron and selenium.

In an embodiment, the magnetic crystal is such that at a temperature of use between -80 and 100 °C it produces a permanent magnetic field (it has a remanent magnetization) that can be sensed when the magnetic crystal is at a temperature higher than 100 °C but still at a temperature such that the analyte of interest maintains its integrity, this permanent field is substantially reduced. As an embodiment, the magnetic crystal is composed of iron selenide (Fe3Se4) with a remanent magnetization of 0.3 emu/g at 25 °C being reduced to 0 emu/g at 50 °C, as shown in Fig lD. The substantial reduction of the permanent magnetic field of the magnetic crystal above the temperature of interest allows an easy manipulation of the direction of this crystal's magnetic field by a minute external field with an amplitude from 0.1 to 1000 Oe.

The temperature of use is defined between -80 and 100 °C, preferably between 4 and 100 °C, more preferably between 4 and 60 °C, as shown in figure Fig. lE.

In an embodiment, the magnetic crystal is composed of one or more nanoparticles with a well-defined shape and with size ranging from 5 to 500 nm. In a particular embodiment, the magnetic crystal is composed of Fe_3Se_4 nanoparticles with size between 50 and 400 nm. In another embodiment, the magnetic crystal is composed of Fe3Se4 nanoparticles with size between 100 and 200 nm.

In an embodiment, the probe element has a second magnetic crystal that does not produce a magnetic field in the absence of an external field at a temperature of use.

In another embodiment, this second magnetic crystal is used to produce an extra response in the presence of an external magnetic field, constant in the temperature range of interest. In another embodiment, this second magnetic crystal is used to generate heat by the application of an external alternating magnetic field. In an embodiment, the second magnetic crystal is magnetite. In another embodiment, the second magnetic crystal is a ferrite.

The capping agent (120) is designed to interface the magnetic crystal and the surrounding media. In this view, the capping agent can include a wide range of possibilities designed for a particular application, from simple termination groups of the magnetic crystal to large molecules and composites. The capping agents can be an organic molecule/coating, an inorganic coating/molecule or an organic-inorganic coating.

The capping agent (121) is such that the probe element is stable in the carrying fluid of interest at least in a temperature within the temperature range compatible with the integrity of the analyte of interest. In an embodiment, the capping agent is the gallic acid and the fluid of interest

is water or an aqueous buffer with pH between 3 and 10. In another embodiment, the capping agent is caffeic acid in similar conditions, allowing further functionalization with a molecule containing a reactive group such as an Amine (- NH2), a Hydroxyl (-OH) or a Thiol (-SH) group. The caffeic acid can be functionalized by a polymer containing an Amine or Thiol as a terminal functional group.

In another embodiment, the capping agent is Levodopamine in similar conditions, allowing further functionalization with a molecule containing a reactive group such as carboxylic (-COOH), Amine (-NH2), hydroxyl (-OH) or a Thiol (-SH) group. The capping agent is obtained after hydrolysis and condensation of alkoxysilanes such as tetraethoxysilane or other organosilanes. Mixtures of different capping agents are also of interest such as but not restricted to, the gallic acid and an amine-functionlized organosiliceouse precursor such as (3-Aminopropyl)triethoxysilane.

In an embodiment, the capping agent (122) is such that the probe element is able to produce a luminescent signal that can be externally detected. The capping agent can contain rare-earth complexes such as Eu3+ beta-diketones. The capping agent can contain carbon dots.

The capping agent (122) is such that the luminescent signal can be used to sense temperature at the probe element and in its surroundings, by a ratio of intensities of by a change in the life-time of the luminescence. The capping agent can contain a mixture of rare-earth complexes such as Eu3+ and Tb3+ beta-di-ketones.

The capping agent (122) is such that the probe element is able to anchor analytes of interest. As an example, the capping agent is the gallic acid and the analyte of interest (150) is a molecule with an amine group. Although other types of reaction between the probe and the analyte can also be used, it includes dopamine as the capping agent and the analyte of interest is a molecule with a carboxyl group.

The ratio between the magnetic crystal and capping agent ranges from 1% to 90% in mass.

One embodiment of a probe element is depicted in FIG. 1A, and includes a magnetic nanocrystal (101) and a capping agent (120). The other embodiment of a probe element depicted in FIG. lB, includes further a capping agent (121) acting as a stabilizer and a second capping agent (122) acting as an anchor for the analyte of interest (150).

One embodiment of a probe element is depicted in FIG. lC, and includes a magnetic nanocrystal (101) that is able to provide a magnetic field (131) with a well-defined direction and a magnetic field (141) with the opposite direction. In this embodiment of a probe element, the intensity of the magnetic fields (131) and (141) depends on temperature and can be reduced by a temperature change. The change with temperature of the intensity of the magnetic fields (131) and (141) is expressed by the change with temperature of the remanent magnetization as depicted in FIG. 1D.

The device provided herein is composed of at least one probe element, at least one analyte of interest, at least one temperature controller, at least one magnetic field reader, and at least one minute magnetic field source.

One embodiment of a device is depicted in Fig. 2, and includes a 3-state temperature controller unit (210), a temperature sensor (211), a peltier heating/cooling unit (212), a magnetic field source (220) composed of permanent magnets, a magnetic field reader (230), an inlet (241) and an outlet (242) unit.

In one embodiment, the device is designed such that the minute magnetic field source is sufficiently far and shielded from the magnetic field reader such they do not interact. In another embodiment, at the time where reading takes place, the magnetic field source is off, such they do not interact during reading.

The device is designed such that the temperature controller is able to control temperature across the device within the temperature range of interest. In another embodiment, the temperature controller includes a feedback and/or feedforward controller such as PI or a PID unit, a temperature sensor and an external heating element such as a resistance.

The heating element can be internal, i. e., it is the probe element itself that is able to absorb energy from an external source and convert this energy into heat. The external source can be a laser and absorption is made by the magnetic crystal. The external source can be an alternate magnetic field and absorption is made by the magnetic crystal.

The device is designed such that the magnetic field source is a miniaturized field source composed of permanent magnets. These magnets may further have a magnetic field circuit to guide the magnetic field lines. The magnetic field source can be a miniaturized field source composed of a coil at a distance from the magnetic field reader used together or not with the permanent magnet. The coil is embedded in the magnetic field reader.

The magnetic field reader (230) can be based on a magnetoresistive sensor, on fluxgate sensors, on miniaturized fluxgate sensors, on hall sensors, on squid sensors, on magnetic force microscopy, or any other sensor used to detect magnetic fields. The magnetic field reader is shielded from the magnetic field sources using, for example, a high permeability tin foil.

The magnetic crystal of the probe element is coupled or embedded in the magnetic field reader. The probe element can be used embedded in the tip of a magnetic force microscope. The probe element can be used coupled to the tip of a magnetic force microscope.

The analyte of interest can be a Cell, maintaining its integrity up to 42 °C. The analyte of interest can be a cancer or a pathogenic cell.

The analyte of interest can be a relevant cell biomarker such as proteins or polypeptides maintaining its integrity up to 60 °C. The analyte of interest can be a cardiac biomarker, such as cardiac troponin T, CK-MB or colon cancer biomarker such as Calcitonin, maintaining integrity up to 60 °C.

The analyte of interest can be a cell biomarker such as nucleic acids or nucleic acid sequences, maintaining their integrity up to 60 °C. The analyte of interest can be a RNA or DNA sequence for detection of a pathogen (Salmonella).

The analyte of interest can be a microRNA sequence for breast cancer detection.

The composite can contain an Aptamer for thrombin detection.

The analyte of interest can be an exosome/vesicle, the analyte of interest is a biomarker for cancer detection.

The analyte of interest can be a cell biomarker such as an organic molecule. The analyte of interest can be a hormone such as Thyroid-stimulating hormone (TSH) for hypothyroidism detection. The analyte of interest can be a small organic molecule such as 5-hydroxyindoleacetic acid for Alzheimer's disease diagnosis.

The analyte of interest can be a cell biomarker and it is detected by a composite that includes one or more synthetic biomolecules, such as a Xeno Nucleic acid, a Peptide Nucleic Acid (PNA), or a Locked Nucleic Acid (LNA) or a Peptoid.

The analyte of interest can be a cell biomarker and it is detected by a composite that includes another nanoparticle or a molecular cluster. Can also be a Sandwich assay between a magnetic nanoparticle and an optically active nanoparticle or a polymeric nanoparticle.

The analyte of interest can be a cell biomarker such as an inorganic molecule. The analyte can be the detection of nitric oxide (NO) as a biomarker for a bowel inflammatory disease.

The process provided herein includes an inlet stage, a proper manipulation of the magnetic field of the crystal stage, a reading stage and an outlet stage.

The inlets and outlets are standard microfluid channels. The inlets and outlets can be made of a polymer or made of an organosilicon material.

The inlet, incubation and manipulation stages occur at a temperature where the magnetic field of the magnetic crystal is small, such that aggregation of the probe element does not occur, and said temperature is within a range that maintains intact and reversible the relevant properties of the analyte of interest. The aggregation of the probe element may occur after incubation and manipulation stages, at a lower temperature where the magnetic crystal creates a relevant magnetic field; in this sense, aggregation of the probe element is controlled by the magnetic field created by the crystal, which in turn is controlled by temperature.

The manipulation stage comprises the application of a small magnetic field and a temperature change such that the magnetic field created by the probe element increases and is set fixed with a defined direction and intensity. The temperature change and small magnetic field created at the manipulation stage are assisted by the temperature controller and the minute magnetic field source, respectively.

The magnetic field is in the 0.5 to 100 Oe range and the temperature change in the 1 to 60 °C range.

In an embodiment, the reading stage comprises the determination of the remanent magnetic field created by the magnetic crystal of the probe element by a magnetic field reader.

The reading stage is made in the absence of an external field, at a temperature different from that used during the inlet and incubation stages, since the magnetic field created by the probe element is stable and aggregation is not a problem at this stage.

The process provided herein can have a second process used to separate and/or increase the concentration of the analyte or the analytes of interest, before the inlet stage, after the outlet stage or in between stages, using a temperature controller and a magnetic field source, as described in previous embodiments.

In one embodiment, this second process involves the application of a magnetic field gradient, using the magnetic field source, at a well-defined temperature, determined by the temperature controller, where the probe element has a given remanent magnetization and magnetic susceptibility that controls the separation velocity.

In one embodiment, analyte determination is not necessary and separation and/or concentration increase stand-alone process where the separation is used as a velocity is controlled by temperature, via the temperature dependent remanent magnetization and magnetic susceptibility of the magnetic crystal of the probe element.

The remanent magnetization and magnetic susceptibility are low, such that velocity is close to zero, while the remanent magnetization and magnetic susceptibility are high, such that velocity is between zero and 5 cm/s.

In one embodiment, this second process involves the use of different probe elements with different magnetic crystals and capping agents, such that each type of capping anchors to a different analyte and the magnetic crystals have different remanent magnetization and magnetic susceptibility such that the velocities of the probe elements under a given magnetic field gradient and at a given temperature are different. The analytes can be concentrated and/or separated by using different temperatures and/or outlets placed at different distances from the magnetic field gradient, as depicted in the part of the device shown in FIG. 3.

This second process involves the use of a general positioning system and a tip, as shown in FIG. 3. As examples of positioning systems and tips we mention atomic force microscopy devices and similar tip-based devices. As embodiments of operation, we mention the following two, both involving a temperature change and control at the tip. In the first one, and in a first stage, at a given temperature, the magnetic crystal of the probe element has a remanent magnetization, such that it is able to attract other magnetic crystals from an inlet system. Said other magnetic crystals can have the same magnetic nature of the magnetic crystal of the probe element or can have other nature, such as: superparamagnetic, hard and soft ferromagnetic, hard and soft ferrimagnetic, spin glasses and mixtures of the previous. In a second stage, at another given temperature, the remanent magnetization of the magnetic crystal of the probe element is reduced, such that attraction between the probe element and the other magnetic crystal is no longer enough to sustain both together and the other magnetic crystal and all elements attached to it can be dropped and counted at an outlet stage.

We mention the use of the tip of said microscopy device containing the other magnetic crystal, with the above detailed properties, and the use of the probe element as the element to be

collected, separated, counted and/or dropped in an outlet stage. The operation of is similar to the first one, except that the positions of the probe element and of the other magnetic crystal are swapped.

Claims

1. A probe element for separation and sensing of analytes, characterized by comprising at least one magnetic crystal composed of one of more nanoparticles with a composition including at least one transition metal or ion and with sizeranging from 5 to 500 nm and at least one type of cappingagent that is either gallic acid, caffeic acid, levodopamine, wherein the magnetic crystal is Fes_3Se_4, wherein the magneticcrystal produces a magnetic field in the absence of an external field at a temperature of use between -80 and 100°Cand the intensity of the magnetic field produced by the magnetic crystal changes by a temperature change.
2. The probe element according to any of the previous claims, wherein the magnetic crystal further produces a magnetic field in a well-defined direction and in its opposite direction.
3. The probe element according to any of the previous claims, wherein aggregation of the probe element is controlled by the magnetic field created by the magnetic crystal of the probe element, which in turn is controlled by temperature change.
4. The probe element according to any of the previous claims, wherein a second magnetic crystal does not produce a magnetic field in the absence of an external field at a temperature of use.
5. The probe element according to the previous claim, wherein the second magnetic crystal generates heat by the application of an external alternating magnetic field.
6. The probe element according to any of the previous claims, wherein at least one of the capping agents is an anchoring agent or a stabilizing agent.
7. The probe element according to any of the previous claims, wherein at least one of the capping agents is luminescent.
8. A device characterized by comprising at least one probe element described in any of the claims 1 to 7 containing at least one analyte of interest, at least one temperature controller, at least one magnetic field reader, and at least one minute magnetic field source, wherein said source does not interact with the said reader; and wherein the temperature controller comprises a heating element, a temperature sensor, and a feedback and/or feedforward controller.
9. A process of analyte determination, characterized by comprising an inlet stage, a stage of manipulation of the magnetic field of the crystal of the probe element described in any of the claims 1 to 7 a reading stage and an outlet stage wherein the manipulation stage is assisted by the temperature controller and the minute magnetic field source;wherein the reading stage comprises the determination of the remanent magnetic field created by the magnetic crystal of the probe element by a magnetic field reader.
10. A process for selective separation of analytes comprising: the capture of analytes using probe elements as described in claims 1 to 7. the application of a magnetic field gradient using the magnetic field source at a well-defined temperature; wherein the probe elements have temperature dependent remanent magnetization and magnetic

susceptibility that controls the separation velocity.

11. The process of selective separation according to theprevious claim, wherein different probe elements have magnetic crystals with different remanent magnetizations and different temperature dependencies
12. The process for selective separation according to any of the claims 10 and 11, wherein it is used together with the first process as a pre- or post- process
13. The process for selective separation according to anyof the claims 10 to 12 wherein it is used as a stand-alone method when analyte determination is not mandatory.

References - Patent

1. Wang X, S., White, R. L., Webb, C. D. & Li, G. Magnetic nanoparticles, magnetic detector arrays, and methods for their use in detecting biological molecules. (2011).
2. Hahlman Josephus A H M & Prins Menno W J. ON-CHIP MAGNETIC PARTICLE SENSOR WITH IMPROVED SNR. (2005).
3. Wang X, S., Osterfeld, S. J., Yu, H., Pourmand, N. & White, R. L. ANALYTE DETECTION WITH MAGNETIC SENSORS. (2009).
4. Wang, P., Guo, Y., Horng, C., Min, T. & Tong, R. MRAM with super-paramagnetic sensing layer. (2010).
5. Prinz, G. A. & Miller, M. M. High efficiency magnetic sensor for magnetic particles. (2005).
6. Wang, J., Xing, C., Li, Y. & Srinivasan, B. High magnetic moment particle detection. (2015).
7. Graham, D. L., Ferreira, H. A. & Freitas, P. P. Magnetoresistive-based biosensors and biochips. *Trends Biotechnol* **22**, 455–462 (2004).
8. Koh I & Josephson L. Magnetic Nanoparticle Sensors. *Sensors* **9**, 8130–8145 (2009).
9. Hsing, I.-M., Xu, Y. & Zhao, W. Micro- and Nano- Magnetic Particles for Applications in Biosensing. *Electroanalysis* **19**, 755–768 (2007).
10. Paleček, E. & Fojta, M. Magnetic beads as versatile tools for electrochemical DNA and protein biosensing. *Talanta* **74**, 276–290 (2007).
11. Ludwig, F., Mäuselein, S., Heim, E. & Schilling, M. Magnetorelaxometry of magnetic nanoparticles in magnetically unshielded environment utilizing a differential fluxgate arrangement. *Review of Scientific Instruments* **76**, 106102 (2005).

Because at the end we are mere specks of stardust striving to flee the “forces” of entropy and avoid the thermodynamic equilibrium, leaving nothing behind but the stories of our experiences, the stamps of our memories and the legacy of the lessons we shared...